WEAR OF ABRASION RESISTING MATERIALS

by

John Thomas Harry Pearce

A thesis presented for the degree of

DOCTOR OF PHILOSPHY

in the

Department of Metallurgy & Materials Engineering,

of the

University of Aston in Birmingham.

April, 1982.

TITLE: Wear of abrasion resisting materials.

NAME: John Thomas Harry Pearce.

DEGREE: Ph.D.

YEAR: 1982.

SUMMARY

The wear behaviour of a series of chromium containing white irons has been investigated under conditions of high stress grinding abrasion using a specimen on track abrasion testing machine. The measured abrasion resistance of the irons has been explained in terms of microstructure and hardness and with respect to the wear damage observed at and beneath abraded surfaces. During abrasion material removal occurred by cracking and detachment from the matrix of eutectic carbides as well as by penetration and micromachining effects of the abrasive grits being crushed at the wearing surface. Under the particular test conditions used martensitic matrix structures gave higher resistance to abrasion than austenitic or pearlitic. However, no simple relationship was found between general hardness or matrix microhardness at wear surfaces and abrasion resistance, and the test yielded pessimistic results for austenitic irons. The fine structures of the 15% Cr and 30% Cr alloys were studied by thin foil transmission electron microscopy. It was found that both the matrix and carbide constituents could be thinned for examination at 100 Kv using conventional dishing followed by ion beam thinning. Many of the rodlike eutectic M_7C_3 carbides were seen to consist of clusters of smaller rods with individual M_7C_3 crystals quite often containing central cores of matrix constituent. Both eutectic and secondary M_7C_3 carbides were found to contain stacking faults on planes normal to the basal plane. In the eutectic carbides in the 30% Cr iron there was evidence of an in-situ $M_7C_3 \longrightarrow M_{23}C_6$ transition which had taken place during the hardening heat treatment of this alloy. In the as-cast austenitic matrix iron strain induced martensite was produced at the wear surface contributing to work hardening. The significance of these findings have been discussed in relation to wear performance.

KEY WORDS: Alloy cast irons, abrasion resistance, eutectic carbides, wear damage, electron microscopy.

ACKNOWLEDGEMENTS.

I would like to express my appreciation to Dr. R.S. Jackson and Dr. W.B. Hutchinson of the University of Aston and to Dr. R.W. Durman of Bradley and Foster Limited for their guidance and comments given during the period of research. I also wish to record my gratitude to Mr. N.N. Brown, Principal, to Dr. G.J.T. Hume, Vice-principal and to Dr. G.G. Storey, Head of Materials Technology for their continued encouragement and support of the work. Finally my thanks to Mrs. J. Davis for the typing of the script.

CONTENTS.

LISTS OF TABLES.

LISTS OF FIGURES.

LISTS OF TABLES.

LIST OF FIGURES

1.0 INTRODUCTION.

A considerable expense is incurred annually in replacing components which have become unserviceable as a result of abrasive wear damage. Only by the development and correct selection and usage of abrasion resistant materials to withstand the various forms of abrasive wear in mining, ore preparation and other industries can equipment such as crushers, grinding mills, pumps etc. be used economically and for the longest possible periods without shutdown and loss of production. The problem of material selection is probably the major difficulty facing both the manufacturers and users of abrasion resistant parts. For example, founders of cast abrasion resistant alloys (1,2) must choose a composition to give a microstructure having the necessary abrasion resistance, toughness and reliability with due regard to cost, section thickness and design, founding characteristics, ease of heat treatment and possible softening for machining. To achieve this the form of abrasive wear and the loading and the environmental conditions under which it takes place must be known.

As an aid to both selection and development of abrasion resistant materials it is important not only to determine their relative resistance to abrasion under given sets of conditions but also to study the nature of the wear damage produced in the structures of the materials being tested so that an understanding of wear mechanisms may be obtained.

The work described in this thesis is concerned with the behaviour of a series of 0-35% chromium cast irons under conditions which simulate high stress abrasion which is the major form encountered in grinding and pulverising mills handling metal ores, cement, coal etc. A review of relevant literature has considered the forms of abrasion, the influence of additional factors such as impact and corrosion, the problem of abrasion testing, the characteristics of various abrasion resistant materials and the selection of these materials to suit specific applications. Experimental work has investigated the use of a specimen on track abrasion testing machine with a standard silica sand as the abrasive in assessing the relative behaviour of the alloy cast irons in both the as-cast and heat treated conditions. The values of relative abrasion resistance obtained from this test have then been discussed with respect to the microstructure and hardness of each alloy iron tested. The investigation has continued to study the nature of damage produced at and beneath abraded surfaces using optical and scanning electron microscopy.

In an attempt to study the finer structural features of the chromium irons a technique was developed for the preparation of thin foils for examination by transmission electron microscopy. This involved determining the correct conditions for dishing followed by ion beam thinning of suitably perforated specimens.

The TEM studies were limited to the 15% Cr and 30% Cr irons. Both the matrix and carbide constituents were successfully thinned and were identified using electron diffraction. Foils produced from unworn structures revealed that the eutectic M_7C_3 carbides in both irons contained structural faulting and that the secondary carbides which were identified as M_7C_3 in the 15% Cr iron were also faulted. Eutectic M_7C_3 rods and plates were found to consist of a number of crystals. Some of the M_7C_3 crystals contained central cores which were not hollow but contained matrix constituent although they appeared to be completely isolated from the surrounding matrix region. Examination of the heat treated 30% Cr iron has produced evidence of an in-situ transformation in the original eutectic carbide of $M_7C_3 \longrightarrow M_{23}C_6$. Attempts to produce thin foils from abraded surface regions met with partial success in that the effect of wear on the austenite matrix in the as-cast 30% Cr iron could be studied. However, the distorted eutectic carbides in these regions tended to be removed during the preparation of foils due to the effects of abrasion which had produced decohesion from the matrix. The results of the transmission electron microscopy observations have been discussed in relation to the earlier wear studies and suggestions have been made for future work.

2.0 TYPES, MECHANISMS AND ASSESSMENT OF ABRASIVE WEAR IN RELATION TO SERVICE CONDITIONS.

2.1 Basic forms of abrasive wear

Wear can be defined as the unintentional removal of material from the surfaces of bodies moving in contact with one another. Wear is believed to occur by the displacement and detachment of small fragments from a surface. The rate at which a given surface wears depends on several factors, such as surface microstructure, type of contact material, type of relative movement, nature of loading, chemical action and temperature. Wear may be due to a combination of elementary mechanisms and it is often difficult to describe accurately the type of wear occuring in any given application.

Industrial conditions producing wear of components have been loosely classified into three main areas. (3)

(a) Abrasive wear which may be dry or wet.

(b) Dry sliding wear which occurs for example in clutch and braking systems.

(c) Lubricated sliding wear in gears, bearings, cams and tappets.

The present work is concerned with the various types of abrasive wear which occur due to the action of abrasive particles or fragments on component surfaces. Abrasive wear results in high annual replacement costs in mining, ore treatment, civil engineering, founding and many other industries.

As a summary of abrasion studies covering a wide range of service conditions Avery (4) has suggested that abrasive wear may be described according to three main types.

(a) Gouging abrasion usually associated with impact.

(b) High stress or grinding abrasion.

(c) Low stress scratching abrasion or erosion.

Gouging takes place when large pieces of abrasive material cut into wearing surfaces with sufficient force to remove relatively large pieces of debris. Worn surfaces tend to show heavy gouge marks. Gouging may occur at low speeds as in a shovel meeting a rock pile or at higher speeds as in hammer bars crushing material in an impact pulveriser. It is usually accompanied by severe impact loads which introduce the problem of achieving high surface hardness to resist penetration combined with adequate toughness to resist cracking.

High stress or grinding abrasion occurs when two working surfaces rub together to fragment granular abrasive materials. The term high stress is used although nominal loads may appear to be small since localised stresses at points of contact between the abrasive particles and the surface are sufficient to exceed the crushing strength of the particles. This causes progressive fragmentation of the particles and wear of the working surfaces. The major example of this type of wear occurs in ball mill grinding but it is also significant in conveyor chains, sprockets and exposed gearing where particles become entrapped between working surfaces.

Low stress scratching abrasion or erosion implies that service stresses do not exceed the crushing strength of the abrading particles. It occurs in applications where freely moving particles which may be suspended in air or water come into contact with a wearing surface. eg. in chutes, pumps, shot blast equipment. Impact forces are likely to be small unless the abrasive becomes contaminated with large pieces of material. Hence the level of toughness required in a material to resist scratching abrasion is significantly less than for the two previous types and maximum resistance is likely to be obtained with the hardest possible material.

Although widely accepted Avery's classification is not fundamental and there is a certain degree of overlap between the three types of wear described above. For example gouging must begin by indentation as in grinding abrasion. Indeed Avery recognised that in many cases a wearing part was subject to more than one of the above types simultaneously but he considered that the predominant mechanism could usually be identified to allow appropriate material selection to resist abrasion to be made.

Another form of classification is to describe abrasive wear in terms either two body or three body conditions. In the case where abrasive particles simply rub against a surface the situation is termed two body abrasion (5). In the case where abrasive is trapped between two sliding surfaces the situation is termed three body abrasion (6).

2.2 Effect of type and size distribution of abrasive

The abrasive nature of granular material is difficult to accurately assess since it can depend on a number of factors. These include hardness, crushing strength and impact properties of the abrasive, shape and size range of the particles and whether the particles are in suspension in a liquid. In order to produce appreciable wear abrasive particles need to be harder than an abraded surface. Typical hardness values for common minerals and phases in ferrous alloys are given in table 2.1. It is recognised that hard materials such as alumina and quartz produce faster wear rates and less variation in the relative wear rates of different ferrous alloys than softer materials such as feldspar and calcite (7). The influence of mineral hardness on the abrasive wear rate of steel grinding balls is illustrated in figure 2.1.

Farmer (8) suggested that there is a transition from a low to high wear rate over a critical range of hardness of abrasive, this critical range being dependent on the hardness of the abraded material as shown in figure 2.2. Haworth (9) concluded that for a given hardness value the abrasive nature of particles increases with increasing degree of angularity and that the influence of shape was as significant as that of hardness. From a series of grinding wear tests Avery (10) found that compressive strength and fracture behaviour of an abrasive were also important, the higher the compressive strength of the abrasive the greater was the grinding wear rate.

Mineral, Material or Phase	Hardness		
	Knoop	HV	Mohs
Talc	20		1
Plastics	25		
Carbon	35		
Gypsum	40	36	2
Calcite	130	140	3
Fluorite	175	190	4
Apatite	335	540	5
Glass	455	500	
Feldspar	550	600-750	
Magnetite	575		
Orthoclase	620		6
Flint	820	950	
Quartz	840	900-1280	7
Topas	1330	1430	8
Garnet	1360		
Emery	1400		
Corundum	2020	1800	9
Silicon carbide	2585	2600	
Diamond	7575	10000	10
Ferrite	235	70-200	
Pearlite, unalloyed		250-320	
Pearlite, alloyed		300-460	
Austenite, 12%Mn	305	170-230	
" " , work hardened	645		
Austenite, high Cr iron		300-600	
Martensite	500-800	500-1010	
Hard Cr electroplate	975		
Cementite	1025	840-1100	
Chromium carbide $(Fe,Cr)_7C_3$	1735	1200-1600	
Molybdenum carbide Mo_2C	1800	1500	
Tungsten carbide WC	1800	2400	
Vanadium carbide VC	2660	2800	
Titanium carbide TiC	2470	3200	
Boron carbide B_4C	2800	3700	

Table 2.1

Typical hardness values.

After (2,16)

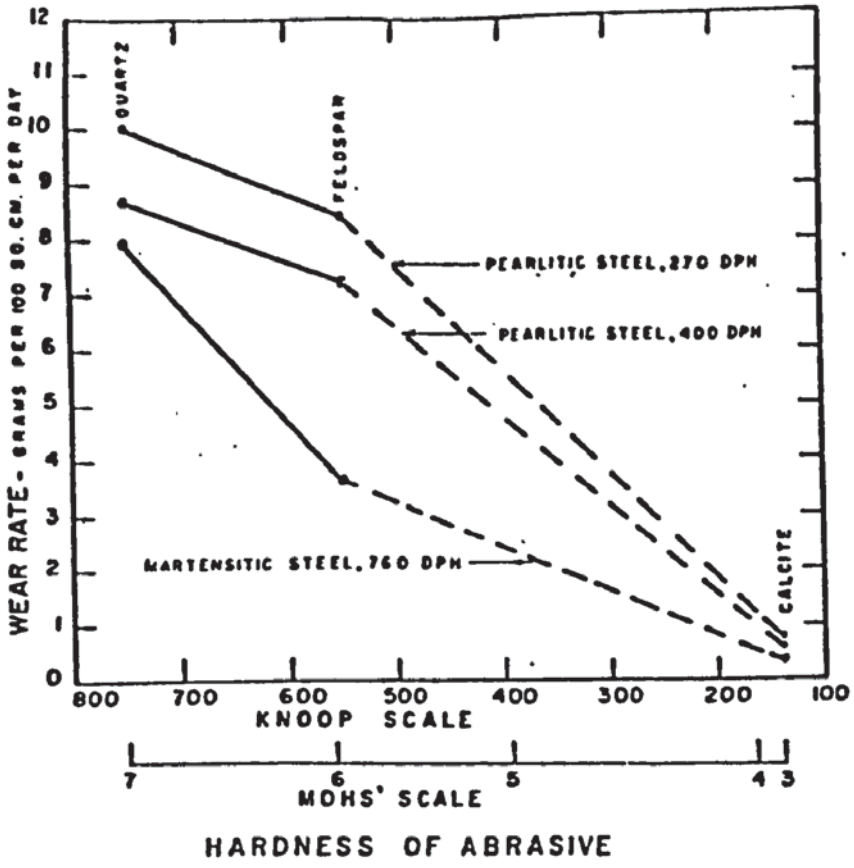

Figure 2.1

Influence of hardness of the abrasive mineral on the wear rate of 0.8%C steel grinding balls.

After Norman (7)

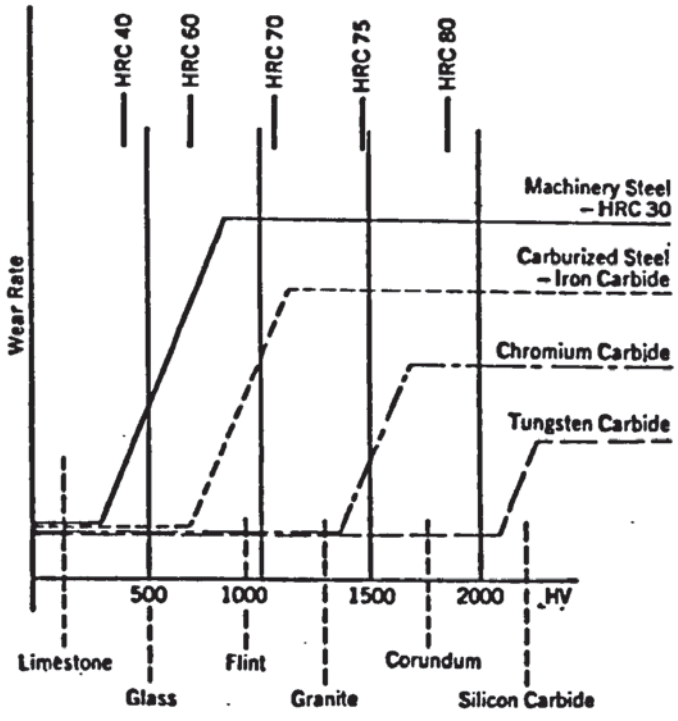

Figure 2.2

Idealized diagram showing wear rate of materials versus mineral hardness.

After Farmer (8)

As abrasive particle size decreases then it has been generally found (10-13) that there is a corresponding decrease in wear rate. This is particularly noticeable in testing hard alloys (10). Finer particles seem to be less abrasive but at the same time the relative performance in relation to different alloys may change (10-12). Fine particles such as silica flour produced wear patterns during grinding tests that were more consistent with low stress erosive wear than with high stress abrasive wear (10). Dunlop and Fellows (12) suggested that this was because the silica flour was so fine that it could flow in a similar fashion to a liquid and consequently no high stress levels were developed at points of contact with the wearing surface. It may be that the larger number of smaller particles abrade one another rather than the surface and that grinding is autogenous.

More recent work (13) suggests that there is a critical particle size below which wear rate decreases and above which wear rate may increase, decrease or remain constant with increasing particle size depending on the material being abraded and the conditions of abrasion. This is shown in figure 2.3 which is based on the data from the above work (13). Because of such variations it was concluded that the use of wear ratios was not suitable for rating the wear resistance of materials under changing conditions such as abrasive particle size or load. Wear ratio can only be used to compare materials when abrasion parameters are constant.

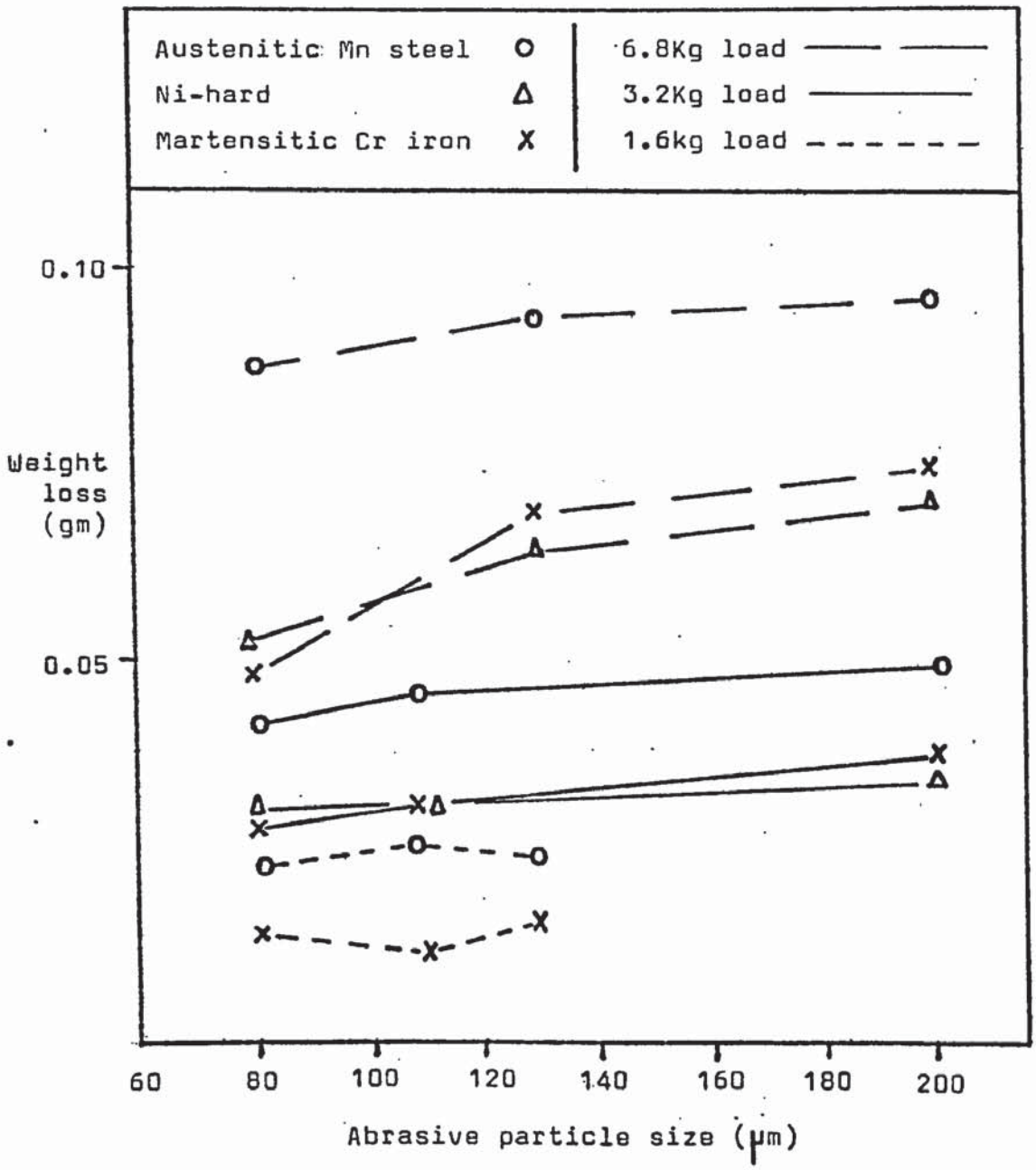

Figure 2.3

Effect of abrasive particle size on wear at different loads for alumina abrasive.
After Muscara et Al (13).

2.3 Effect of magnitude, velocity and direction of loading.

The particle size and shape of abrasive media cannot be studied in isolation since the level of stress during abrasion could produce marked changes in both these factors. During high stress grinding abrasion where particles are fragmented the abrasive may be initially round and smooth but on fracture it can quickly become angular and reduced in size. In erosive wear service stresses are seldom sufficient to produce fracture of the abrasive and wear rate can be related to the original shape and size range of the particles.

In grinding abrasion load must be considered in relation to the compressive strength and fragmentation characteristics of the abrasive. In a series of grinding tests Boyes (14) showed that in general wear increased by a disproportionate factor depending on test conditions as load increased, the increase at high loads being greater than that at low loads. This is shown in figure 2.4 which describes the relationship between load and volume loss in a low alloy white iron. To explain this effect Boyes studied the breakdown of the Erith silica sand which was used as the abrasive in his tests. The relationships obtained between sand grain size, load and testing time are illustrated in figure 2.5. This shows that average grain size was progressively reduced as time of testing and load were increased. Boyes concluded that it was abrasive fragmentation rather than any variation in wear behaviour of the alloy which resulted in a increase in wear

rate with time at any given load and in a non-linear increase in wear rate with load.

The velocity of abrasive action can vary depending on the application particularly where gouging or low stress abrasion are involved. Both velocity and direction are characteristics of a specific process and it is difficult to change either without altering the nature of the process. The effect of velocity during abrasion has not been investigated in detail but Haworth (9) concluded that increasing the velocity of abrasive action produces disproportionate increases in wear rate. The direction of abrasion has been studied in shot blast equipment and in slurry transport. It has been found that the characteristic wavy wear patterns on eroded surfaces depend on the direction of abrasive particles (15). The effect of direction is important in determining the respective levels of deformation and cutting wear which are discussed below and must also be considered when designing components constructed from abrasion resistant rubbers.

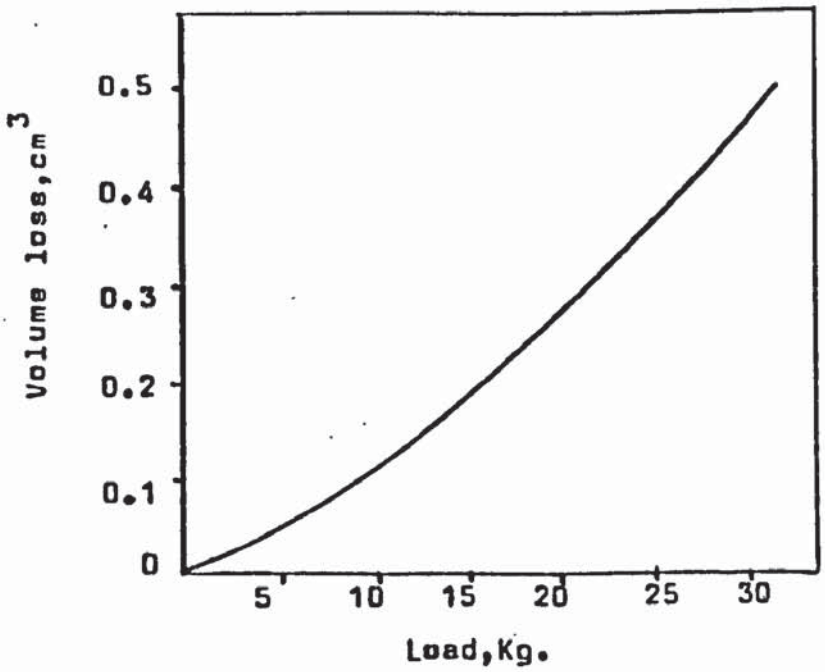

Figure 2.4

Effect of testing load on volume loss during grinding wear of a low alloy white iron.

After Boyes (14)

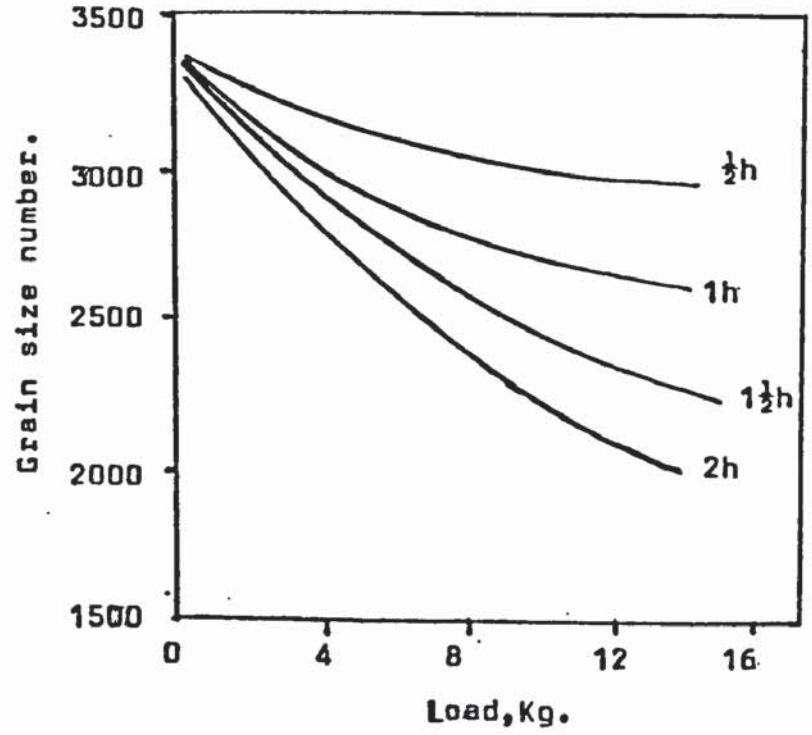

Figure 2.5

Relationship between testing load and grain size of silica abrasive at various times.

After Boyes (14)

2.4 Mechanisms and theories of abrasive wear.

2.4.1 Deformation and cutting wear.

A number of attempts has been made to define the mechanisms which might occur during abrasive wear (16-24). In general the stress involved during abrasion can be considered in terms of a component normal to the wearing surface and a component parallel to the surface. The normal component may cause hard particles to penetrate the surface. The parallel component, which gives relative movement between the abrasive and the surface, may cause chipping of the surface by suitably oriented particles of abrasive or may cause other particles to groove the surface by ploughing (16) or rubbing (18).

During ploughing or rubbing by smooth edged or rounded particles, the surface material is pushed transversely to the direction of particle movement to form a groove, the displaced material piling up at groove edges rather than being removed from the surface (16). Ductile surfaces abraded by sharp edge particles wear by cutting of chips similar to machining. In brittle materials grooves are said to be formed by crack propagation. In grinding abrasion since the particles of abrasive are crushed at the surface, ductile materials may wear by a fatigue mechanism, where surface material is displaced to and fro by repeated indentation. (16).

Wear mechanisms have been analysed in two ways depending on the application of force to the abrasive particles.

(a) When force is applied to entrapped loose particles between two surfaces as in grinding, gouging etc.

(b) When force results from kinetic energy of moving abrasive particles as they meet a surface as in erosion in liquid or pneumatic systems.

The first case, as illustrated in figure 2.6a, has been studied by several authors (16, 18-20). Their general conclusion can be described by an expression in which V, the volume wear rate per unit length of sliding, is given by

$$V \propto \frac{\text{load}}{\text{hardness of surface}}$$

This cannot be applied to grinding abrasion since it assumes that abrasive particles are rigid and not crushed. The equation has been developed for annealed single phase metals and does not include factors such as particle size and shape, presence of fluid and brittleness of abraded material.

It has been suggested (16) that a deformation wear mechanism as outlined by Bitter (21) could be the basis for the development of relationships to describe grinding wear. The proposed mechanism of deformation wear resulted from studies of the second case where abrasive particles impinge

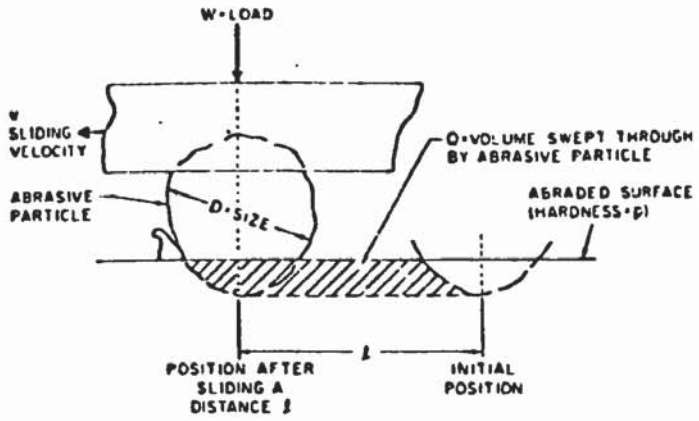

(a)Direct mechanical application of force to abrasive particle.

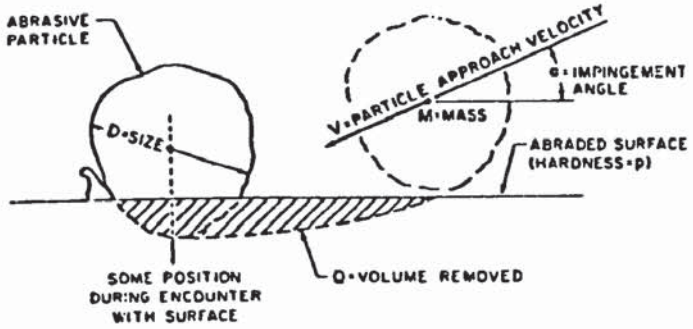

(b)Kinetic application of force to abrasive particle.

Figure 2.6
Models of abrasive wear.
After (16)

on a surface (Figure 2.6b.) Here there are two kinds of action depending on angle of impingement and nature of the surface. These are deformation wear and cutting wear. Deformation wear results from repeated deformation during collisions of particles with a surface. It is most likely to occur at large impingement angles. If a particle impinges on a surface then elastic or plastic deformation may occur at the point of collision. If the collision is elastic frequent repetition would be expected to cause no damage unless fatigue behaviour occurs. If the elastic limit is exceeded during the collision then plastic deformation will occur and repeated collisions with a large number of particles will form a plastically deformed surface layer. Deformation hardening will increase the elastic limit and on further plastic deformation the limit will eventually become equal to the strength of the material embrittling the surface layers and leading to spalling.

If the impinging particles strike the surface at an acute angle the surface is subject to a shearing force which may give cutting wear (21) i.e. each particle 'machines' material from the surface. The relative levels of deformation and cutting wear will also depend on the particles velocity at impact and on whether the surface is ductile or brittle. Figure 2.7 shows how cutting and deformation wear are combined to give total wear for a ductile and a brittle material. In the case of a soft ductile material maximum wear occurs at lower angles, whereas a hard brittle material suffers maximum

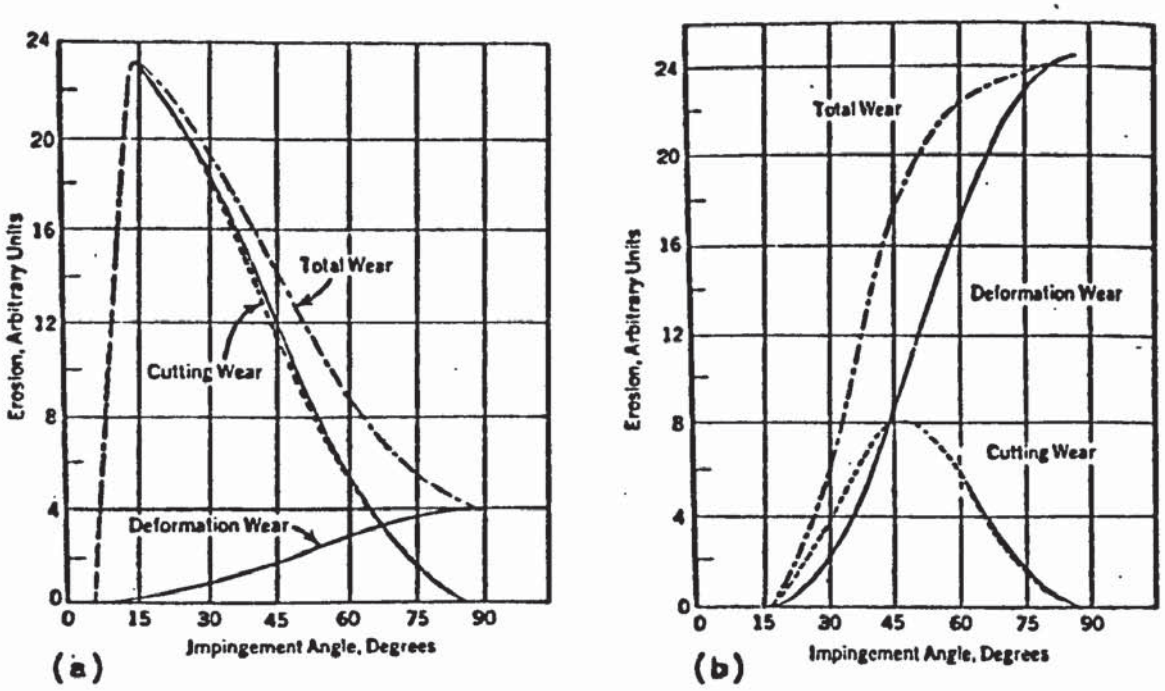

Representation of deformation, cutting and total wear versus impingement angle for (a) soft ductile material
(b) hard brittle material.

Figure 2.7

Influence of impingement angle on erosive wear.

After (21-23)

Alloy	0.2offset yield MNm^{-2}	ultimate MNm^{-2}	change in length. %	test
Ni-Cr iron (martensitic)	280 1200	280 1800	0.2 2-3	tension compression
28%Cr iron (austenitic)	- 750	650 1250	- 3-4	tension compression
28%Cr iron (martensitic)	- 1000	710 2200	- 3	tension compression

Table 2.2

Yield and ultimate strength values in tension and compression.

wear at high impingement angles. The work of Bitter (21) and Finnie (22) was based on the use of tensile stress-strain relationships but in abrasion compressive stresses are also involved. Avery (25) has correctly suggested that any wear equations developed must take due account of this since for brittle materials such as white cast irons stress-strain relationships in tension and compression are not similar. This point is illustrated by the data in table 2.2.

Although the stress at the point of impact of a moving object with a surface or the stress where an indenter presses into a surface as in a hardness test is basically compressive it is recognised that the indentation is surrounded by a cone of shear stress. In practice this could cause chipping of edges of brittle materials.

2.4.2 Indentation of surfaces.

A knowledge of the way in which a surface is indented by an object under load has been important for a very long time since this forms the basis of static indentation tests to measure hardness of materials. Surface indentation has been analysed by Tabor (26) and Westbrook (27) in order to explain the influence of the constraint factor and work hardening. The behaviour of material in and adjacent to the plastic zone which develops beneath an indenter has also been considered in terms of slip line field and elastic theories.

In the slip line field theory the material in the plastic zone is assumed to flow upwards and the material outside this flow region is assumed to be rigid (28). The elastic theory considers that material outside the zone behaves elastically and suggests that the displaced volume on indentation can be accomodated by an elastic decrease in volume instead of by upward flow (29). The elastic theory is claimed to be correct for blunt indenters only (for half cone angles of $\geqslant 80^{o}$) and it is recognised that for sharper indenters some upward flow as suggested by slip line field theory will occur. The process of shot peening which gives rise to residual compressive stresses is forwarded as evidence for the inclusion of elastic considerations in indentation theory (30). It has been shown that deformation under a wedge indenter depends on the friction condition at the interface and that an undeformed zone can develop immediately under the indenter for high friction conditions (28). The shape of flow fields, the extent of resultant plastic deformation and the nature of any residual stresses after indentation will therefore depend on the geometry of indenting particles during abrasion.

By considering the energy expended in plastically deforming material on indentation, Moore (31) has developed the following relationship:

$$\mu w \approx p^2 \int \sigma \, d\varepsilon$$

where μ = friction coefficient between abrasive particle and wear surface.

w = load on the abrasive particle.

p = depth of indentation of the particle.

$\int \sigma \, d\varepsilon$ = energy under stress-strain curve of the material integrated to strain at surface.

Moore (31) suggested that volume wear is proportional to the cross sectional area of grooves made by abrasive grits and is hence proportional to p^2. Hence volume wear increases with increase in grit size and load and decreases as the value of the integral increases. This value will be larger for a material with a high elastic limit and high strain hardening rate. This and the above discussion assumes that the material indented is capable of plastically deforming under load. Abrasion resistant materials however, normally contain a high proportion of hard brittle constituents in their structure and the possibility of indentation induced microcracking must also be considered. The theories and evidence of such cracking have been the subject of a review by Lawn and Wilshaw (32) who have attempted to define indentation stress fields for various indentation systems and to relate these fields to the nature

of cracking in indented brittle solids. The review restates the development of the Hertzian elastic field and its variants for cases involving spherical indenters on flat surfaces in the light of the cone shaped cracking that circumvents the contact circle and spreads downwards into the indented material at critical loading. The relevence of such a mechanism to particle size reductiom by comminutiom during crushing and milling is then discussed.

Studies of indentation of surfaces by a point force or sharp indenter (30-33) have examined the Boussinesq stress field around such an indenter and have developed models for indentation cracking. Lawn and Swain (33) proposed the model of crack formation given in outline form in figure 2.8 Initially the sharp point of the indenter produces an inelastic deformation zone. Fracture is initiated in this zone and develops into a crack downwards, this crack is called a median vent. A median vent develops as a circular shape crack and several mutually intersecting median vents may form during indentation (33-35). At a later stage a median vent can grow outwards and can break through the surface forming a semicircular configuration centred on the indentation point. This is illustrated in figure 2.9. On unloading the median vents close but do not heal and sideways extending cracks called lateral vents develop. These lateral cracks can extend to surface causing chipping damage. Since the lateral vents develop on unloading it is suggested that they must be

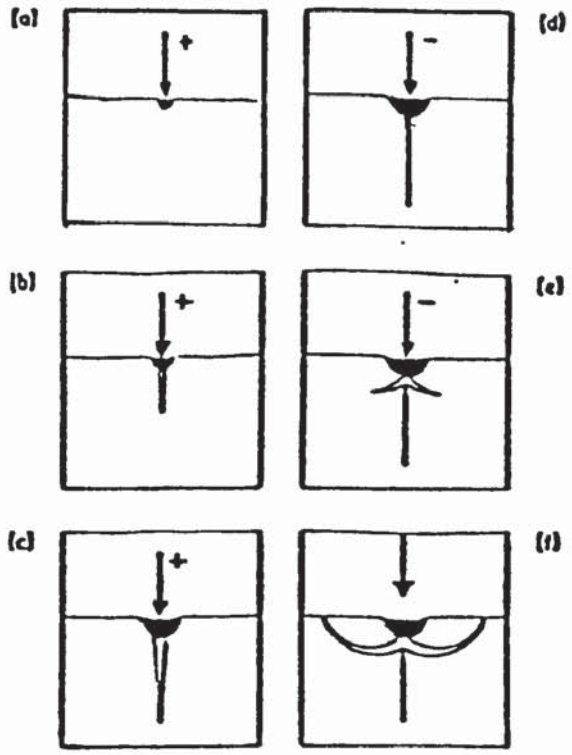

Figure 2.8

Model of vent crack formation under point indention. Median vent forms during loading (+) half-cycle, lateral vents during unloading (-) half-cycle. Fracture initiates from inelastic deformation zone (dark region) After Lawn et Al(33)

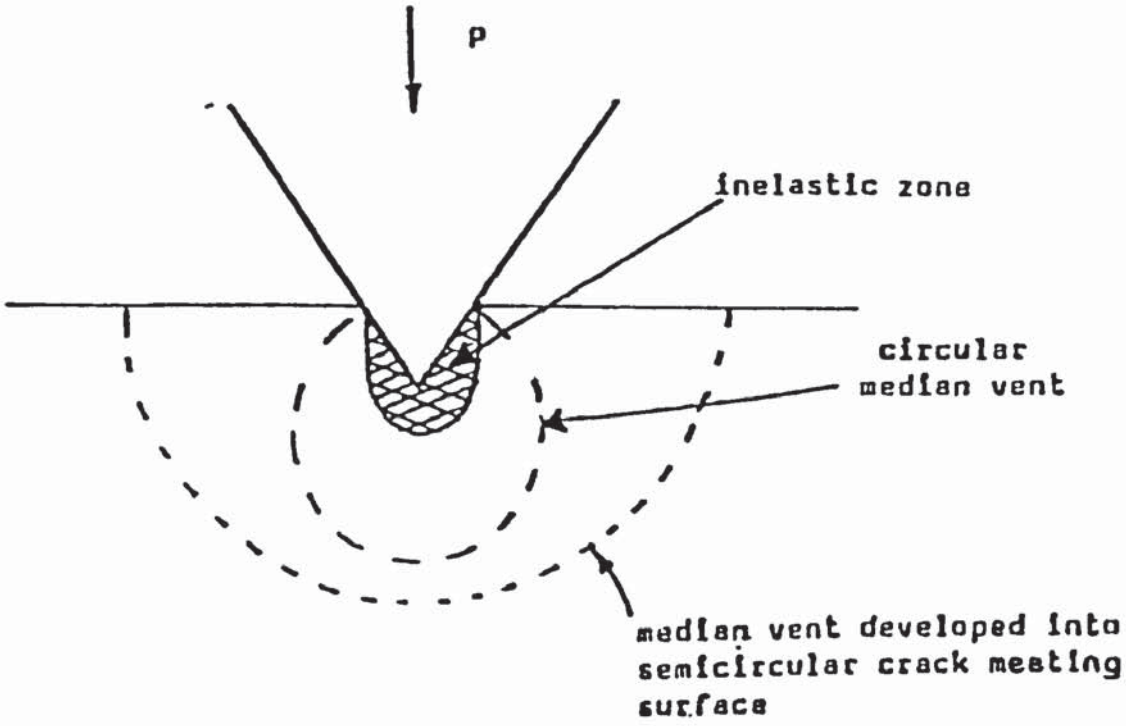

Figure 2.9

Model of median vent cracking on indention of brittle solid. After Lawn et Al (35)

connected with the residual stresses resulting from the inelastic deformation zone. Further work is considered necessary to determine if such a relationship exists (33,34) and also to study whether measurement of surface traces of vents in opaque materials such as carbides can be used to assess fracture toughness (36).

Indentation models of abrasion where abrasive grits indent and move relative to a surface forming grooves have not yet been sufficiently developed to interpret abrasion damage resulting from microcracking of brittle constituents. Although studies of abrasion of fused silica surfaces by silicon carbide papers indicate that very sharp abrasive particles give more lateral cracks than blunt particles. Material removal from the surface appears to result from the linking up of neighbouring cracks and by crack overlap (33).

2.4.3 Abrasive wear mechanisms in duplex structures

The work discussed in the preceeding sections on abrasion and indentation mechanisms deals mainly with either ductile or brittle single phase structures. In practice, service damage to wear resisting alloys will result from more complex wear modes since these alloys are duplex and normally contain hard brittle phases dispersed in a ductile matrix.

A number of studies (5, 14, 18, 23, 24, 37-43) have been made in order to relate wear damage to microstructure in duplex materials such as steels, white irons and cemented carbides. Much of this work concentrates on describing the structures in terms of volume fraction and morphology of the hard dispersed phase and relates this to volume or weight loss under varying abrasion conditions. Only limited attempts have been made to study damage at worn surfaces in order to develop models of wear mechanisms.

For pearlitic steels containing over 10% by volume of pearlite, Moore (37) found that wear resistance and bulk hardness were linear functions of pearlite volume. In martensitic steels an empirical relationship showed that abrasion resistance was a linear function of the square root of the % carbon present.

For steels containing spheroidised carbides wear resistance was thought to depend on particle size and mean free ferrite path (37). Larsen-Badse et al (38, 39) in studying a range of cementite particle spacings, found that abrasion resistance was inversely proportional to the square root of cementite particle spacing; later work (37) suggests that the role of cementite particles in providing wear resistance may well change according to the size of abrading grits and the relative sizes of the carbide spacing and debris formed during abrasion. The situation is further

complicated by the possible fracture of certain shapes and sizes of carbides during abrasion which can contribute to the overall wear mechanism (40).

Richardson (41) suggested that hard phases such as carbides in steel are only effective in imparting abrasion resistance if their size is at least as large as the wear debris produced during abrasion. When the depth of penetration of the abrasive becomes greater than the size of the dispersed phase then the properties of the matrix assume greater importance (37).

Increased abrasion resistance is therefore obtained when the hard particles are present in a massive form as in white irons or hard facing materials. In hypo-eutectic alloy white iron it is known (1, 2, 42) that increasing the volume fraction of eutectic carbides will increase the abrasion resistance for a given matrix structure. There is little published information however on the relative behaviour of eutectic carbides and the matrix at the wearing surface. Several workers (14, 18, 25, 44) have observed bending and fracturing of the carbides in the surface regions of worn components and of wear test specimens. None of the work has investigated how the carbides deform or crack although Richardson suggests the carbides can flow plastically and may work harden (18). Garber et al (42) conclude that alloys with carbides in their structure will have satisfactory

abrasion resistance only when the matrix is sufficiently strong to prevent the removal of deformed or cracked carbides from the surface.

Blomberry et al (43) have investigated wear mechanisms during abrasion of tungsten carbide-cobalt composites in rock drilling. They found that in the initial stages of damage fine abrasives preferentially remove cobalt from the surface forming small pits with intergranular facets. They suggest that the removal of cobalt lowers the fracture strength of the surface layers since it leads to intergranular cracks growing from the pits and eventually microfracture of the tungsten carbide skeleton. This is followed by removal of tungsten carbide grains from the surface and repeated surface microspalling. Composites with the highest measured fracture resistance had the highest cobalt contents and therefore suffered greater cobalt removal and more severe abrasion. They considered that even though much of the volume loss resulted from fracture at the surface, fracture tests such as transverse rupture strength or crack length determination on indentation could not give a valid assessment of abrasion resistance; recent work (24) does however suggest that wear rate due to spalling can be determined in terms of fracture toughness and hardness values and microstructual parameters. Above a critical load both wear grooving and removal of material is said to be due to crack propagation. Fracture toughness models can be used to calculate this critical load

for two body abrasion in which it is assumed that abrasive particles are not crushed. This work also considers that the product of abrasive wear resistance and fracture toughness which is called the "wear strength" can be useful in comparing different structures but this is of questionable value.

From the above discussion possible mechanisms which might operate during abrasive wear can be summarised as follows:

(a) Cutting wear of the matrix by softer abrasives and of both matrix and carbide phases if the abrasive is sufficiently hard.

(b) Deformation wear of the matrix.

(c) Selective removal of matrix.

(d) Microfracture of carbides due to indentation and/or plastic flow of surrounding matrix or removal of matrix.

(e) Pulling out or chipping of fractured carbides.

and (f) Fatigue cracking due to repeated indentation and grooving.

2.4.4 Effect of service conditions.

The wear mechanisms discussed above may be influenced by the effects of impact loading, corrosive environment and heating of the wear surface. Toughness requirements become more demanding as the speed and size of equipment increases

particularly in components subject to gouging or grinding abrasion. Resistance to impact is the one factor that frequently dictates the selection of a material with less than maximum hardness (45). Published work on impact and abrasion relates to the problem of avoiding failure or excessive plastic flow (1, 2, 7, 10, 45, 46).

In many applications e.g. wet grinding, components are subjected to abrasion in the presence of corrosive agents. Under these conditions wear rates are generally higher than for dry abrasion (44, 47-56). This increase is due to a combination of both physical and chemical effects. In wet abrasion fine abrasive particles are washed away and abrasion may result from coarse particles meeting the surface, in contrast in dry abrasion there may be a layer of fine abrasive powder protecting the surface and autogenous grinding occurs. Enhanced fracture of abrasive particles under wet conditions may also contribute to faster wear (57, 58). Chemical effects result from the removal of passive films by wear (48, 49) and from the selective attack of the matrix in duplex alloys (42, 56). The latter causes hard wear resistant dispersed phases such as eutectic carbides to be undermined and they then lack support and are more easily broken away (44, 59). Some components must resist abrasion while operating at elevated temperatures. Examples of such conditions occur in breaker bars and pallets for sinter plants, fire bars (60) and rolls for hot mills (61). The effects of increased

temperature during abrasion may also be of interest during dry grinding of ores (54) and during accelerated laboratory abrasion tests (9).

Hot hardness characteristics of abrasion resisting alloys have been examined but no definite correlation between these characteristics and elevated temperature abrasion has yet been established (62, 63). Apart from affecting microstructure high temperatures might also influence wear in other ways. For example the wear debris of oxides may give enhanced abrasion and heating and cooling of a surface may cause crazing. This is the formation of a network of fine shallow cracks resulting from thermal fatigue. It is recorded as little wear in terms of weight loss but the cracks may increase the effectiveness of an abrasive so that wear rates accelerate (61, 64).

The effect of heating during wear testing has been studied (65, 66). Moore (66) considered that observed temperature rises of 300-900^{o}C could significantly affect surface structure and influence rates of diffusion of oxygen and nitrogen into the surface. Further work was said to be needed to determine whether frictional heating was an important factor in abrasive wear mechanisms.

2.5 Assessment of abrasion resistance.

The mechanisms by which abrasive wear occurs are complex and are difficult to describe accurately. Consequently any assessment of abrasive wear in terms of obtaining useful data as a basis for service life predictions is equally as difficult. The development of wear testing procedures is well recognised as a tedious process and it is generally accepted that a universal wear testing machine is unlikely to be developed (10). Workers in the field have concentrated their efforts in developing tests in which one of the three accepted abrasion forms i.e. gouging, high stress and erosion predominates. Whichever form of wear is studied there are certain basic criteria which need to be borne in mind if the test is to be successful and the results of value in predicting service performance.

2.5.1 Requirements of an abrasion test.

The requirements of a useful abrasion test and the problem of interpretation of the results have been discussed by a number of review papers (4, 9, 10, 14, 67-69). Avery (10) recommended that any test should satisfy the following:

(a) It should have proven reliability or reproducibility. This should be expressed in quantitative terms and be used in judging how far the test evidence may be trusted when comparing materials.

(b) It should have a proven ability to rank various materials. If the range of values obtained on a variety of materials is too small even if reproducibility is good it will be difficult to predict service behaviour.

(c) It should be validated by correlation with service tests.

The latter condition of validation is the most difficult to achieve since a test must either simulate accurately the conditions encountered in service or if the test is simplified it should represent the same basic mechanism of abrasion as that in service. In addition the opportunity must exist to allow correlation of the test results with those obtained in controlled service trials. Even then few service trials include sufficient replication to enable reliability and experimental error to be calculated.

The assessment of abrasion resistance on site under actual conditions of service is limited in that tests must be performed whilst causing the minimum distruption to production. This will naturally tend to restrict the type and number of variables that can be studied in any one situation. In addition a technician is required on site to record the wear data. Hence the majority of tests developed are laboratory tests where there is more choice and control over the conditions of study.

A further problem confronting the investigator is that of duration of testing since results are usually required after a relatively short time of testing. To achieve this the severity of the test must be increased and this may impair its ability to be selective in terms of assessing competitive materials. Acceleration of testing could also cause excessive rises in temperature at the wearing face which could influence relative abrasion resistance of materials.

To overcome the above difficulties so that abrasion resistant materials can be compared or tested to judge suitability for use in particular applications a variety of wear testing rigs has been developed. The nature of these tests and their success in predicting service behaviour and in allowing a better understanding of wear processes is reviewed in the following sections.

2.5.2 Assessment of resistance to gouging wear.

Gouging, where lumps of abrasive material cut into a surface under force, is a difficult mechanism to simulate on a small scale (16). Borik (69) suggested that small jaw crushers can be modified to rank materials for gouging abrasion applications, while Avery (70) claimed that a fixed abrasive grinding wheel test using a brake shoe type specimen could simulate gouging. The use of a fixed abrasive however differs from what is experienced in service since it is argued

that the matrix is differentially worn by loose abrasives. It has also been suggested (16) that bonding of fixed abrasives can be variable and that this might influence the accuracy of the test. A further criticism is that the grinding wheel test does not involve impact loading that so frequently occurs in service. Avery recognised these deficiencies and concluded (10) that the grinding wheel test had good reproducibility and ranking ability but the service conditions with which it could be correlated could not be accurately defined. The test has shown some correlation with crusher service but this was not as close as desired (25). This may be due to the high hardness of the alundum wheel used for the test since this is harder than the materials usually encountered in service. Special wheels made from bonded quartz having a lower more appropriate hardness have not proved sucessful (25). Results obtained using an alundum wheel are shown in figure 2.10. Austenitic high chromium irons and martensitic irons are seen to have lower rates of wear than austenitic manganese steel whereas the steel is most likely to be selected for a gouging application because of its superior toughness.

Borik has used a jaw crusher as a gouging wear test in which a stationary test plate is paired with a moveable plate made of a reference material. The jaw plates are set to a standard opening and are used to crush a known amount of siliceous rock of a standard size range. The results are expressed as a wear ratio by dividing the weight loss of the

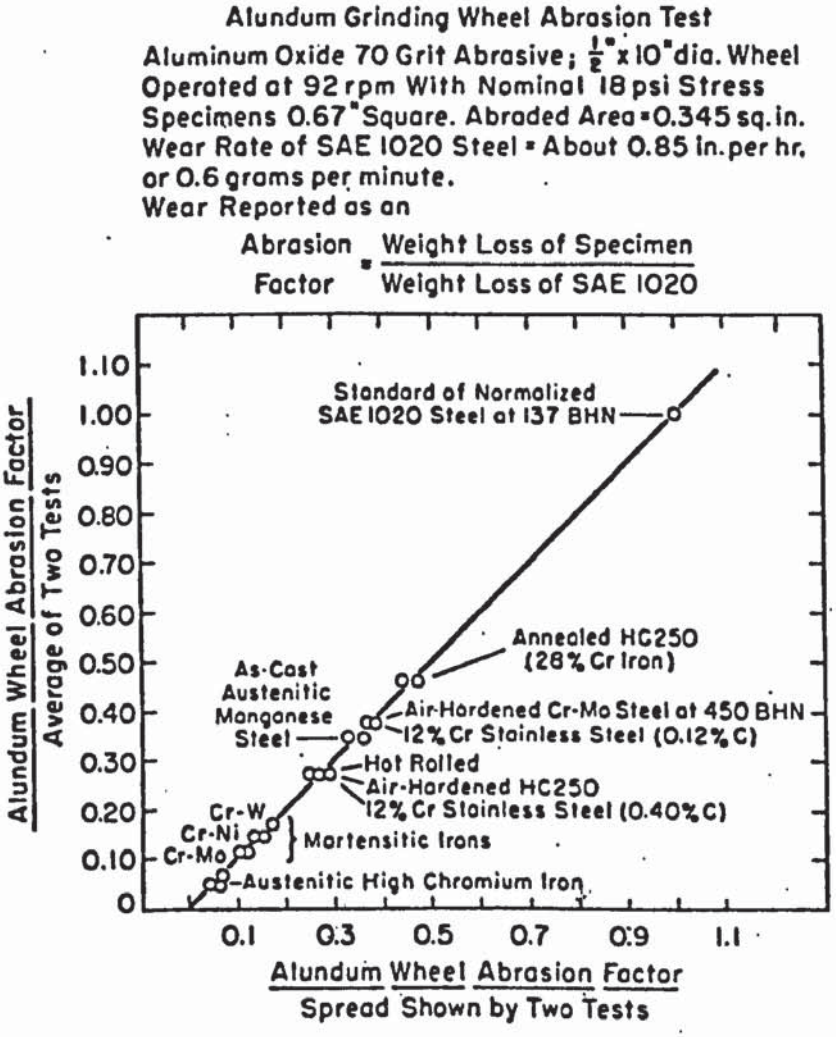

Figure 2.10

Results from Alundum wheel test.

After Avery (10)

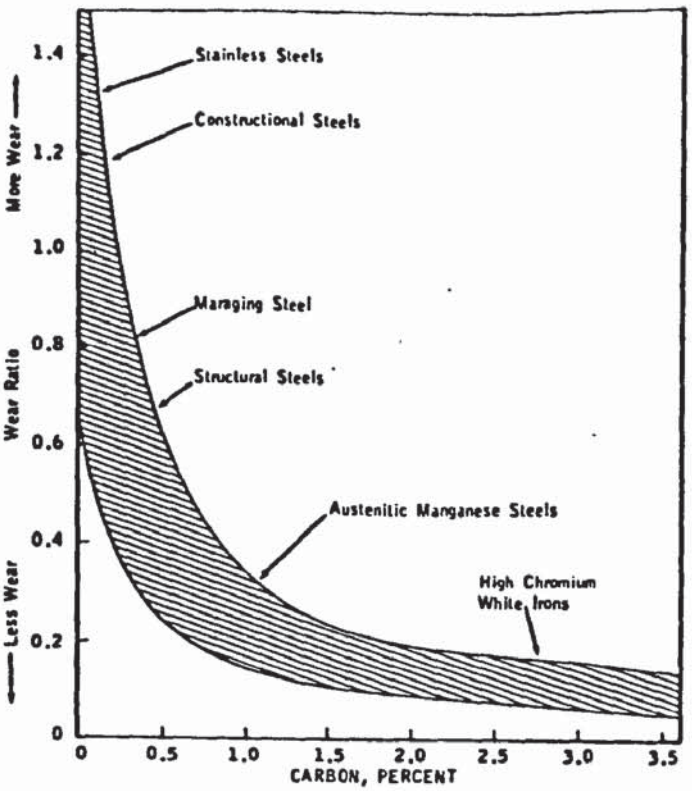

Figure 2.11

Relationship between the gouging wear ratio and the carbon content of various ferrous materials.

After Borik et Al (69,71)

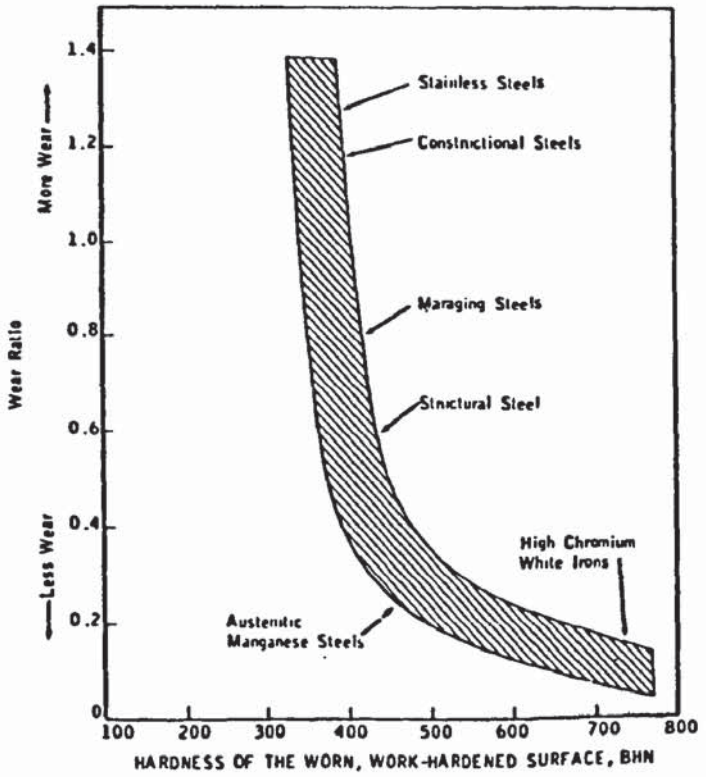

Figure 2.12

Gouging wear ratio plotted versus work hardened surface hardness of various ferrous materials.

After Borik et Al(69,71)

fixed test plate by that of the reference plate. The test is claimed to give reproducible results enabling small differences in gouging wear resistance of materials to be detected. Typical results are given in figures 2.11 and 2.12.

Figure 2.11 shows how as carbon content increases then gouging wear resistance is improved. At lower carbon levels the improvement is due to the influence of carbon on martensite hardness and at higher carbon levels it is due to increased amounts of hard carbides in the structure. Borik (69, 71) relates the spread in the vertical direction to matrix structure, alloys with martensitic structures being close to the lower boundary and those with austenitic structure lie nearer the upper boundary. Figure 2.12 shows a clear relationship between wear resistance and the hardness of the worn work hardened surface layer especially at values over 400 H_B, similar relationships have been found in high stress abrasion tests.

2.5.3 Assessment of resistance to high stress abrasion

The high rates of metal loss from mill liners and grinding media during the grinding of ores, cement and other materials have given rise to increasing development of materials to resist high stress abrasive wear. Such wear results from scratching, local plastic flow and microcracking of surfaces as they grind entrapped abrasive grains.

A large number of testing procedures has been suggested over the years as suitable means of assessing the materials developed. Some involve the study of marked balls in production mills while others involve simulative laboratory tests.

A number of investigators (7, 69, 73-77) have used marked ball tests and although much of the resultant data is from short time tests it is claimed (7) that these give excellent correlation with large scale tests over prolonged time periods. Typical relative wear rates that have been determined in this way are given in table 2.3. Since these values were obtained using oversize (125 mm dia) balls it is said (7) that they can be used to evaluate liner materials since the larger balls have cast structures similar to those of liner plates, which have coarser structures than the usual 75 mm dia. balls. Reproducibility is claimed to be good since in a set of five identical balls the abrasion factor had a range of 2% of the mean.

The use of short time tests and their correlation with long term consumption is discussed by Farge (73). For smaller diameter balls there was good agreement between short and long term results but for larger balls differences could arise due to core effects particularly in forged balls. The so called short time tests require several weeks to complete hence in alloy development the use of much quicker laboratory tests must be considered.

Alloy	Hardness R_c	Relative wear rate
15%Cr-3%Mo cast iron	66	89
27%Cr cast iron	64	98
Martensitic 1%C,Cr-Mo steel	55	100(std)
Martensitic Ni-Cr-Mo iron	59	107
Martensitic .7%C,Cr-Mo steel	58	111
Martensitic Ni-Cr iron	55	116
Martensitic .4%C,Cr-Mo steel	55	120
Pearlitic .8%C,Cr-Mo steel	39	127
Austenitic Mn steel	49	138
Pearlitic low Cr iron	48	195

Hardness values on worn surfaces after service in mill

Table 2.3

Relative wear rates of cast materials for mill liners grinding siliceous ore.After Norman (7)

Material	Condition	H_v	Wear resistance relative to Armco iron		
			SiC 180grit	SiC 60grit	corundum 180grit
White iron	Chill cast,stress relieved at 400°C	676	2.26	2.08	2.33
Ni-hard	Chill cast, 8h at 275°C	710	2.33	-	2.31
Ni-hard	Chill cast, 4h at 450°C, 8h at 275°C.	750	-	-	2.06
SG iron	Normalised	325	-	-	1.50
Stellite	As cast plate	630	1.97	1.67	2.60
Delfer	"	630	2.81	2.43	3.09
Delcrome	"	613	2.60	2.20	3.23

Table 2.4

Relative wear rates of cast materials on SiC and corundum. After Richardson (18)

Two main types of laboratory tests have been developed. One type involves the wearing of pin specimens under load on abrasive cloths (11, 13, 16, 17) and the other involves the sliding of a specimen over a circular wear track while the specimen and track are immersed in dry loose abrasive (14) or in abrasive slurry (4, 10, 23).

Kruschov (11) and Richardson (18) constructed similar tests in the form of a rotating disc abrasive paper on which two special tracks were used. A standard control material was run on one track and a test material on the other. Richardson improved the technique of Kruschov by modification of the loading arrangements to eliminate loading variables. A wide range of pure metals and alloys was tested against a range of abrasive papers such as silicon carbides, corundum and flint. Wear resistance was quoted as a wear ratio in relation to a standard Armco iron pin. Experimental error was reported as $\pm$ 3% for hard abrasive and $\pm$ 10-12% for softer abrasives (18). Typical wear ratios are shown plotted against initial bulk material hardness in figure 2.13. These results show that the proportionate relation of hardness to relative wear resistance is only approximate and varies from one material to another. Final hardness after testing would give better correlation to account for work hardening of materials during testing. The significance of Richardsons results is discussed in detail elsewhere (25) but the following comments illustrate the major points.

(a) Heterogeneous alloys such as steels, white and alloyed irons and hardfacing alloys give lower values of relative wear resistance when tested on silicon carbide than when tested on corundum (Table 2.4). The reduction was marked in the hardfacing alloys which contain hard alloy carbides and was less obvious in the white iron and Ni-Hard which contain softer M_3C type carbides.

(b) These alloys were sensitive to grit size. Even when the abrasive was considerably harder than the unstrained carbides they become less effective as the relative sizes of the scratches increase, i.e. wear resistance decreases as the scale of deformation gets larger compared to size of carbides.

(c) Richardson concluded that it was not clear whether carbides can work harden. They are said to flow plastically at work surfaces.

Richardson (78) claims good correlation between results from his tests and those from field tests obtained during ploughing.

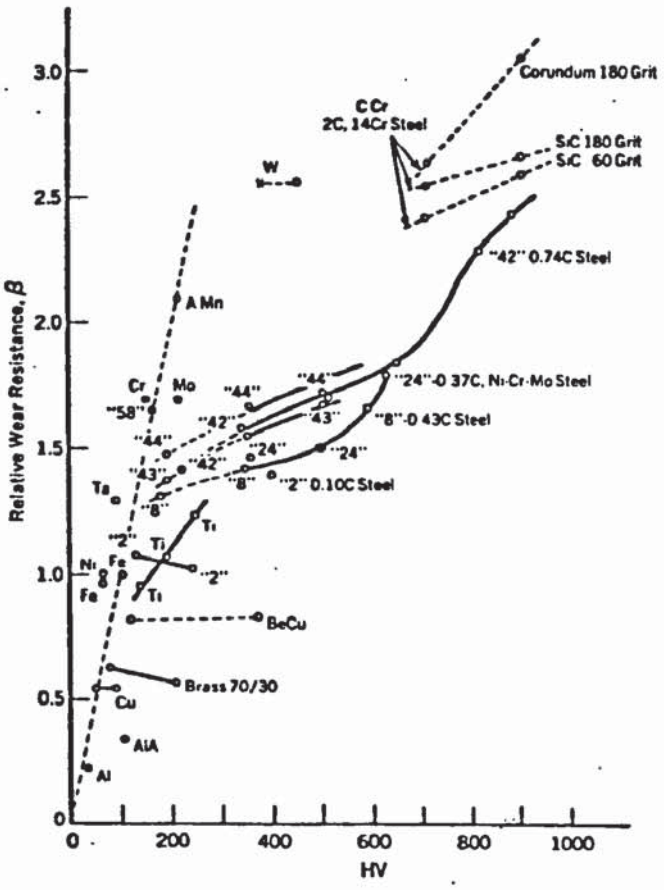

Figure 2.13

The relative wear resistance of metals abraded on 180 grit corundum cloth versus initial bulk hardness. After Richardson (18)

Muscara and Sinnot (13) outline the operation of a test apparatus based on a converted milling machine which is claimed to give high reproducibility of wear data. This uses a pin specimen (6 mm in dia) which is made to rotate as it travels against fresh abrasive cloth. Specimen rotation avoids unidirectional abrasion which is said to produce abnormal wear scars as abrasives tend to follow pre existing scratches. Alumina was the abrasive most suited to testing ferrous alloys and the test ranked the alloys in a similar order to field testing in an ore grinding mill. Examples of these results are given in table 2.5.

Avery (23) suggested that the above test was not a true high stress abrasion test since the abrasive is cushioned on one side by a mounting cloth and the abrasive is not ground between two metal surfaces. The test was said to accentuate cutting wear and minimise deformation wear whereas both these forms are important in grinding.

The second type of test involving the running of a specimen in loose abrasive against a metal wear track gives three body abrasion associated with sufficient force to fragment the abrasive particles. This combines varying proportions of deformation and cutting wear. The use and results from this type of test have been the subject of a number of papers (4, 10, 23, 70). Since grinding is normally carried out wet Avery (4) used a slurry of quartz

Abrasion-Resistant Irons and Steels

Designation	Type of Alloy	Composition							Heat Treatment	Hardness on* Worn Ball Surface, Rc	Wear Ratio†
		C	Mn	Si	Cr	Mo	Ni	V			
A	Martensitic high-chromium white iron	3.0	0.68	0.44	19.71	1.39	0.67	–	1750°F/5 hr, Air-cooled; 400°F/4 hr	66.2	90
B	Cr-Mo Steel	0.88	0.42	0.53	6.61	1.13	–	–	1875°F/3 hr, Air-cooled; 450°F/4 hr	63.0	100
C	2Si-1Mo Steel	0.24	0.68	1.90	–	0.92	–	0.086	1700°F/2 hr, 1540°F/1 hr, Water-Quenched; 400°F/4 + 4	44.6	148
F	Ni-Cr White Iron	3.4	0.5	0.5	2.1	–	4.2	–	As-cast; Tempered 450°F	61.9	108
G	Pearlitic Cr-Mo Steel	0.8	0.7	0.5	2.1	0.3	–	–	Air-quenched and tempered	40.8	120
I	Austenitic Manganese Steel	1.1	13.0	0.7	–	–	–	–	1900°F; Water-quenched	51.0	136

*Rockwell C hardness on surface of ball after being tested in an ore grinding mill.
†Wear ratio determined from ball mill test data using Alloy B as a standard.

Mean Weight Losses and Ranking of Tested Alloys

Alloy	Mean Weight Loss, g			Ranking*		
	105μ, 7 lb.	80μ, 15 lb.	Ball Mill	105μ, 7 lb.	80μ, 15 lb.	Ball Mill
A	0.02964	0.04823	404	2	1	1
B	0.03792	0.06876	445	3	3	2
C	0.05568	0.10296	634	5	5	5
F	0.02946	0.05154	486	1	2	3
I	0.04588	0.08214	605	4	4	4

*The alloys are ranked 1 through 5; number 1 is the most abrasive resistant, number 5 is the least.

Table 2.5

Wear data obtained by Muscara et Al (13) in laboratory tests and in ball mill trials.

sand in water to wear specimens 40 x 40 x60 mm in size at speeds of 0.6 m/sec. under compressive stresses of 0.4 N/mm^2. Two specimens are tested together, one of which is a standard of annealed steel. Wear damage is given in terms of comparative weight loss and is expressed as a wet sand abrasive factor. A run in period is used prior to weighing to obviate errors due to irregularities in specimen and track surface contours. This test is claimed to be reliable and reproducible and has been validated by ball mill tests (4, 10). Figure 2.14 shows how the wet sand abrasion factor compares with wear rates obtained in marked ball tests in production mills. The two tests appear to rank materials in a similar order but their relationship is not simple since service in a mill involves impact conditions which are absent from the laboratory test.

Boyes (14) in a study of abrasion by sand which occurs in foundry equipment, investigated various methods of producing wear in laboratory tests. The highest wear rates were obtained when the sand was crushed using a rolling or sliding action. The use of weighted rollers was not developed since the sand abrasive was rapidly broken down and larger amounts of fresh sand would be required. Boyes used a sliding test similar to that of Avery and used Erith silica sand as an abrasive against an annealed mild steel wear track. Typical results from this test are given in figure 2.15 showing relative performance of various irons and steel.

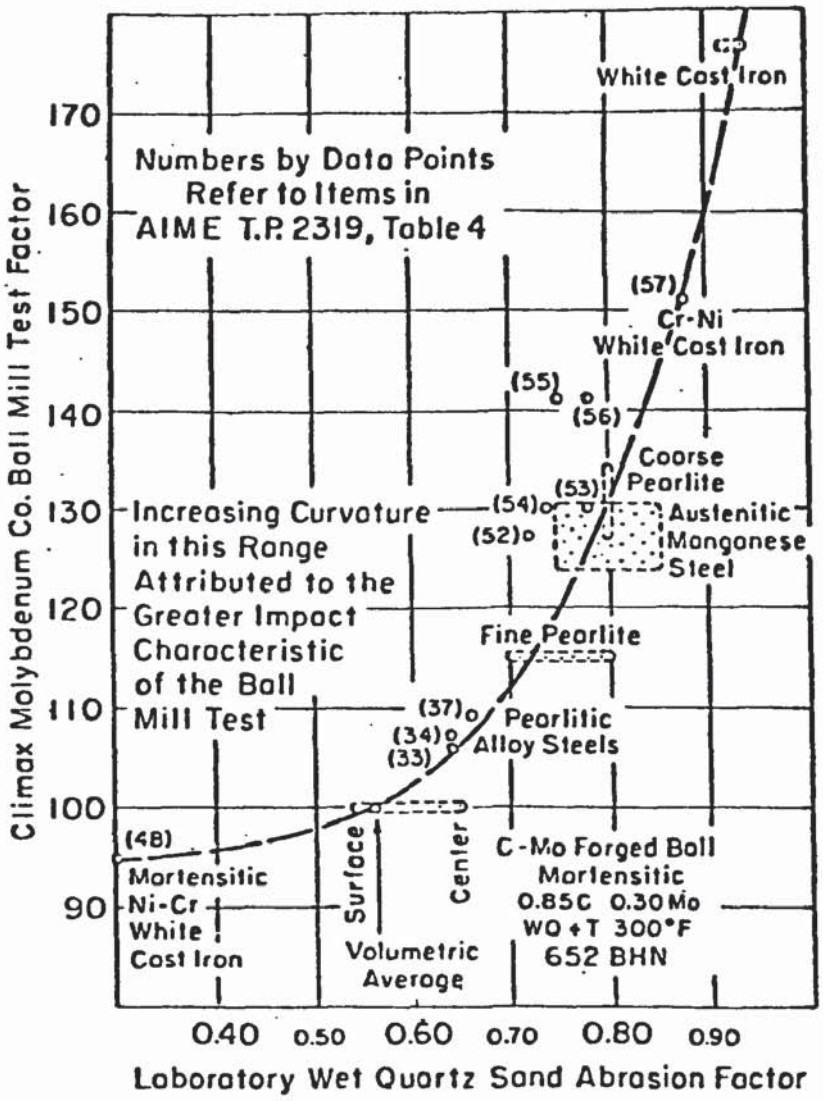

Figure 2.14

Comparative performance of various alloys under high stress abrasion conditions.

After Avery (10)

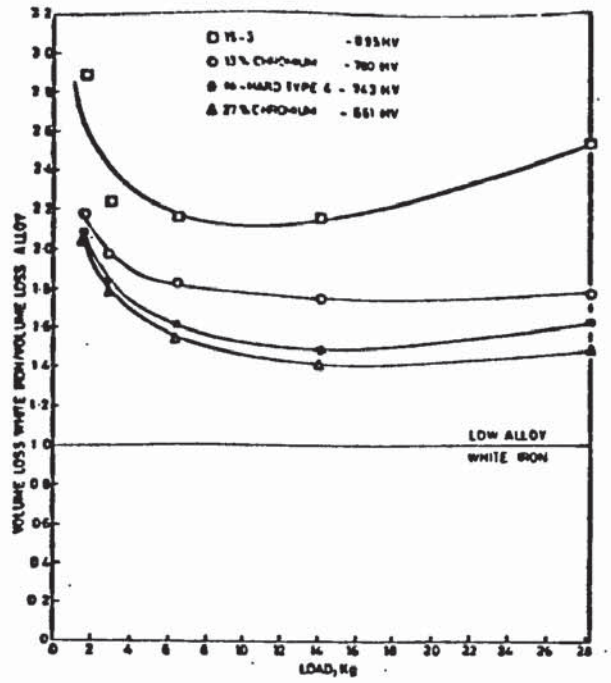

Figure 2.15
Relative wear performance of high Cr irons.
After Boyes (14)

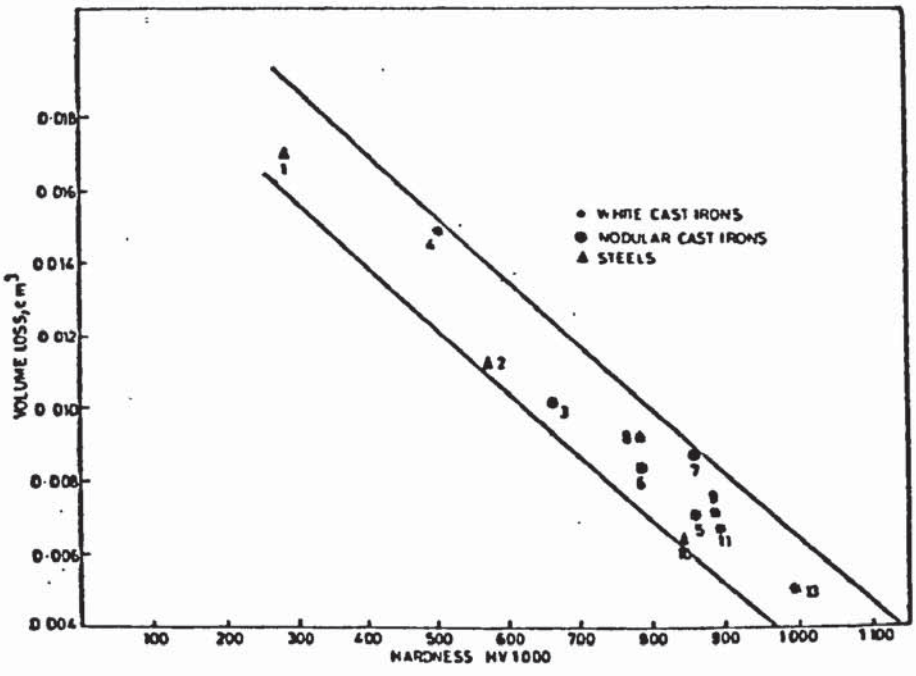

figure 2.16
Relationship between hardness after strain hardening and volume loss at low testing load.
After Boyes (14)

Reproducibility was calculated at ± 5% at high loads and ± 14% at small loads. Boyes confirmed the findings of other workers in that abrasion resistance can be related to surface hardness after testing. This is shown in figure 2.16. Boyes (14) did not give a detailed discussion on the relationship between his wear results and the structure of the alloys and did not relate his test to any field results. He observed that the surface deformation as seen during microscopic examination did not differ significantly with testing load. The deformation was said to be similar to that observed in plough share test specimens and grinding mill balls although it was not as severe as in the latter.

In a recent study of high manganese cast iron Lambert (79) reports wear test results obtained on a machine consisting of a shaft turning inside a loaded split bearing. The abrasive of 30 μm mill scale was introduced via the lubricant. The test is said to show the superiority of high manganese cast iron over Hadfield steel under these conditions. This was related to increased work hardening during service.

2.5.4. Assessment of resistance to low stress abrasion

Abrasive wear in which the stresses imposed on the abrasive particles do not exceed their crushing strength is known as low stress or scratching abrasion or erosion.

Three main types of testing procedures have been developed for its study.

(a) Bowl grinding tests which rotate pin type specimens in a bowl containing loose dry abrasive or slurry. (8, 16, 72, 80).

(b) Pneumatic devices using a blast nozzle to direct abrasives at rotating specimens (15, 69).

(c) Rubber wheel tests in which a revolving rubber wheel is used to carry wet or dry abrasive against the wear face of a stationary specimen. This is the most popular of these three types and its use is widely reported (10, 15, 69, 81, 82).

Two other tests of interest have been used by Lui (50) and Shabuev (83). The test described in (50) was developed to study the effects of corrosion during abrasion. It is a variation of the bowl grinding machine but instead of pin specimens it uses thin disc specimens rotated at high speed in slurry. The other test (83) is a variation of the rubber wheel test in that it uses rubber counter specimens to slide relative to metal specimens immersed in abrasive slurries. The results of this test are to be discussed

later since the irons tested had carbon and chromium contents of similar levels to those of the present work.

The rubber wheel test is the best recognised of the above tests to produce reproducible erosion wear data. Its development is outlined by Borik (81) and its application to practical situations by Stolk (82). The range of materials tested is wide since the factor between the best and worst reported erosion resistance is about 1500. (see figure 2.17). The results of rubber wheel tests are said to correlate with those from bowl grinding (69) and soil tilling tests (82).

Further results from bowl grinding are shown in table 2.6. This test rotated 50 mm x 10 mm dia pins at 700 rpm in a 1.1 mixture of water and graded silica sand. Values are given relative to a mild steel standard. (72).

Pneumatic tests have been less popular in erosion studies and the ranking of materials in sand blast type tests does not agree with that from the rubber wheel test (15). This is because the pressures involved give conditions approaching high stress abrasion in that some break down of the abrasive occurs. The results of tests on shot blast blade materials are given in table 2.7.

SAND SLURRY ABRASION TEST RESULTS

Material	Condition	Hardness, Rc	Relative Abrasion Resistance
5% Cr–1% Mo–1% C steel	½h – 1760 F (960 C) AC	59	2.50
	½h – 1870 F (1020 C) AC	64	2.34
4% Ni–2% Cr–2.8% C	As Cast	51	3.44
	24h – 525 F (275 C) AC	54.5	3.32
	2h – 1560 F (850 C) AC	59.5	3.12
12% Cr–0.5% Mo–2.5% C	As Cast	46	2.12
	1h – 1920 F (1050 C) AC	59.5	5.31
15% Cr–2% Mo–3% C	As Cast	54	3.47
	1h – 1920 F (1050 C) AC	62	7.77
27% Cr–2.9% C	As Cast	56	3.46
	1h – 2010 F (1100 C) AC	59.5	8.26

Table 2.6

Sand slurry abrasion test results.

After(84)

WEAR TEST RESULTS FOR SHOT-CLEANING BLADE MATERIALS

Material	Condition	Hardness, Rc	Life, h
15% Cr–2% Mo–3.5% C	Oil quenched and tempered	61-65	283
16% Cr–3% Ni–2.5% C	As Cast	48-54	39
	Oil quenched and tempered	58-63	92
25% Cr–2% C	As Cast	49-50	37
	Oil quenched and tempered	62-65	90
Alloy cast iron*	As Cast	48-51	18
	Oil quenched and tempered	49-52	40
3.5% Cr–0.2% Ni–2.5% C	As Cast	49-50	5
	Oil quenched and tempered	58-63	7
12% Mn–1% C	Water quenched	Rb-180	14

*1.3% Cr–1.7% Mo–0.3% Ni–1% V–0.6% Ti–1.8% C

Table 2.7

Life of shot cleaning blades.

After (84)

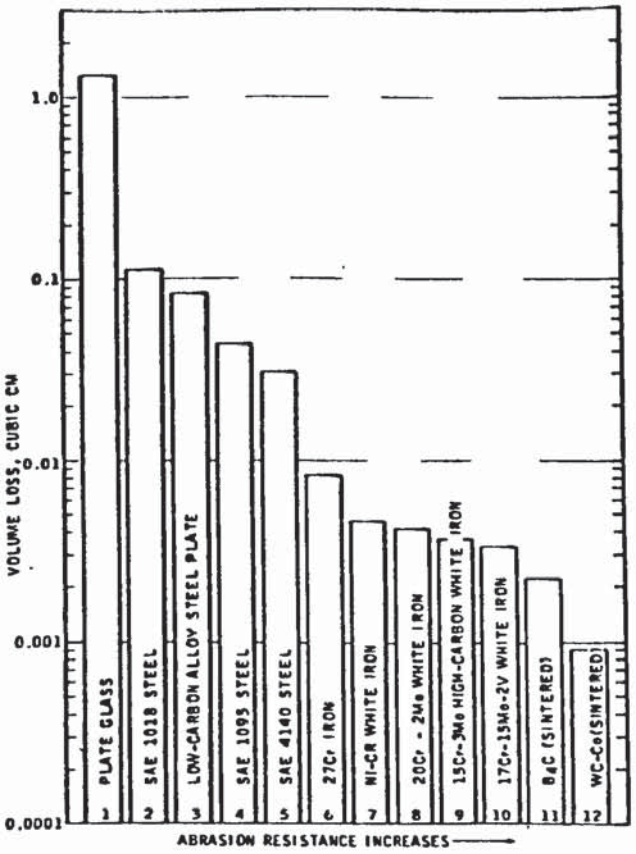

Figure 2.17

Abrasion resistance of various materials as determined by the rubber wheel abrasion test.

After Borik (81)

2.5.5. Summary of abrasion testing.

From the preceeding discussion it is seen that by means of relatively basic procedures the wear resistance of different materials can be sufficiently evaluated to produce data relatively quickly and probably at reasonable cost. This data can be reported in a number of ways. Most investigators appear to favour the use of wear ratios where wear of a material under test is related to wear of a standard material. It must be remembered however, that such wear ratios can only be used to compare materials when the conditions of abrasion are constant. A less popular approach is to calculate abrasion damage in terms of depth of metal removed per unit of time. This requires measurement of density, area and time as well as weight loss and it is questionable what the calculated values could relate to in terms of service performance.

In designing a test, attention must be given to the type of abrasive used since harder abrasives wear more rapidly giving less spread in results for a given material but they may also be less selective between different materials. Quartz sand has been used for many of the tests described above because it is commonly encountered in practical situations e.g. in rocks, in mineral gangue, in soils and as contaminant in cooling waters. It is cheap and readily available in a consistent form as standard sands.

The above tests do not include tensile and bending stresses and the impact conditions encountered in many service applications. Hence as well as wear test data additional information on mechanical properties is necessary in selecting materials for a given use in order to minimise premature replacement due to fracture.

Abrasion tests can be concluded to have two main values. The first of which is that they can grade with reasonable accuracy and reproducibility available abrasion resistant materials. The most promising of these can then be evaluated in service trials. The second value is that the damage produced in an abrasion test can be studied to aid in understanding wear mechanisms. For example the degree of surface deformation, the extent of microcracking and the amount of work hardening can be observed and measured. These features can also be compared to those in components which have been in service. Laboratory tests may enable various stages of wear to be examined and this is often not possible in service testing since the effects of initial mechanisms are removed as cumulative damage proceeds.

3.0 DEVELOPMENT AND PERFORMANCE OF ABRASION RESISTANT ALLOY WHITE IRONS.

A wide range of cast irons, steels and other materials such as ceramics and rubbers have been developed to withstand abrasive wear. The basic characteristics of these materials have been reviewed by the author in an earlier report (85). The present review considers the production, structural characteristics and behaviour of alloy white irons particularly those containing 10-35% chromium. These irons rely on the presence of hard carbides within their microstructures for wear resistance and during their solidification the formation of soft grey iron structures must be avoided. The addition of carbide stabilising elements such as chromium promotes the white iron eutectic reaction and enables graphite free structures to be obtained in useful section sizes.

3.1 Addition of chromium to cast irons

Small additions of up to 3% chromium are made to improve the strength, hardness and wear and heat resistance of ordinary grey and white irons (86). The effect of chromium on chill and mottle formation in these irons has been reviewed by Boyes (87, 88). Additions of 2-2.5% chromium can be made to rolls and to produce white iron castings for low duty abrasion resistance (61, 86, 89). Martensitic white irons contain 1-3% chromium to offset the graphitising

effects of nickel additions which are needed for hardenability. (86).

Small additions of chromium to white irons as in the nickel containing martensitic types (Ni-Hards) do not alter the form of the eutectic carbides which tend to form as a continuous network in the eutectic structure. Larger additions of 8% chromium give a discontinuous carbide structure in the martensitic Ni-Hards thus improving toughness (44). The development of these compositions has been reviewed by Durman (90) who also outlines the reasons for using chromium contents of 10-35% in white irons. At these higher chromium levels the eutectic carbides become harder and less continuous increasing toughness. According to chromium content, other alloy additions e.g. molybdenum, section size and heat treatments these high chromium irons can be made austenitic, martensitic, ferritic or pearlitic to suit given applications or machining requirements.

3.2 The iron-chromium-carbon system

Early studies of this system by Tofaute (91), by Bungardt (92) and by Griffing (93) have been reviewed by Boyes (60) and by Jackson (94). Jackson suggested that much of the earlier work was limited in accurancy due to use od impure materials and measurement difficulties at the high temperatures involved. He re-investigated the austenite

liquidus surface and has combined his results with those of Griffing and other workers to produce a revised ternary constitutional diagram. The three dimensional space model of this diagram is shown in figure 3.1. This plots the relative positions of the invariant planes which are shown in plan form in figure 3.2. These figures show that the system contains the following peritectic reactions:

$$L + M_{23}C_6 \longrightarrow \alpha + M_7C_3 \quad \text{at} \quad 1449^{\circ}C$$

$$L + \alpha \longrightarrow \gamma + M_7C_3 \quad \text{at} \quad 1292^{\circ}C$$

$$L + M_7C_3 \longrightarrow \gamma + M_3C \quad \text{at} \quad 1184^{\circ}C$$

Also the following peritectoid reaction occurs:

$$\gamma + M_7C_3 \longrightarrow \alpha + M_3C \quad \text{at} \quad 795^{\circ}C$$

The primary phases which form were plotted by Jackson and are seen in figure 3.3. A recent study (95) of the phase relationships at 870°C has confirmed earlier findings (96, 97) that the only carbides present in the system are M_3C, M_7C_3 and $M_{23}C_6$.

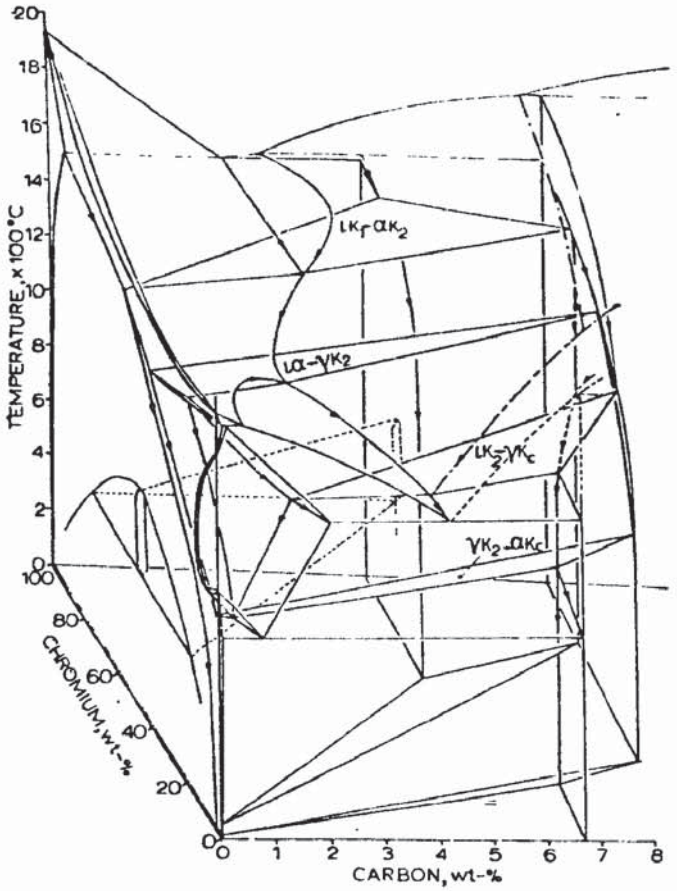

$K_1=(Cr,Fe)_{23}C_6$, $K_2=(Cr,Fe)_7C_3$, $K_c=(Fe,Cr)_3C$

Figure 3.1

The Fe-Cr-C system:three dimensional model.
After Jackson (94)

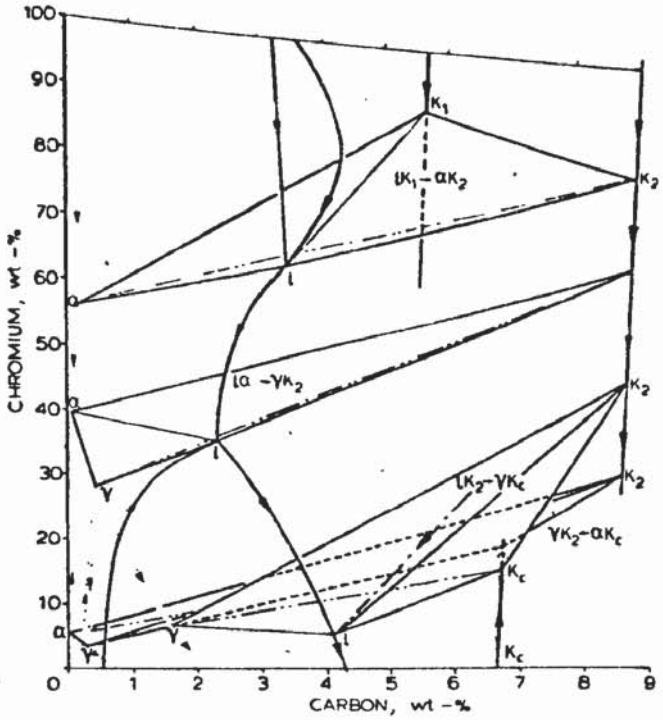

Figure 3.2

Plan of invariant planes in Fe-Cr-C system.

After Jackson(94)

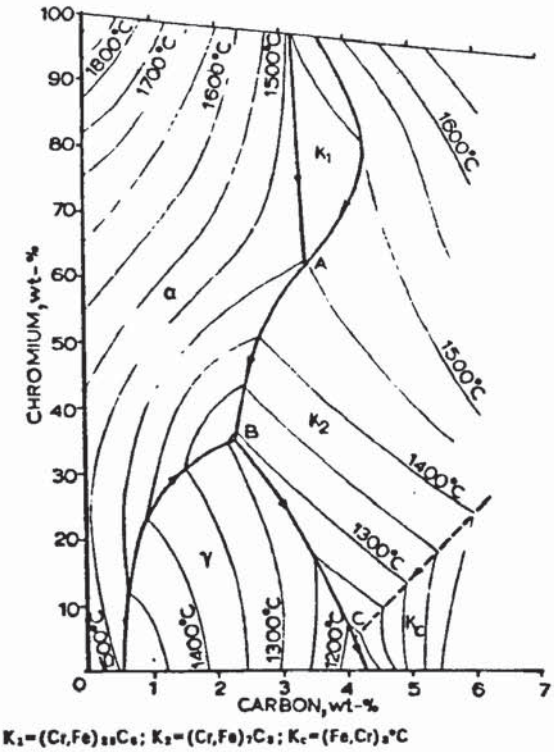

$K_1=(Cr,Fe)_{23}C_6$; $K_2=(Cr,Fe)_7C_3$; $K_c=(Fe,Cr)_3C$

Figure 3.3

Liquidus surface in Fe-Cr-C system.

After Jackson(94)

3.3 Solidification of unalloyed and alloyed white irons

3.3.1 Eutectic structures in the iron-cementite system

The solidification behaviour of the white iron eutectic has been studied by a number of authors (98-103). Use of quenching and thermal analysis techniques has shown that this eutectic solidifies by progressive growth of columnar forms from the edge to the centre of a casting section. The delineation of eutectic cells in white irons is difficult, it is not clear whether a austenite-cementite eutectic cell consists of one or more columnar forms or crystals (98).

Merchant (99) recognised that cementite in the eutectic has a tendency to form flat faces and suggested that the eutectic was nucleated by cluster formation of cementite plates . Hillert & Steinhauser (100) proposed a model for subsequent growth which is shown in figure 3.4. This suggests sidewise and edgewise mode of eutectic growth on a cementite plate. Sections cut perpendicular or parallel to the sidewise growth direction of the eutectic give either globular or rodlike structure known commonly as the ledeburite eutectic. Williams (101) noted that the ledeburite structure was usually associated with the columnar type eutectic structure whereas another microstructural form which he called platelike was associated with a equiaxed

type structure. Rickard and Hughes (102) investigated these two forms and proposed models for each. These are shown in figure 3.5. The ledeburite eutectic, which is the more usual form, solidified with only moderate undercooling below the equilibrium white iron eutectic temperature and was usually nucleated at the mould face. The platelike form however, required more undercooling and was nucleated at numerous points within the melt producing equiaxed eutectic cells. In both structures the nucleating phase was found to be cementite in plate form. The ledeburite eutectic developed by sidewise growth of austenite and cementite in a manner similar to that proposed earlier (100). When this sidewise growth was replaced by the growth of additional plates separated by austenite the platelike eutectic resulted. In the ledeburite eutectic it was suggested (102) that growing crystals could change direction by the formation of fresh plates at the growing tip giving rise to an interlocking cluster of crystals which should be considered as a eutectic cell. The formation of the platelike structure was said to be due to the development of serrations on the initial carbide plates into other plates with areas of austenite in between them with much of the eutectic austenite forming on original austenite dendrites. Such a mechanism may be significant in the formation of platelike eutectic structures in alloy irons, in that chromium may modify the undercooling required to form the platelike structure.

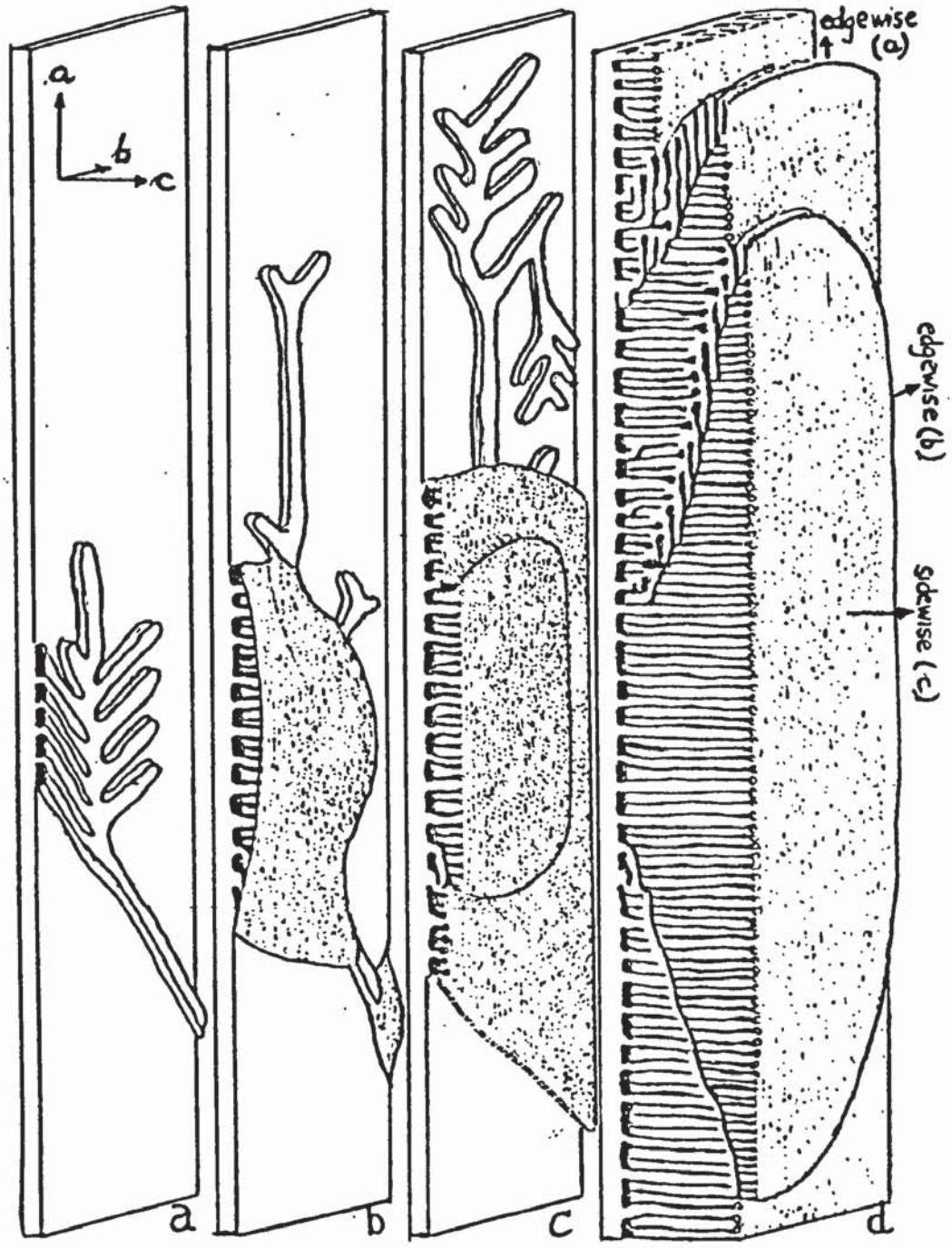

Figure 3.4

Sidewise and edgewise mode of development of ledeburite eutectic on cementite plate in white iron.

After Hillert et Al (100)

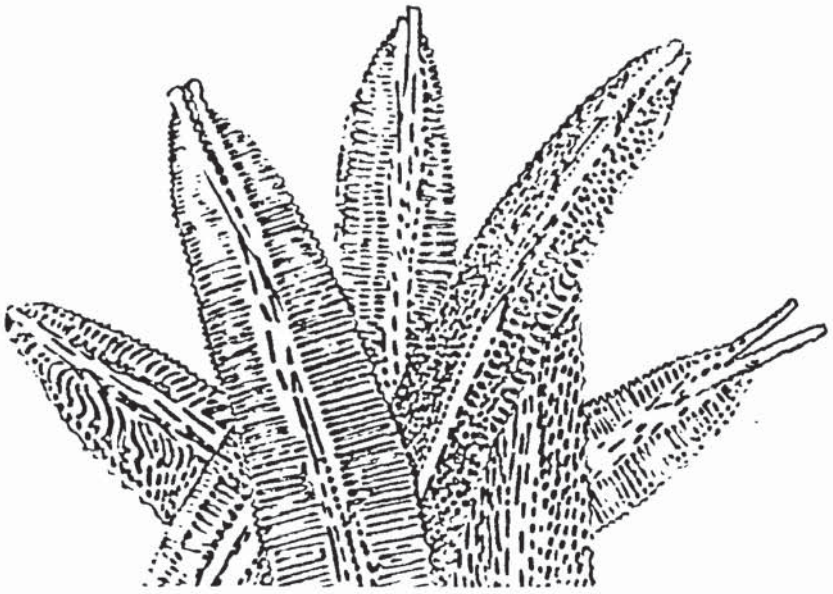

(a)Model of ledeburite eutectic.

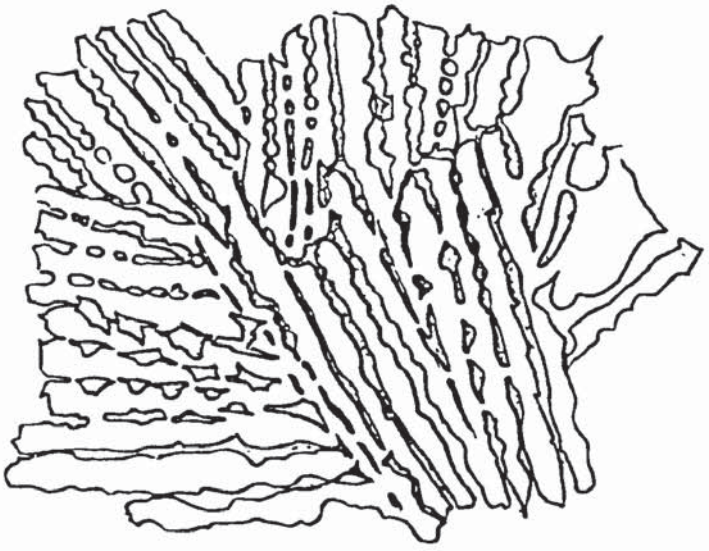

(b)Model of platelike eutectic.

Figure 3.5
Eutectic models in white iron. After (102)

3.3.2 Eutectic structures in chromium cast irons.

Durman (90) states that above about 12% chromium the eutectic carbides in chromium cast irons are discontinuous in nature due to the formation of M_7C_3 type carbides instead of the M_3C type. Durman (1) and Maratray (104, 105) have also recognised that the actual morphology of the M_7C_3 eutectic carbides depends on the composition of an iron relative to the eutectic trough (see figure 3.3). In hypoeutectic alloys the eutectic carbide solidifies in the spaces between primary austenite dendrites and the form of the carbide depends on the size of these available spaces. When the austenite leaves only a small volume to solidify as eutectic, the carbides form in between the dendrite arms. As the amount of eutectic solidifying increases i.e. as the amount of eutectic carbide increases to between 20-30% then the eutectic takes the form of clusters containing lamellae of carbide radiating from centres located in the interdendritic spaces. The eutectic structure becomes completely lamellar when above about 30% carbide is present and the primary austenite no longer interfers with the eutectic formation. In hypereutectic alloys with carbide contents of over 35% large hexagonal primary M_7C_3 carbides replace the primary austenite and are distributed in a matrix containing lamellar M_7C_3 eutectic carbides (106).

In lower chromium irons a discontinuous type of M_3C carbide forms peritectically (94, 106). This is illustrated by the example of a 6% Cr iron which contains discontinuous M_7C_3 carbides and peritectic M_3C carbides, Jackson explains that this structure is the basis for eutectic Ni-Hard with improved toughness (107).

From results of carbide counts in a range of irons Maratray (104, 105) suggests that the formula

$$\% \text{ carbides} = 12.33\ (\%C) + 0.55\ (\%Cr) - 15.2$$

can be used to estimate carbide content in the microstructure. High chromium irons often contain small amounts of molybdenum to improve heat treatment response. Molybdenum gives rise to small patches of Mo_2C eutectic carbide which can be revealed by selective etching.

3.3.3 Distribution of chromium and molybdenum between carbide and matrix.

Preliminary work (108) on irons with chromium contents of 2.5 to 9.5% showed that the carbide phase contained between 3 to 4 times more chromium than the matrix. The chromium content of the carbide can vary from 30% in alloys with a low Cr:C ratio (3.5) to about 60% in alloys with a high Cr:C ratio (>8) (104, 107). The chromium content of the matrix

increases linearly with Cr:C ratio (104, 105). At Cr:C ratios of around 3 the chromium content of the carbide corresponds to $(Cr_2 Fe_5) C_3$ and at ratios exceeding 8 the corresponding carbide formula is $(Cr_5 Fe_2) C_3$. The extent of substitution of chromium for iron decreases as the Cr:C ratio increases. This is shown in figure 3.6. Replacement of iron by chromium in M_7C_3 is believed to be on a random basis (105). The M_7C_3 carbides also contain molybdenum when this is present as an additional alloying element. The amount is found to increase with increasing % Mo in the iron and with decreasing amounts of carbide (105). It is not as yet known whether molybdenum replaces iron or chromium in the M_7C_3 structure. About 50% of a molybdenum addition to a chromium iron goes into Mo_2C type carbides which do not contain chromium or iron. The remaining 50% is equally divided between M_7C_3 carbides and the matrix (105). The chromium content of the matrix $\%Cr_m$ can be related to Cr:C ratio according to:

$$\%Cr_m = 1.95\% \text{ Cr:C} - 2.47$$

and the molybdenum content of the matrix $\%Mo_m$ is given by:

$$\%Mo_m = 0.23 (\%Mo) - 0.029$$

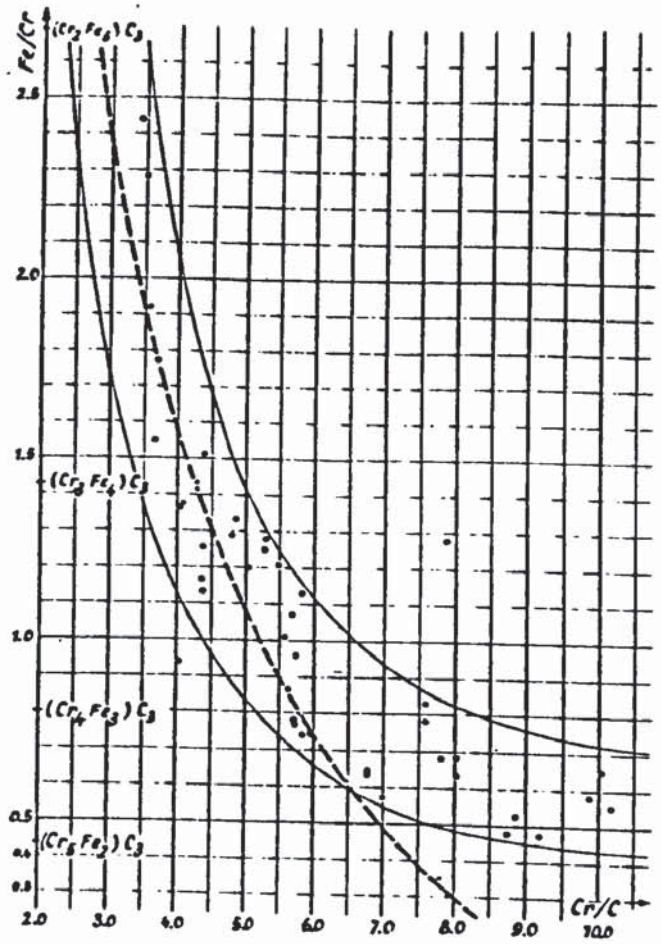

Figure 3.6

Relation between the Fe/Cr and Cr/C ratios of the M_7C_3 carbides.

The dashed line indicates the theoretical relation for stoichiometric carbides.

After Maratray (105)

3.3.4 The effect of refining additions on cast structures.

Hypoeutectic chromium irons contain a primary dendrite "grain structure" and a eutectic "grain structure" since solidification takes place by nucleation and growth of primary dendrites of austenite or ferrite followed by the formation of eutectic carbides. Attempts have been made to refine these "grain structures" in order to improve toughness and possibly wear resistance (109-113) Rickard (109) found that fine grain eutectic structures were produced in ferritic 30% Cr irons by using low pouring temperatures or by making small refining additions of titanium or nitrogen. Titanium additions also refined the dendrite size and changed the columnar dendrite pattern to an equiaxed form giving improved hot tearing resistance (110-1). Subsequent work (112) on unalloyed white irons has shown that refinement of primary austenite dendrites by cobalt or zinc powder coatings on moulds can markedly improve hot tearing resistance. The coatings did not affect the eutectic grain structure and it is reported (113) that there are no available ladle additions which will consistently modify either the primary or eutectic grain structures of unalloyed white iron. A cobalt mould coating could refine the austenite dendrites in irons containing up to 5% Cr but could not refine the austenite or ferrite dendrites in higher chromium irons (113). Under foundry conditions it seems that refining additions have no practical advantage in austenitic abrasion resistant alloys and are only used for the heat resisting ferritic high Cr irons to reduce brittleness.

3.4 Production of alloy white iron castings.

The production and founding characteristics of alloy white iron castings have been outlined by a number of authors (60, 86, 90, 106, 114-6). Cupola melting is restricted to low chromium grades and to nickel chromium (Ni-Hard) irons. High chromium irons cannot be cupola melted due to the difficulty in obtaining low carbon contents and sufficiently high metal temperatures; electric arc or induction melting is therfore required. In electric melting charges can be based on high grade steel scrap, low phosphorus pig iron and high carbon ferrochromium to ensure low sulphur and phosphorus levels (114). Acid furnace linings in spite of attack by the chromium bearing slag are generally thought to be more economic than basic materials. For low carbon 30-35% Cr irons melting temperatures of 1600-1650^{o}C are needed to ensure solution of low carbon ferrochromium and to achieve sufficiently high pouring temperatures of 1450-1550^{o}C. For higher carbon lower chromium grades melting temperatures of 1500^{o}C are usual to give pouring temperatures of 1300-1400^{o}C for 15% Cr irons (116) and 1400-1500^{o}C for 23-28% Cr irons (90).

To produce castings conventional moulding is used including greensand, Co_2, furan, air set and shell techniques (90). Gravity die casting has so far proved uneconomic due to rapid die wear (106). Running and feeding of castings must be designed to minimise dross defects from the viscous

oxide films which form on the metal and to minimise unsoundness due to high shrinkage on solidification. In addition casting design should avoid sharp sectional changes and employ generous fillets to reduce hot tearing tendency.

To aid fettling breaker cores can be used. Heavier feeders are removed by slitting so long as overheating is avoided. Flame cutting will cause thermal cracking and cannot be used. Similarly high chromium irons cannot be easily fusion welded although limited repair may be possible using powder techniques (117).

3.5 Commercial compositions for abrasion resistant castings.

The recently drafted BS 4844 now covers unalloyed white irons, the chromoium irons and the nickel-chromium irons (118). Typical chemical compositions from this standard are given in table 3.1, all irons are hypoeutectic. The lower carbon grades generally have improved toughness at the expense of wear resistance and are used where impact loading is significant. The compositions of the 14-28% Cr irons are designed to give austenitic or martensitic matrices. Molybdenum is added to avoid the formation of pearlite in as-cast austenitic irons and to improve hardenability. Silicon content is important for deoxidation, improving fluidity and surface finish, but silicon contents above 0.8% will lower hardenability (2).

BS.4844. Part 2.

Nickel—Chromium Grades

Chemical Composition %

Grade	*C*	*Si*	*Mn*	*Ni*	*Cr*	*Mo (max)*	*S (Max)*	*P (Max)*
2A	2·7–3·2	0·3–0·8	0·2–0·8	3·0–5·5	1·5–2·5	0·5	0·15	0·3
2B	3·2–3·6	0·3–0·8	0·2–0·8	3·0–5·5	1·5–2·5	0·5	0·15	0·3
2C	2·4–2·8	1·5–2·2	0·2–0·8	4·0–6·0	8·0–10	0·5	0·15	0·3
2D	2·8–3·2	1·5–2·2	0·2–0·8	4·0–6·0	8·0–10	0·5	0·15	0·3
2E	3·2–3·6	1·5–2·2	0·2–0·8	4·0–6·0	8·0–10	0·5	0·15	0·3

BS. 4844. Part 3.

High Chromium Grades.

Chemical Composition %

Grade	*C*	*Si (max)*	*Mn*	*Cr*	*Mo*	*Ni*	*Cu*	
3A	2·4–3·0	1·0	0·5–1·5	14–17	0–2·5	0–1	0–1·2	0·1
3B	3·0–3·6	1·0	0·5–1·5	14–17	1–3	0·1	0 ·1·2	0·1
3C	2·2–3·0	1·0	0·5–1·5	17–22	0–3	0–1·5	0–1·2	0·1
3D	2·4–2·8	1·0	0·5–1·5	22–28	0–1	0–1	0–1·2	0·1
3E	2·8–3·2	1·0	0·5–1·5	22–28	0–1	0–1	0–1·2	0·1

Table 3.1

Compositions of abrasion resistant alloy irons.

After BS.4844

The compositions of the Ni-Cr series are selected to give martensitic structures as cast. Silicon contents are lower to avoid graphite formation but ideally must be at least 0.5% to avoid blowhole formation (86). Phosphorus has an embrittling effect and must be as low as possible.

Table 3.1 does not include alloys for heat and corrosion resistance. These are the 30-35% Cr grades where the structure consists of ferrite + eutectic carbides. Their development is discussed by Boyes (60).

Typical compositional ranges are:-

Carbon	1.0 - 2.0%
Chromium	30 - 35%
Silicon	2.0 max %
Manganese	0.5 - 0.7%
Phosphorus	0.05 max %
Sulphur	0.06 max %

Compositions such as these may be of use in helping to develop alloys to resist abrasion at high temperatures or under corrosive conditions.

3.6 Control of as-cast matrix structures.

As can be seen from the liquidus surface in figure 3.3. Hypoeutectic chromium irons can solidify with primary austenite or primary ferrite dendrites before eutectic carbides form. In the 30-35% Cr series the ferrite is retained in the as-cast condition. In lower chromium irons the austenite can

be retained or it can fully or partially transform to ferrite + carbides or to martensite depending on composition and cooling rate of the casting. Generally a martensitic matrix will provide the best resistance to abrasion although in some applications an austenite matrix may give equivalent or superior abrasion resistance since it can work harden during service to give a self replacing wear surface.

Pearlite must be avoided in the matrix of either as-cast or heat treated irons since it will lower abrasion resistance (1, 119, 120). Control of matrix structure therefore involves the use of alloying elements to produce either an austenitic or a martensitic matrix in the as-cast condition. Martensitic matrix structures can also be produced by suitable heat treatment although in some castings this may lead to cracking. As size and complexity of design of castings increase the as-cast hardenability is of increasing importance in choice of composition (119). It is accepted that for some castings e.g. large pump bodies an austenitic matrix must be used because of the difficulities involved in producing a martensitic matrix (104). This avoids the build up of residual stresses due to martensite transformation (2).

3.6.1 Austenitic matrix structures.

To obtain an as-cast austenite matrix the composition of the iron must be in the austenite liquidus region and be such that austenite is retained at ambient temperatures for a given casting section.

Jackson (94, 106) has shown that austenite decomposes peritectoidally to produce carbides and ferrite and is not a room temperature equilibrium phase. However, the presence of chromium in spite of being a ferrite former will slow down the rate of austenite decomposition such that under non-equilibrium cooling austenite will be retained. Alloy additions such as manganese, nickel and molybdenum aid austenite retention (106). In studying 17.5% Cr irons Gundlach (119) found that nickel in combination with molybdenum efficiently suppressed pearlite formation. Copper and manganese additions were less effective than nickel. Jackson (106) has investigated the retention of austenite in a series of irons containing 1.1 - 4.1% C and with Cr equivalents ranged from 14.5 to 32.5. (Equivalent values are given by Cr + 2Si + 1.5Mo - 2Ni - Mn - 15N).

Austenite content was estimated using magnetic permeability readings since it is difficult to distinguish austenite from ferrite by metallographic means. The results of these measurements are shown in figure 3.7 which plots permeability values with respect to the liquidus surface. The low values of permeability correspond to the retention of austenite. The diagram shows that at higher chromium levels austenite can be retained over a wider range of carbon contents. This is also shown by plotting permeability against carbon content for constant chromium levels as in figure 3.8. The field of austenite retention was found to expand to lower chromium and higher carbon contents for sections smaller than 35 mm dia and to contract for heavier sections.

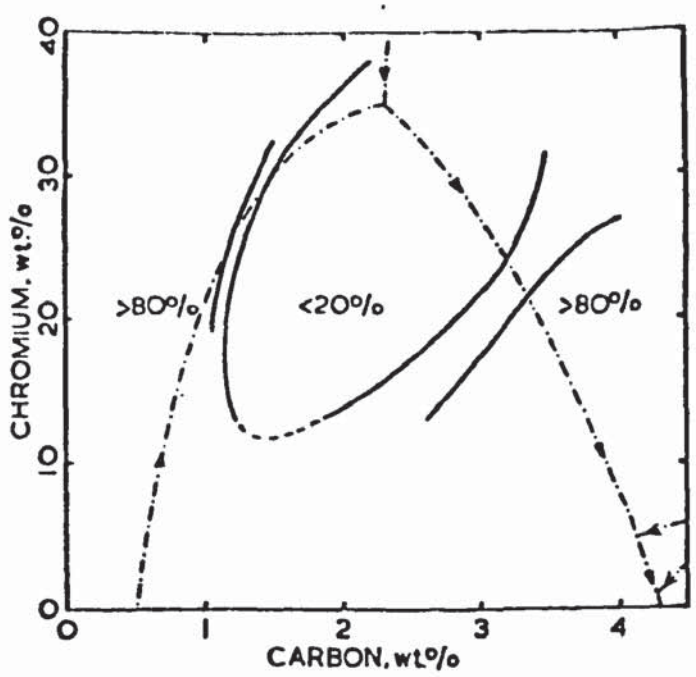

Figure 3.7

Permeability/ composition relationships for 35mm dia. sand cast bars.

After Jackson (106)

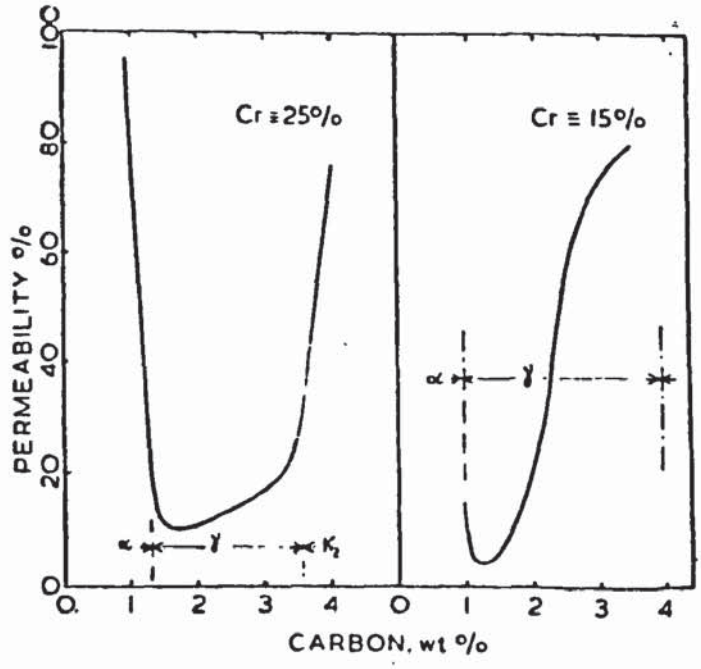

Figure 3.8

Permeability/carbon relationships at 15% and 25% Cr equivalent.

After Jackson (106)

In irons in which the chromium level is insufficient to retain fully austenite it was found (106) that the chromium rich centres of dendrites remained untransformed whereas their edges did not. At higher chromium levels it was noted that austenite in the eutectic region may transform to martensite in preference to the dendritic austenite (105, 106). Maratray (105) related this to heterogeneity of austenite but does not provide microanalysis data to illustrate this view.

The selection of composition to give austenitic irons which can be used in the as-cast condition centres on the 25-27% Cr irons (90, 106, 120). Maratray (104, 105) has shown that for sand cast 25 mm rounds the Cr:C ratio must be at least 7.2. He found that adding molybdenum decreased the value of Cr:C ratio necessary to ensure an austenitic matrix. This effect is shown in figure 3.9. Hence for a given chromium level transformation products can be suppressed at higher carbon levels if molybdenum is present. Maratray suggests that the Cr:C ratio should be as low as possible with a molybdenum addition to give an austenitic matrix. Figure 3.10 can then be used to select carbon and chromium levels to give the required amount of eutectic carbide in the structure (104). It was noted that variations in Cr:C ratio or in molybdenum content had no significant effect on the microhardness of austenite (105).

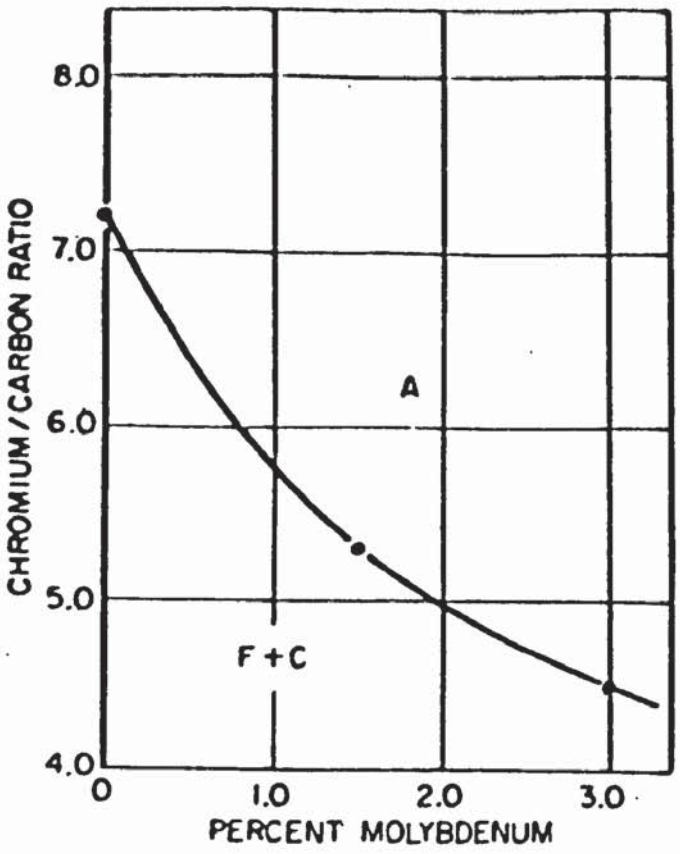

Figure 3.9

Relation between Cr/C ratio,Mo content and as-cast microstructure for sand cast 25mm dia. rounds.

After Maratray (105)

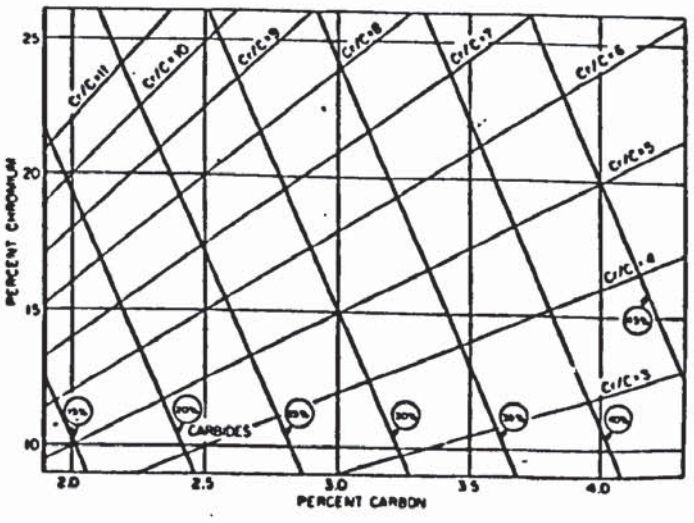

Figure 3.10

Relation between C and Cr contents and the amount of carbides.

After Maratray (104)

3.6.2 Martensitic matrix structures.

The characteristics of as-cast martensitic white irons have been discussed by several authors (2, 44, 53, 73, 86, 90, 115, 119-122). To obtain a martensitic matrix the iron is alloyed with nickel and chromium (see grade 2A-E in table 3.1). The levels of alloy addition to produce martensitic structures depend on section thickness. If there is insufficient alloying addition the iron may contain graphite and some pearlite. If there is excessive alloying the iron may contain increased amounts of retained austenite. As section size increases nickel and chromium contents should be raised and silicon content reduced. The nickel addition suppresses the austenite $\longrightarrow$ pearlite transformation and the chromium addition counteracts the graphitising effect of the nickel. In the higher chromium grades chromium is used to produce discontinuous carbides.

Isothermal transformation curves (123) for these irons show a pearlite nose at about 540^{o}C and a bainite nose at about 250^{o}C. The Ms is about 150^{o}C but M_f is as low as -130^{o}C. These temperatures are modified by composition and cooling rate. To avoid cracking castings must be cooled slowly from about 200^{o}C to room temperature and should not be knocked out until they are cold. Since M_f is subzero the structure of as-cast Ni-Hard will contain carbides in a matrix of martensite and residual austenite. To obtain maximum hardness and wear resistance this austenite must be transformed by heat treatment or refridgeration.

Since the introduction of the Ni-Cr white irons a number of other compositions have been suggested to produce martensitic matrices in the as-cast condition (115, 116, 124, 125). In these irons other elements notably manganese and copper which are less expensive than nickel are used to replace all or part of the nickel addition. The irons also contain chromium and molybdenum.

Typical recommended alloying levels are:-

Ref	%Mo	%Cu	%Cr	%Mn	%Ni
116, 117	2-3	2	2	0.7-1	1
125	0.3	2.5	1.5	1.5	0.65
126	0.2	1	-	3.2	-

These irons have similar structures and hardness levels to the Ni-Hard types and are claimed to be comparable on a cost-wear basis. There was a good deal of interest in these low nickel irons during the nickel shortage of 1969 when due to the industrial disputes at the Canadian mines nickel prices increased from £1000/ton to over £6000/ton. However, this interest subsided when nickel became available again and its price reduced. Since then it is reported that these irons have gained only limited acceptance in ore grinding operations (73). A new alloy which is said to be becoming accepted as grinding media is a martensitic mottled iron called Ferro-M (73). Its structure contains graphite nodules which counteract solidification shrinkage and improve soundness in sections where feeding is difficult.

3.7 Heat treatment of abrasion resistant irons.

Suitable thermal treatments of abrasion resistant irons are used for the following reasons:

(a) to relieve internal stress.

(b) to transform retained austenite in as-cast martensitic irons

(c) to austenitise and susequently quench harden irons with low alloy content.

(d) to destabilise austenite in high chromium irons to allow hardening.

(e) to temper martensitic structures.

(f) to soften for machining.

The above effects will be discussed in relation to relevant alloy compositions.

3.7.1 Heat treatment of as-cast martensitic irons.

The Ni-Cr martensitic irons can be put into service in the as-cast condition but their service life may be improved if they are given a low temperature heat treatment (44, 126-8). The usual treatment applied to the lower chromium grade is for 4-16 hrs at 275^{o}C followed by air or furnace cooling. This relieves casting stresses, tempers the as-cast martensite and transforms any residual austenite to martensite and bainite. If the iron is to withstand severe impact under repeated loads a double treatment of

4-6 hrs at 450°C followed by furnace and air cooling and then by reheating to and holding at 275°C can be used.

The higher chromium grades are normally held for 6-12 hrs at 775-825°C and then air or furnace cooled. This conditions the retained austenite for transformation to martensite and bainite and the iron has then a reasonable combination of hardness, strength and impact resistance. In complex castings where there is a danger of cracking or when decarburisation is a problem an alternative treatment is available (90). This requires holding for 4 hours at 550°C, air cooling and then reheating and holding for 16 hours at 450°C and air cooling. The higher chromium grades can be subsequently tempered at 200-350°C to increase toughness and spalling resistance. The conditioning of austenite mentioned above is of particular importance in treating high chromium irons. Similar treatments to those described above are also recommended for the nickel replaced, Cu-Mo-Cr irons (115, 116). The hardness of the lower chromium Ni-Hards is relatively unaffected by heat treatment and Hv values of 550-600 are usual depending on carbon content. Heat treatment slightly raises the hardness of the higher chromium grades from 550 Hv to 600 Hv for 2.5% C and from 650 to 700 Hv for 3.5% C iron. The improvement in service life on heat treatment is attributed to removal of residual stress and residual austenite. The residual austenite can transform to martensite at the wearing surface causing a volume increase

which can result in spalling of the surface layers under impact conditions. In a ball drop test as-cast balls lasted only 100-200 drops whereas heat treated grinding balls lasted for several thousand drops (128).

Heat treatment is not so important if the iron is used under sliding wear conditions where working stresses are unlikely to produce spalling. Under these conditions such "work hardening" can raise surface hardness to 800-850 Hv (90) and the iron gives satisfactory performance. The residual austenite can also be transformed by refridgeration since Mf is about -130^{o}C. Refridgeration of 50 mm dia grinding balls increased the amount of martensite in their structure and increased wear resistance (129). When followed by tempering refridgeration is said to give optimum hardness and toughness (129).

3.7.2 Reaustenitising and hardening of pearlite irons.

Irons with lower chromium levels which have as-cast pearlite matrix structures and higher chromium irons which have been annealed for machining can be hardened by reaustenitising at 950-1100^{o}C depending on composition and quenching. Hardening is normally carried out by forced air quenching or a quench in a mild quenching liquid such as oil or molten salt. Fraser (130) claims that savings can be made in cost of alloy elements over the as-cast martensitic irons

since pearlite formation on quenching can be suppressed with less alloy addition than that needed to prevent pearlite formation on cooling in the mould after casting. The potential saving in alloy additions may more than offset the cost of heat treatment (130). However, the lower chromium irons have poor hardenability and to suppress pearlite in heavier sections even on quenching other alloy additions of Mo, Ni, Cu and Mn must be used.

Pearlite structures may be fully austenitised but high solution treatment temperatures of less than 50°C below the solidus are required (104-105). On cooling a highly alloyed austenite matrix is retained. In practice this is not used due to the narrow margin of allowable temperatures.

3.7.3 Hardening of as-cast austenite matrix irons.

3.7.3.1 Destabilisation treatments.

Austenite formed on solidification can be retained at room temperature since it is super-saturated with carbon, chromium and other alloy elements. These elements retard the transformation rate of austenite such that on normal cooling of sand castings austenite does not break down. To obtain martensitic structures on heat treatment the alloy content of the austenite matrix must be lowered. This is achieved by a destabilisation treatment (1, 2, 104, 120).

This involves soaking castings within the range 920°-1000°C to allow the precipitation of secondary carbides thus decreasing both the chromium and carbon contents of the matrix. Destabilisation and soaking for quenching are usually performed at the same temperature and combined as a single treatment (2). On cooling from this temperature austenite can now transform to martensite if the cooling rate is sufficiently fast to prevent pearlite and bainite formation. The effect of destabilisation on transformation characteristics is illustrated in figure 3.11. It is seen that precipitation of secondary carbides results in a retardation of the pearlite transformation and a raising of the Ms temperature so that hardening to martensite is possible.

Maratray (104, 105) has studied the morphology of the precipitated carbides. He noted that the most uniform and finest distribution of carbides is obtained by reaustenitising a pearlite structure and then soaking. He considered that this would give better impact resistance than the structure obtained by soaking an as-cast austenite which gives a less uniform distribution of secondary carbides although the hardness values of the two structures are similar.

The destabilisation temperature used has a marked influence on hardness and Ms temperature. This is shown in figure 3.12 for a 12% Cr, 3% Mo iron. The maximum hardness is seen to be achieved after destabilising and quenching from around 975°C.

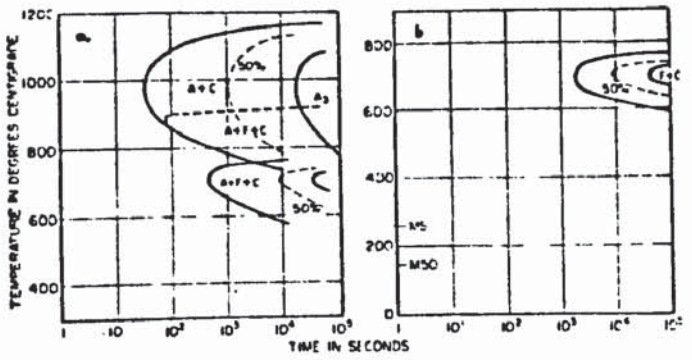

Figure 3.11

Schematic isothermal transformation diagrams for (a)undestabilised and (b)destabilised austenite. After Maratray (104)

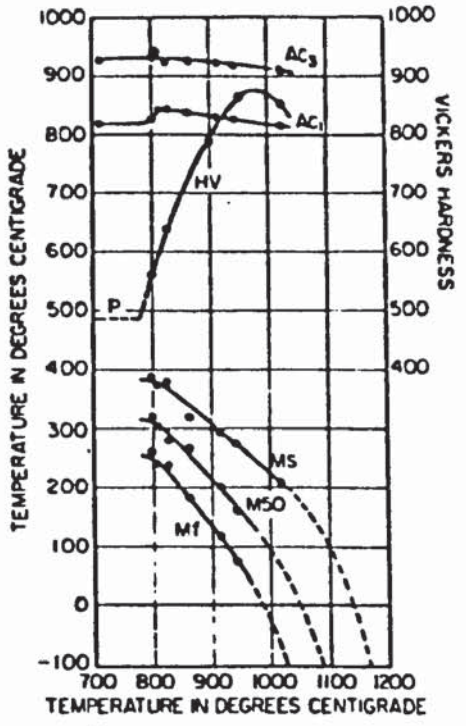

Figure 3.12

Effect of destabilisation temperature on hardness and martensite transformation in a 2.4%C, 12.8%Cr, 3%Mo iron completely destabilised.
After Maratray (104)

Precipitation of the secondary carbides is normally complete within 4-6 hours and typical treatments (1, 2) for high Cr-Mo grades are as follows:

Grade	°C	Soaking time *	
15 Cr-3 Mo	920-960	½ - 1 hr	Air quench
15 Cr-2 Mo-1 Cu	920-960	4 hr min	"
20 Cr-2 Mo-1 Cu	950-1000	6 hr min	"
23-28 Cr	1100	"	"

(* + 1 hr per 25 mm of section)

To avoid cracking on heating to soaking temperatures the castings should be heated very slowly to at least 800°C. This minimises intensification of residual casting stresses by steep temperature gradients. These irons are normally air hardened since liquid quenchants may cause cracking. Air hardening can be accelerated by fans and spray techniques but cooling must be uniform on all sections of the casting to minimise residual stresses.

3.7.3.2 Hardenability.

Since chromium is present in both the eutectic and secondary precipitated carbides only part of the total chromium content of the iron is retained in the matrix to increase hardenability. Hence unalloyed chromium irons have relatively poor hardenability. Supplementary additions of Mo, Ni, Mn or Cu are needed to improve hardenability if heavier sectioned castings are required to be fully hardened.

Fairhurst (2) has shown that hardemability is increased if the chromium content is increased for a constant carbom level and is decreased if the carbon content is increased for a constant chromium level. The point was illustrated by plotting the time taken to cool through half the difference between the quenching temperature and ambient in terms of avoiding pearlite formation against Cr:C ratio. The composite diagram is shown in figure 3.13 which shows that for typical Cr:C ratios of 4-8 the maximum half cooling time to avoid pearlite formation is around ten minutes, corresponding to a 25 mm section on air cooling. If 3% Mo is added the half cooling time increases to over 2 hours, corresponding to full hardening of a 100 mm section (2).

These effects are further illustrated by consideration of the influence of section size in relation to Cr:C ratio and to molybdenum addition. Figure 3.14 shows that to maintain hardness and avoid pearlite in heavier sections additions of molybdenum are necessary.

Maratray (104) has developed a relationship to calculate hardenability from chemical composition. For air hardening after 20 mins at 1000^{o}C then

$$\log d = 0.32 + 0.158 \frac{Cr}{C} + 0.385 (\% Mo)$$

where d = maximum diameter in mm that can be air hardened without pearlite forming.

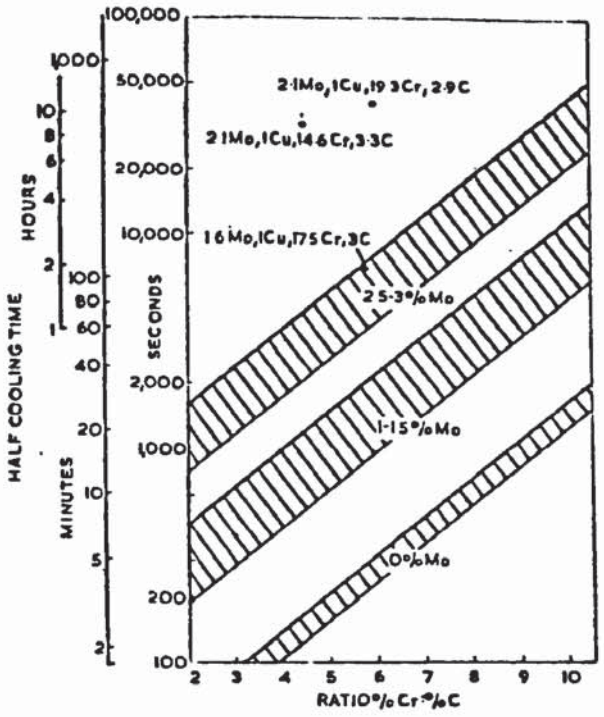

Figure 3.13

Influence of Cr/C ratio and Mo content on half cooling time to avoid pearlite formation.

After Fairhurst (2)

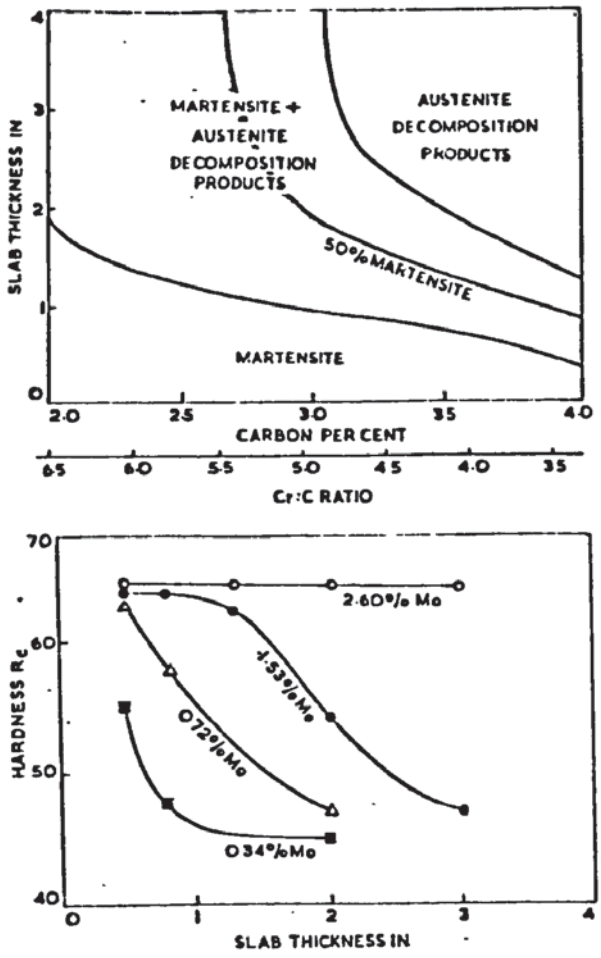

Figure 3.14

Influence of the carbon and molybdenum content on matrix structure and hardness in various sections of high Cr iron after air quenching. Top. Influence of C content at 12-14%Cr, 1.5%Mo. Bottom. Influence of Mo at 12-14%Cr, 3%C. After Fairhurst (2)

Further improvements in hardenability can be made by supplementary additions of nickel and copper as shown in figure 3.13. Fairhurst and Rohrig (2) suggested that the extra additions of copper or nickel should be about 0.5% and must not exceed 1.2%. They report that the presence of copper or nickel increases the soaking time required for destabilisation since their amounts in solution in austenite cannot be lowered by heat-treatment. Increased soaking times result in a lower carbon austenite which transforms to a lower carbon martensite which is less hard and less abrasion resistant. Copper and nickel are also said to increase the tendency to retain austenite after quenching giving possible loss of abrasion resistance. It was concluded that for maximum abrasion resistance plain Cr-Mo irons must be used.

However, work by Cox (131) claims that nickel additions of up to 3.5% can be used to improve hardenability without the problem of retained austenite if the molybdenum content is lowered. He investigated a series of compositions in the range 3.0% C, 0.5% Si, 0.5% Mn, 15% Cr, 0 - 3.75% Ni, 0 - 3.75% Mo. From these he suggested a 15% Cr, 3% C, 2% Ni, 0.25% Mo iron which was designated IN-3503. This iron is claimed to fully air harden in sections up to 200 mm. For smaller sections 0.5 - 1% Ni + 0.25% Mo is said to be adequate. Cox suggested that these irons should compete favourably on a cost wear basis with the existing irons which contain more molybdenum.

Manganese has a similar effect to copper and nickel and the most recent claims for the use of high manganese contents in 15% Cr irons have been made by Stefanescu (132) who recommended manganese levels of up to 5% to improve hardenability and replace molybdenum. However, it is suggested (2) that manganese is not very effective in suppressing pearlite on slower cooling and also tends to encourage retained austenite. In contrast in 17.5% Cr irons Cias (133) found that manganese contents of 2.5-3.0% were more effective in improving hardenability than 2% copper or 2% nickel additions. They did increase tendency to retain austenite but this was less of a problem in heavier sections. Nevertheless Fairhurst (2) concluded that manganese could be used to improve hardenability at low cost but the structures so produced could contain excessive amounts of retained austenite. The recommended manganese level is 0.8 - 1%.

3.7.3.3 Tempering.

There is little published information on the effects of tempering on structure and properties of high chromium irons although tempering is normally recommended after hardening to reduce residual stress and to transform retained austenite which may be present after quenching. (90). Tempering temperatures lie within the range 200 - 450^{o}C. Fairhurst (2) however, claims that for many applications tempering is not necessary and suggests that there is evidence that tempering above 200^{o}C can decrease toughness.

But Durman (134) found that in 15% Cr irons with carbon contents below 1.5% fracture toughness is increased with increased temperature of tempering. For carbon contents above 1.5% the toughness was found to be controlled by the volume fraction of eutectic carbides and was relatively unaffected by matrix characteristics. Secondary hardening during tempering was observed by Boyes (135) in 27-33% Cr irons, by Cox (131) in 15% Cr, 1.5% Ni, 0.25% Mo irons and by Allen (136) in 27% Cr irons containing cobalt. Increases in hardness up to 50 Hv are quoted.

Fairhurst (2) in reviewing the results of Kamaras and Korsnak (137) has related secondary hardening to transformation of retained austenite. Tempering in the region 400-600^{o}C is said to destabilise austenite such that it transforms on cooling. An iron with little retained austenite decreased in hardness with increased tempering temperature. In irons with larger amounts of retained austenite, secondary hardening is seen to result in a higher hardness than that of the as-quenched condition. In spite of this it is reported (2) that abrasion resistance even after secondary hardening is likely to be lower than in the as-quenched condition.

3.7.4 Softening treatments.

Annealing of high Cr irons produces a soft granular pearlite matrix which allows tool machining to be carried out although grinding in either the hard or soft condition is said to be more usually employed (106). It must be remembered that the presence of eutectic carbides will have a large influence on machinability since they remain unaffected by the annealing treatment. The lower carbon grades with less eutectic carbide will be the most easily machined grade, machining becoming more difficult above 3% C. Distortion on hardening of chromium irons is reported (2) to be small such that surfaces can be machined to close tolerances so that only a small amount of final grinding will be needed after heat treatment. Annealing of 15% Cr 3% Mo grades involves heating at a slow rate to a reaustenitising temperature between 920-975^{o}C, holding for 1 hour minimum, furnace cooling to 820^{o}C and then cooling at a rate below 40^{o}C/hour down to 590^{o}C. This is followed by air cooling to room temperature (115). The 23-28% Cr grades are held for 1-4 hrs at 750-820^{o}C and then furnace cooled to 600^{o}C followed by air cooling to room temperature. Annealed hardness values generally lie between 300-400 Hv and depend on the temperature of transformation to ferrite + M_7C_3 or $M_{23}C_6$ (104). This product is often referred to as granular pearlite. Its hardness is found to increase as the temperature of its isothermal formation is decreased and as cooling rate under continuous cooling conditions is increased. The formation of granular pearlite is retarded by higher Cr:C ratios, by Mo additions and by destabilisation treatments (105).

3.8 Properties of abrasion resistant white irons.

3.8.1 Tensile strength and hardness.

Typical values for tensile strength and hardness of alloy white irons are given in table 3.2 which has been compiled from published data (1, 2, 86, 90, 115, 138). Durman (134) studied tensile properties and fracture toughness of 15% Cr irons and found that up to the point where the eutectic carbide network became continuous, at approximately 1.4% C, the alloy behaved similarly to a ductile matrix containing hard particles. The greater the volume of hard particles i.e. eutectic carbides the stronger and harder the structure became but any change in matrix properties was also found to affect the properties of the composite. At higher carbon contents when the eutectic carbides formed a complete network around the primary dendrites it was found that it was the strength of this network which dominated the properties of the alloy and any change in matrix strength had little effect. The higher the chromium or carbon content the greater is the amount of eutectic carbide in the structure and the smaller is the influence of matrix type on strength. This is illustrated in table 3.2 by considering the 15 Cr/3 Mo iron with a 3.6% C content. There is little difference in UTS between a austenite matrix (510 MN/m^2) and a martensite matrix (490 MN/m^2) but in the lower carbon grade the difference in UTS is larger with austenite and martensite giving respectively 615 and 1000 MN/m^2.

Grade	Condition	Matrix	%C	UTS MNm^{-2}	Hv
4%Ni-2%Cr	AC	M+A	2.8	350	630
"	AC	M+A	3.5	310	660
15%Cr-3%Mo	AC	A	2.5	615	500
"	QT	M+A	"	1000	780
"	AC	A	3.6	510	680
"	QT	M+A	"	490	810
"	FC	P	"	690	450
15%Cr-2%Mo-1%Cu	AC	A	3.3	460	510
"	QT	M	"	620	830
20%Cr-2%Mo-1%Cu	AC	A	2.9	550	460
"	QT	M	"	700	825
25%Cr	AC	A	2.0	660	520
"	QT	M	"	700	700
"	FC	P	"	700	350
33%Cr	AC	F	1.1	550	300

AC-as cast
QT-quench & temper
FC-furnace cool

M-martensite
A-austenite
P-pearlite
F-ferrite

Table 3.2

Typical values for tensile strength and hardness of Cr irons

3.8.2 Fracture toughness and impact properties.

Conventional impact testing of alloy white irons is of questionable value since the low energy of fracture requirements of these brittle materials dictates the use of non-standard test specimens. No correlation can be obtained with impact properties of other alloys or between section sizes. In addition the results give a wide scatter band since the test gives poor sensitivity and lack of reproducibility (1, 106). In general a conventional test will show that irons with discontinuous carbides absorb more energy in fracture than irons with continuous carbides. Fairhurst (2) illustrates this by giving the values from un-notched impact tests as follows:

a) Low alloy martensitic white iron 30-75 Nm

b) Quenched and tempered 15Cr/3 Mo iron 70-120 Nm

These values correlate with practical experience which has shown that the 15/3 irons can be used for applications where the low alloy irons would break after short periods of use. In applications involving severe abrasion wear rates can be so high that the wear resistance of different alloys is similar such that fracture resistance can be the main criteria in material selection. To assess fracture resistance two alternative methods have been developed; these are the use of simulated impact tests or the use of fracture toughness techniques.

3.8.2.1 Simulated impact testing.

Simulated impact tests have been developed to study the effect of repeated impact loads. A common test is the ball drop test which is used to test grinding balls that cannot be tested by conventional impact or fracture toughness tests (1, 73, 106, 126, 134). The test simulates conditions in a grinding mill and involves the repeated dropping of test balls from 6-8 m onto an anvil. The number of ball-anvil impacts to failure is recorded to give an assessment of the repeated impact resistance of both ball and anvil material. The test can evaluate the effects of casting defects as well as the effects of microstructure and hardness on the fracture behaviour of various alloys. Typical results are quoted by Durman (106). Examples are given below as number of drops to failure of ball samples:

a) Low alloy Ni-Cr martensitic iron	500 - 1000 Drops
b) Austenitic 25% Cr iron (3% C)	1000 - 3000 "
c) Martensitic 25% Cr iron (3% C)	5000 - 7000 "
d) Martensitic 18% Cr iron (2% C)	upto 20,000 "

Castings defects can seriously reduce these values. Shrinkage cavities can cause early fracture and surface defects such as sand inclusions can induce surface spalling.

Another approach to this problem involves the use of a reciprocating shaking machine which determines the impact abrasion resistance of a number of small balls or cylindrical pebs (106). A weighed sample of balls or pebs is shaken with wet or dry abrasive in a hardened steel cylinder which moves in a vertical plane at 300 times/minute. The samples are weighed and examined for a fracture at convenient intervals. This test is particularly useful in that the degree of impact, the type of abrasive and wet or dry conditions can be selected.

3.8.2.2 Fracture toughness.

The application of fracture toughness testing to alloy white irons has been described in a number of papers (1, 2, 45, 106, 131, 134, 139-14). The measure of fracture toughness gives a quantitative description of the resistance of a material to propagation of a pre-existing crack. Fracture toughness is sensitive to variations in microstructure and is of value in determining the seriousness of defects such as microshrinkage, inclusions and hot checks.

The fracture toughness index K_{Ic} is determined by application of a tensile load across a pre-cracked notch and by measurement of the load at which the crack begins to propagate. The pre-cracking is achieved by producing a fatigue crack at the root of a notch.

The root radius of this crack must be smaller than a limiting value below which sharpness has no further effect, low stress fatigue conditions are standardised to produce a crack with a root radius smaller than the limiting value. The crack subsequently blunts to the critical value which is structure dependent. Hence fracture toughness tests measure cracking under the worse possible condition. In addition tests are performed under plane strain such that the measured K_{Ic} value is independent of specimen geometry.

Typical values of K_{Ic} for abrasion resistant alloys are given in table 3.3. The values given suggest that fracture toughness cannot be related directly to hardness. Diesburg and Borik (45) found that martensitic irons were always harder than austenitic irons but their fracture toughness could be higher or lower. Carbon content has been found to be the main factor which influences toughness (134, 141).

Increasing carbon levels lowered toughness since it increased the proportion of carbides in the structure. At carbon contents above 1.5% in 15% Cr iron toughness was found (134) to be controlled by the volume fraction of the carbides which formed a continuous network and was relatively unaffected by matrix characteristics (see figure 3.15). In lower carbon irons, in which the carbide network is discontinuous, toughness was improved by reducing the volume fraction of the carbides, by decreasing the primary dendrite arm spacing at a given

Material	Carbon, %	HRC	Fracture Toughness, ksi$\sqrt{in.}$ ($MN/m^{3/2}$)
Pearlitic Cr-Mo Steel	0.63	27	38 (42)
C-Mn Rail Steel	0.8	31	31 (34)
Mn-Si-Cr-Ni-Mo Steel (highly tempered)	0.55	34	90 (100)
Pearlitic Cr-Mo Steel	0.88	37	31 (34)
27Cr Iron	2.7	50	28 (31)
9Cr-6Ni Iron	3.4	50	23 (25)
Cr-Mo (Austenitic) Iron	2.9 to 3.6	49 to 53	16 to 31 (18 to 24)
Cr-Mo (Martensitic) Iron	2.9 to 3.6	55 to 64	19 to 29 (21 to 32)
Mn-Cr-Mo Steel	0.65	57	21 (23)
Mn-Si-Cr-Ni-Mo Steel	0.55	58	32 (35)
Mn-Si-Cr-Mo Steel	0.63	58	25 (28)

Table 3.3

Fracture toughness of various abrasion resistant alloys. After(45)

Matrix Microstructure	
Order of Decreasing Abrasion Resistance	Order of Decreasing Fracture Toughness
Austenite plus Secondary Carbides	Austenite
Austenite.	(Spheroidite)
Martensite	Martensite
(Pearlite)	Austenite plus Secondary Carbides
(Spheroidite)	Pearlite

* Parentheses mean the order of ranking is based on results from one iron.

Table 3.4

Effect of matrix structure on abrasion resistance and toughness of alloy white irons.

After (45)

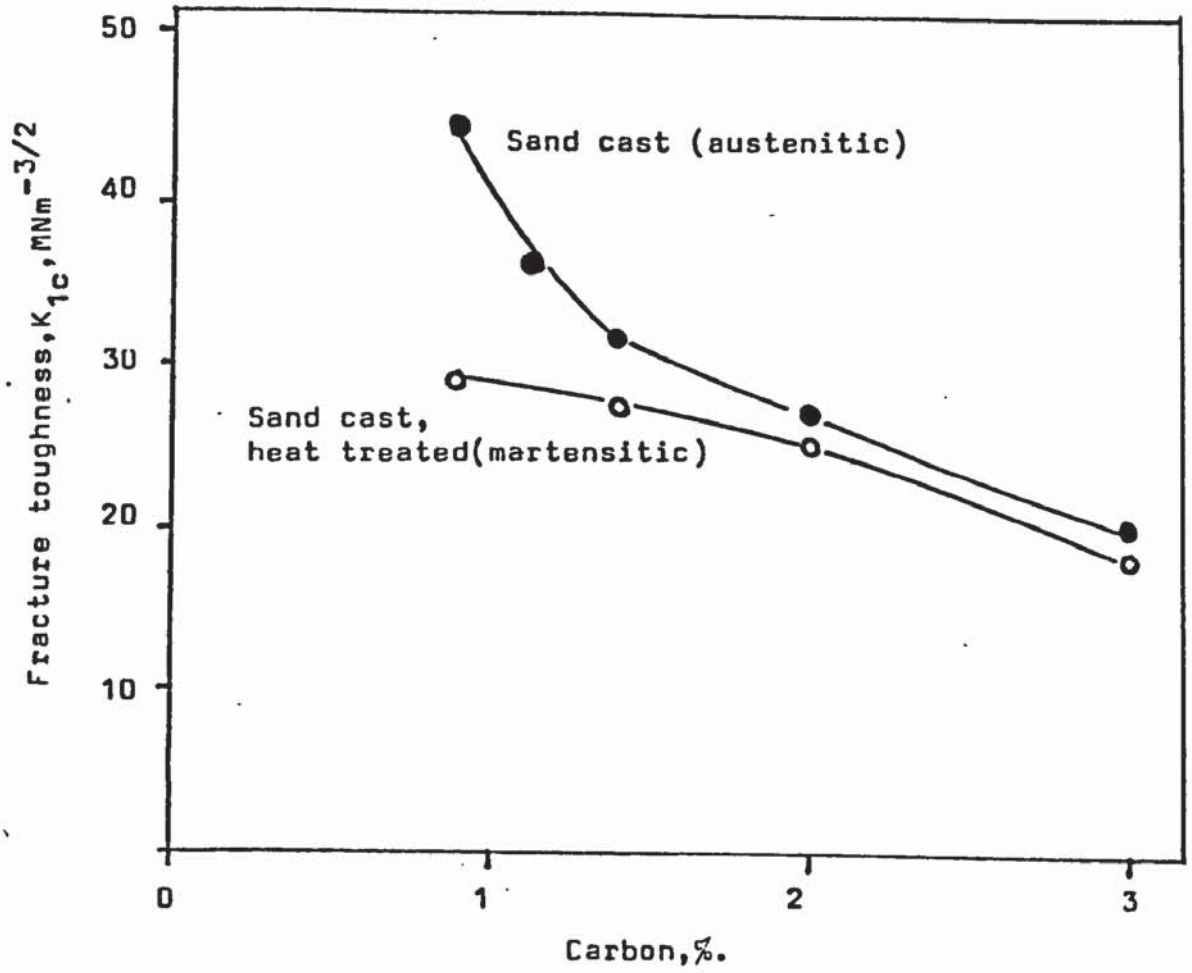

Figure 3.15

Effect of carbon content on fracture toughness of 15%Cr irons.

After Durman (134)

carbon level, by increasing the tempering temperature of martensitic irons, by spheroidisation of as-cast carbides and by hot working of the cast structure. Improvements in toughness clearly relate to the refinement of the embrittling eutectic carbide. Similar conclusions were reached by Diesburg (45) who studied the effects of the variables given in tables 3.4 and 3.5 on both toughness and abrasion resistance. Refinement of dendrite arm spacing of the primary austenite resulted in a corresponding refinement of interdendritic carbides and improvement in toughness. Durman (134) however, concluded that this improvement in toughness was not sufficiently large to warrant a change in moulding technique i.e. from sand to chill, since a comparable improvement could be made more easily by reducing carbon content by 0.4%. Embrittling carbide networks could be broken down by spheroidisation heat treatments but these may be uneconomic due to the very high temperatures required. Thermomechanical treatments have been used to refine eutectic carbide and are said to be worthy of further development (134, 142-143). Hot working of low carbon white irons (2-2.4% C) has given improvements in strength and toughness (142, 143) and is more promising than in higher carbon irons which tend to crack. Harrison and Dixon (40) successfully forged Ni-Hard grinding balls between flat dies and showed that the carbide network was broken up into a discontinuous form. The forged structure was said to be tougher than the as-cast structure without loss of hardness or abrasion

Increasing Amount of Variable	Pin Test Abrasion Resistance		Plane Strain Fracture Toughness	
	As-Cast	Heat-Treated	As-Cast	Heat-Treated
Carbon	Large Increase	Large Increase	Large Decrease	Large Decrease
Silicon	No Effect	Small Decrease	Large Increase	No Effect
Molybdenum	Small Increase	Small Increase	No Effect	No Effect
Eutectic Carbide Refinement	Large Decrease	Large Decrease	Large Increase	Large Increase
Eutectic Carbide Globularization	No Effect	No Effect	Large Increase	Large Increase
Secondary Carbide Precipitation	Small Increase	No Effect	Large Decrease	Large Decrease
Retained Austenite	NA[a]	No Effect	NA	Large Increase
Presence of 0 to 10% Martensite	No Effect	NA	No Effect	NA
Presence of 0 to 10% Pearlite	Small Decrease	ND[b]	Small Increase	ND
Presence of 0 to 30% Ferrite-Carbide Aggregate	ND	Large Decrease	ND	Large Increase
Tempering at 410 F (210 C)	ND	Large Increase	ND	Large Increase
Tempering at 600 or 800 F (315 or 425 C)	ND	No Effect	ND	Large Decrease

[a] NA = not applicable.
[b] ND = not determined.

Table 3.5

Effect of certain variables on abrasion resistance and toughness of alloy white irons.

After (45)

resistance. As yet there is no available liquid metal addition that will spheroidise or refine the eutectic carbides by modifying their solidification behaviour.

The influence of the eutectic carbides on fracture was found to be greater in austenitic matrix irons (134). In martensitic alloys the nucleation of voids during the fracture process occurs due to the presence of secondary carbide particles and fracture is thus less dependent on eutectic carbide. Any fracture toughness increase gained by refining eutectic carbides is said to be not retained when secondary carbides are present in the matrix after heat treatment (141). The toughness of the as-cast austenite matrix irons was also lower when patches of carbide precipitate were present (141). Durman (134) found in austenitic alloys that fracture paths tended to follow strain induced martensite which formed in lower carbon irons, whereas in higher carbon irons the eutectic carbides controlled fracture. A summary of the general effects of matrix structure is given in table 3.4. The term spheroidite is used to describe a microstructure of general spheroidal carbides in a ferrite matrix (45). Toughness requirements dictate therefore that a low carbon iron should be selected, but process reasons and the demands of abrasion resistance require higher carbon contents. From a practical viewpoint higher carbon levels are preferred for two reasons. Firstly they enable the use of pig iron in place of low carbon steel scrap and the use of higher

carbon ferrochromium. Secondly if the carbon level is reduced from 3 to 1% in a 15% Cr iron the melting temperature increases from 1275 to 1450°C and this is accompanied by a widening in the freezing range (134). As well as being more costly to melt the lower carbon irons would be more prone to shrinking defects and this could seriously influence toughness since shrinkage pores are likely initiation sites for fracture. The problem could be magnified in heavy sections where it is common practice to accept a certain amount of central unsoundness provided it is limited to the interior of the casting.

3.9 Abrasion resistance and service performance.

The abrasion resistant alloy white irons compete with a range of other abrasion resistant materials including steels (144-153), hardfacing alloys (154-162), ceramic materials (163-172) and rubbers (173-177). When selecting a material for a given application consideration must be given to the service requirements of the wearing part, to its method of production, to its ease of installation and replacement and to the costs involved. The relative performance of available materials must also be known with respect to the expected conditions of service. This information should result from the use of controlled service trials to reinforce data from laboratory wear tests.

There is extensive literature on selection and performance of abrasion resistant materials much of which relates to specific applications or industries (178-200). This literature has been discussed in detail with respect to gouging wear, high stress abrasion and erosion (85). The present review is limited to high stress abrasive wear encountered in grinding applications but some brief comments on both gouging and erosion are considered relevant to the overall discussion.

3.9.1 Gouging abrasion.

Resistance to gouging abrasion and its associated impact damage is important in many applications ranging from crushing

plant to materials handling. To resist gouging Hadfield manganese steel is the normal choice (90, 114) since its toughness and plasticity is such that fracture under impact conditions seldom occurs in service. The limitations to the use of this steel are the problem of spreading and lack of work hardening in certain applications. This means that alternative materials such as low alloy martensitic steels, low-medium carbon grades of high chromium irons, ceramics and rubber are also used, the final choice depending on the levels of impact expected in a given application. The stresses from impact blows can be estimated but Avery (4) suggests that the usual recourse in material selection is to choose a material that is somewhat tougher than necessary following the principal that sudden failure should be avoided even at the expense of rapid wear. Gouging conditions involving high levels of impact are met by scraper and dipper teeth (178, 179), gyratory and cone crusher mantles and liners (77, 151, 180), roll and jaw crushers (180), hammers and liners in hammer mills (2, 180). Lower levels of impact are encountered in tertiary stage roll and jaw crushers, in screen decks, shovels and chutes (180).

Figure 3.16 and table 3.6 illustrate how various materials compared in a laboratory jaw crusher gouging test described earlier. Although the results show that steels and cast irons with martensitic matrix structures show greater gouging resistance than austenitic matrices (71),

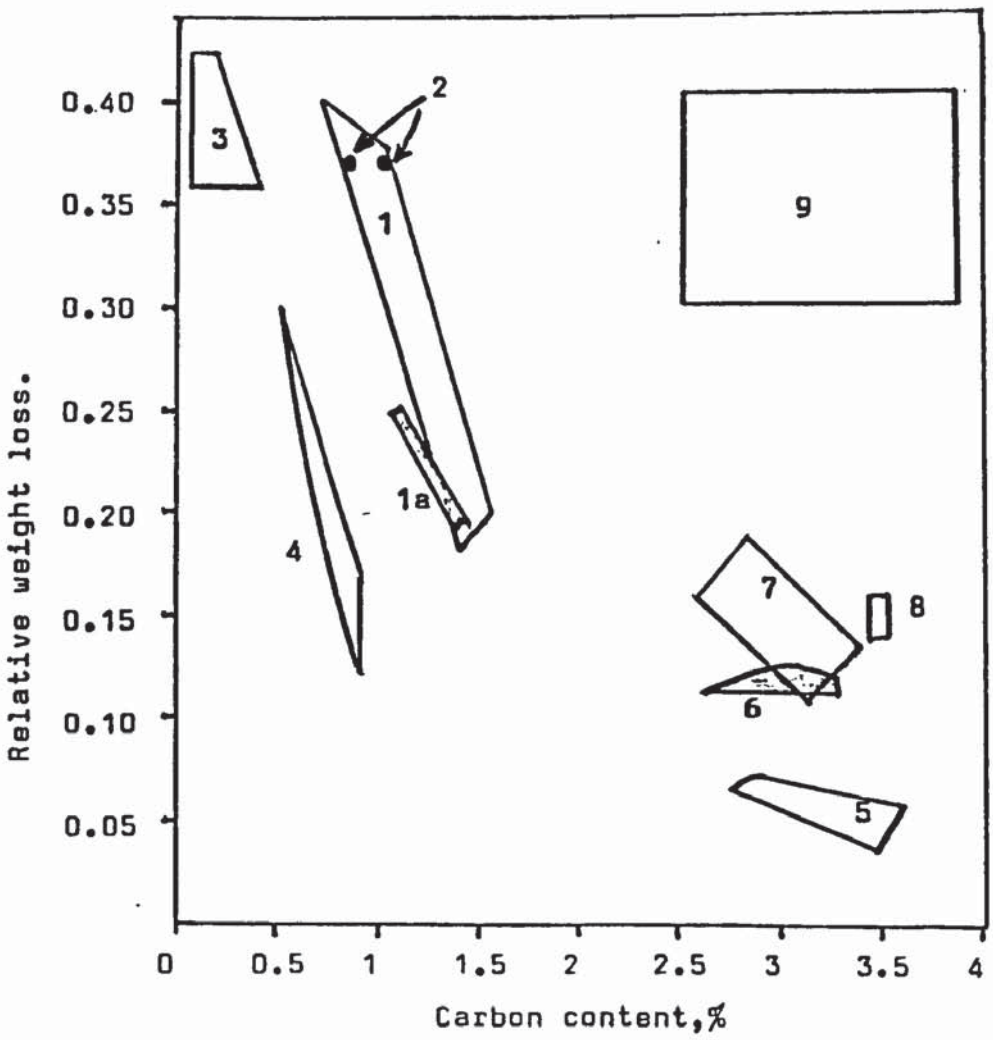

1.Austenitic 12% Mn steels.
1a.Austenitic 6% Mn-1% Mo steels.
2.Pearlitic cast steels.
3.Quenched and tempered wrought steels.
4.Quenched and tempered Cr-Mo steels.
5.Martensitic 15% Cr-Mo irons.
6.As-cast 12-20% Cr-Mo irons.
7.Quenched 26% Cr irons.
8.6% Ni-9% Cr irons.
9.Pearlitic white irons.

Figure 3.16

Laboratory jaw crusher test results.

After (84)

GOUGING ABRASION TEST RESULTS

Material	C, %	Condition[1]	BHN Before Test	BHN After Test	Wear Ratio
ALLOY STEELS					
Type 304 Stainless Steel	0.08	Annealed	165	377	1.192
Type 316 Stainless Steel	0.04	1900 F (1035 C) WQ	193	381	1.291
AISI 4340	0.40	1750 F (955 C) AC	320	368	0.674
AISI 4340	0.40	1600 F (870 C) OQ + 450 F (230 C)	520	627	0.232
AISI 4340	0.40	1600 F (870 C) OQ + 1200 F (650 C)	340	356	0.716
Ni–Co–Mo Maraging Steel	0.01	1500 F (815 C) AC + 900 F (480 C)	419	431	0.705
6 Cr–1 Mo	0.90	1950 F (1065 C) AC + 450 F (230 C)	600	642	0.112
6 Cr–1 Mo	0.90	1950 F (1065 C) AC + 1000 F (540 C)	600	623	0.148
Pearlitic Cr–Mo Steel	0.60	1800 F (980 C) AC + 1050/1100 F (565/590 C)	326	344	0.377
Pearlitic Cr–Mo Steel	0.85	1800 F (980 C) AC + 1050/1100 F (565/590 C)	342	362	0.379
AUSTENITIC MANGANESE STEELS					
6 Mn–1 Mo	1.27	1900 F (1035 C) WQ	200	440	0.192
6 Mn–1 Mo + Ti	1.23	1900 F (1035 C) WQ	200	436	0.170
12 Mn	0.93	1900 F (1035 C) WQ	185	400	0.328
12 Mn	1.00	1900 F (1035 C) WQ	199	461	0.279
12 Mn	1.24	1900 F (1035 C) WQ	198	375	0.212
12 Mn	1.27	1950 F (1065 C) WQ + 140 F (60 C)	211	411	0.207
12 Mn–1 Mo	1.12	1950 F (1065 C) WQ	–	–	0.244
12 Mn–1 Mo + Ti	1.23	1950 F (1065 C) WQ + 140 F (60 C)	204	451	0.209
12 Mn–1 Mo + Ti	1.28	1950 F (1065 C) WQ	200	512	0.200
12 Mn–1 Mo + Ti	1.28	1950 F (1065 C) WQ	200	512	0.182[2]
HIGH-CHROMIUM IRONS					
12 Cr–0.7 Mo	3.25	1750 F (955 C) OQ + 400 F (205 C)	712	–	0.073
15 Cr–3 Mo (LC)	2.51	1850 F (1010 C) AC + 450 F (230 C)	716	–	0.076
15 Cr–3 Mo (HC)	3.60	1650 F (900 C) OQ + 400 F (205 C)	870	–	0.048
15 Cr–2 Mo–1 Cu	3.26	As Cast	477	551	0.093
15 Cr–2 Mo–1 Cu	3.32	1750 F (955 C) AC + 400 F (205 C)	726	–	0.072
20 Cr–2 Mo–1 Cu	2.87	As Cast	503	547	0.109
20 Cr–2 Mo–1 Cu	2.89	1750 F (955 C) AC + 400 F (205 C)	706	–	0.081
27 Cr	2.68	As Cast	481	555	0.135
27 Cr	2.58	1850 F (1010 C) AC + 450 F (230 C)	662	719	0.144

[1]AC = air cooled OQ = oil quenched WQ = water quenched [2]Crushing taconite

Table 3.6

Results of gouging abrasion tests. (72)

	Material	Wear Index
1	Ni-Cr martensitic white cast iron	0.065
2	Cr-Mo-W-Nb hardfacing	0.079
3	High-chrome martensitic white cast iron No.1	0.115
4	Nodular graphite-based cast iron	0.137
5	Fusion-cast alumina special	0.172
6	Sintered alumina	0.173
7	Tungsten carbide hardfacing	0.192
8	Fusion-cast alumina	0.221
9	Low-alloy steel plate, quenched and tempered No.2	0.382
10	Slagceram	0.518
11	Low-alloy cast iron	0.704
12	Fusion-cast basalt	0.846
13	Low-alloy steel plate, quenched and tempered No.1	0.952
14	High-phosphorus pig iron	0.953
15	En8 steel plate	1.000
16	Low-alloy steel plate, quenched and tempered No.3	1.336
17	Acid-resisting ceramic tile	2.030
18	Silicon carbide ceramic No.1	2.265
19	Polyurethane No.5	2.490
20	Silicon carbide ceramic No.2	4.710
21	Concrete No.3	6.350
22	Silicon carbide ceramic No.3	8.470
23	Concrete No.2	10.320
24	Concrete No.1	18.000

(a) Sliding abrasion.

	Material	Wear Index
1	Cr-Ni-Mo martensitic white cast iron	0.144
2	Ni-Cr martensitic white cast iron	0.157
3	High-chrome martensitic white cast iron No.1	0.158
4	Nodular graphite-based cast iron	0.274
5	High-chrome hardfacing	0.295
6	Fusion-cast alumina	0.323
7	Extruded alumina	0.350
8	13% Mn cast steel	0.536
9	Low-alloy cast iron	0.595
10	Low-alloy steel plate, quenched and tempered No.3	0.750
11	En8 steel plate	1.000
12	Concrete No.4	1.110

(b) Medium impact abrasion.

(Low value of index indicates high wear resistance)

Table 3.7

Wear indices of materials subjected to abrasion by blast furnace sinter. After Hocke (186)

the latter are almost invariably used as crusher linings since the former tend to break in service (77). Improvements in materials for use in crushers have been limited to modification of austenitic (12-14% Mn) steels using molybdenum (151), to the use of high carbon, Cr-Mo white iron hardfacing on wear zones (77), to reinforcement of martensitic irons by cast in members (182) and to the use of composite structures in which martensitic iron is bonded to and supported by a tough steel backing (130, 183).

Service conditions involving the handling of crushed material are somewhat less severe than those encountered in crushing. Impact forces tend to be lower and less tough materials can be considered for use. The performance of several materials including alloy irons has been assessed by Hocke (185, 186) who tested chute materials subjected to wear by coke and sinter. On a cost-wear basis martensitic alloy white irons were said to be the most economic choice. Examples of wear performance are given in table 3.7.

3.9.2 High stress (grinding) abrasion.

Selection of materials to resist high stress abrasion is important in grinding applications such as mill liners and grinding media and crushing discs and rolls. Typical applications and examples of materials selected and their performance are given in a number of papers (2, 7, 25, 44, 45, 53, 73, 74, 76, 77, 90, 107, 114-6, 126, 147, 163, 176, 177, 180, 187-191).

As previously discussed the major problem is to obtain a material which combines wear resistance with toughness although final choice will depend also on material availability, replacement costs and the importance attached to avoiding product contamination. The latter arises from abraded metal fragments from liners and the grinding media which may cause discoloration of ceramic, pottery and paint pigments, may be poisonous in foodstuffs or be detrimental in later production processes such as ore flotation separations where they can act as a depressent.

Much of the development of metallic and other materials for grinding has been aimed at reducing the high consumption due to wear in ball mills. For example at one plant metal loss due to wear in all operations was estimated at 0.8 kg per ton of ore processed and about 85% of this was attributed to loss in grinding balls and mill liners (4).

A ball mill is a cylindrical vessel which rotates on its horizontal axis. As the mill rotates a stepped lining or lifter bars lift the balls and charge up the rising wall of the mill imparting a cascading action and giving rise to fragmentation of the charge material (pulp) between balls and between balls and liner plates. Materials ground in this way include metallic ores, refractories, coal, limestone, shale, cement etc. Grinding will involve varying levels of impact depending on the size and speed of the mill and may be

performed under dry or wet conditions. Grinding operations may take place in a number of stages in primary, secondary and tertiary mills depending on the sizes of pulp particles ground which range from 6-8 mm (from crushers) down to -100 mesh. In the cement industry all three stages are combined in a single multiple chamber mill. Figure 3.17 is a view of the interior of the first chamber of a dry cement mill showing stepped lining plates, the ball charge and diaphragm segments which separate adjacent chambers and classify ground material. Mill shell liner plates generally have section thickness ranging from 110-170 mm and weights of 150-350 kg.

The grinding balls used generally range from 120 mm down to 12 mm in diameter, the larger balls being used for larger particle feed sizes and harder materials and smaller balls or cylpebs for small particle sizes. The action by which the balls grind is determined by the speed of revolution of the mill and by the load factor (the volume of the charge of ball + pulp relative to that of the mill) (177). At low speeds or high load factors the balls roll against each other and the pulp is broken down by pressure and friction. The balls move in layers as is illustrated in figure 3.19 (a). As speed increases the balls rise to a higher limit point from which they are thrown from the shell and move in paths as shown in figure 3.19 (b). The speed and load factor should be such that the balls then fall against the charge and not the liners causing fragmentation by impact crushing.

Figure 3.17

Interior of first chamber of dry cement mill showing stepped lining plates, ball charge and diaphram segments.

Figure 3.18

Specification for ball mill parts. After (90).

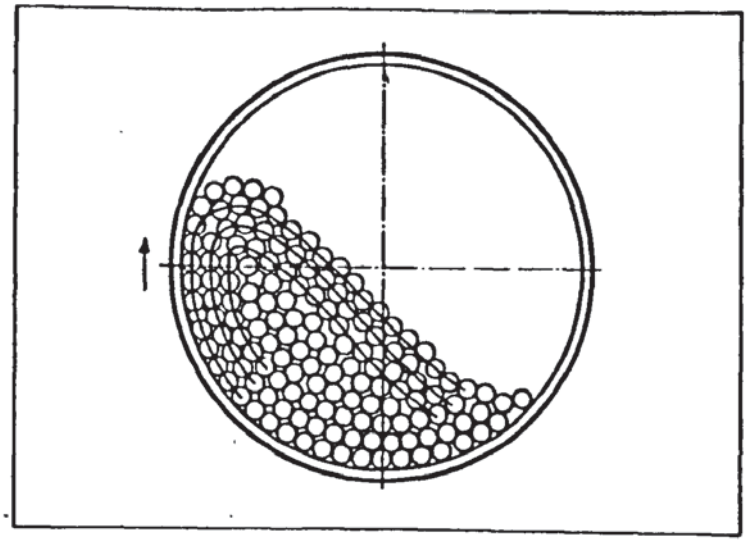

(a)at low speeds

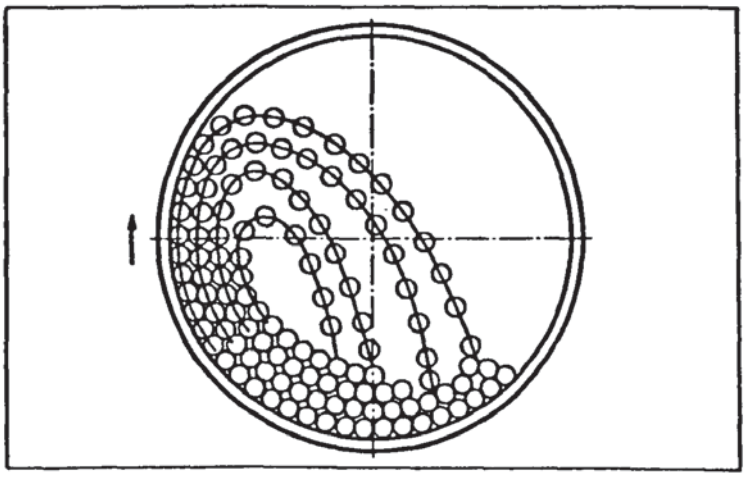

(b)at higher speeds

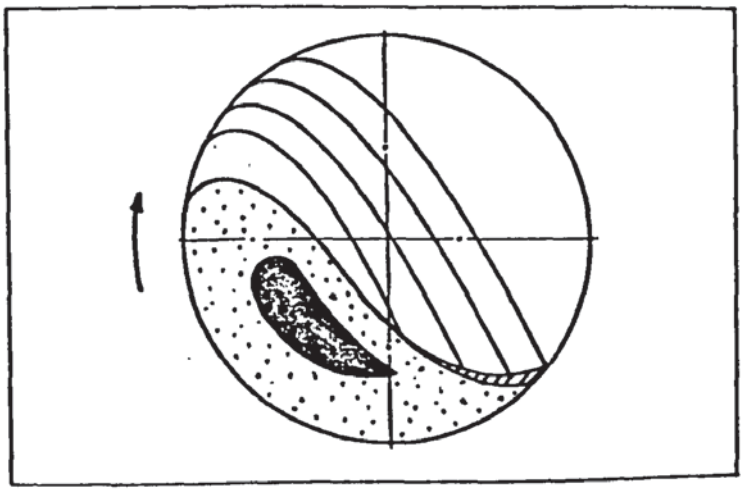

(c)grinding areas

Figure 3.19

Movement of balls in a mill and grinding action.

After (177)

The combined grinding effect is shown in figure 3.19 (c). In the dark shaded region grinding results from friction between balls, in the lighter shaded region grinding is said to result from compression and shear forces between the balls and the pulp and the cross hatched region grinding results mainly from impact crushing (177). The point at which the balls are thrown from the shell depends on the profile of the lining or lifter bars and this will influence grinding efficiency and impact loads on the balls.

The revolving speed of the mill should be sufficient to cause cascading but should not exceed a critical value at which the load centrifuges. Wear of media and liners has been found to be at least as proportional to the square of the mill speed (190). Higher speeds can also reduce charge pressure by increasing the cataracting effects resulting in less efficient grinding and can give more impact damage since the balls are thrown onto the opposite shell wall above the toe of the charge (176). For example in a mill grinding sulphide ore at a speed of 93% critical the life of the steel lining was 5800 hrs, when the speed was reduced to 62% critical the lining lasted 18,000 hrs. Mill speed is of even greater significance when rubber linings are used. Other factors influencing wear are relative hardness and sizes of balls and pulp particles, mill diameter and mill retention time.

The historical development of mills and wear resisting materials has been reviewed by Norman (163) and Dodd (188-9). Over the last twenty five years the trend has been to replace batches of smaller 300-450 hp mills by larger diameter + 3000 hp single units. Approximate maximum diameters quoted (163, 189) at the present time are 5 m for rod mills, 6 m for ball mills and about 10.5 m for autogenous mills where the ball charge is replaced by pieces of ore (100-500 mm in diam.). Typical wear performances by ferrous materials in mills has been given earlier in table 2.3. The majority of smaller mills were once lined with either pearlitic or high manganese steels and grinding balls of over 40 mm dia were always forged. Steels suffer from high wear rates but they are still used in applications involving high impact conditions due to their superior toughness. The wear rates given in tables 2.3 were obtained during milling a high silica ore and this has resulted in a smaller range in wear rates of different materials than would be obtained with a less abrasive material. Experience has shown that under less arduous conditions and in rod or autogenuous mills for the same materials greater differences in relative wear rates are found although their ranking remains the same (7, 163).

The present trends in the use of hard linings involve the replacement of pearlitic high carbon steels by more abrasion resistant martensitic steels and irons. The former were used because of their relatively low first cost and in

USA much of this steel was used in the form of worn railway rails but some was specially made into liners from rolled plate (163). Pearlitic white irons which were also in widespread use because of low cost have also been replaced by alloy martensitic irons except in wet applications where wear rates are very high for both types of material (90, 114, 163, 189).

The most promising steels for grinding abrasion resistance appear to be the medium carbon low alloy (Cr-Mo) series which may be wrought or cast. They contain 1-2% Cr, 0.5% Mo, 0-1.5% Ni and are oil hardening. They are said to be suitable for use under high impact conditions and have generally completely replaced the less abrasion resistant 12% Mn steels. However, higher carbon series have been limited in their development due to cracking problems both in foundry production and in subsequent service (163).

As an alternative to steels three types of alloy irons have been used in ball mills, they are the martensitic Ni-Cr irons (Ni-Hard), 25-27% Cr irons and 15% Cr - 3% Mo irons. The Ni-Hards have tended to replace steels as liner material in small (low impact) mills or where the size of the grinding balls is limited (90). For example in the second chamber of cement clinker mills where steel linings lasted only 2-3 years Ni-Hard replacements have given lives of over 10 years (188). Attempts however to use Ni-Hard

in the coarser chamber were less successful due to the use of larger balls and due to greater exaggeration of liner plate contours. Some improvements were obtained by redesigning the liner plates to be smaller and thicker but spalling was still a problem particularly when the balls used were made in 25% Cr - 3% C iron. Hence the Ni-Hard liners have been replaced by 25-27% Cr irons with slightly higher carbon levels than the balls (188). Figure 3.18 shows the present stage of lining development for dry cement mills. It is seen that in the first chamber the high chromium irons have themselves been replaced by 15% Cr - 3% Mo iron with carbon levels of about 2% to ensure adequate toughness (90). In ore grinding also the 15% Cr - 3% Mo irons are replacing quenched and tempered low alloy and austenitic manganese steels for both shell and end liners in ball and autogenous mills (2) although under more severe conditions of ore grinding e.g. for very hard ores such as taconite or for wet milling the advantages of the higher chromium irons are less pronounced.

In the last fifteen or so years metallic liners have faced increasing competition from rubber materials which are claimed to have several important advantages (173, 176-7). These include longer life and no corrosion or breakage problems, reduced maintenence costs and downtime, more predictable wear rates and pattern of wear, noise reduction, low weight permitting easy handling and installation and

reduced driving power consumption and loads on mill bearings. To date economical use of rubber liners has been limited to fine grinding conditions where there are no larger angular particles in the feed material since these can cut into the rubber giving rapid wear (163). For optimum use of rubber linings it is recommended that as small as possible grinding balls should be used (176). The rate of rubber linings wear is also highly dependent on mill speed and it has been found that at speeds over 80% critical wear rates become so high that the use of rubber is uneconomical (177). Since many mills operate at speeds above 75% critical, Norman (163) suggests that rubber liners will need to undergo significant improvements with respect to rubber properties or liner design for them to be competitive with steel or iron liners. The use of rubber is also limited in dry grinding applications by restrictions to maximum working temperatures of 100^{o}C. Norman also suggests that rubber linings are unsuitable in rod mills although claims by rubber liner producers (176) say that they can give more than satisfactory performance so long as the mill head remains lined with steel to avoid risks of rod spearing. The high elasticity of rubber has allowed it to successfully replace steel as the material for end grates in grate discharge mills. Since rubber grates reinforced by steel reduce unnecessary stops and high maintenance costs that were associated with the clogging of steel grates by pieces of grinding media (176-7). The most likely area for the successful use of rubber liners appears

to lie in the field of fine grinding particularly under wet conditions.

It is in this area where polyurethane materials are currently being examined with respect to their behaviour in controlled service trials (191). To date polyurethane has given disappointing performance when used as a liner plate in a mill grinding wet chalk and clay for cement production using a nominal 90 mm dia. ball charge and pieces of railway line (125 mm in length). Wear was produced over the entire working surface of the polyurethane plates and was most severe near the inlet end of the mill causing them to be replaced after 1080 hours service. The usual material for mill lining plates is a 25% Cr - 3% C iron which generally lasts for about 7000 hours and usually fails through breakage and not excessive wear. Such service conditions appear to be too severe for rubber or polymer type materials unless mills are redesigned to use smaller balls and to avoid the use of larger angular pieces of material such as the railway line lengths which are included to prevent balling of the charge. At present it seems that polyurethane is likely to be restricted to its already successful use in low stress abrasion (175).

One type of high stress grinding application in which rubber type materials are less likely to be of use is for the roller and tracks of pulverising equipment used to grind

coal for power stations, limestone, cement and phosphate ore (2, 84, 90). For this type of service steels have generally been replaced by martensitic Ni-Cr irons and high Cr irons which give between 4 - 5 x improvement in life for both rollers and tracks. As for ball mills the trend towards larger units and more output means a constant demand for improvements to be made both in general properties and abrasion resistance. The alloys currently receiving most attention for continued use and development in pulverising are the 15 - 20% Cr, 2 - 2.8% C irons containing both molybdenum and nickel additions to improve hardening response.

3.9.3 Low stress abrasion

Low stress abrasion, scratching abrasion or erosion is the main form of wear in mixing, handling and transport of fine grained solids, slurries or liquids contaminated with fine particles. Typical applications involving this type of wear are sand milling, sand and shot blasting, slurry pumps, hydro-cyclones, classifiers, plough shares in sandy soils, chutes etc. A number of studies has been made to evaluate suitable erosion resistant materials (69, 81-84, 192, 193). It is generally considered that since impact resistance is a minor consideration the higher the hardness of a material then the greater is its resistance to low stress abrasion. However, recent work (192) has suggested that hardness of microstructurally heterogeneous solids such as white irons

is a poor indicator of resistance to this form of wear. The volume fraction and dispersion of hard carbides is said to be the main factor which controls erosion resistance (192). At present the most commonly used materials are Ni-Hard (53, 90) or 15% chromium - 3% molybdenum iron (2, 77) the former material being selected where the complex nature of a casting such as a pump part would cause heat treatment problems and a high hardness is required in the as-cast condition (90). For applications where impingement angles of the abrasive on a surface are high and cutting wear is minimal rubber materials may also be considered (144, 173). In contrast where impingement angles are small and cutting wear prevails very hard ceramic materials have been successfully used (21, 168, 169). This latter group are claimed to be finding increasing application as liners in pipes transporting powders, slurries, cereals etc. (168) where erosion is a problem at bends and as pump parts where metallic materials suffer from corrosion and erosion damage (168, 169). Impellors and housings for pumps are one group of components for which conventional cast alloys, rubbers and ceramics are competitive materials. Apart from basic wear resistance, selection will also depend on resistance to corrosion, complexity of shape, need for machining, size and cost, etc. Typical applications for abrasive handling pumps include handling of mineral slurries in ore preparation, slurried ash, sand and gravel from quarries and on dredgers. Chromium irons containing molybdenum are being increasingly used in pump manufacture

since they are said not only to have better abrasion and corrosion resistance and better toughness than Ni-Hards but also are capable of being machined after suitable annealing (2). Durman (90) also reports that an as-cast 25% Cr iron has been in successful use in pumps handling gravel dredged from the sea bed, an application requiring toughness (gravel sizes range 3-50 mm) and corrosion resistance. It is generally accepted that Ni-Hards or high Cr irons give about 2 - 3 X better life than either 12% Mn steel or Cr-Mn-Mo martensitic steels when used in a variety of pumps (83, 90). In erosive wear tests to determine the most suitable alloy for use as cylindrical pump liners Shabuev (83) found that maximum wear resistance corresponded to near eutetic composition in chromium irons (see figure 3.20). The reduction in erosion resistance at high carbon levels was said to be due to the presence of brittle hypereutectic carbides. The best results were obtained with an iron containing 30% Cr and 2.4 - 2.9% C corresponding to optimum erosion and corrosion resistance. In fact 30% chromium irons are the subject of current development to improve resistance to combined corrosion and abrasion under both high stress (e.g. wet milling) and low stress (e.g. pumps) conditions.

Because of their resistance to chemical attack rubbers and polyurethane are often employed as liners in slurry pumps and as pump wheels and agitators (192). The rubber is usually bonded onto a light weight steel casing or section and this

is claimed to give easy installation. Polyurethane has also been considered for use in pipelines handling steelworks slurries (193) and for plates and guards in shot blast cabinets where it has given promising results when used in positions not too close to the impellor wheel. Impellor blades have been made of polyurethane but have been reported to be unsatisfactory for use with metallic shot. However, complete impellor wheel and blade assemblies of polyurethan have been successfully used in sand reclamation plants (175).

For use with metallic shot impellor blades of high chromium iron are claimed to give maximum wear resistance. A typical composition is 25% Cr, 2.8%, 1% V and the iron is used in the hardened condition. It has been found that the wear on shot blast blades is markedly affected by impellor wheel design and blade arrangement (195). Improvements in design can reduce the severity of the eddy currents which can produce severe localised wear and the smoother shot flow is also combined with less shot bounce on the blade faces (196).

In erosion wear contamination can also influence wear rates. For example contamination of shot returning to the impellor wheel can cause large increases in wear in the shot blast equipment; 2% by weight of sand contamination has been found to increase wear by up to 5 times. Where rubber materials have been used in pumps and in Humphrey spirals contamination of ore slurry by flotation oils has led to

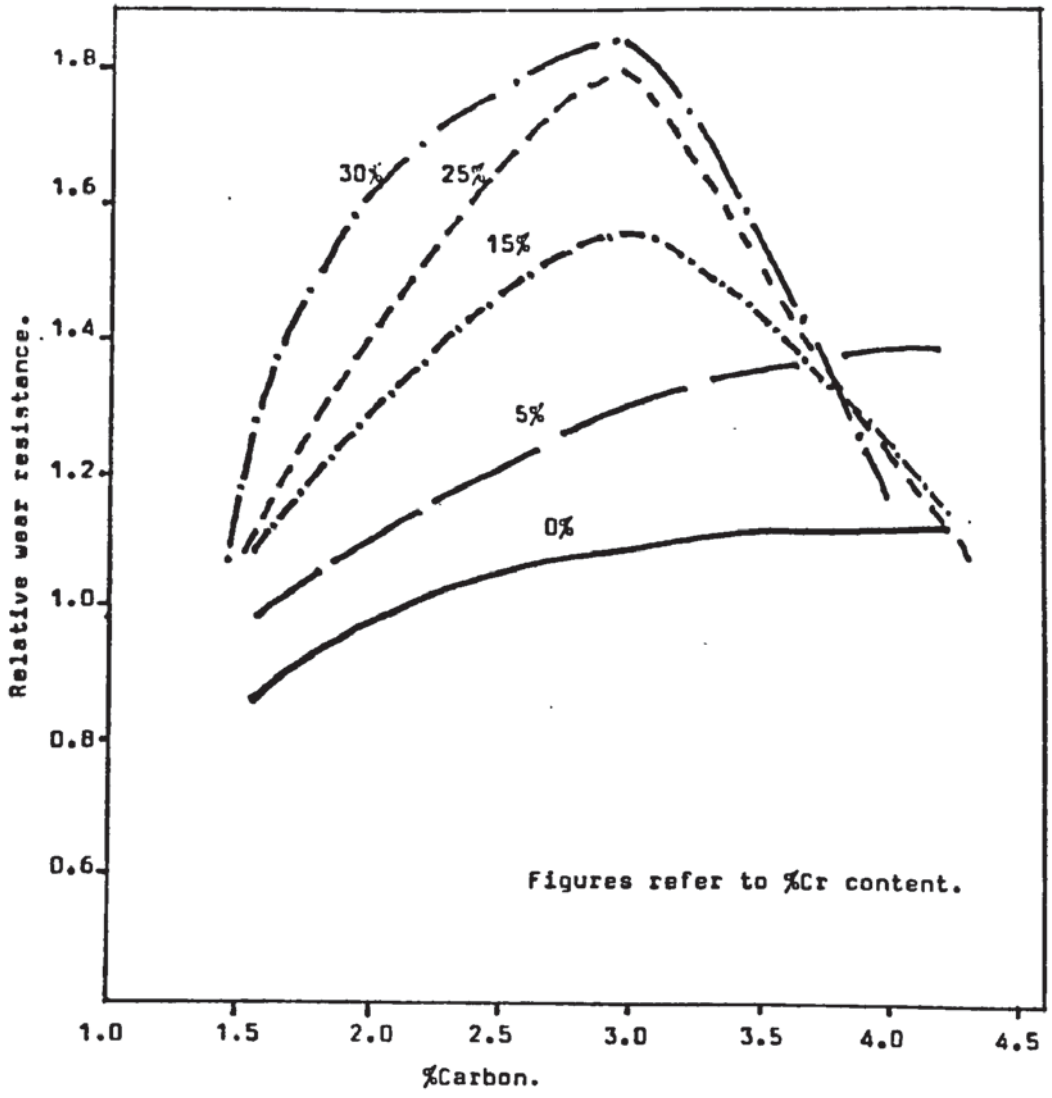

Figure 3.20

Relative low stress abrasion resistance of chromium irons.

After (83)

Application	Ball diameter (mm)	Weight Loss (gm./tonne ground) Superwet	White Iron	Forged steel
Wet raw cement mill				
First chamber	90-60	50-100	-	200-500
Second "	60-30	50-100	140-160	200-300
Third "	25-20	50-100	130-150	200-250
Iron ore--semi-dry	60-30	70-150	-	300-500
Iron ore--wet	60-30	100-200	250-750	400-1000

Table 3.8

Comparative wear losses for wet grinding.

After (200)

fairly rapid deterioration of the rubber (77).

3.9.4 Abrasion in corrosive environments.

The problem of combined abrasion and corrosion has already been introduced in section 2.4.4. It was noted that some authors considered that under "wet wear" conditions corrosion played a significant part in producing higher wear rates while others suggested that under wet wear these higher rates were due to a change in the physical nature of the wear or due to the enhanced fracturing of the abrasive. In either case the result is that for wet wear conditions the differences in wear rate between the most abrasion resistant material and the least resistant become much smaller. Hence the wear resistance: cost ratio for the more expensive highly alloyed cast irons has not to date been sufficiently large enough to encourage their use at the expense of cheaper materials such as steel or low alloy white irons in wet applications, particularly wet milling. The only other alternatives to cheap steels or white irons are rubber materials or ceramic materials.

One area of current development is the use of 28 - 30% chromium levels combined with up to 1.5% molybdenum in irons containing 2.5 - 2.7% carbon (197). The molybdenum additions are designed to improve hardness and hardenability and to improve corrosion resistance by replacing chromium in alloy carbides thus allowing more chromium to remain in the matrix

to encourage passivity. At these higher Cr levels both chromium and carbon must be carefully controlled to produce a hardenable austenitic iron instead of a non hardenable ferritic matrix which is favoured by the presence of molybdenum and also faster cooling rates.

An alternative development may be the use of smaller additions (up to 5%) of chromium to improve the performance of cheap unalloyed white iron which has had widespread use in media in small diameter wet mills. Further investigation could examine the effects of rare earth additions which are claimed by Soviet workers to improve erosion-corrosion resistance of high chromium irons (198, 199).

A comparison between the 30% Cr (Superwet) alloys and cheap low phosphorus unalloyed white irons and forged steel balls is given in table 3.8. The Superwet material is said to be up to six times more wet wear resistant than forged steel and can be produced in balls up to 90 mm dia. Unalloyed white iron is limited to 40 mm diameter due to its brittleness (200).

4.0 ABRASIVE WEAR STUDIES.

4.1 Development and construction of wear testing apparatus.

In the preceeding literature review it was seen that a wide variety of both in-service and laboratory testing procedures have been developed to study the various forms of abrasive wear. It was decided to confine the present work to high stress abrasion in order that the information obtained might prove useful in understanding the high wear rates in grinding media and liners. It was also thought that high stress abrasive wear damage could be more easily studied in a simulative laboratory test rather than attempt to examine material after use in production mills. Of the simulative high stress abrasion tests developed it appeared that the most reliable and reproducible results were obtained when specimens slide over a circular track while immersed in wet or dry abrasive (4, 10, 14, 25). Such a test is claimed to have been validated by ball mill production tests (4, 10). A wear test apparatus was therefore developed on the basis of specimens under load sliding on a track in the presence of a suitable abrasive material.

The apparatus was constructed from a foundry core sand mixer which had been converted to a bowl grinding abrasion test. This test which involved the rotation of finger type specimens in loose abrasive had proved unsatisfactory for abrasion resistant white irons since it

had given very low rates of wear (201). The mixer was further modified by the fixing of a grey iron track which is held in position by three equidistant plates as illustrated in figures 4.1 and 4.2. A support and loading arrangement was then built on to the centre drive shaft of the mixer so that two specimens could be tested together.

Grey iron was used as the track material since it is softer than alloy white irons and was thought likely to wear away in an even manner. A number of tracks were cast and the pattern equipment remained available to produce further tracks if required. The internal diameter of each track was 300 mm and its width was 20 mm in the initial series of tests. The track width was reduced to 16 mm for later series of tests. The apparatus was powered by a 2 HP electric motor and the centre shaft rotated at 90 rpm to give a linear speed of the specimens over the track of 1.4 m/sec.

The type of specimen selected for the abrasion tests was based on that which was claimed to be successfully used by previous workers (4, 10, 14). Details of the specimen and holding shoe arrangement are given in figure 4.3 The angled faces at the front and rear of the specimen ensure ease of entry and exit of the abrasive particles between the specimen and wear track. The specimens were cast to shape but were made slightly oversize so that the casting skin could be removed from each face by grinding. The face to be abraded was then finished ground to remove 1 mm depth.

The abrasive selected for the tests was a clean washed silica sand which is normally used for foundry mould production. Silica sand was chosen since it could be readily obtained in consistent quality with a controlled particle size range. In addition quartz is commonly found as gangue material in minerals which are to be crushed and ground. The sand used in the tests was Chelford 60 sand which has a mean particle size of 245 μm and grains which are round to sub-rounded in shape with medium sphericity (202). After a few trial runs it was found that 7 kg of dry sand was suitable for satisfactory operation of the test in that there was sufficient sand covering the track to produce wear without unnecessary overloading of the mill.

4.2 Selection and production of alloys for wear testing.

The nominal compositions of iron produced for use as wear test samples are as given in table 4.1. The unalloyed 3% C white iron (iron 9) was selected as standard material for use in initial proving of the wear test method and for later comparison purposes with the alloy irons. The 3.5% C - Cr - Mo iron (iron 10) was produced so that when tested in the fully hardened condition it would provide a guide to the smallest wear rate to be expected. This is because this material is believed to give the highest resistance to high stress abrasive wear of all the alloy white irons.

The series of 0 - 35% Cr irons (irons 1-8) was selected since it covers the complete range of chromium contents commercially used for abrasion resistance. With increasing chromium content the form of the eutectic carbides is expected to change from the continuous M_3C type to the discontinuous M_7C_3 type. In addition the form of the matrix will change from pearlite to austenite and then to ferrite in the as-cast irons and heat treatments can be used to produce martensitic matrices. As chromium content increases the carbon contents are reduced in order to ensure a hypoeutectic composition and so avoid the formation of coarse primary carbides. The carbon contents have been selected to follow the line xy in figure 4.4 so that there will be approximately the same proportion of eutectic carbide in each iron. The line xy follows the normal level of carbon in commercial 15-27% chromium irons.

4.2.1 Production of test samples

All the irons were melted in a 50 kg capacity acid lined high frequency induction furnace using commercial purity raw materials. A furnace temperature of 1550°C was used to ensure complete solution of ferrochromium and the irons were poured at 1450°C into synthetic greensand moulds. Twelve wear test samples were cast in a box from a common runner bar. Three boxes of test samples were cast from each melt together with a 50 x 50 x 75 mm and a 125 x 125 x 150 mm block.

These blocks were made available so that the influence of section size on wear behaviour could be studied at some future time. They have not been used for wear test specimens in the present work. The analysis of each melt was obtained from coin specimens using an automated direct reading vacuum spectrograph (polyvac). The results are given in table 4.2.

4.2.2 Heat treatment of test samples.

Irons 2-7 and 10 in table 4.1 were subjected to heat treatments which corresponded to industrial practice. The treatments were carried out in small electric muffle furnaces. A controlled atmosphere was not used. The lower chromium irons were hardened by oil quenching whereas the higher chromium irons were believed to have sufficient hardenability after destabilisation to be hardened by natural cooling in air. All the irons were air cooled after tempering. Iron 10 was not tempered so that it could be tested with the highest possible initial hardness. Irons 1 and 9 are normally heat treated and iron 8 is ferritic and consequently non-hardenable.

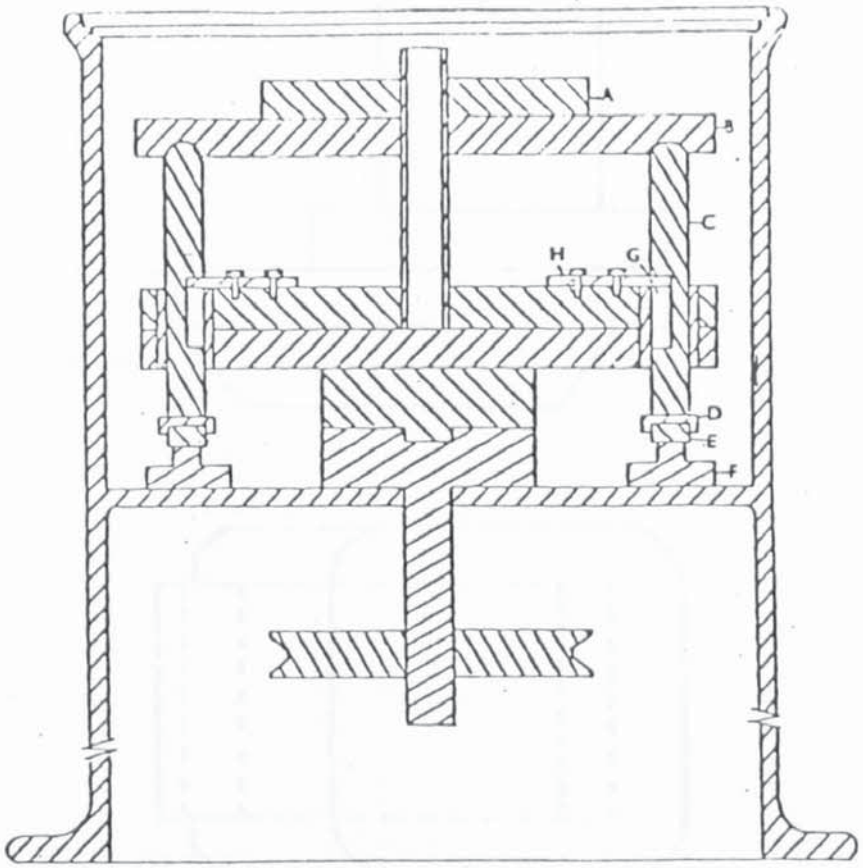

A&B - Applied weights Scale 1:5
C - Arm
D - Shoe
E - Specimen
F - Track
G - Groove
H - Plate

Figure 4.1 Diagram of wear test apparatus.

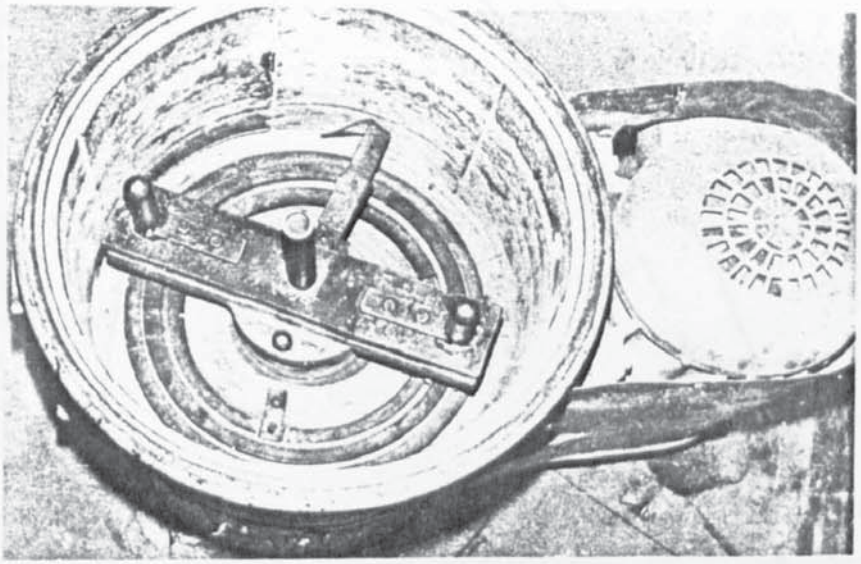

Figure 4.2 Wear test apparatus.

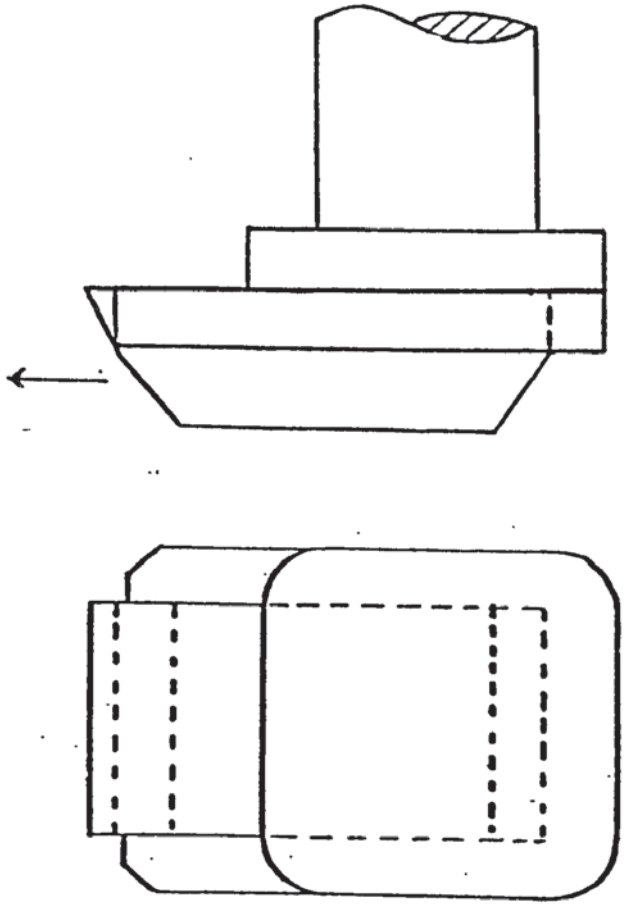

Figure 4.3

Diagram of wear test specimen and shoe arrangement.

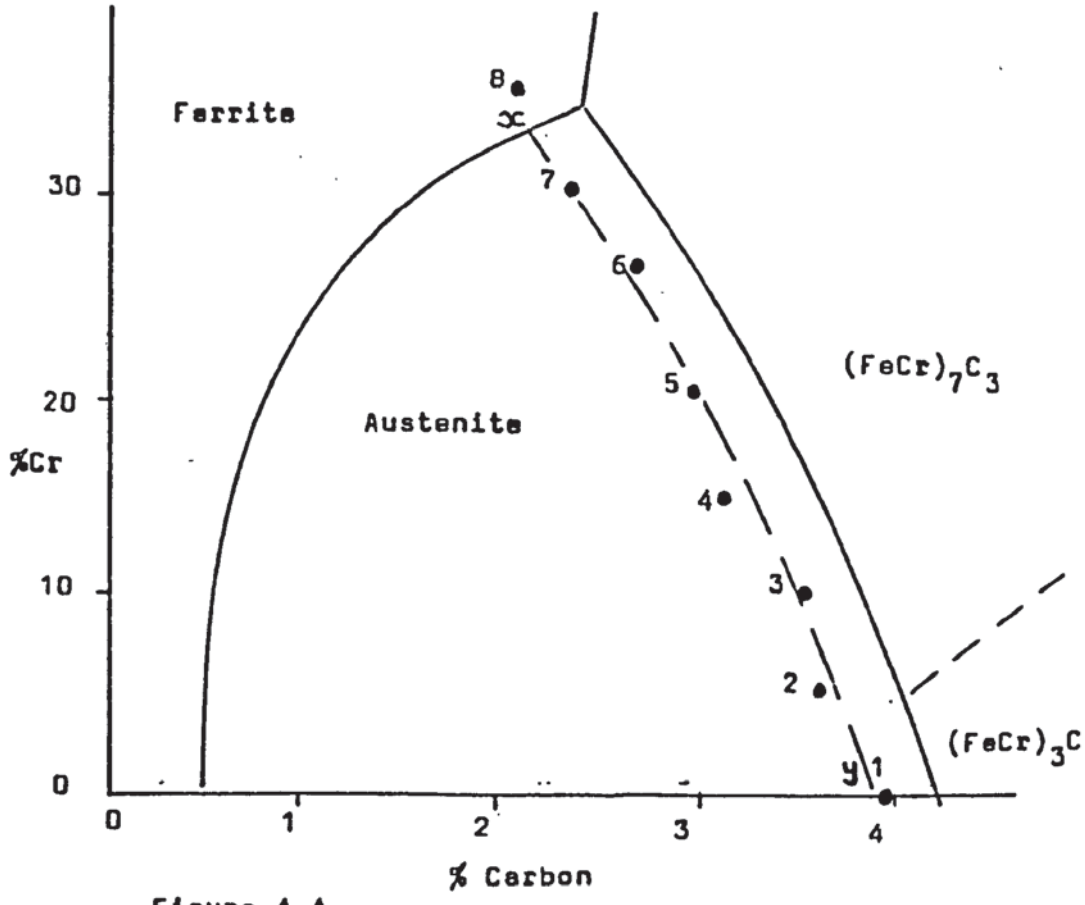

Figure 4.4

Plot of compositions for 0-35%Cr irons.
(Compositions planned to lie along —— ——)

Iron No.	%C	%Cr	%Mo	Heat Treatment
1	4.0	-	-	-
2	3.7	5	-	1hr 900°C OQ, 1hr 200°C AC.
3	3.5	10	-	1hr 900°C OQ, 1hr 300°C AC.
4	3.2	15	-	1hr 800°C FC, 1hr 1025°C AC, 1hr 450° AC.
5	3.0	20	-	" " "
6	2.7	25	-	" " "
7	2.4	30	-	" 1hr 1100°C AC "
8	2.2	35	-	-
9	3.0	-	-	-
10	3.0	15	3	1hr 800°C FC, 1hr 1025°C AC.
				FC-furnace cool; AC-natural air cool; OQ-oil quench.

Table 4.1

Nominal compositions of irons for abrasion testing and details of heat treatments.

Iron No.	%C	%Cr	%Si	%Mn	%S	%P	%Ni	%Cu	%Sn	%Mo	%Al
1	3.99	0.14	0.80	0.22	0.018	0.055	0.07	0.26	0.07	0.02	-
2	3.67	5.54	0.75	0.30	0.020	0.046	0.09	0.21	0.05	0.02	0.003
3	3.57	10.09	0.80	0.26	0.040	0.057	0.11	0.24	0.03	0.02	-
4	3.10	14.68	0.67	0.19	0.031	0.041	0.15	0.24	0.03	0.02	-
5	3.00	20.40	0.66	0.26	0.034	0.047	0.15	0.23	0.02	0.02	0.003
6	2.72	26.60	0.78	0.25	0.025	0.043	0.16	0.22	0.02	0.02	0.006
7	2.44	30.60	0.71	0.21	0.024	0.042	0.17	0.21	0.02	0.02	0.004
8	2.13	36.00	0.75	0.14	0.022	0.041	0.17	0.20	0.02	0.03	0.002
9	2.81	0.11	0.83	0.32	0.030	0.034	0.08	0.27	0.02	0.02	-
10	3.58	14.10	0.62	0.59	0.050	0.032	0.16	0.28	0.02	3.21	-

Table 4.2

Analysis details of irons 1-10.

4.3 Wear testing procedures and results.

4.3.1 Initial series of tests (1-12).

4.3.1.1 Details of tests.

The first series of tests (nos 1-3) were made on iron 9 (3% C unalloyed white iron) in the as-cast condition. The purpose of these tests was to investigate the amount of wear that could be produced using the apparatus. The effects of variations in testing load and test duration were also studied. Test loads of 10.2, 16.7 and 22.6 kg were used for testing times of up to 2 hours. The same procedure was adopted for each test. Each of the two samples was washed in alcohol, dried and then weighed to 0.01 gm using a Oertling single pan balance. The weighed samples were tested for 30 minutes and then removed from the wear apparatus, washed in alcohol to remove abrasive, dried and reweighed. They were then replaced in their original holder shoe on the wear apparatus and tested for a further 30 minute period and again reweighed. This was repeated for a total testing time of 2 hours. Fresh sand was not used for each 30 minute period, the same weighed 7 kg of sand being used throughout each 2 hour test.

Based on the experience gained from the first three tests further tests (Nos 4-8) were performed to determine the

reproducibility of this type of wear measurement. A test load of 10.2 kg was used for five repeat tests on standard 3% C white iron samples. This enabled reproducibility to be assessed from 10 weight loss determinations. Tests 9-12 were then made in order to compare the amount of wear produced in the unalloyed white iron samples with that produced in 3.5% C, 15% Cr, 3% Mo iron samples in the fully hardened condition. This comparison was made at testing loads of 4.3 and 10.2 kg.

All the above tests were carried out using the same wear track which was 20 mm wide and the same batch of Chelford 60 sand as abrasive. Before each test each loading arm (C in figure 4.1) was lightly greased to ensure its free movement during testing. This free movement was also checked after each test.

4.3.1.2 Results of tests.

Table 4.3 gives the weight loss values produced at different testing loads and testing times in iron 9 (2.8% C white iron). Test No. 3 was ended after 1.5 hrs since the amount of wear produced was such that the unworn part of the specimen would not have cleared the track fixing plates if the test had been continued. For ease of comparison these results have been plotted in figures 4.5 and 4.6. Table 4.4 gives the weight loss at different times for 5 repeat tests on iron 9 under a standard load of 10.2 kg.

Tables 4.5 and 4.6 record the respective weight losses in iron 9 and iron 10 (15% Cr 3% Mo fully hardened) when tested at two different loads. For visual comparison the results of tables 4.4 and 4.5 have been plotted in figure 4.7. It is seen from these results that the fully hardened Cr-Mo iron was approximately 2.5 X more abrasion resistant than unalloyed pearlitic white iron. This gave some indication i.e. (4-12 gm) of the weight losses to be expected in the range of chromium irons to be tested. The extent of the wear damage produced in these two irons can be compared in figure 4.8. Figures 4.5-4.7 show that the weight loss-testing time and weight loss-testing load plots followed non-linear relationships. This confirmed previous work (14) carried out on this type of abrasion test.

To assess reproducibility of the test the results of table 4.4 were used to calculate the standard deviation in weight loss determined at testing times of 0.5, 1.0, 1.5, and 2.0 hrs. The standard deviation was calculated using the formula (203):

$$\sigma = \sqrt{\frac{\sum x^2 - \sum x.\bar{x}}{n - 1}}$$

where n = no of results and $\bar{x}$ = mean

The values obtained were as given in table 4.7. To compare the variation in the results for each testing time a value of 3 standard deviations (99% confidence limits) has been expressed in terms of a percentage of the mean value.

Test number	Sample number	Test load (Kg)	Testing time (hr)			
			0.5	1.0	1.5	2.0
1	1	10.2	2.60	6.03	10.05	13.05
	2		2.42	5.35	9.42	11.40
2	1	16.7	3.85	9.01	14.10	18.63
	2		5.21	9.94	14.72	18.35
3	1	22.6	6.48	12.73	18.20	-
	2		7.62	15.02	20.11	-

Table 4.3

Weight loss in gm. of 2.8%C white iron standard (iron 9).

Test number	Sample number	Testing time (hr)			
		0.5	1.0	1.5	2.0
4	1	2.36	5.35	8.72	11.98
	2	2.20	5.73	9.02	11.72
5	1	2.62	6.10	10.07	13.31
	2	2.64	6.02	9.61	12.53
6	1	2.35	5.33	8.50	11.87
	2	2.48	5.30	8.21	11.36
7	1	2.09	4.95	7.92	11.90
	2	2.31	5.26	8.48	12.85
8	1	2.65	5.30	8.86	13.01
	2	2.61	5.07	8.75	12.72

Table 4.4

Weight loss in gm. of reproducibility tests on 2.8%C white iron standard (iron 9).Testing load -10.2Kg.

Test number	Sample number	Testing time (hr)			
		0.5	1.0	1.5	2.0
9	1	1.02	2.41	3.68	4.71
	2	1.03	2.39	3.35	4.63
10	1	1.27	2.33	3.41	4.60
	2	1.34	2.28	3.60	4.12

Table 4.5

Weight loss in gm. of hardened 15%Cr/3%Mo iron (iron 10)
Test load - 10.2Kg.

Test number	Sample number	Material	Testing time (hr)			
			0.5	1.0	1.5	2.0
11	1	Iron 9	0.78	1.91	2.93	3.92
	2	Iron 10	0.45	1.02	1.53	2.05
12	1	Iron 9	0.90	2.10	3.25	4.15
	2	Iron 10	0.48	1.04	1.70	2.10

Table 4.6

Weight loss in gm. of as cast 2.8%C white iron(iron 9) and hardened 15%Cr/3%Mo iron (iron 10).Test load 4.3Kg.

Iron 9 H_v=440

Iron 10 H_v=950

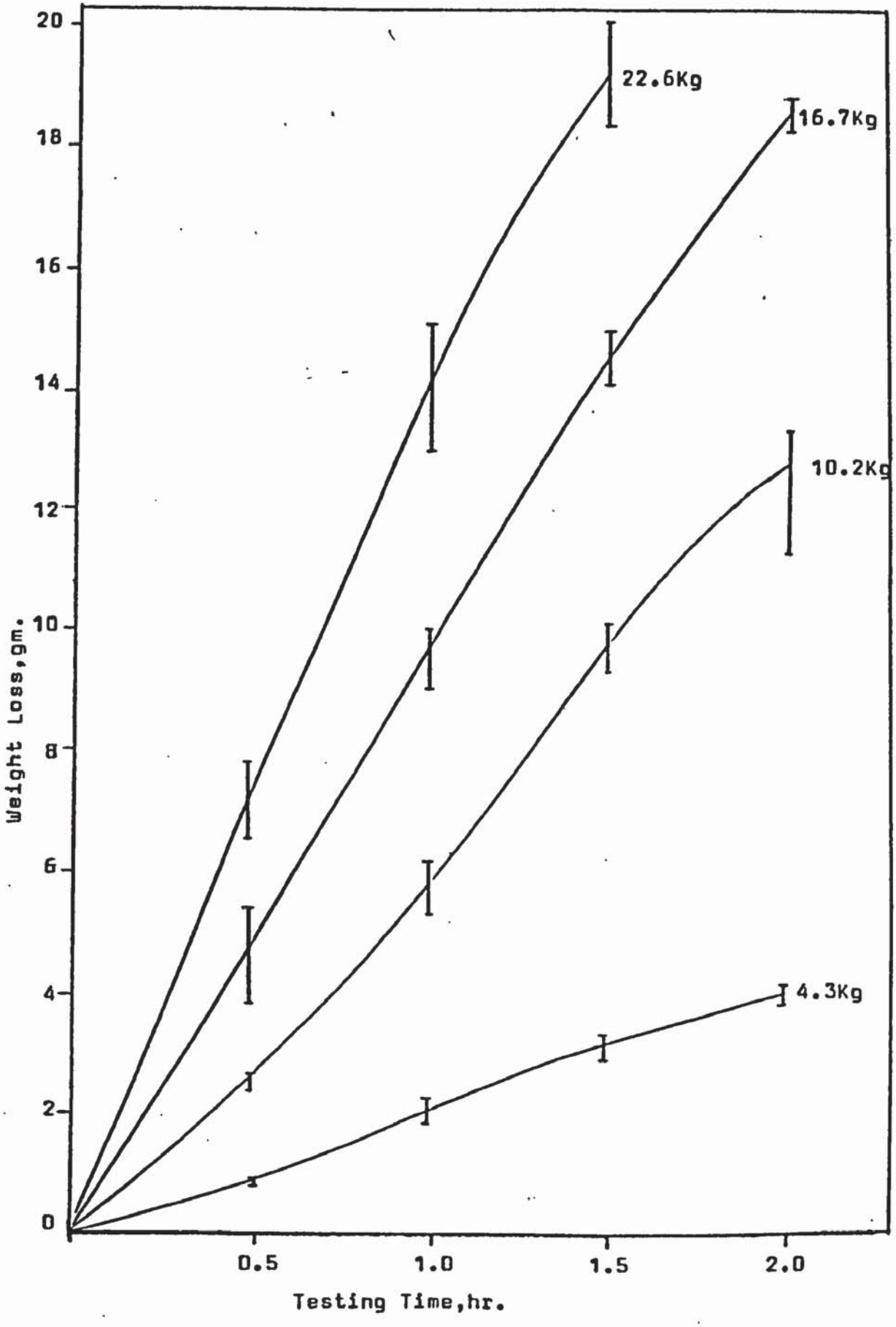

Figure 4.5

Effect of testing time and load on weight loss of 2.8%C white iron standard (iron 9).

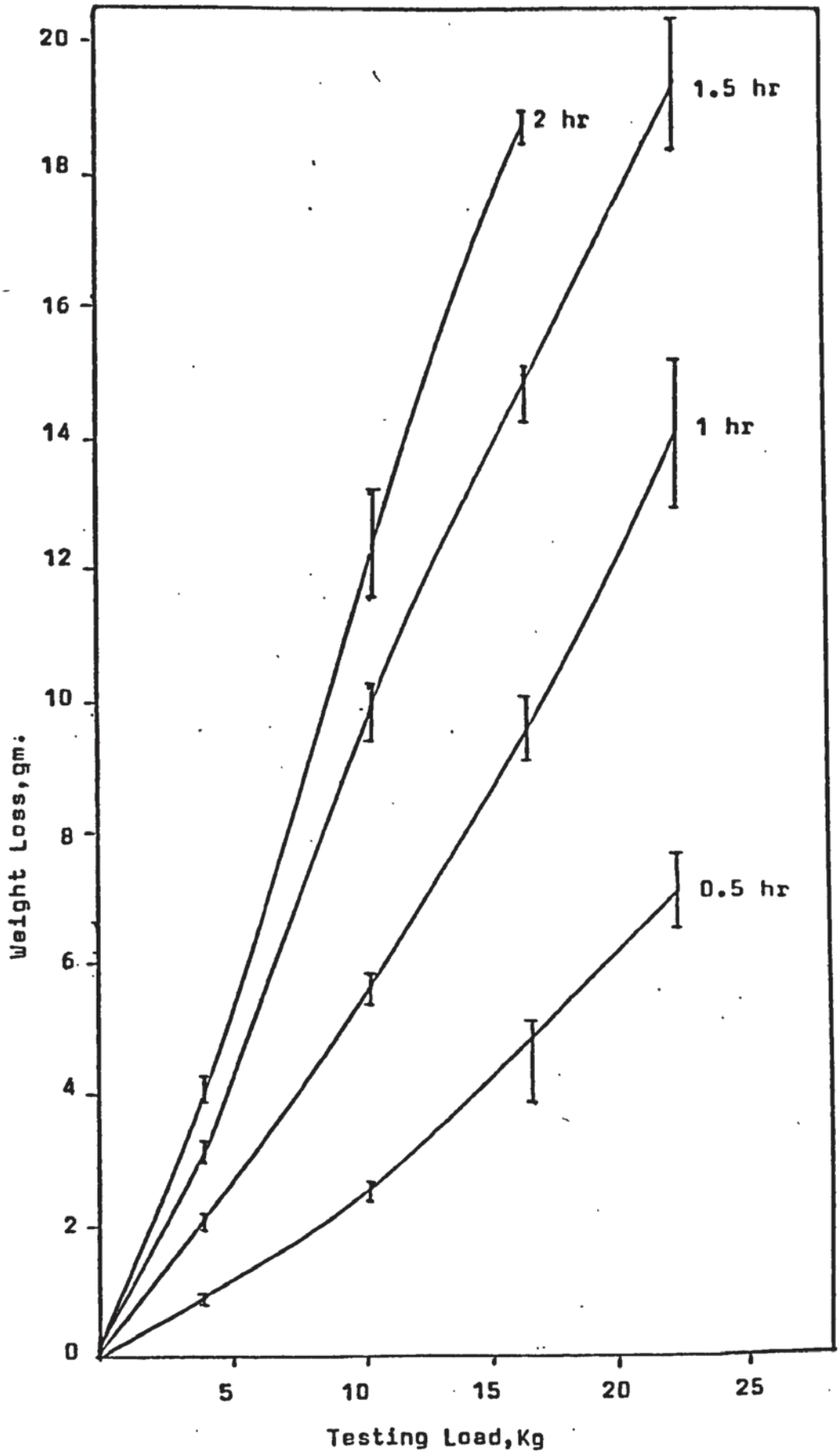

Figure 4.6

Effect of testing load at various times on weight loss in 2.8%C white iron standard (iron 9).

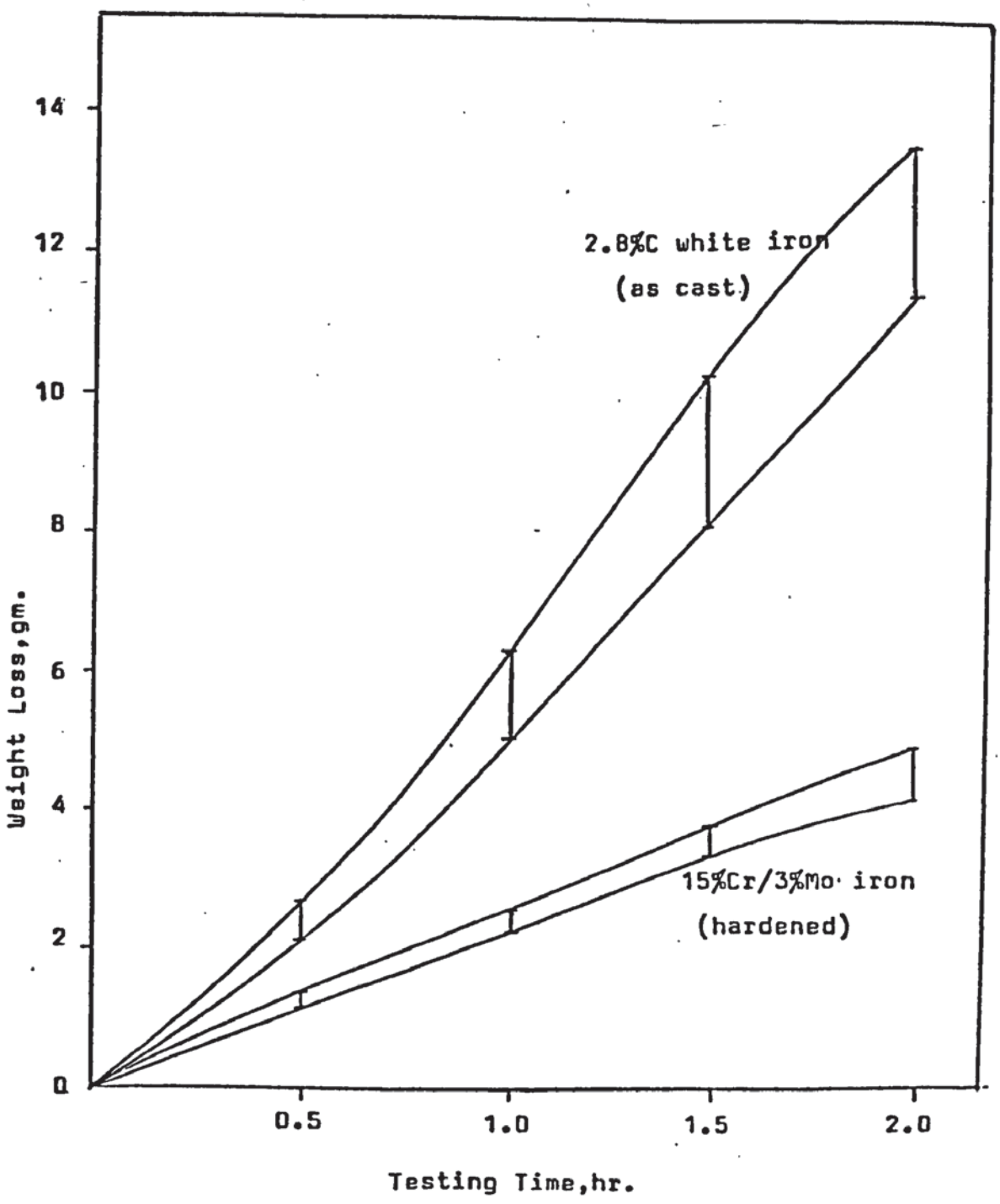

Figure 4.7

Weight loss of 2.8%C white iron (iron 9) and hardened 15%Cr-3%Mo iron (iron 10).Testing load was 10.2 Kg.

Testing time (hr)	Mean weight loss (gm.)	Calculated standard deviation σ	3σ as % of mean value
0.5	2.431	0.198	24.4
1.0	5.441	0.384	21.2
1.5	8.814	0.636	21.6
2.0	12.325	0.643	15.6

Table 4.7

Standard deviation calculated for repeat tests on 2.8%C white iron (iron 9).

As cast series		Heat treated series	
Test no.	Iron nos. tested	Test no.	Irons nos. tested
13	1+R	23	2+6
14	4+8	24	4+R
15	2+7	25	3+5
16	3+R	26	7+6
17	5+6	27	2+R
18	1+4	28	3+7
19	5+R	29	4+5
20	8+2	30	10+R
21	3+6	31	2+7
22	7+R		

R-reference samples (iron 9)

Table 4.8

Randomised testing order for 0-35%Cr irons.

The results show that there was less variation for the longest testing time (i.e. the largest weight loss). The values of ± 15.6 to 24.4% are higher than those obtained by previous workers, ± 7 to 21% by Boyes (14) and ± 5.7 to 8% by Avery (4) for a wet abrasion test. In an attempt to reduce this level of variation the width of the track was reduced as mentioned earlier to prevent chipping damage to the unworn area and also a run in period was used prior to the actual wear test. During these initial tests it was also noted that there was an equal distribution of the load to each of the two samples under test since specimens loaded on one arm did not give repeatedly higher or lower weight losses than specimens tested on the other arm.

4.3.2 Tests on 0-35% Cr irons (Nos 13-31)

4.3.2.1 Details of tests.

In the initial series of tests (Nos 1-12) machine loads of 4.3 to 22.6 kg were used producing nominal compressive stresses on the wear surface of each specimen from 0.04 N/mm^2 to 0.22 N/mm^2. In the later tests on the as-cast and heat treated 0-35% Chromium irons the track was machined to reduce its width from 20 to 16 mm. This gave greater clearance (i.e. unworn area) at the edges of each specimen and prevented the chipping away of unworn edge material during wear testing. In this later series of tests a standard

10.2 kg machine load was used for all tests to give a nominal compressive stress on each specimen of 0.12 N/mm^2

In order to reduce the time required for testing the samples the duration of each wear test was set at 1 hour. In addition to minimise the influence of variations occuring during the initial stages of each wear test a 10 minute run in period was used. Each ground sample was run in for this period before being cleaned and weighed. The weight loss was then determined after a 1 hour test period using a standard 7kg amount of Chelford 60 silica sand as abrasive. Weight losses were determined to 0.0001 gm using a Stanton CL40 Unimatic balance. Duplicate tests were made on each iron in the as-cast and heat treated conditions and during the course of testing standard white iron samples were used. In order to spread the duplicate and standard determinations with respect to time, life of track etc. a randomized testing order was used as given in table 4.8. The use of the standard white iron samples enable reproducibility during the course of testing to be determined.

4.3.2.2 Results of tests.

The results of the wear tests on the as-cast series of 0-35% Cr irons are given in table 4.9 together with information on the microstructures and mean hardness values of the iron.

The wear index has been calculated for comparison purposes and is given by:

$$\text{wear index} = \frac{\text{mean weight loss of white iron standard}}{\text{mean weight loss of alloy iron tested}}$$

Hence the as-cast 5% Cr iron has been found to be 1.25 x more resistant to abrasion than the standard white iron under these particular conditions of testing. The figure R_n given in the table refers to when a reference sample was tested together with a alloy iron specimen. The weight losses recorded for each particular reference test are given in the small supplementary table.

The results of the wear tests on the heat treated series are given in a similar manner in table 4.10. All of these irons were treated to produce martensitic matrix structures. For visual comparison the as-cast and heat treated wear samples are shown in figure 4.9 and 4.10.

The standard deviation of the weight loss determinations from the standard white iron samples was calculated as before. These results gave a mean weight loss of 8.5552g with a calculated standard deviation of 0.204. Three standard deviations calculated as a percentage of the mean value was found to be 7.2%

The index was calculated using weight loss measurements, as used by other workers, since the densities of the irons tested do not vary significantly. The lower chromium irons

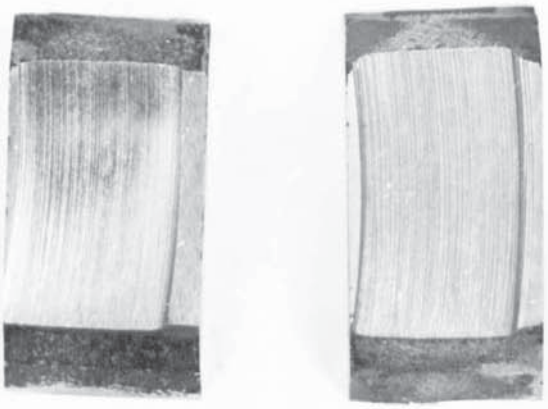

Hardened
15% Cr-3% Mo
iron

As-cast
2.8% C white
iron

Figure 4.8

Initial tests. Wear test samples in hardened 15-3 iron and as cast unalloyed white iron.

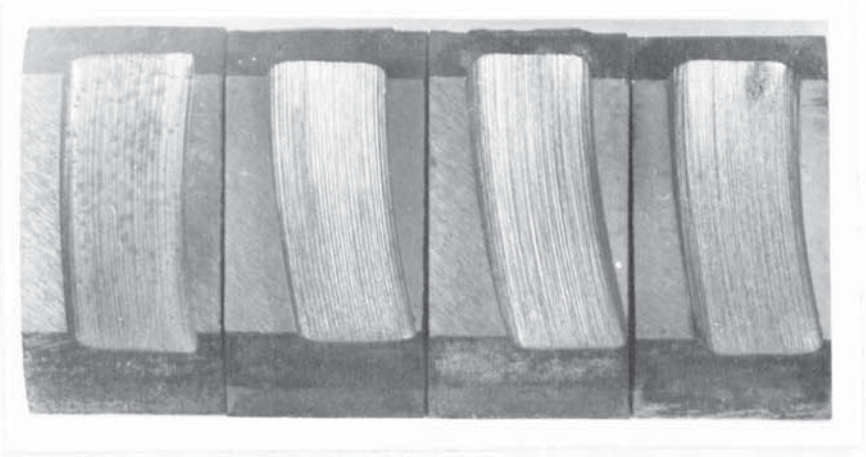

Iron	1	2	3	4
% Cr	0.1	5	10	15

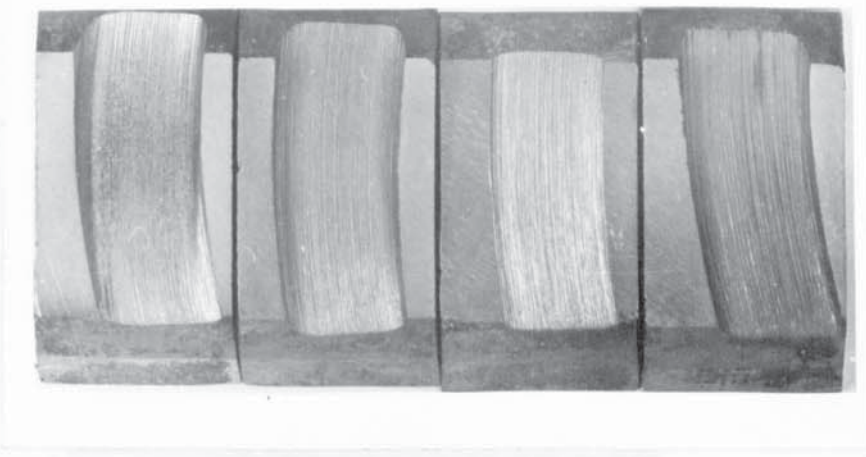

Iron	5	6	7	8
% Cr	20	26	30	36

Figure 4.9

Wear test samples. Irons 1-8 in as-cast condition.

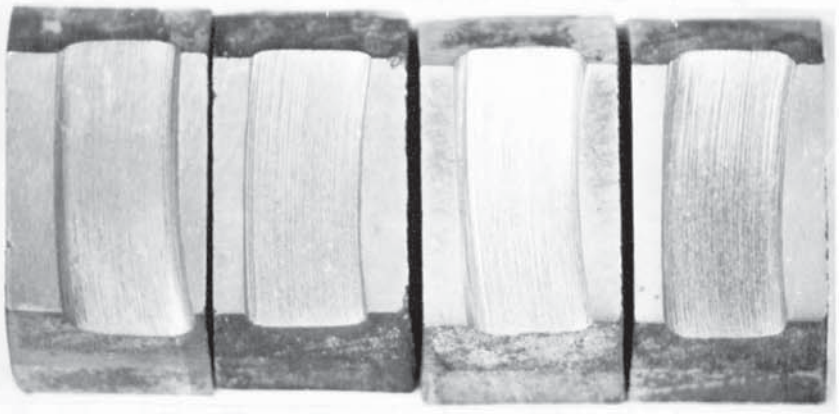

Iron	9AC	2	3	4
% Cr	0.1	5	10	15

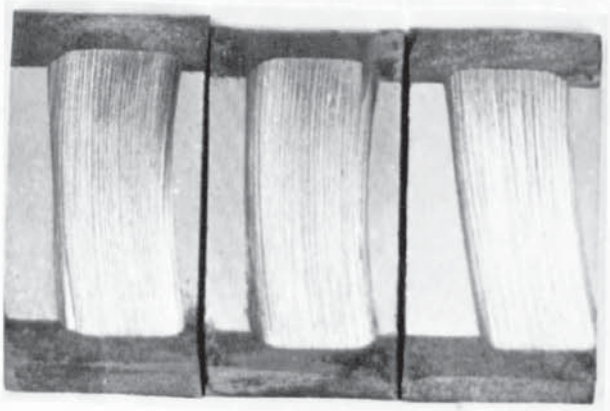

Iron	5	6	7
% Cr	20	26	30

Figure 4.10

Wear test samples. Irons 2-7 in heat treated condition and iron 9 (as-cast) used as reference.

Iron No.	%C	%Cr	Weight Loss (gm.) Test 1	Test 2	Mean	Wear index	Hv_{30}	Structure.
1	3.99	0.14	9.0627(R_1)	8.4143	8.7385	0.98	535*	Continuous M_3C eutectic +pearlite.Mottled areas.
2	3.67	5.54	6.8981	6.8775	6.8568	1.25	606	Continuous M_3C eutectic +pearlite.
3	3.57	10.09	9.6194(R_2)	9.3197	9.0200	0.95	564	Discontinuous M_7C_3 +pearlite.
4	3.10	14.68	7.6680	7.8557	7.7618	1.10	590	" "
5	3.00	20.40	10.6782	10.2434(R_3)	10.4608	0.82	580	Discontinuous M_7C_3 +pearlite +austenite.
6	2.72	26.60	11.5328	10.7930	11.1629	0.77	505	Discontinuous M_7C_3 +austenite.
7	2.44	30.60	8.7260(R_4)	8.0900	8.4080	1.02	498	" "
8	2.13	36.00	9.7770	10.7350	10.2560	0.83	314	Discontinuous M_7C_3 +ferrite.

R_1	8.8418
R_2	8.5328
R_3	8.4223
R_4	8.3900

(* away from mottle)

Table 4.9 Results of wear tests on 0-35% Cr irons in as cast condition.

Iron	%C	%Cr	Weight loss (gm.)			Mean	Wear index	Hv_{30}
			Test 1	Test 2	Test 3			
2	3.67	5.54	4.6908	5.3700(R_5)	4.6139	4.8915	1.74	954
3	3.57	10.09	6.1912	6.6060	-	6.3986	1.34	917
4	3.10	14.68	6.7960(R_6)	6.1430	-	6.4695	1.32	800
5	3.00	20.40	6.9196	6.5460	-	6.7328	1.27	858
6	2.72	26.60	8.2855	7.9358	-	8.1106	1.05	825
7	2.44	30.60	8.4016	7.7910	7.9800	8.0575	1.06	794
10	3.58	14.10	3.7303(R_7)	-	-	3.7303	2.29	950

R_5	8.2940
R_6	8.6753
R_7	8.7303

Table 4.10 Results of wear tests on heat treated irons.

have density values of 7.65 - 7.7 and the higher chromium irons values of 7.4 - 7.5 gm / cc. A comparison based on volume loss would mean only very slight changes in the value of the wear index (e.g. from 0.83 to 0.80 for the as-cast 36% Cr iron). The volume losses in the range of irons tested varied from 0.48 cm^3 for the hardened Cr-Mo iron to 1.49 cm^3 for the 26% Cr iron (as-cast).

4.3.3 Abrasive breakdown during testing.

The nature of the silica sand used as the abrasive in the tests was examined by SEM at low magnification and was studied by sieve analysis. Figure 4.11 compares the sand before and after testing. Figure 4.12 presents the results of a standard sieve analysis on samples of sand before and after testing. It is seen that the sand particles were broken into much smaller and angular fragments during wear testing confirming that the test gave high stress abrasion conditions.

4.3.4 Profiles of worn surfaces.

The grooved wear pattern produced by the test was studied using a Rank Taylor Hobson surface profile measuring instrument. This uses a stylus which is moved across the worn surface in order to produce a magnified trace of that surface. The wear surfaces examined were much more deeply grooved than

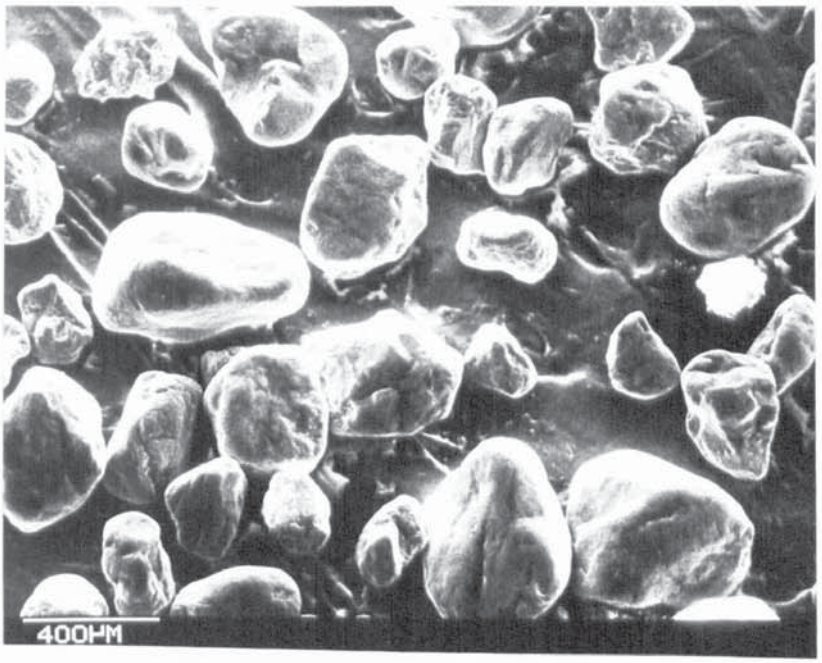

(a) Before testing.

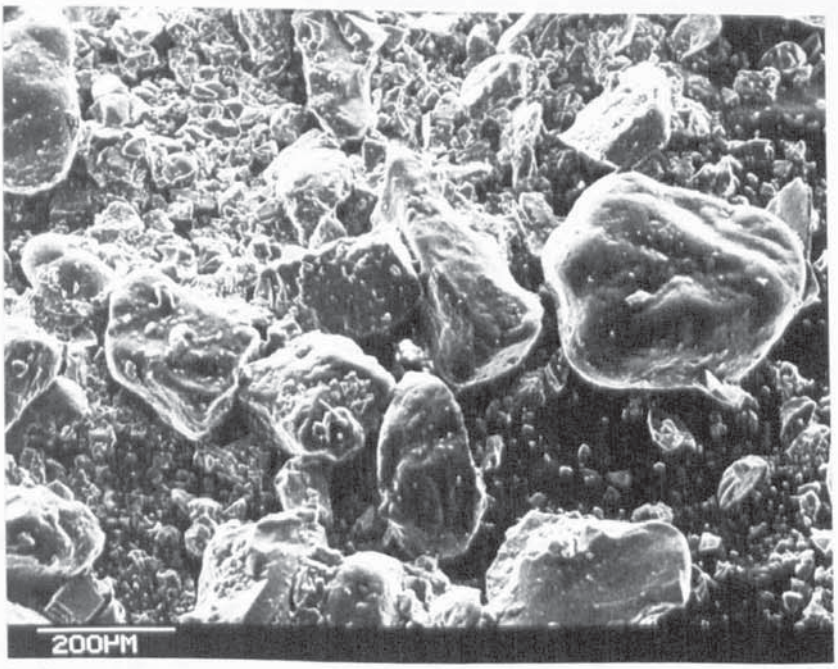

(b) After testing.

Figure 4.11

SEM views of silica sand abrasive before and after wear testing.

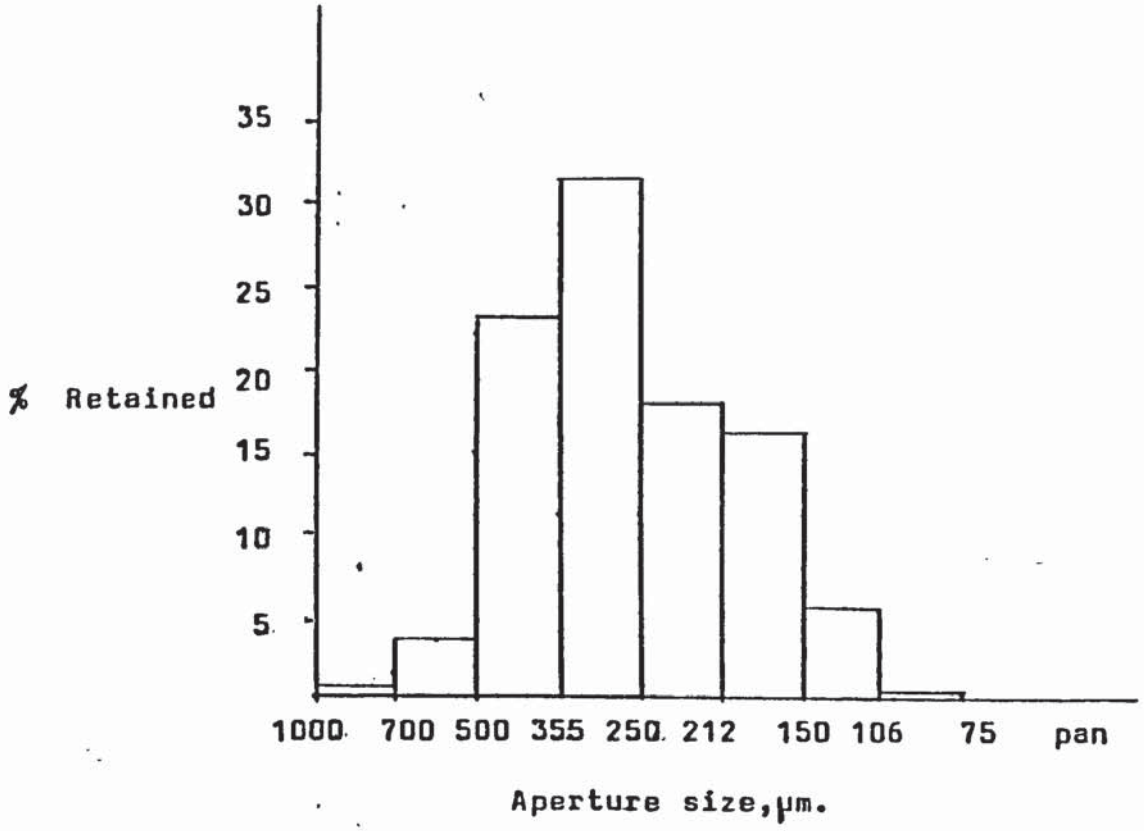

(a)Before testing.

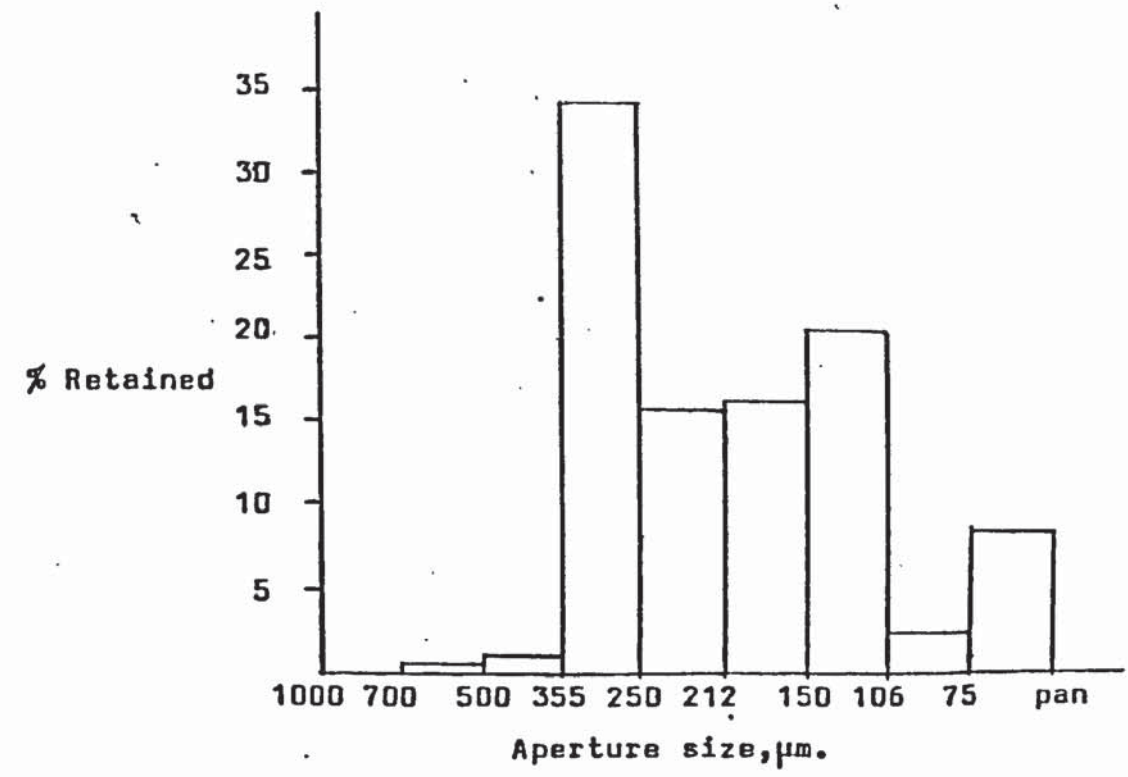

(b)After 10 min. run in +1 hr. testing period.

Figure 4.12

Sieve analysis of sand abrasive.

(a) Machine test load 10.2Kg.

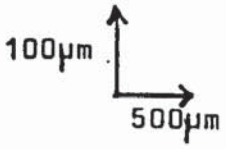

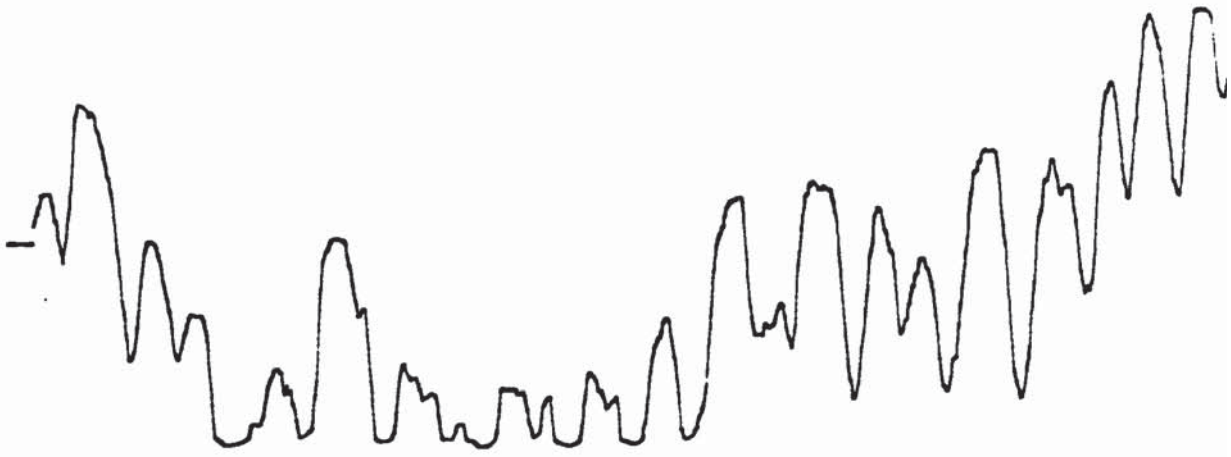

(b) Machine test load 16.7Kg.

Figure 4.13
Traces of worn surfaces of white iron standard specimens at two different testing loads.

(a) Iron 2 (5%Cr) as cast.

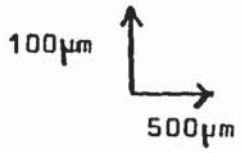

(b) Iron 2 (5% Cr) hardened

(c) Iron 4 (15%Cr) as cast.

Figure 4.14
Traces of worn surfaces.

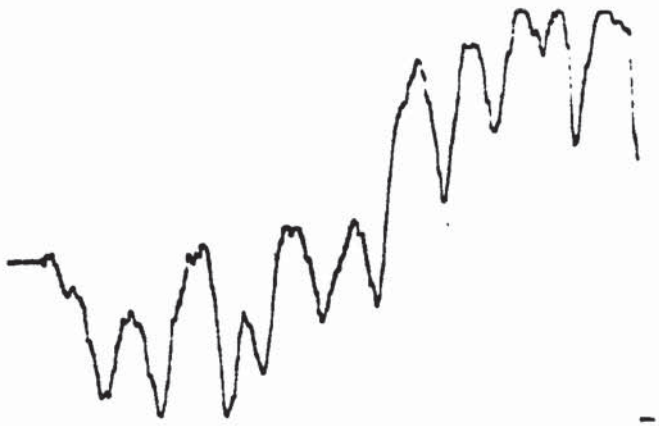

(d) Iron 7 (30% Cr) as cast.

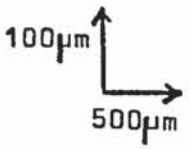

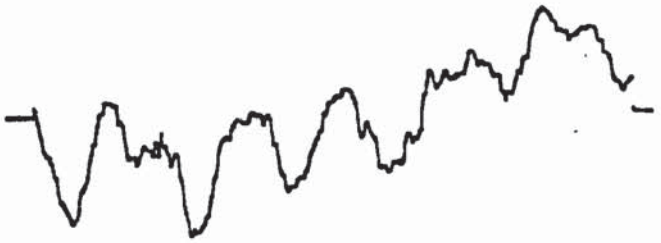

(e) Iron 7 (30% Cr) hardened.

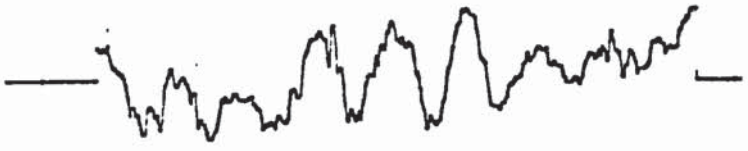

(f) Iron 8 (36% Cr) as cast.

Figure 4.14cont.
Traces of worn surfaces.

machined surfaces for which the instrument was designed. Consequently it was adjusted to give the minimum possible magnifications of X100 in the vertical direction and X20 in the horizontal direction. Figure 4.13 shows the traces of the wear surfaces of the white iron reference material tested at different loads. The depth of the grooves (valley to peak height) varies from 50 to 150 μm for the sample tested at 10.2 Kg load and this depth increases to a range 50-280 μm for the test at the 16.7 Kg load. Traces of wear surfaces for a representative selection of irons from the second series of tests (see tables 4.9 and 4.10) are given in figure 4.14. The significance of these are discussed later with respect to both abrasion resistance and microstructure of the irons concerned.

4.4 Metallographic examination.

4.4.1 Practical details.

Since white irons are hard and brittle specimens for microexamination had to be carefully taken in order to avoid fracturing either the sample or the cut off wheel. To achieve this a Discotom cut off machine fitted with a 1.5 mm wide o1 grade wheel was used. Sufficient coolant was pumped onto the sample during cutting to prevent heating and thus avoid structural changes and thermal cracking. The irons were examined after wear testing using specimens taken parallel to and transverse to the wear track.

In order to preserve the wear damage at the surface each specimen was nickel plated and then mounted in bakelite before preparation. After normal metallographic preparation the majority of the samples were etched in a freshly prepared solution of picric acid (1gm) in methanol (100cc) acidified with hydrochloric acid (5cc). Iron 8 (35% Cr) which had a ferritic matrix was etched electrolytically in 10% oxalic acid. Iron 7 (30% Cr) was subjected to several etchants in order to identify the carbides present in its structure.

General views of the as-cast microstructures were recorded at X150 and representative views of wear damage in the sub-surface microstructures were recorded at X1800 using an oil immersion objective. All the photomicrographs were taken using a PM6 Oympus microscope fitted with a 35 mm camera. Commercial black and white film was used and this was developed and printed in the normal way.

The proportions of eutectic carbides in the as-cast microstructures were determined using a microscope fitted with a crosswire eyepiece and a step movement stage. The results were expressed as the mean of five determinations taken at a depth of 2-4 mm below an unworn surface. This depth corrosponded to a value typical of that reached after wear testing.

4.4.2 Microstructures of irons 1-10.

Figure 4.15 shows that iron 1 containing 4% C and 0.14% Cr was not fully white but contained areas of flake graphite. The eutectic carbide in this iron was of the M_3C type in ledeburitic form. Iron 2 containing 3.7% and 5% Cr was fully white and figure 4.16 shows that the ledeburite eutectic in this iron was finer than the eutectic in iron 1. In both irons the primary and eutectic austenite has transformed to pearlite on cooling.

Figure 4.17 illustrates that when 10% chromium is present the form of the eutectic carbides is changed from the continuous M_3C type as shown in the two previous micrographs to the discontinuous M_7C_3 type. This level of chromium did not influence the transformation of austenite on cooling and a pearlite matrix has been produced. The structure of iron 4 containing 3.1% C and 15% Cr is shown in figure 4.18. It is similar to that of iron 3 in that it consists of discontinuous lamellar M_7C_3 carbides in a pearlite matrix. The structure of iron 5 containing 20% Cr is also similar but the austenite dendrites appear to have only partially transformed to pearlite, as seen in figure 4.19. In iron 6 containing 2.7% C and 26% Cr there was sufficient chromium in the matrix to fully suppress the austenite transformation on cooling after solidification. The structure therefore consisted of fine lamellae of M_7C_3 carbides in a austenite matrix as shown in

figure 4.20. An austenite matrix has also been retained in iron 7 which contained 2.4% C and 30% Cr. However, as can be seen in figure 4.21 the eutectic carbides in this iron were finer than those in iron 6 or those in any of the other irons.

The composition of iron 8 (2.1% C, 36% Cr) was such that primary dendrites of ferrite formed on solidification instead of dendrites of austenite as for the previous irons. The ferrite remained unchanged during cooling and hence the final structure of iron 8, as seen in figure 4.22, consisted of fine eutectic carbides in a matrix of ferrite. Figure 4.23 represents the microstructure of iron 9 which was used as a reference material. Because of its lower carbon content there was proportionately less ledeburite eutectic in its structure than in irons 1 and 2. Figure 4.24 shows the structure of the 15% Cr, 3% Mo iron in the fully hardened condition. The form of its matrix is discussed later.

The results of phase counting of the % eutectic carbides are given in table 4.11. Each determination was made by step counting a 10 mm traverse in 0.05 mm steps using a Swift point counting stage, at a magnification of X600. The table also lists a calculated value according to Maratray (105), this formula is not applicable to chromium contents below 10% where the carbides are of the M_3C type.

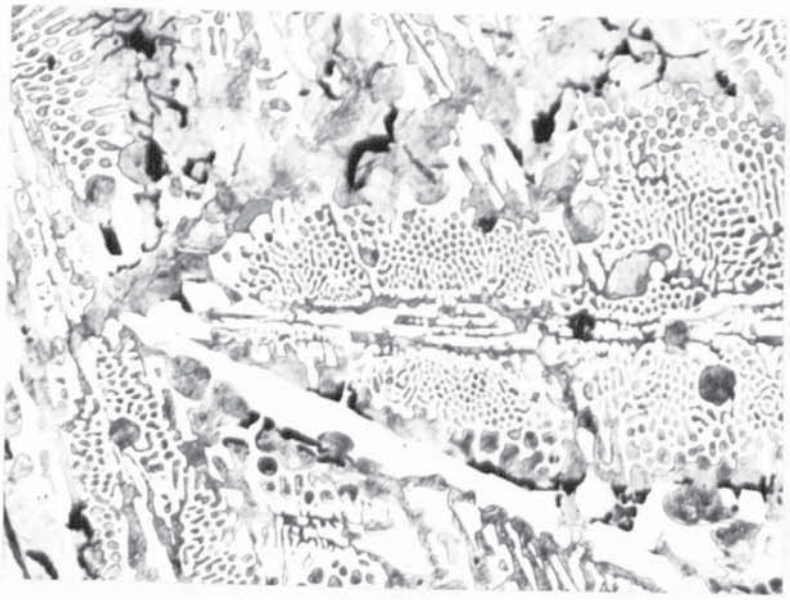

Figure 4.15
As cast microstructure of iron 1 (4%C-0.1%Cr)
Ledeburite eutectic + areas of mottle. X150

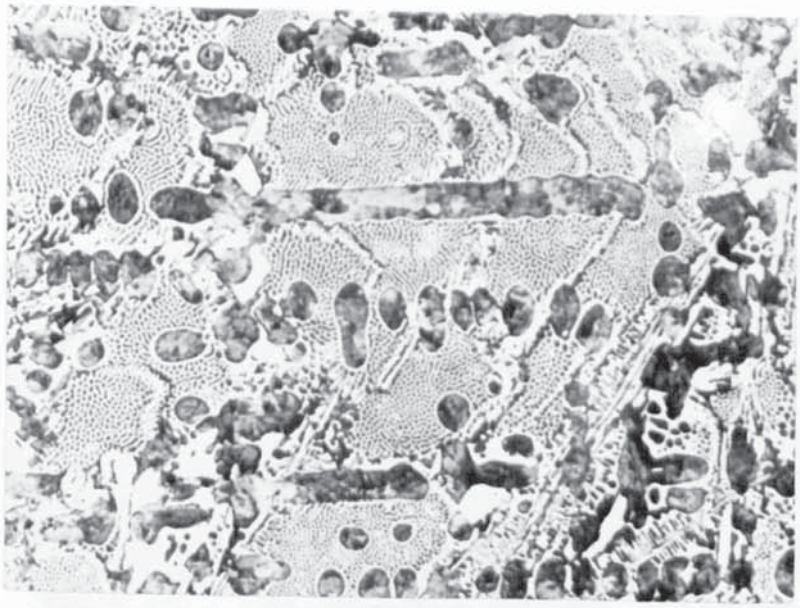

Figure 4.16
As cast microstructure of iron 2 (3.7%C-5%Cr)
Ledeburite eutectic.

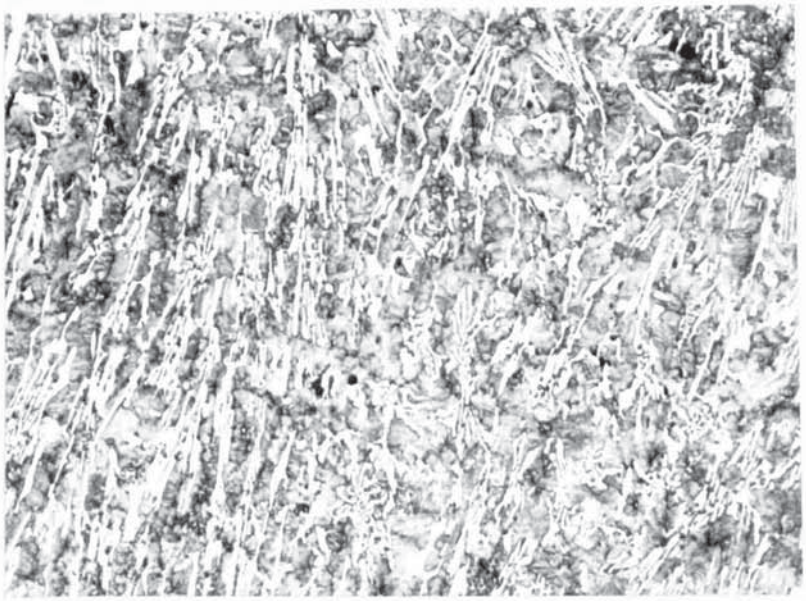

Figure 4.17
As cast microstructure of iron 3 (3.5%C-10%Cr)
Discontinuous eutectic carbide in pearlite
matrix. X150

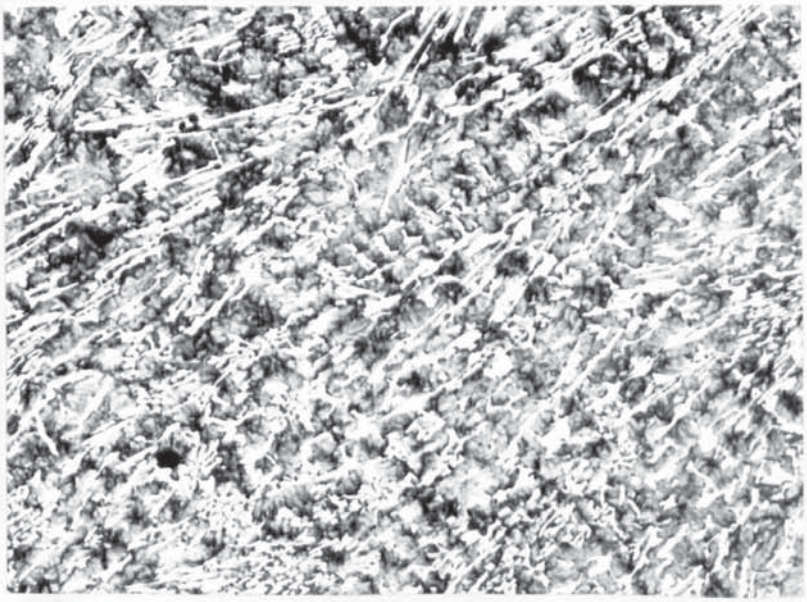

Figure 4.18
As cast microstructure of iron 4 (3.1%C-15%Cr)
Discontinuous eutectic carbide in pearlite
matrix. X150

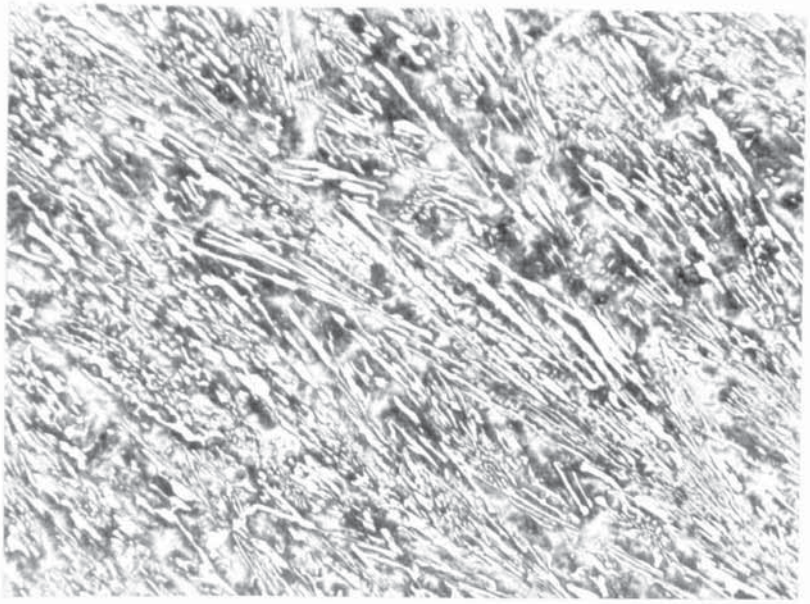

Figure 4.19
As cast microstructure of iron 5 (3%C-20%Cr) Discontinuous lamellar eutectic carbides in matrix of granular pearlite and austenite.
x150

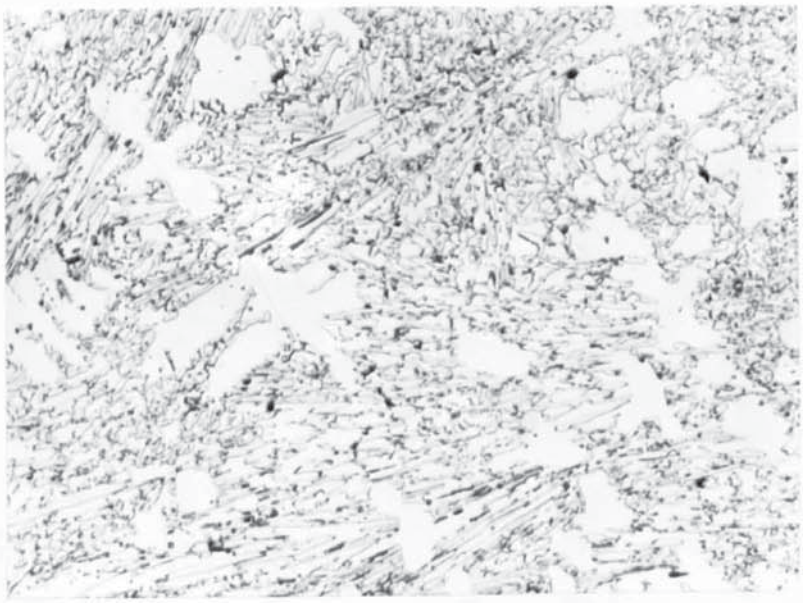

Figure 4.20
As cast microstructure of iron 6 (2.7%C-26%Cr) Discontinuous eutectic carbides in austenite matrix.
X150

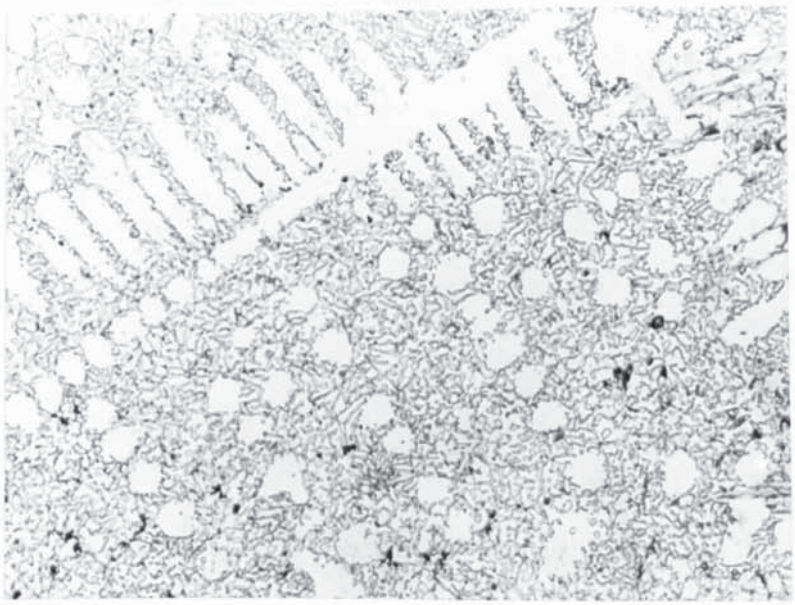

Figure4.21
As cast microstructure of iron 7 (2.4%C-30%Cr)
Fine discontinuous eutectic carbides in austenite matrix. x150

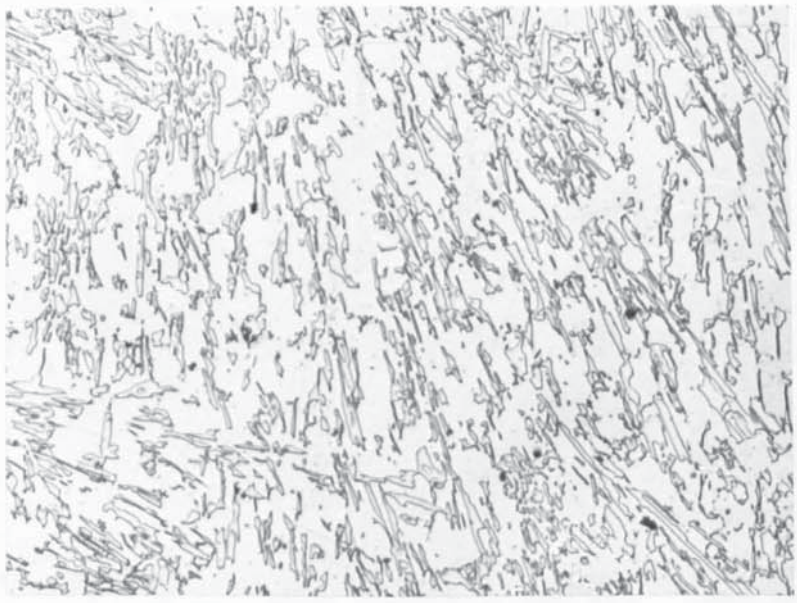

Figure 4.22
As cast microstructure of iron 8 (2.1%C-36%Cr)
Discontinuous eutectic carbides in ferrite matrix. x150

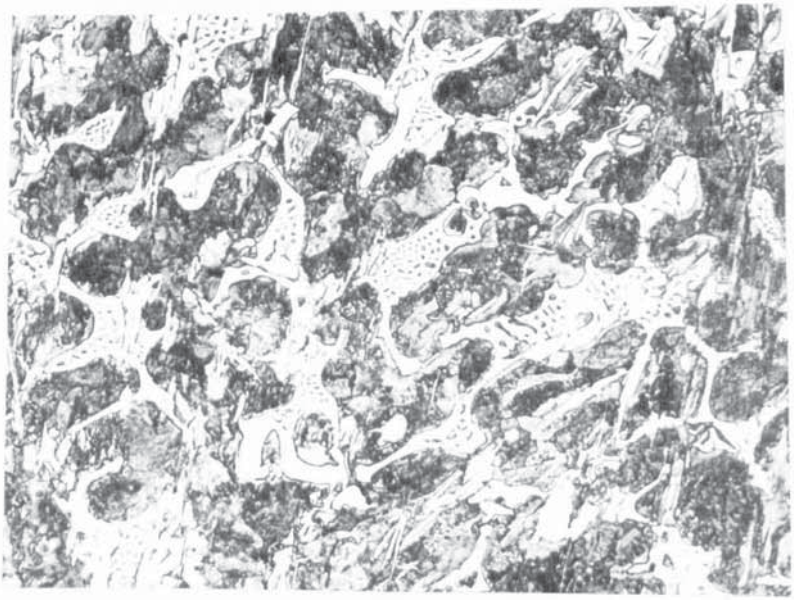

Figure 4.23
As cast microstructure of iron 9 (2.8%C-0.1%Cr)
Ledeburite eutectic + pearlite. X150

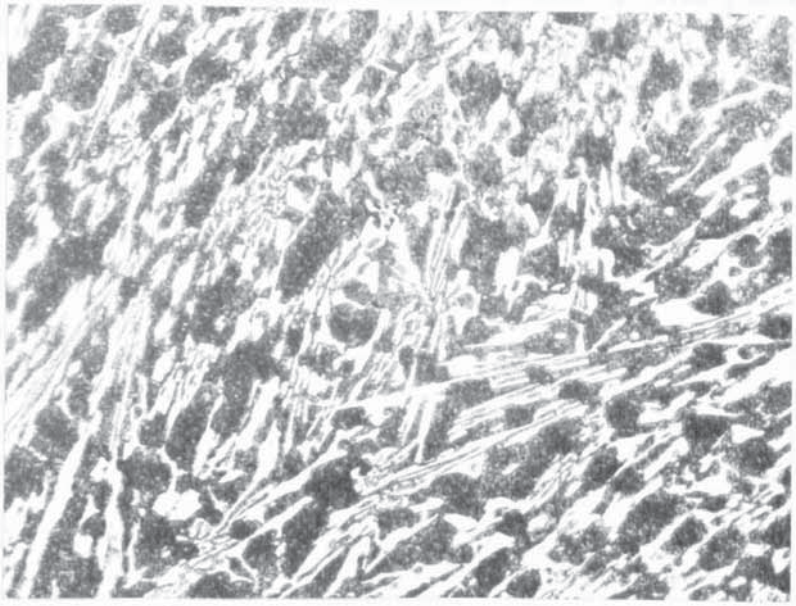

Figure 4.24
Microstructure of iron 10 (15%Cr- 3%Mo -3.5%C)
in the hardened condition. X150

Iron	%C	%Cr	Determination number					Mean	Calc. value*
			1	2	3	4	5		
1	3.99	0.14	50.0	60.4	45.2	55.4	57.2	53.6	-
2	3.67	5.54	50.6	55.0	57.7	50.1	51.3	52.9	-
3	3.57	10.09	33.6	32.7	32.7	29.8	30.0	31.8	34.3
4	3.10	14.68	36.3	32.8	32.3	36.2	32.2	33.9	31.1
5	3.00	20.40	33.1	33.3	31.8	32.8	32.4	32.7	33.0
6	2.72	26.6	31.0	31.5	29.0	31.8	29.2	30.5	32.9
7	2.44	30.6	33.0	32.6	32.2	32.0	33.2	32.6	31.7
8	2.13	36.0	27.8	26.8	26.4	27.2	27.6	27.2	30.9
9	2.81	0.11	30.0	31.3	27.6	31.9	31.3	30.4	-
10	3.58	14.1	33.6	32.9	34.6	33.4	33.2	33.5	36.5

*value calculated from:

$$\%\text{carbides} = 12.33(\%C) + 0.55(\%Cr) - 15.2 \quad \ldots.(104,105)$$

Table 4.11

Phase count results: %eutectic carbides present in irons 1-10.

The 10-30% Cr irons all contained approximately similar proportions of eutectic carbide, the mean values ranging from 30.5 to 33.9%. The 35% Cr iron contained slightly less carbide with a value of 27.2%. The values for iron 1 vary between 45.2 and 60.4% due to the occurrence of isolated mottled areas containing graphite.

4.4.3 Microstructures at wear surfaces.

Figure 4.25 - 4.36 illustrate the wear damage observed in the as-cast and heat treated irons. They represent sections taken parallel to the direction of travel of the test specimens over the wear track. The arrows indicated with the figure captions represent the direction of wear which is opposite to the direction of travel.

4.4.3.1 As-cast irons.

Representative views of the damage observed at the surface of iron 9 which was used as the standard reference material are given in figure 4.25. Fracturing and apparent bending of the M_3C eutectic carbide is seen at the immediate surface. Similar forms of damage were noted in iron 1 but there was less flow at the surface in this iron because of its greater proportion of carbide. Figure 4.26 shows distortion and cracking of carbides in the 5% Cr iron and reveals a layer of fragmented wear debris which has been smeared

along the wear surface. In this iron relatively few cracks were observed in the larger eutectic carbides.

Figure 4.27 represents damage in iron 5 which was typical of the 10-20% Cr irons where the discontinuous M_7C_3 carbides become fractured just below the surface and flow along in the deforming matrix at the surface. Figures 4.28 and 4.29 illustrate the damage seen in the two irons with fully austenitic matrix structures. Figure 4.28 shows the severity of cracking in eutectic carbides in the 25% Cr iron (iron 6). The carbides contain branched cracks which lead to pieces of the carbide becoming detached from the matrix. Penetration of the austenite matrix by the silica abrasive is also seen. Figure 4.29 shows that the finer carbides in the 30% Cr iron (iron 7) were less severely cracked than those in iron 6. However, it is seen that fractures across the carbides lead to their eventual removal from the matrix. Figure 4.30 shows that when the matrix is soft then the eutectic carbides become fragmented. This represents damage in the 35% Cr iron which has a ferritic matrix. The surface regions are heavily deformed and penetration of the abrasive grits into the surface is a common feature. Sub-surface cracking in the ferritic matrix was also observed.

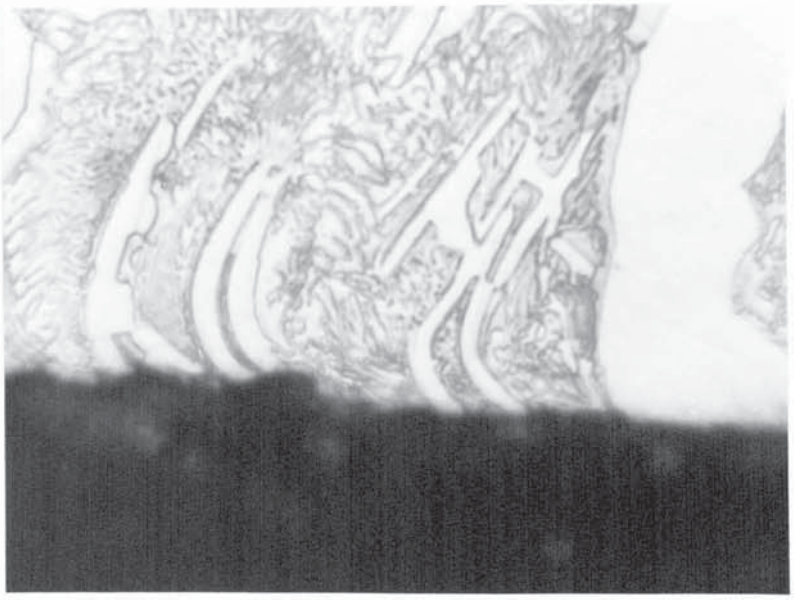

(a) Apparent bending of finer M_3C carbides.

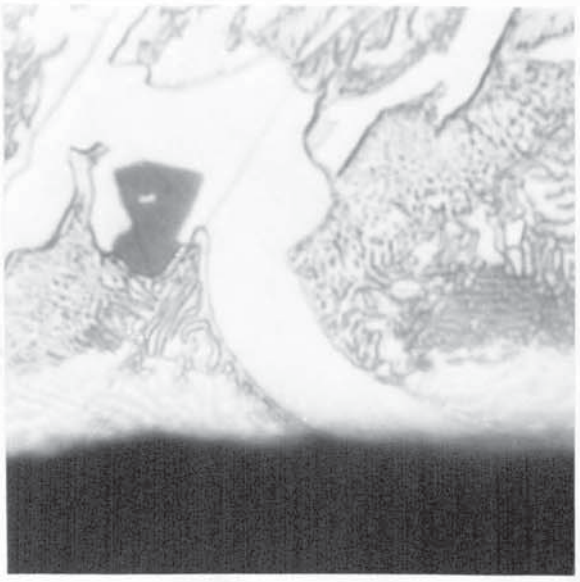

(b) Bending of M_3C and white non-etching layer.

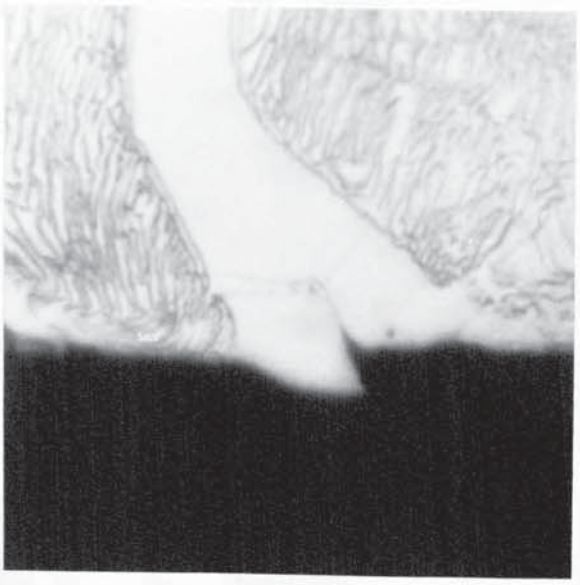

(c) Cracking in distorted M_3C carbide.

Figure 4.25

Microstructures at wear surface of iron 9 (2.8%C-0.1%Cr) tested in as cast condition. Wear direction ---→ ×1800

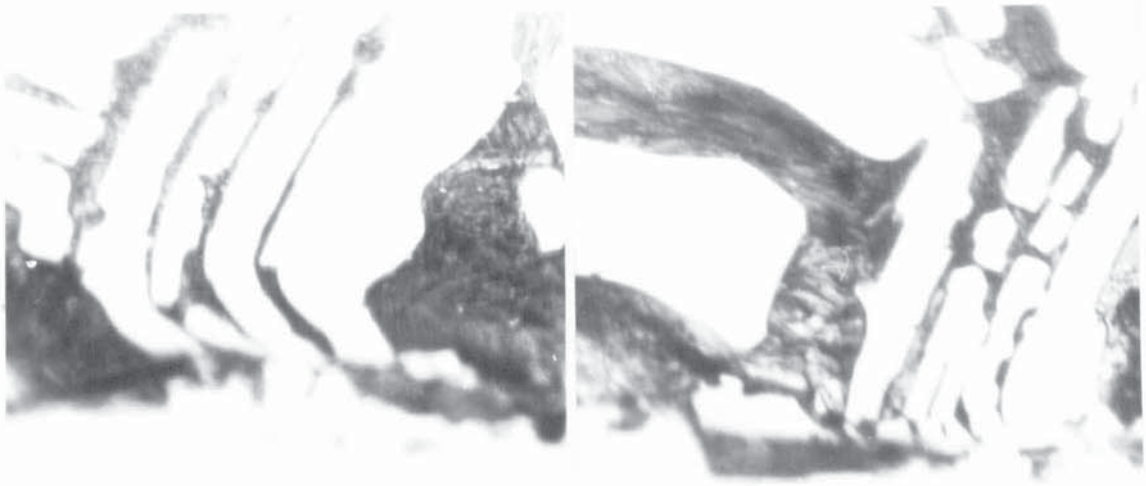

(a) distortion of carbides at surface.

(b) Sub-surface fracture in carbides.

Figure 4.26
Microstructure at wear surface of iron 2 (3.7%C-5%Cr) tested in as cast condition.Wear direction --→ x1800

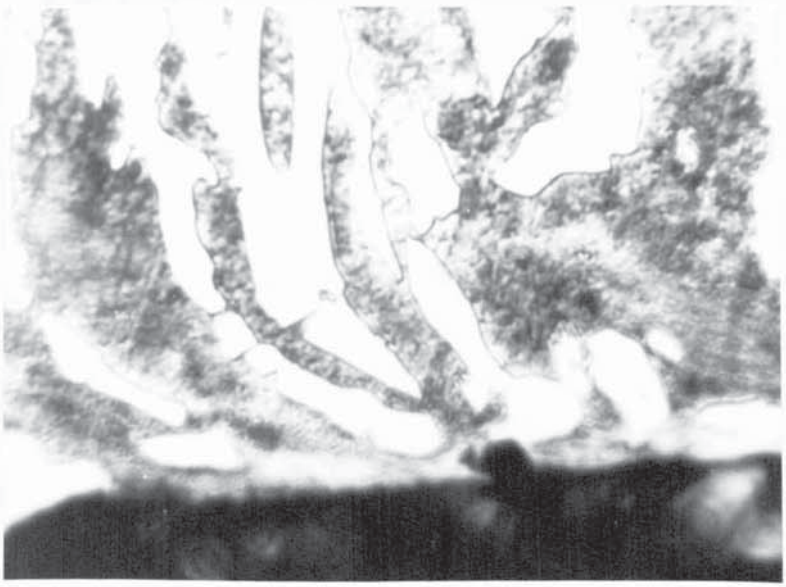

Figure 4.27
Microstructure at wear surface of iron 5 (3%C-20%Cr) tested in as cast condition.Wear direction --→ x1800

(a) Severe cracking of eutectic carbide.

(b) Branched crack in carbide & abrasive penetration into austenite matrix .

Figure 4.28
Microstructures at wear surface of iron 6 (2.7%C-26%Cr) tested in as cast condition.Wear direction --→ x1800

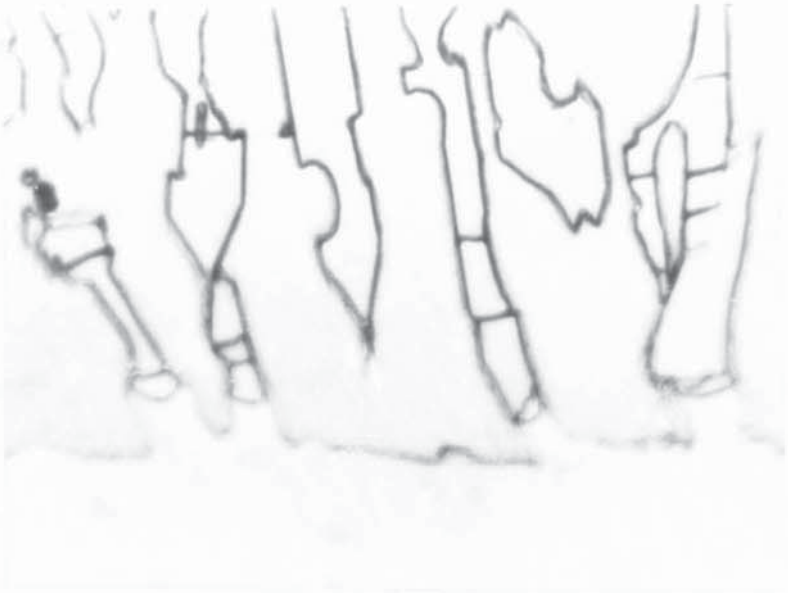

Figure 4.29
Microstructure at wear surface of iron 7 (2.4%C-30%Cr) tested in as cast condition.Wear direction ---→ x1800
Fracture & removal of carbides from austenite matrix.

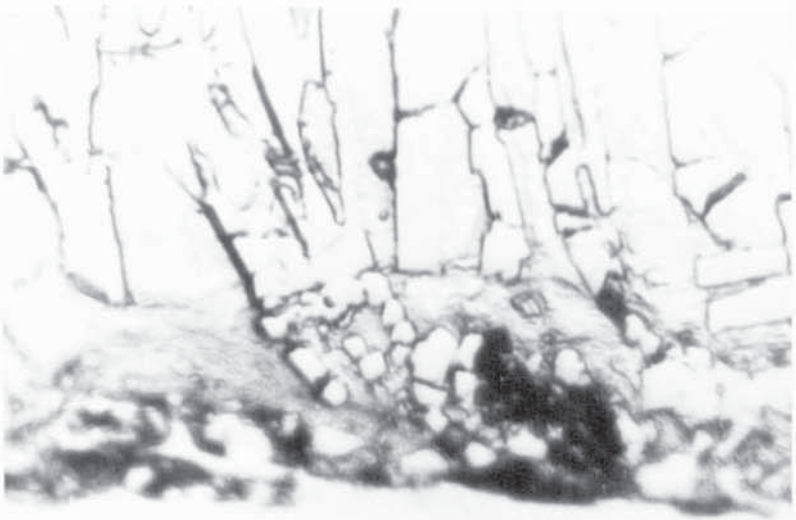

Figure 4.30
Microstructure at wear surface of iron 8 (2.1%C-36%Cr) tested in as cast condition.Wear direction ---→ x1800
Fragmentation of carbide & penetration of ferrite matrix by crushed abrasive.

4.4.3.2 Heat treated irons.

Figures 4.31 - 4.36 represent the wear damage which was typical of the heat treated irons. The treatments were designed to produce hardened matrices of tempered martensite, the higher chromium irons (irons 4-7 and 10) were destabilised before air hardening so that their structures also contain dispersions of secondary carbides. Figure 4.31 shows that even when there was a matrix of tempered martensite there was still appreciable deformation at the wear surface. This micrograph shows the hardened 5% Cr iron and reveals apparent bending of some of the eutectic carbides as in the as-cast iron (Figure 4.26). In contrast figure 4.32 shows the wear surface of the hardened 15% Cr-3% Mo iron in which there was very little sign of deformation or cracking at the wear surface.

Figure 4.33 is typical of the damage seen in the 15% Cr iron; this iron did not fully harden and the darker areas visible in the matrix are fine pearlite. Stepped fractures can be seen in the eutectic carbide lamellae, some of which appear to have deformed without fracturing. Figures 4.34-5 can be considered together since these show the effects of wear in the 20 and 25% Cr irons which have similar microstructures. The eutectic carbides tend to break just below the surface as a result of parallel fractures but in some carbides vertical cracks were also seen. (4.34a). In both

irons the tempered martensite matrix was unable to prevent penetration by the silica abrasive grits.

On examination of the microstructure of the heat treated 30% Cr iron after etching in acidified picral it was found difficult to distinguish the boundary between the protective nickel plate and the edge of the broken carbides. To make the carbides move clearly visible the specimen was etched for 5-10 seconds in Murakami's reagent (10 gm K_3 Fe $(CN)_6$ + 10 gm KOH + 100 ml H_2O). This revealed that the eutectic carbide had a duplex structure as shown in figure 4.36a. It was also seen that the eutectic carbides fracture just below the wear surface and that the broken fragments became detached as for the 20-25% irons. It was noted that the carbide in contact with the matrix contained cracks but some of these appeared to be halted at the interface with the inner carbide (see figure 4.36b and c).

4.5 Hardness testing.

Hardness tests were made on the irons in the as-cast and heat treated conditions using a Vickers machine fitted with a standard pyramidal diamond indenter under a load of 30 kg. The hardness value of each sample was expressed as the mean of four determinations. The mean values for the irons have been given in tables 4.9 and 4.10 of wear test results.

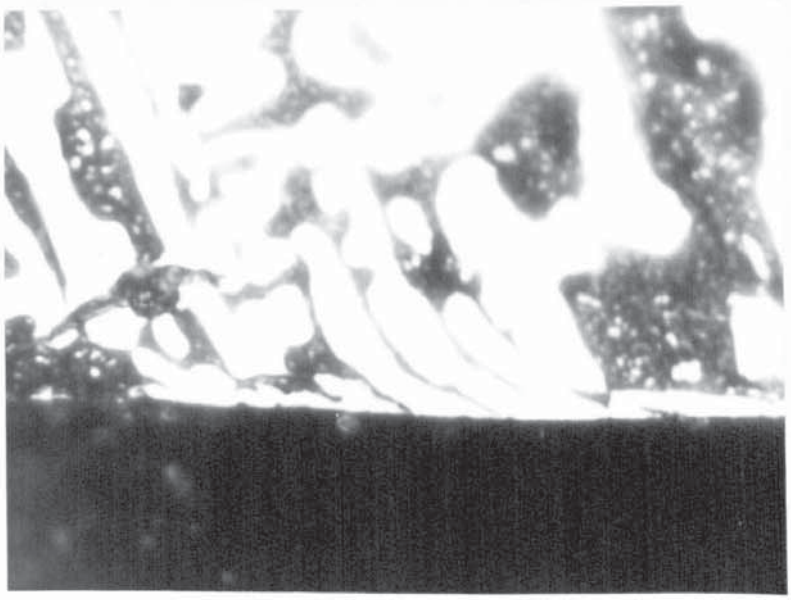

Figure 4.31
Microstructure at wear surface of iron 2 (3.7%C-5%Cr) tested in heat treated condition.Wear direction --→
x1800

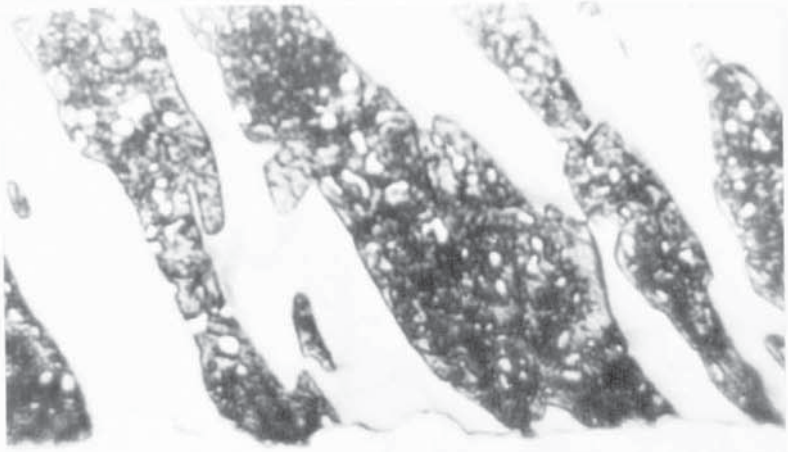

Figure 4.32
Microstructure at wear surface of iron 10 (3%C-15%Cr-3%Mo) tested in heat treated condition.Wear direction --→
x1800

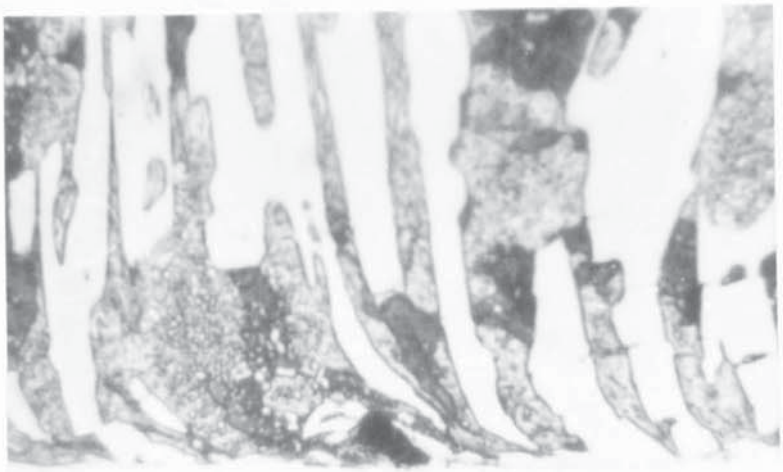

Figure **4.33a**

Microstructure at wear surface of iron 4 (3.1%C-15%Cr) tested in hardened & tempered condition. Initial Hv_{30}=800 Cracking and distortion of carbides in wear direction. Dark regions in matrix are non-martensitic transformation product. Wear direction --→ X1800

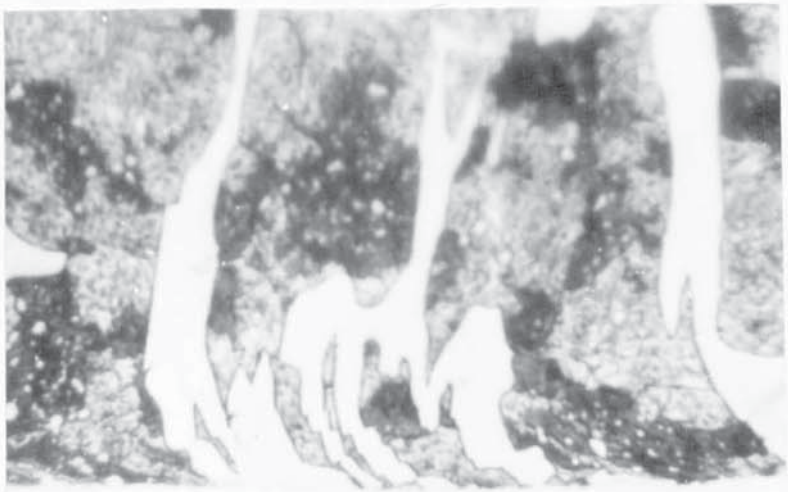

Figure **4.33b**

As above. Another view showing fracturing of carbides. X1800

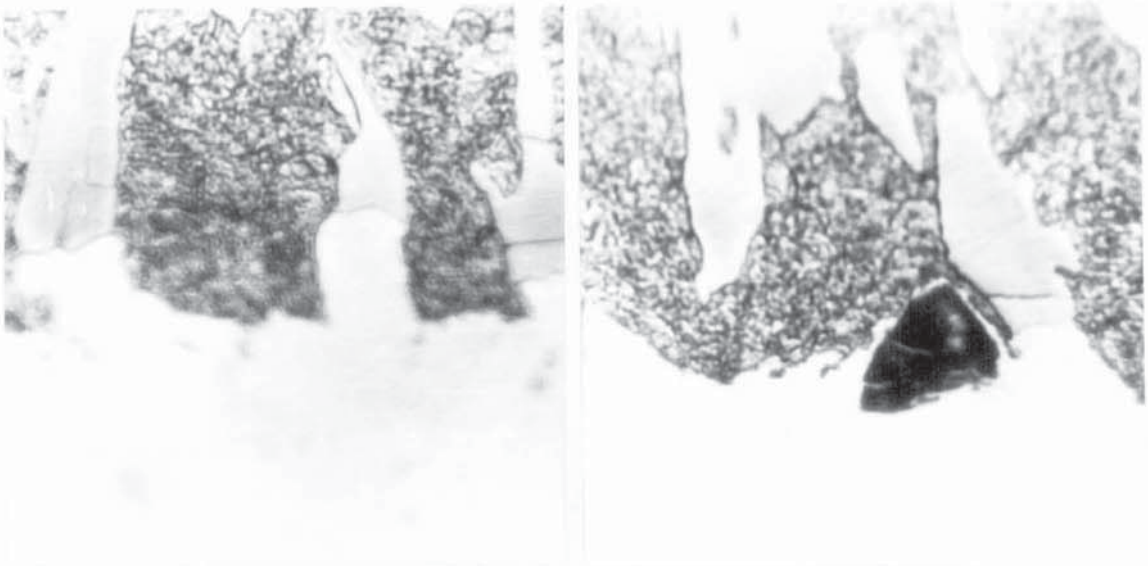

(a)Transverse & vertical cracks in carbide.

(b)Penetration by abrasive.

Figure 4.34
Microstructure at wear surface of iron 5 (3%C-20%Cr) tested in heat treated condition.Wear direction ---→
×1800

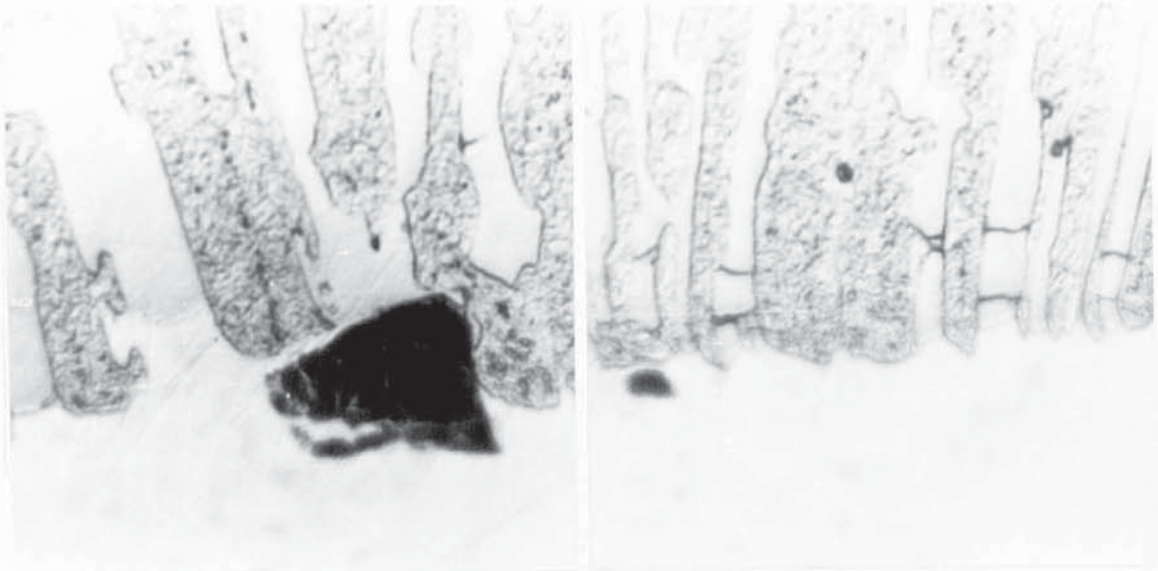

(a)Penetration by abrasive.

(b)Transverse cracking in eutectic carbides.

Figure 4.35
Microstructure at wear surface of iron 6 (2.7%C-26%Cr) tested in heat treated condition.Wear direction ---→
×1800

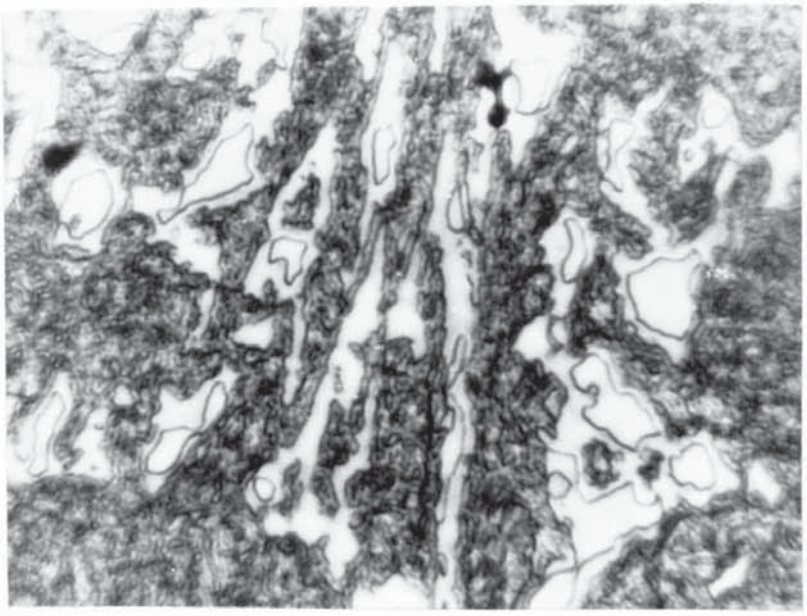

(a)General microstructure showing duplex nature of carbides after heat treatment. x1000

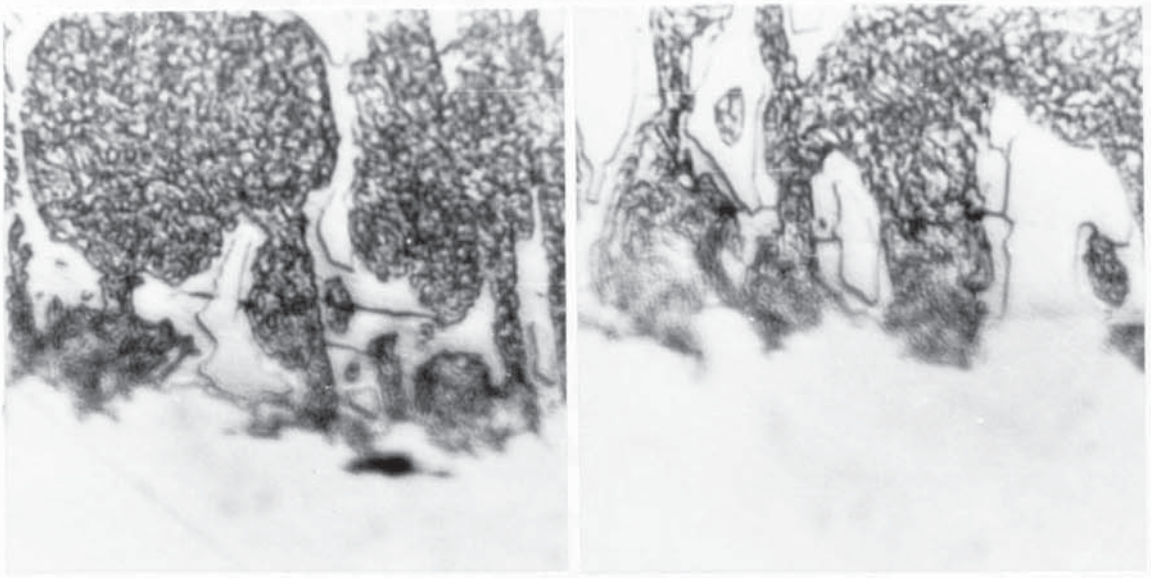

(b)Views at wear surface.Wear direction ---→ X1800
Cracking in outer carbide appears to halt at inner carbide.

Figure 4.36

Microstructure of iron 7 (2.4%C-30%Cr) in heat treated condition.

Microhardness tests were also carried out using a Vickers M12a microhardness tester. Variations in matrix microhardness were studied using traverses from the worn edges to inner undamaged regions. A number of attempts was made to determine the hardness of the eutectic carbides but the values obtained varied widely particularly in the case of the discontinuous fine lamellar type carbides which were so small that very small loads had to be used in testing.

The results of microhardness determinations for the as-cast and heat treated irons are given in tables 4.12 and 4.13. Determinations were made at the immediate wear surface and at given distances in from the wear surface. The figures in the tables are expressed in terms of maximum, minimum and mean values of matrix hardness away from the worn edge and at the worn edge. The latter values were obtained from determinations made within 50 μm of the surface. The difference in mean values is given as a guide to the extent of matrix work hardening during the course of the wear test. For example, irons 3, 4 and 5 which when tested in the as-cast condition with pearlitic matrix structures gave hardness increases of 30-50. Irons 6 and 7 which were austenitic gave hardness increases of over 300 due to the greater work hardening characteristics of the austenite. The ferritic iron (iron 8) which was heavily distorted in the surface regions also gave appreciable hardening with an increase of over 100 points.

Iron	Matrix	Centre			Edge			Difference in means
		max	min	mean	max	min	mean	
1	Pearlite	282	251	262	374	328	354	92
2	"	473	423	447	554	453	500	53
3	"	554	473	517	644	515	561	44
4	"	578	542	562	642	554	596	34
5	P +A	590	565	574	677	590	620	46
6	Austenite	415	381	397	947	542	744	347
7	"	447	374	415	950	565	757	342
8	Ferrite	310	290	300	453	375	414	114
9	Pearlite	344	318	334	455	423	436	102

Table4.12 Results of microhardness tests on 0-35% Cr irons (as cast condition).Microhardness of matrix away from and at worn edge.

Iron	Centre			Edge			Difference in means
	max	min	mean	max	min	mean	
2	902	834	850	978	835	898	48
3	880	845	866	953	902	927	61
4	869	834	842	927	902	910	68
5	814	785	798	869	795	822	24
6	814	775	780	880	775	826	46
7	739	673	705	835	749	788	73
10	953	880	910	1034	953	1004	94

Table4.13 Results of microhardness tests on heat treated irons.Microhardness of matrix away from and at worn edge.

The extent of work hardening in the two austenitic irons and in the ferritic iron is shown in graphical form in figures 4.37-9. For comparison in terms of depth of hardening figure 4.40 has been plotted from values obtained by Durman (59). This represents the hardness of a 25% Cr, 3% C austenitic ball which has been in service in a grinding mill. Values were determined at different depths using a Vickers hardness tester with a 5kg load.

Microhardness determinations made on the eutectic carbides were subject to wide variation particularly for the discontinuous lamellar carbides. The M_3C type continuous carbides gave less variation and in irons 1 and 2 values ranging from 1070-1280 were obtained. There was no significant difference in hardness between the M_3C carbides in the 0.1% Cr iron (iron 1) and the 5% Cr iron (iron 2). In the higher chromium irons the values obtained varied from 1440 to 1910. In these irons the carbides were lamellar and consequently a small load of 10gm had to be used to ensure that the impression was not wider than the carbide plate and to avoid cracking around the impression. At this load small errors in ocular reading could give differences of 100-150 hardness points at the 1400-1900 level. Because of these variations it was not possible to determine whether carbides at the wear surface had work hardened as a result of wear deformation or if the M_7C_3 carbides varied in hardness according to the chromium content of the iron.

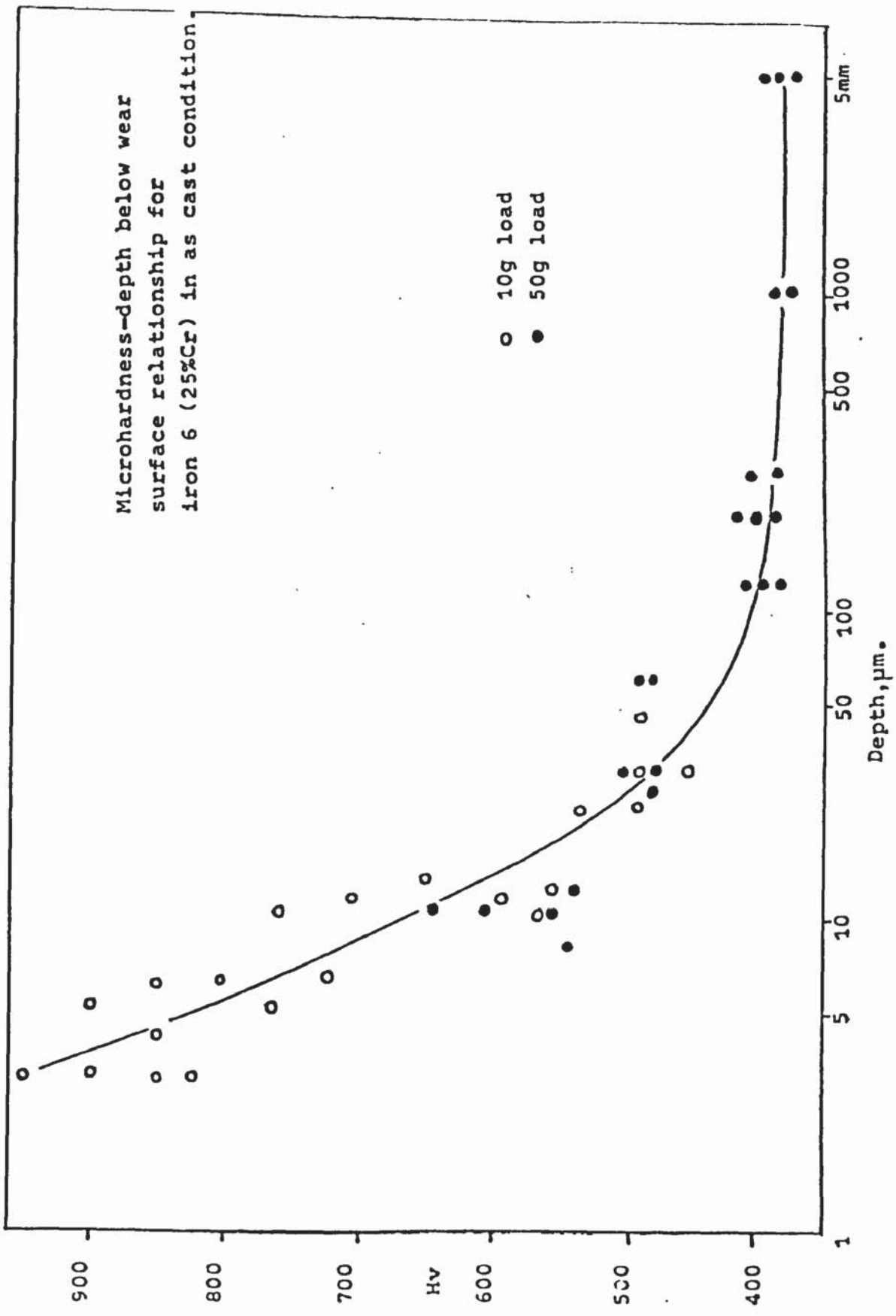
Microhardness-depth below wear surface relationship for iron 6 (25%Cr) in as cast condition.
o 10g load
• 50g load
Hv
900
800
700
600
500
400
1
5
10
50
100
500
1000
5mm
Depth, µm.

Figure 4.37

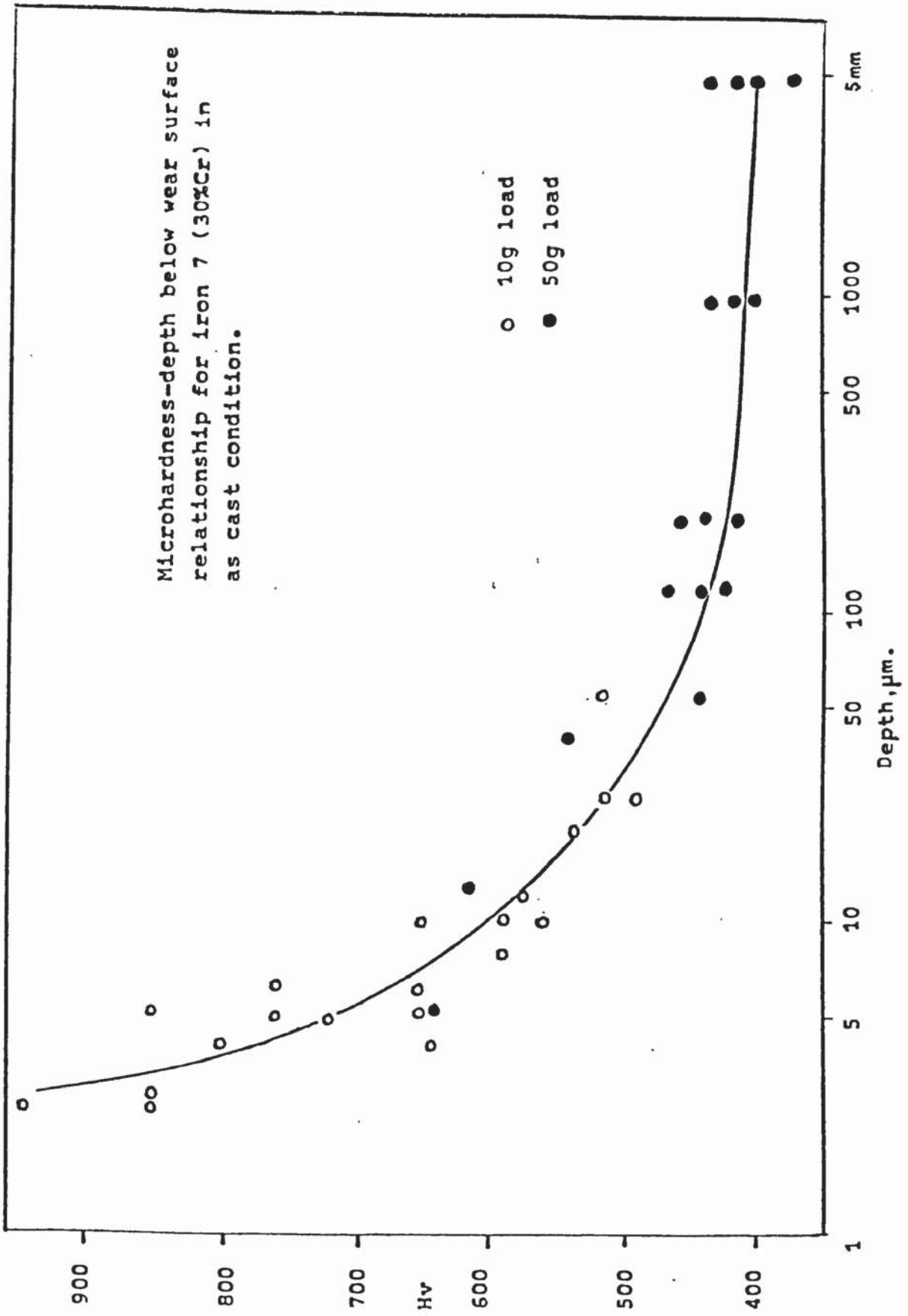
Microhardness-depth below wear surface relationship for iron 7 (30%Cr) in as cast condition.
o 10g load
● 50g load
Hv
900
800
700
600
500
400
1
5
10
50
100
500
1000
5mm
Depth, µm.

Figure 4.38

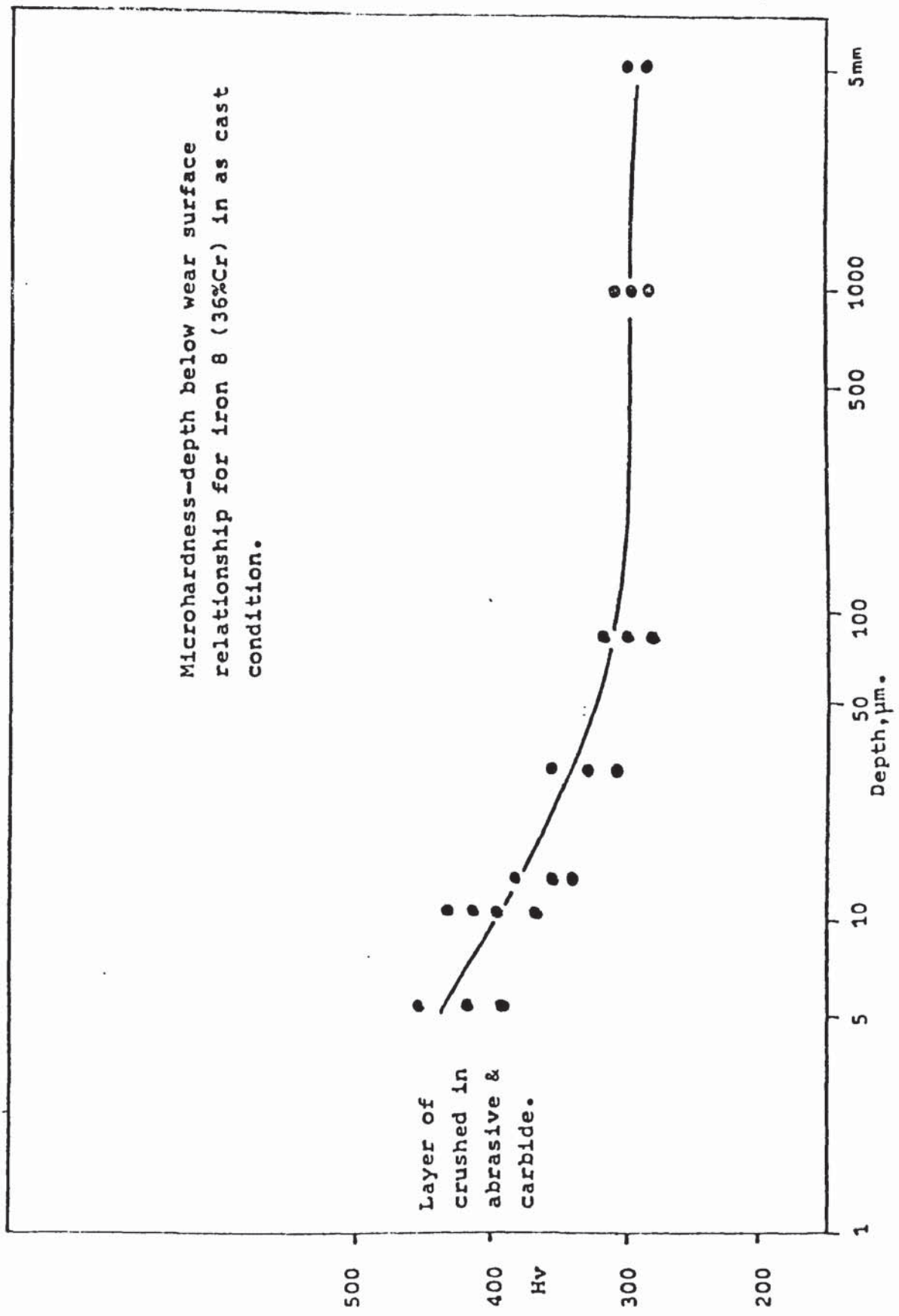
Microhardness-depth below wear surface relationship for iron 8 (36%Cr) in as cast condition.
Layer of crushed in abrasive & carbide.
Hv
500
400
300
200
1
5
10
50
100
500
1000
5mm
Depth, µm.

Figure 4.39

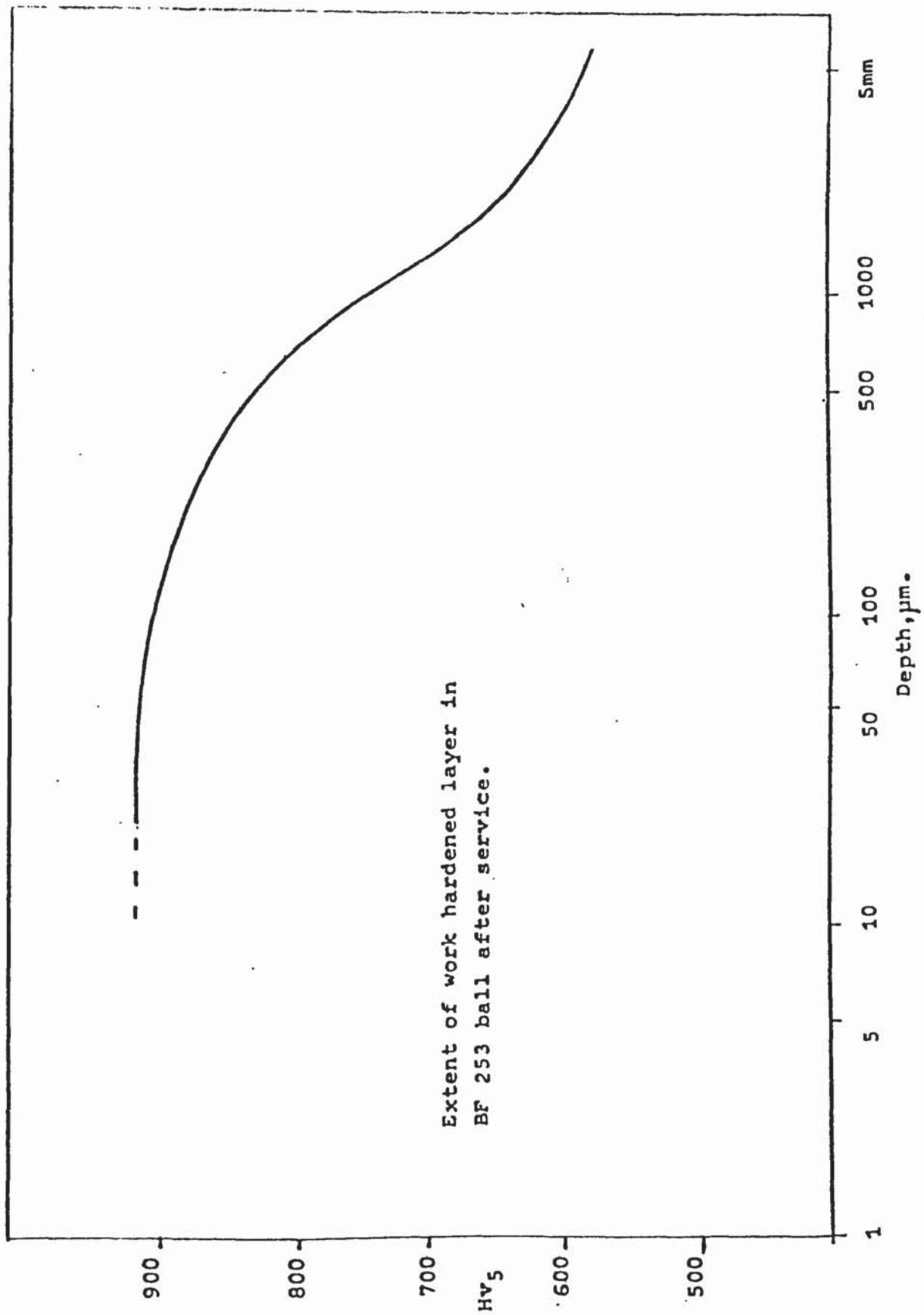
Extent of work hardened layer in
BF 253 ball after service.
900
800
700
600
500
Hv_5
1
5
10
50
100
500
1000
5mm
Depth, µm.

Figure 4.40

With the exception of iron 4 all the heat treated irons were fully martensitic with the matrix microhardness decreasing with increase in chromium content. Iron 4 contained between 10-20% non-martensite transformation product. Microhardness values of 570-644 were obtained in areas containing this product.

4.6 Scanning electron microscopy.

Worn surfaces of representative irons were examined using specimens 10 x 10 mm square x 5 mm high. After cutting the specimens were cleaned in an ultrasonic bath using chlorothene to remove debris from sectioning and were stored in a dessicator prior to examination on a Cambridge Stereoscan microscope. This was also used to study the microspecimens which had already been examined by conventional microscopy. To achieve this the specimens were re-prepared and then carefully removed from their plastic mounts without damage to the prepared surface so that they would fit onto a small specimen stub for the microscope. This type of observation was used instead of a replica technique since it did not give interpretation difficulties. A small number of shadowed two stage carbon replicas of microstructures at the wear surfaces were prepared and examined by transmission electron microscopy. The field of view at the worn surface was limited by the wires of the supporting grid. The use of a finer grid caused cracking of the replica, such that it was difficult to

determine whether observed cracks were in the original specimen or were actually in the replica. Using SEM the structure at the worn edge was clearly seen and the extent of damage could be surveyed.

4.6.1 Examination of Metallographic sections.

Studies of the damage in irons 1 and 2 in the as-cast condition revealed cracking of the eutectic carbide at the wear surface and removal of the pearlite from between the eutectic carbide. Figure 4.41 shows how the silica sand abrasive has been crushed into the pearlite areas in iron 1. The black flakes seen are eutectic graphite which was present in the as-cast structure. Examination of iron 2 in the heat treated condition revealed less cracking of the M_3C eutectic carbide but the matrix which was tempered martensite was removed from between the carbide as in the pearlitic iron. This effect is seen in figures 4.42 and 4.43. In both the as-cast and heat treated irons because the eutectic carbide was continuous it tended to remain in position unless it was severely cracked.

Figure 4.44 illustrates the damage observed in the irons containing discontinuous eutectic carbides in a pearlite matrix. It shows more clearly the extent of cracking seen earlier by conventional metallography. Figures 4.45-6 represent the effects of wear in iron 7 which had an austenitic matrix in the as-cast condition. The carbide plates contained several

parallel transverse fractures with the larger carbides being severely cracked. A small number of sub-surface cracks were seen in the austenite matrix as shown in figure 4.45 (b) which also reveals the void left by a piece of eutectic carbide removed on preparation. This is due to the effect of wear in loosening the carbide in the matrix since examination of the structure away from the wear surface did not reveal any cracking or indeed any removal of the eutectic carbides. In figure 4.47 the severe fragmentation of the carbides in the soft ferrite matrix of the as-cast 35% Cr iron is seen. In this case the wear surface consists of a heavily deformed layer containing crushed abrasive and carbide fragments.

A survey of the damage in the hardened 15% Cr iron (iron 4) revealed several interesting features. Cracks were observed in both the eutectic carbides and the matrix which was tempered martensite with a small amount of pearlite. In addition wear caused separation at the eutectic carbide-matrix interface. Figure 4.48 presents general views of the sub-surface damage and figures 4.49-51 show the separation of the carbide from the matrix as the structure deforms in the direction of wear. The large matrix crack seen in figure 4.50 (a) was not typical and the more usual form of matrix cracking seen is illustrated by that shown in the top RH corner of figure 4.51. This crack appears to follow a sub-boundary in the matrix. Figure 4.51 shows how cracks in the eutectic carbide coincide with voids which have developed at the eutectic carbide-matrix interface.

Figure 4.52 confirmed the metallographic evidence described earlier where the eutectic carbides in the higher chromium irons tend to crack and then become detached from the matrix. This shows the hardened 25% Cr iron in which there is little evidence of deformation in the wear direction but the carbides have fractured just below the immediate surface. Figures 4.53 and 4.54 represent the effects of wear in the heat treated 30% Cr iron in which the eutectic carbide is believed to be duplex in nature. The outer carbide which appears lighter in shade contains cracks which do not always propagate into the second carbide which appears darker.

The wear damage in the hardened 15% Cr - 3% Mo iron which was the most abrasion resistant of all the irons tested is shown in figures 4.55 and 4.56,little deformation of the matrix is evident and the carbides contain very few cracks. The shallow crack seen in figure 4.56(b) is typical and this leads to removal of small fragments of carbide from the surface.

4.6.2 Examination of worn surfaces.

Representative samples from the wear test specimens were also examined directly using SEM. The results of this examination are summarised in figures 4.57-4.68. In each figure the front of the wear test specimen is at the top of the photograph so that the direction of wear is from the top to the bottom. The figures taken at low magnification allow general comparison over the range of irons tested.

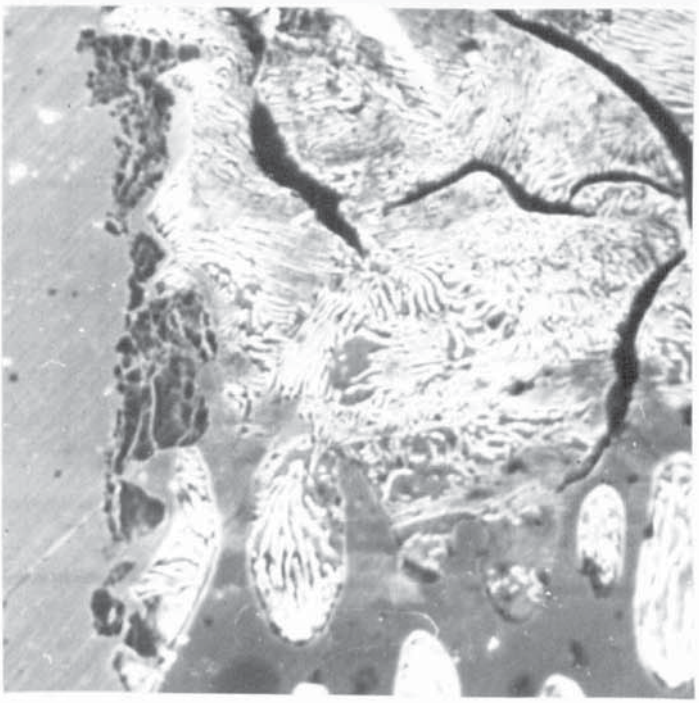

Figure 4.41
SEM view at wear surface of iron 1 (4%C) in as cast condition.Wear direction ↓ x1800

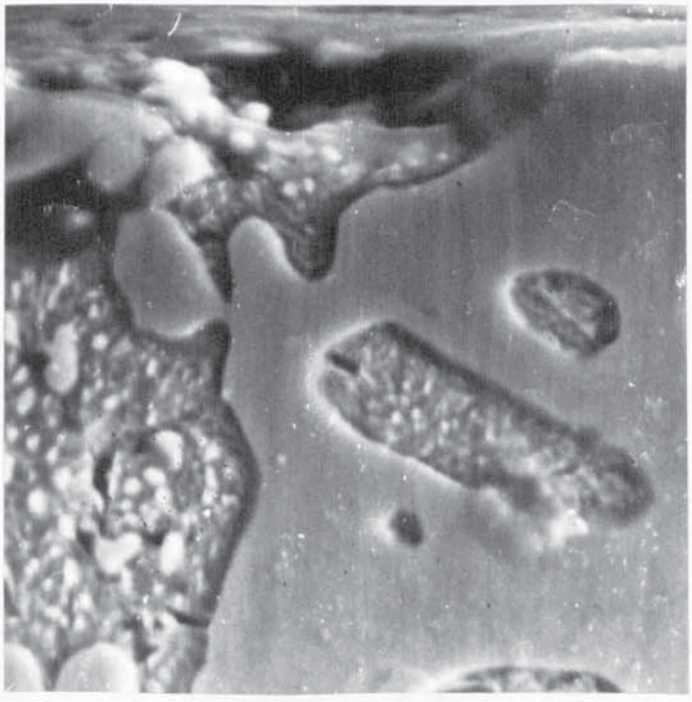

Figure 4.42
SEM view at wear surface of iron 2 (3.7%C-5%Cr) in heat treated condition.Wear direction ---→ x4500

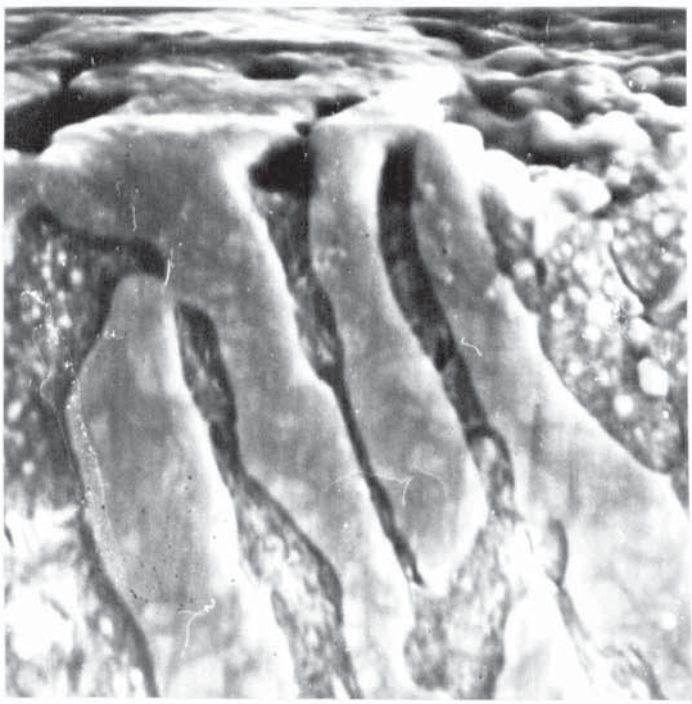

(a)Removal of matrix,no cracks seen in carbides.

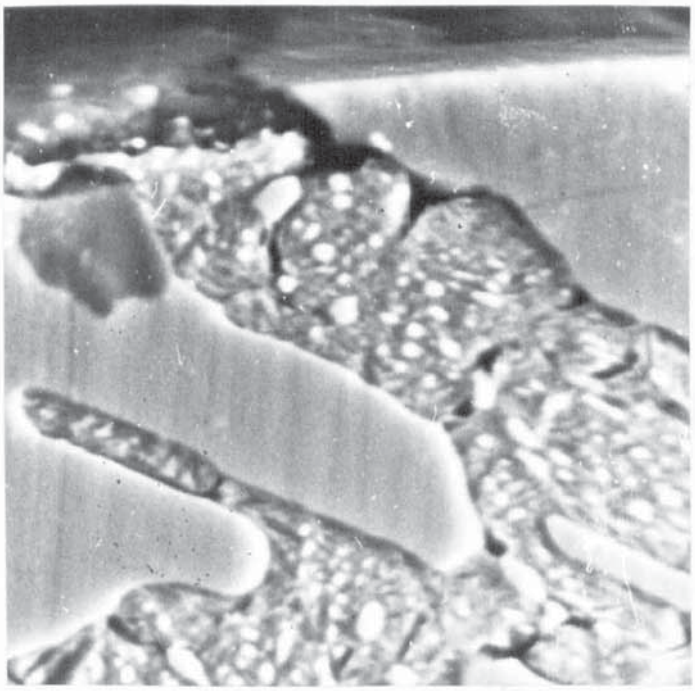

(b)Cracks in matrix around tempered carbide particles and separation at matrix-carbide interface.

Figure 4.43
SEM views at wear surface of iron 2 (3.7%C-5%Cr) in heat treated condition.Wear direction ---→
x4500

(a)Sub-surface cracking of eutectic carbides.

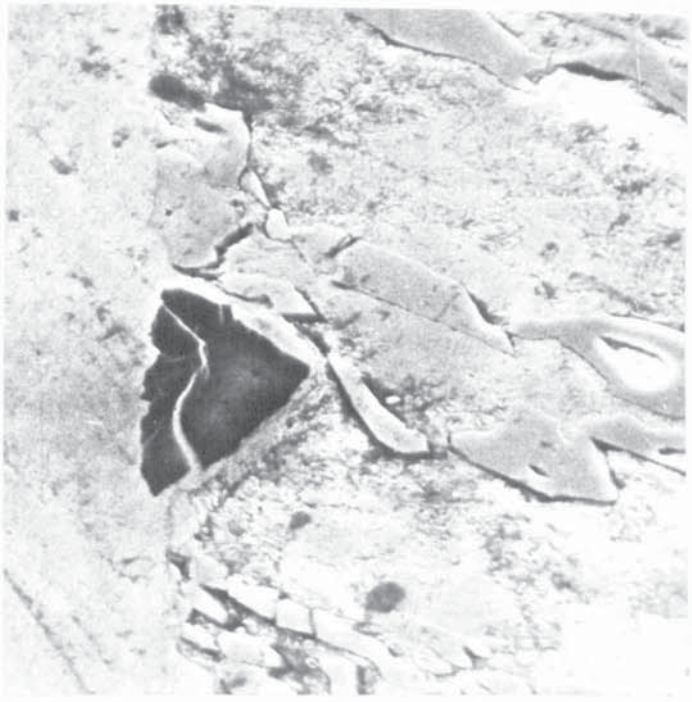

(b)Deformation around penetrating abrasive grain.

Figure 4.44

SEM views at wear surface of iron 4 (3%C-15%Cr) in as cast condition.Wear direction ↑ x2250

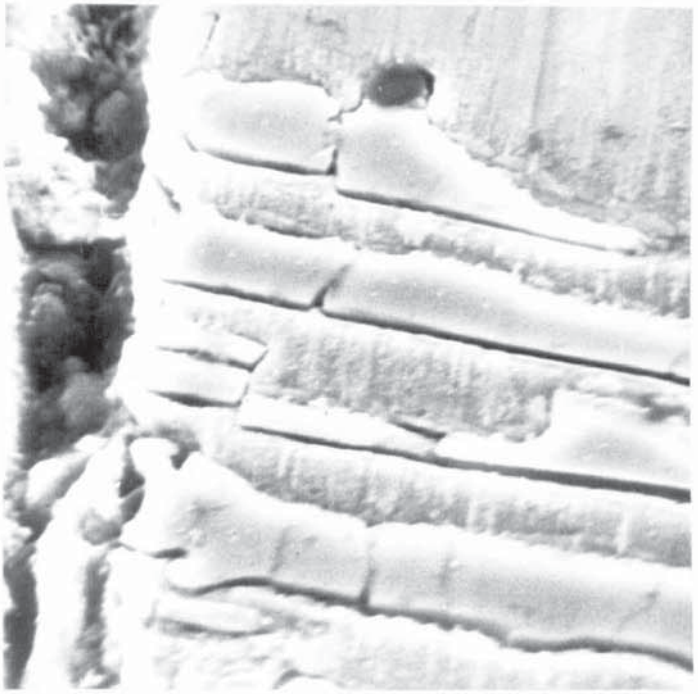

(a) Transverse cracks in eutectic carbides.

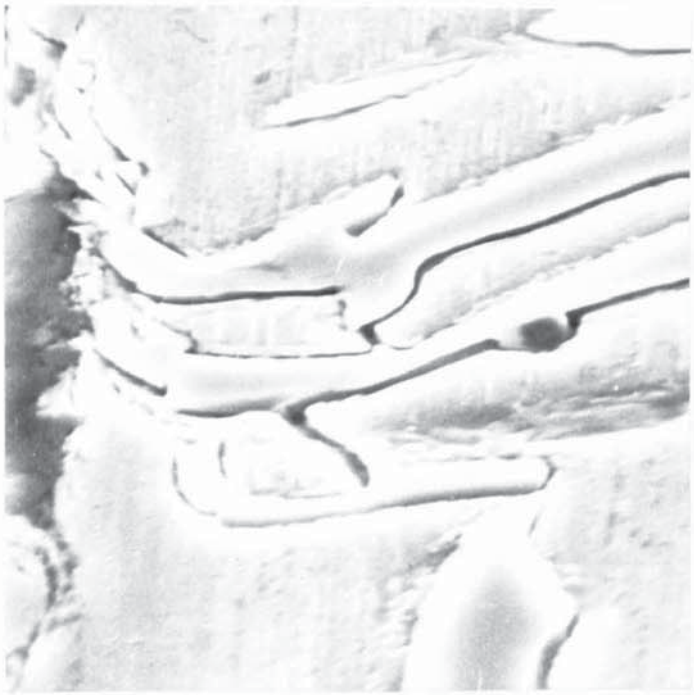

(b) Interface separation and cracking in eutectic carbides and in austenite.

Figure 4.45

SEM views at wear surface of iron 7 (2.4%C-30%Cr) in as cast condition. Wear direction ↑ x6000

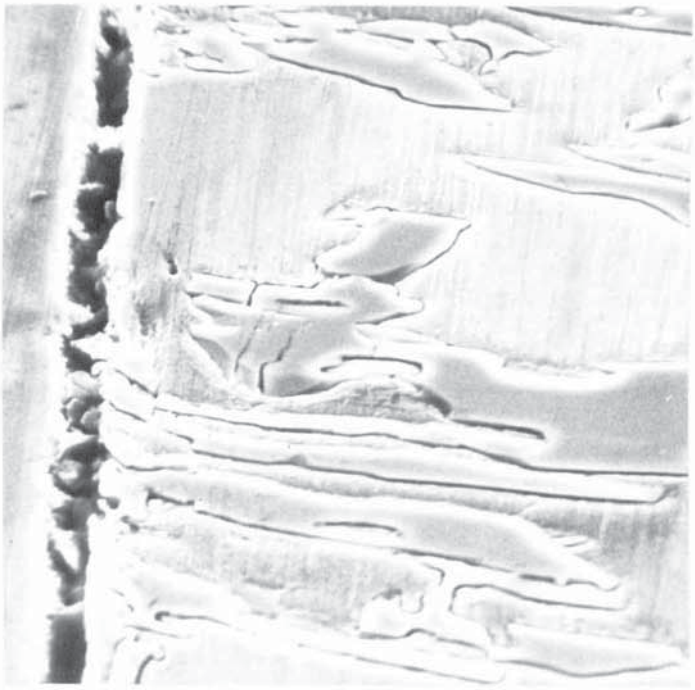

(a) General view (x2500)

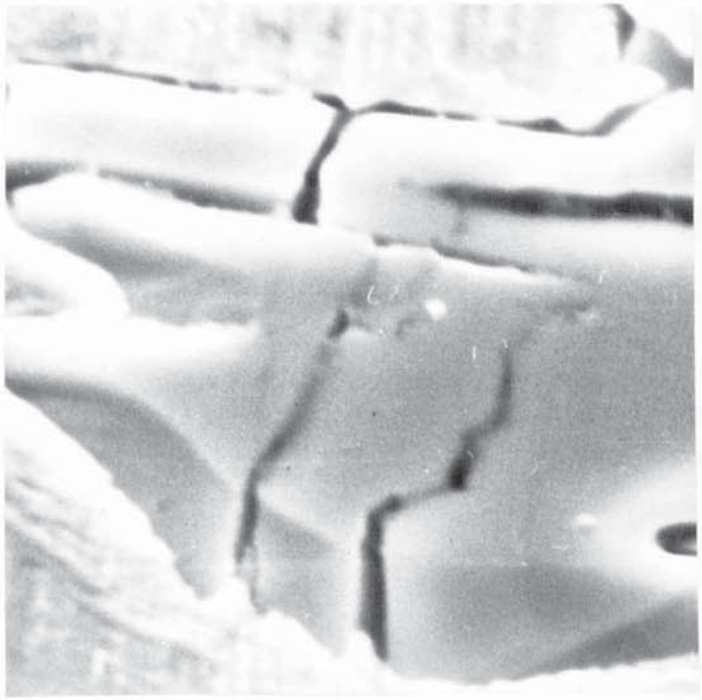

(b) View of severely cracked eutectic carbide in (a) (x10K)

Figure 4.46
Further SEM views of iron 7 (as Fig.4.45).Wear direction ↑

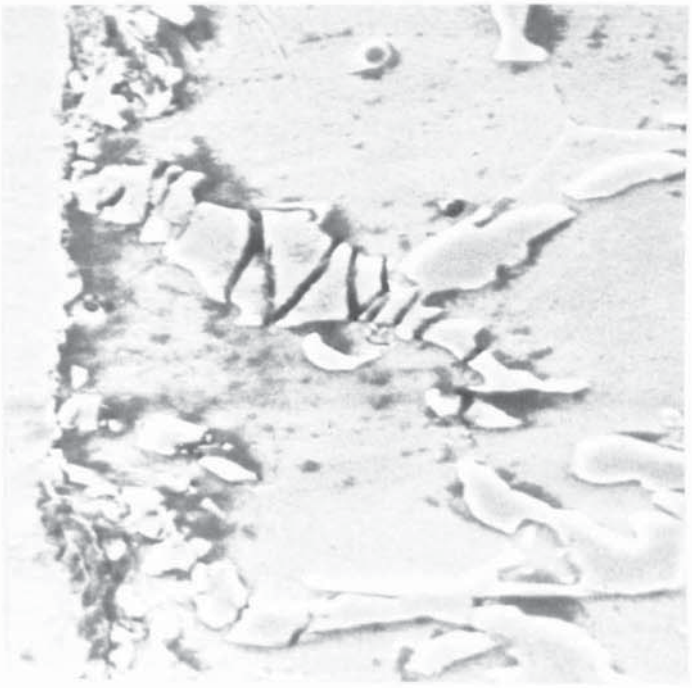

(a) Cracking causing fragmentation of eutectic carbide.

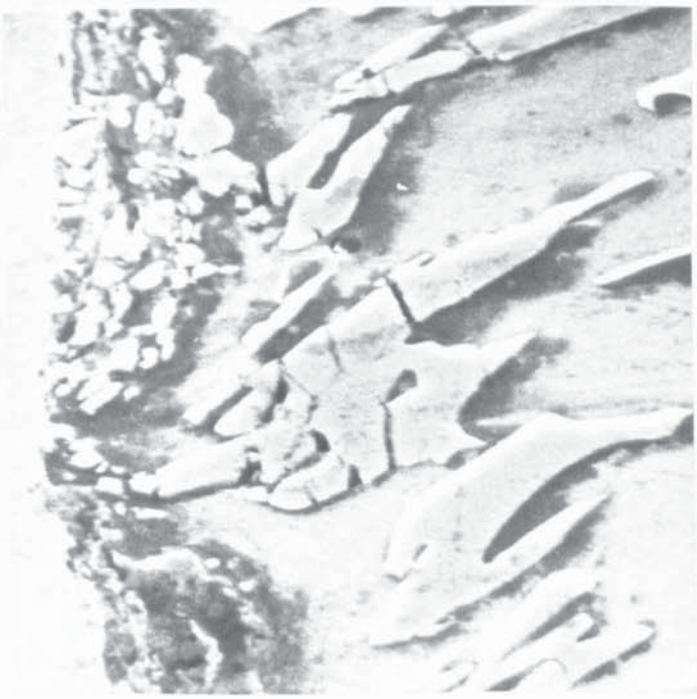

(b) Extent of crushed in layer at surface.

Figure 4.47

SEM views at wear surface of iron 8 (2%C-36%Cr) in as cast condition (ferrite matrix). Wear direction ↑ x5000

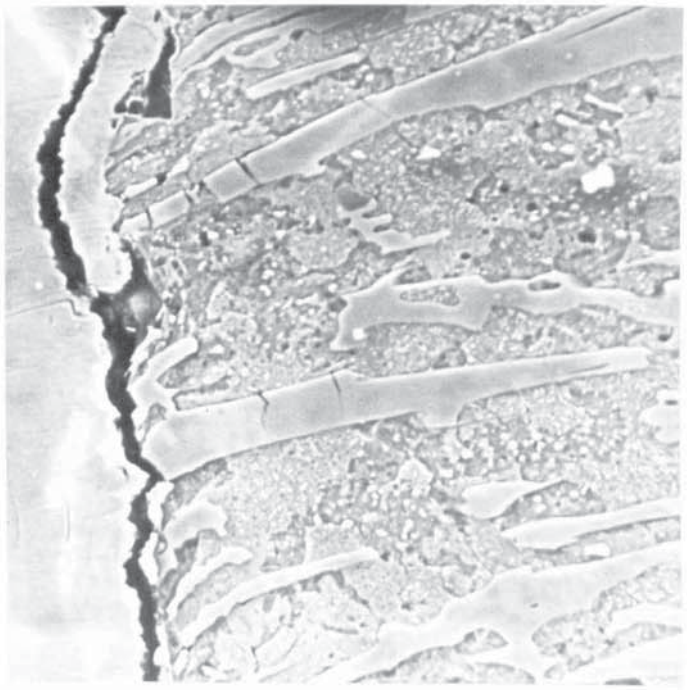

(a) Sub-surface cracks in eutectic carbides. ×1300

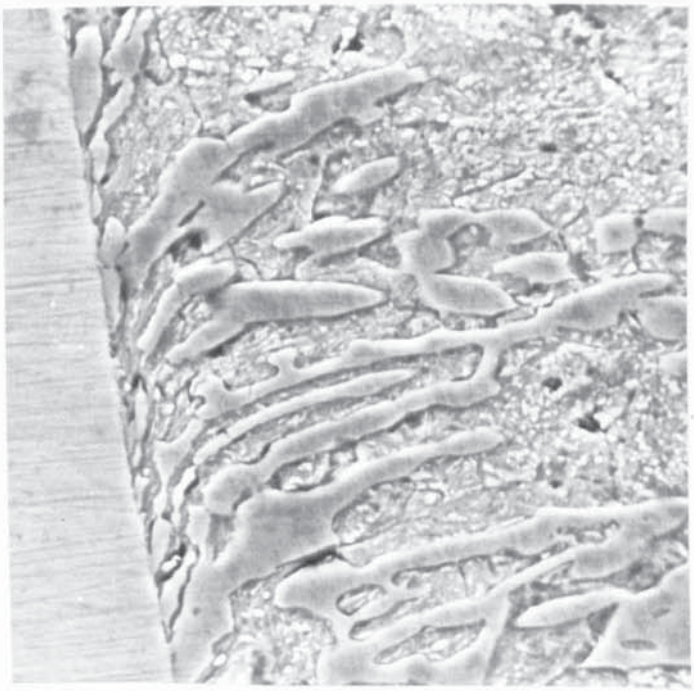

(b) Flow in wear direction. ×2000

Figure 4.48

SEM views at wear surface of iron 4 (3%C-15%Cr) in the heat treated condition. Wear direction ↓

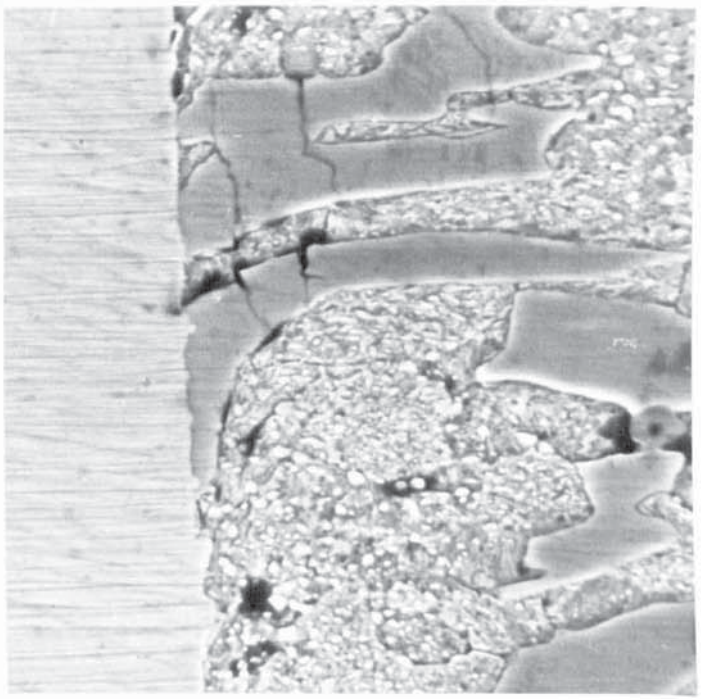

(a) Cracking of carbides with voids at carbide-matrix interface.

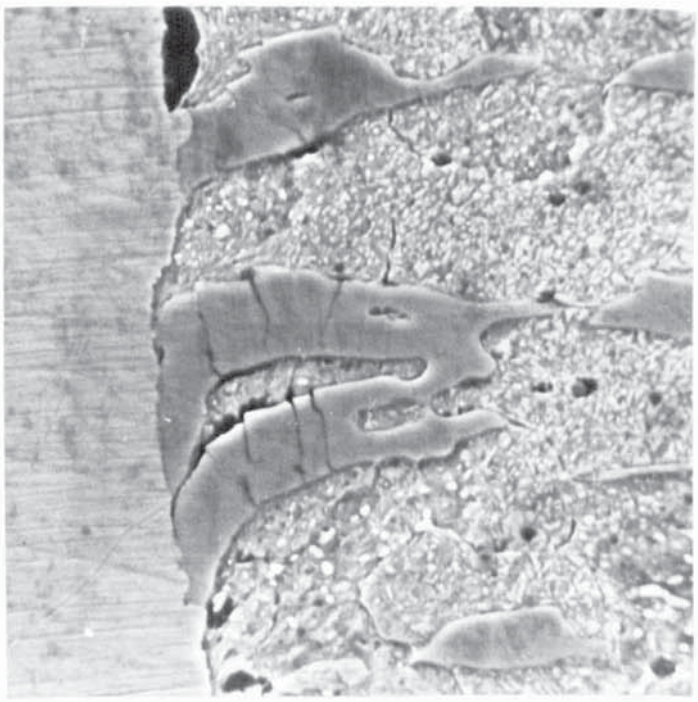

(b) Similar effects as in (a).

Figure 4.49
Further SEM views of iron 4 (as Fig. 4.48) ↓ x2000

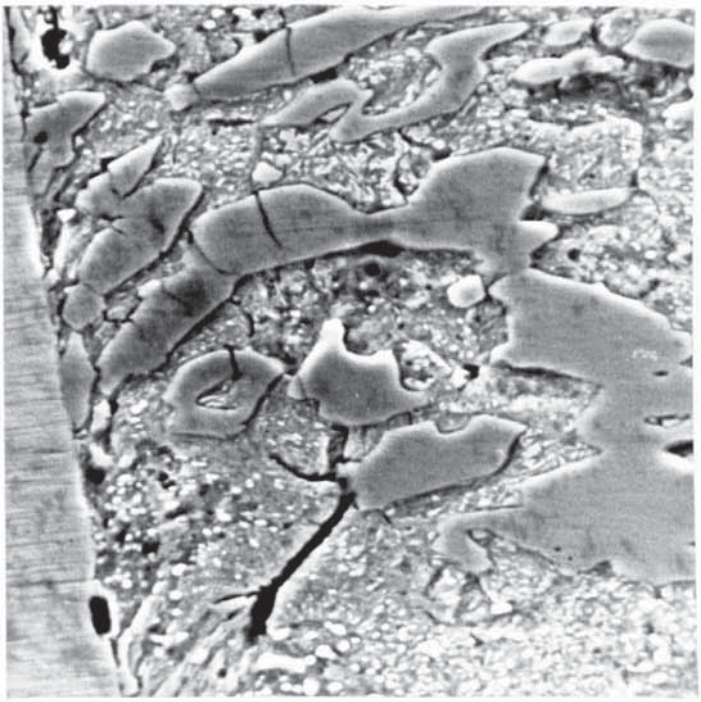

(a) Sub-surface crack in matrix.

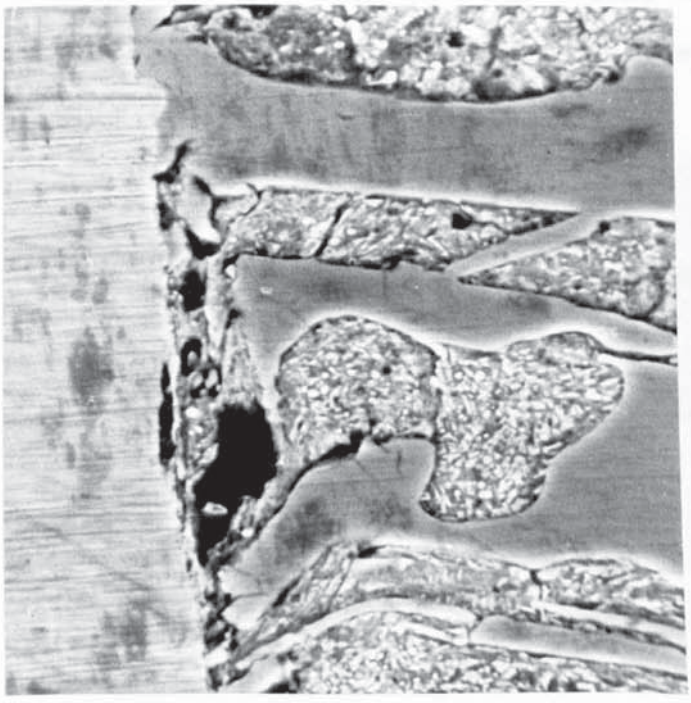

(b) Void at surface due to carbide removal and bending of thin carbide.

Figure 4.50

SEM views of iron 4 (as Figs. 4.48-9) ↓ x2000

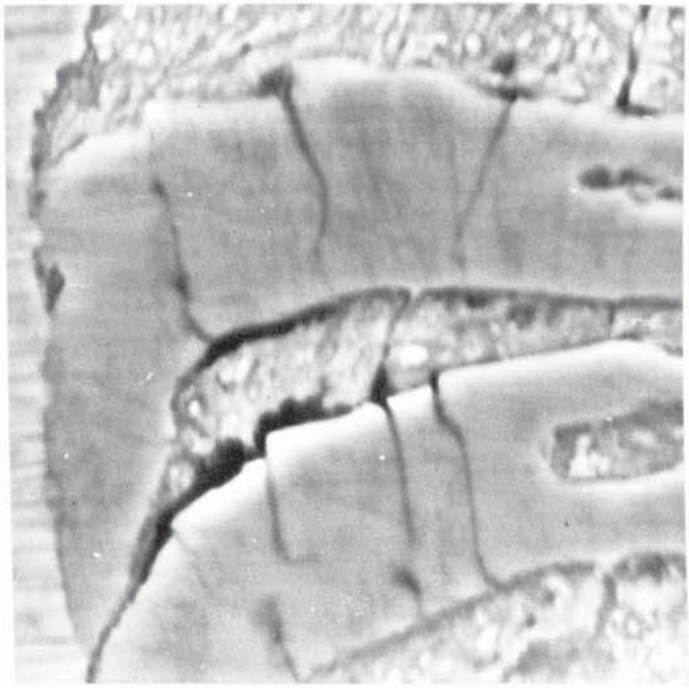

Figure 4.51
Iron 4.Cracking seen in Fig.4.49(b) at higher mag. (x6000)
Cracks in carbide coincide with voids at interface. ↓

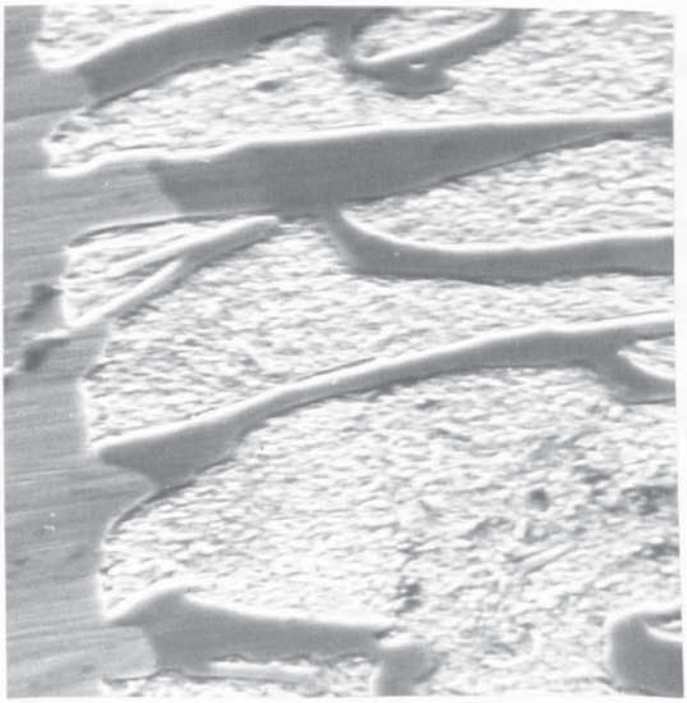

Figure 4.52
SEM view at wear surface of iron 6 (2.7%C-26%Cr) in heat treated condition.Sub-surface fracture of carbide leading to its removal. ↓ x2000

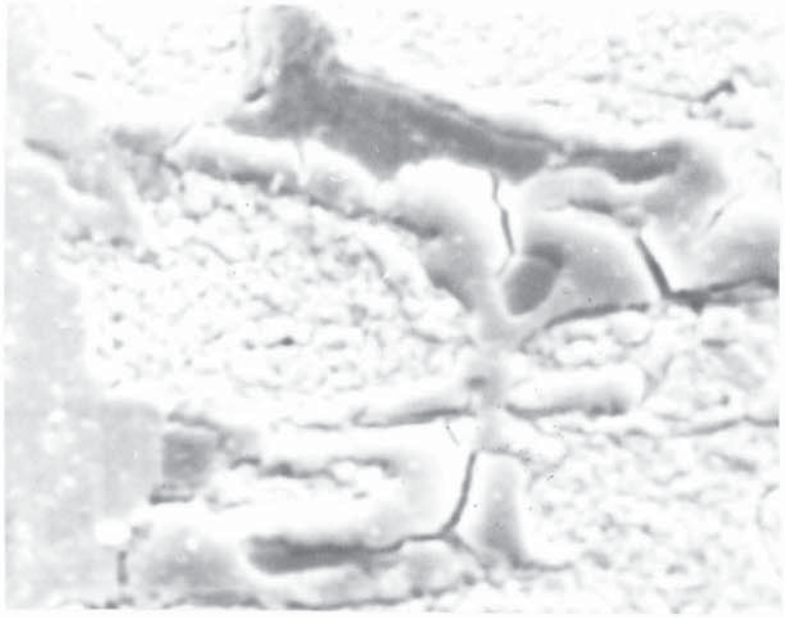

(a) Cracking in outer(lighter) carbide,cracks appear to arrest at inner(darker) carbide.

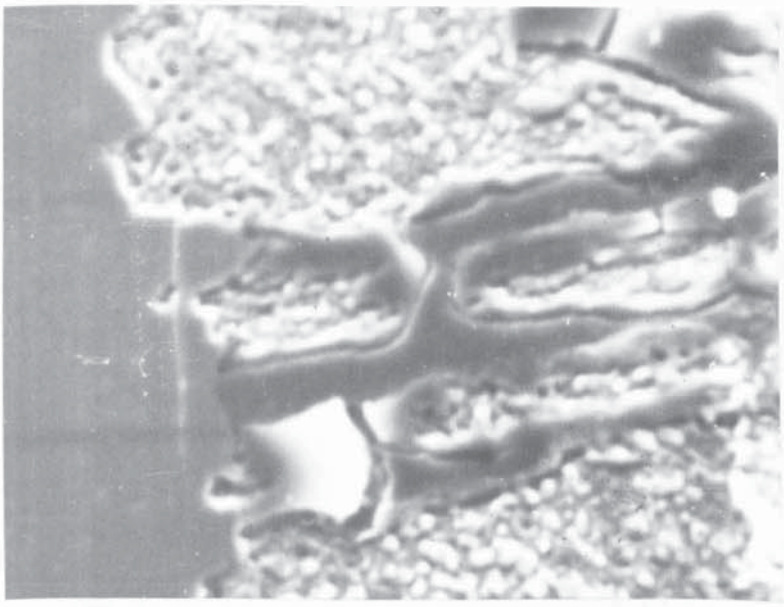

(b) Crack in lighter carbide.

Figure 4.53

SEM views at wear surface of iron 7 (2.4%C-30%Cr) in heat treated condition.Wear direction ↑ x4500

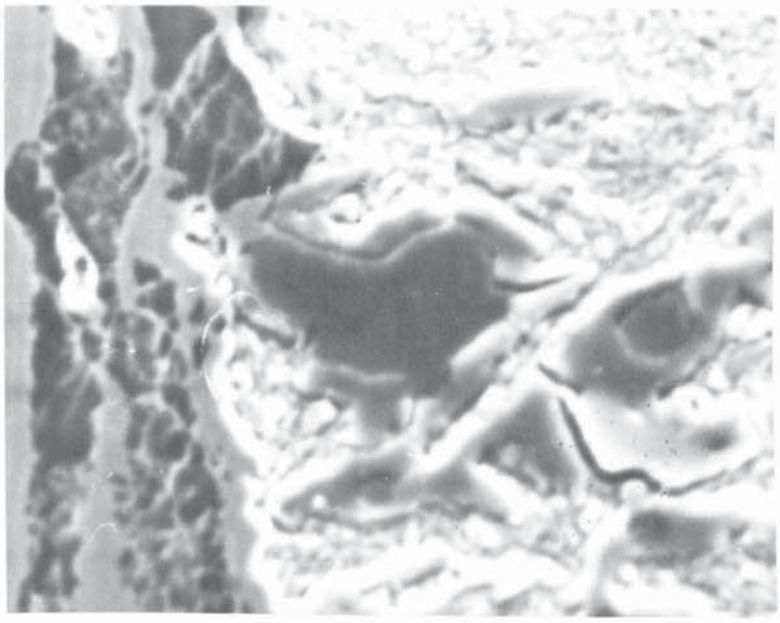

Figure 4.54
Further view of iron 7 (as Fig.4.53) showing surface penetration by crushed abrasive & cracking of carbide. x4500

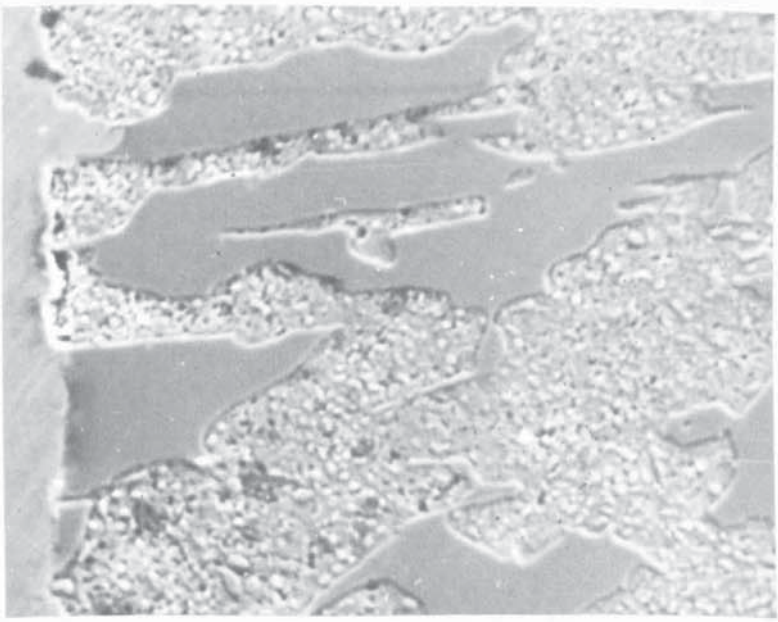

Figure 4.55
SEM view at wear surface of iron 10 (3%C-15%Cr-3%Mo) in heat treated condition. Wear direction ↓ x1800

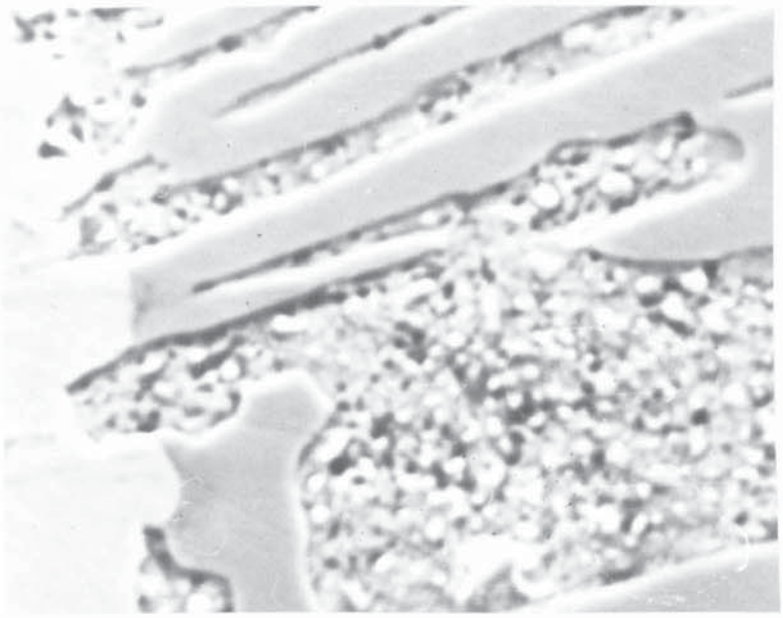

(a) Removal of eutectic carbide from just below surface.

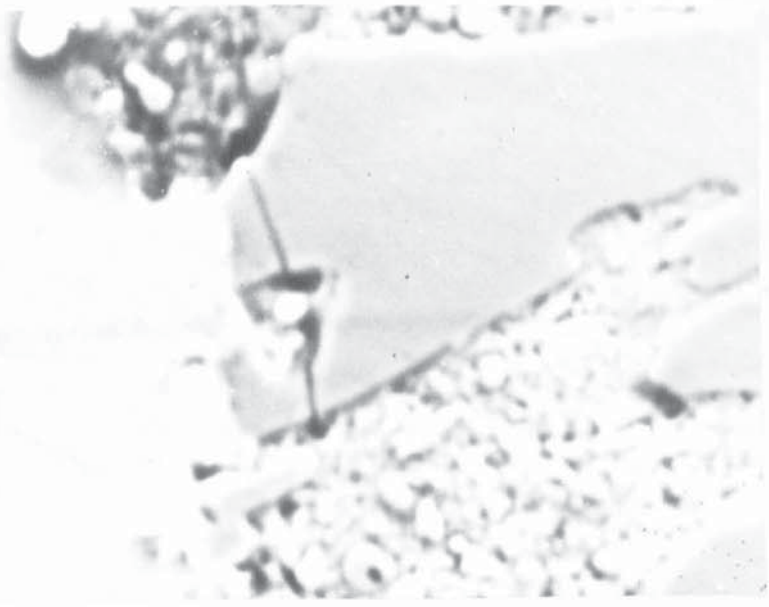

(b) Typical shallow depth of cracking in eutectic carbide.

Figure 4.56
SEM views at wear surface of iron 10 (as Fig.4.55) ↓ x4500

Figure 4.57(a) shows the grooved wear pattern produced in the as-cast 4% C iron (iron 1). The severely damaged area corresponds to an area of mottle and is seen more clearly in figure 4.57(b). Figure 4.58 shows the reduced damage in the fully white 5% Cr iron tested in the as-cast condition. Figure 4.59 allows comparison between the wear grooves in the 10% Cr iron (iron 3) before and after a hardening heat treatment. Figure 4.60 compares the damage in the as-cast 20% Cr iron with a matrix of austenite and pearlite with that in the as-cast 25% Cr iron which was fully austenitic.

Figure 4.61 reveals the severity of the surface disruption in the soft ferritic matrix 35% Cr iron. Figure 4.62 shows that in irons with martensitic matrix structures the wear surfaces are smoother with fewer pitted areas than in the as-cast irons which had softer pearlitic, austenitic or ferritic matrices.

Figures 4.63-4.68 present higher magnification views of the damage in selected irons. In figures 4.63 and 4.64 the pitted areas resulted from the removal of pearlitic and martensitic matrices respectively from between continuous M_3C eutectic carbides. In the higher chromium irons where the eutectic carbides are discontinuous the pitted areas were due to fracture and removal of these carbides from the matrix. In irons where the matrix is soft wide continuous wear scars can be seen running along the surfaces of the grooves (see

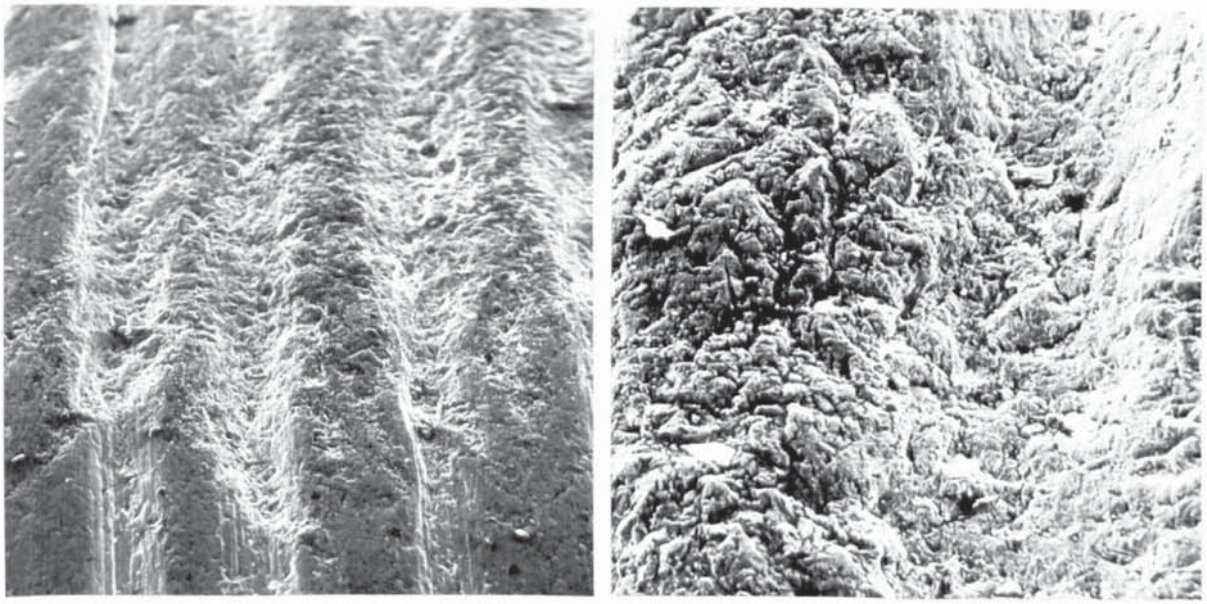

(a)Increase in wear damage mottled regions Hv=350. x60

(b)Severe damage in region containing eutectic graphite. x130

Figure 4.57

SEM views of wear surface of iron 1 (4%C-0.1%Cr) in as cast condition.(Hv=535 in fully white region of eutectic Fe_3C and pearlite.Wear index=0.98)

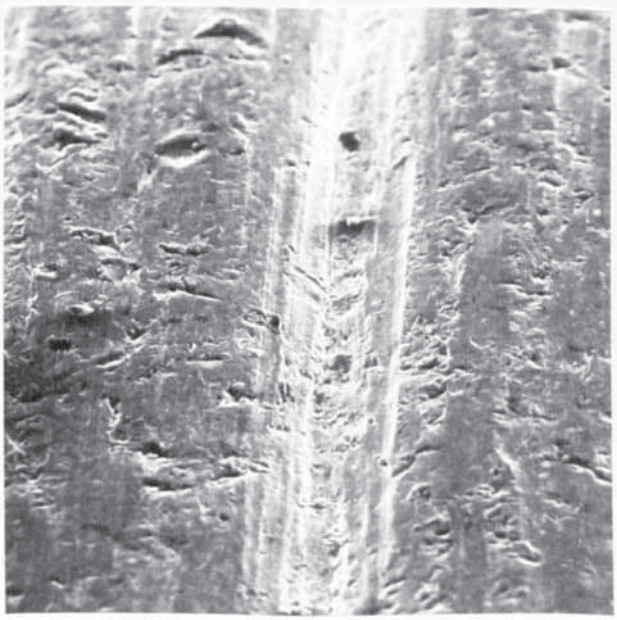

Figure 4.58

Wear surface of iron 2 (3.7%C-5%Cr) in as cast condition. (Hv=606,eutectic M_3C and pearlite.Wear index=1.25) x130

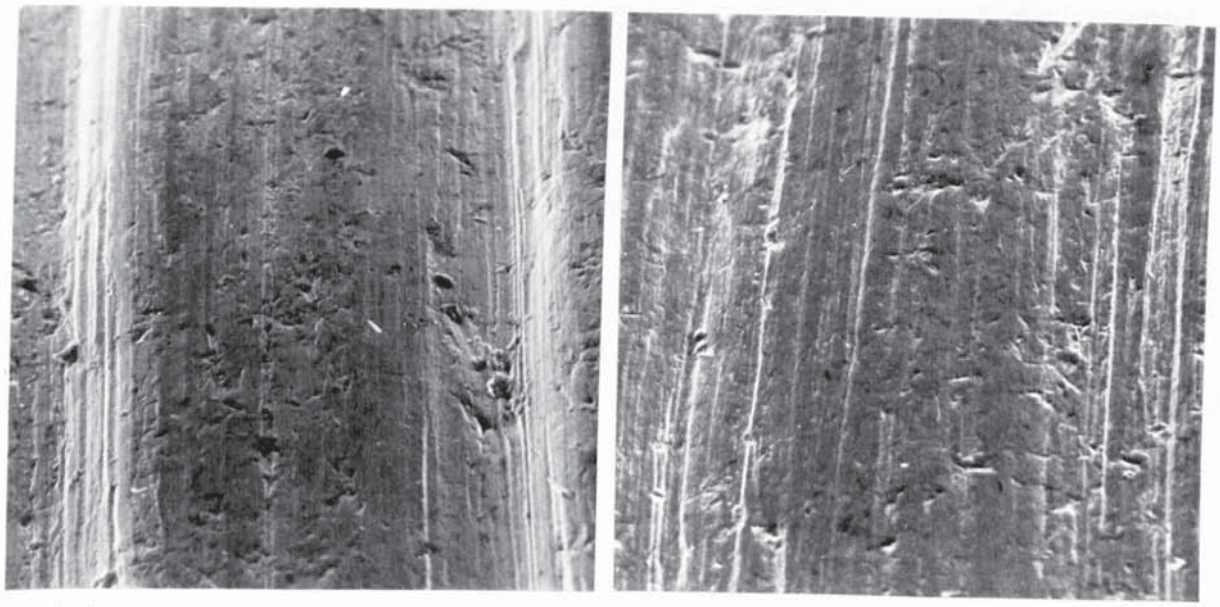

(a)As cast,pearlite matrix
Hv=564,wear index=0.95

(b)Heat treated,tempered martensite matrix.Hv=917,wear index=1.34

Figure 4.59

Wear surfaces in iron 3 (3.5%C-10%Cr) tested in (a) as cast & (b) heat treated conditions. ×120

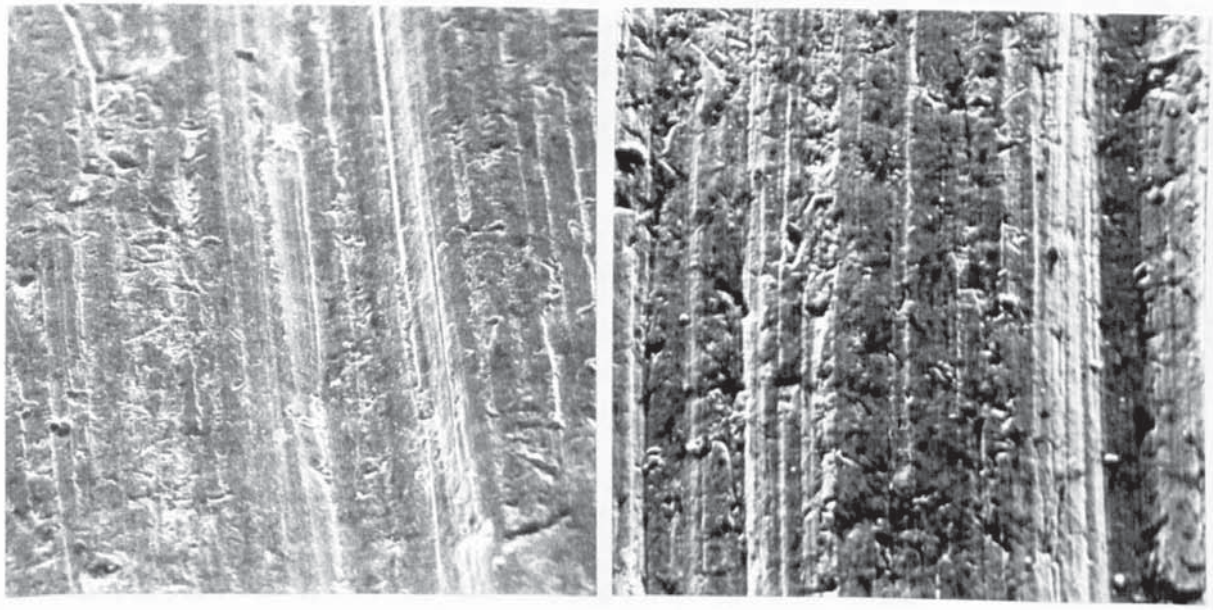

(a) 3%C-20%Cr iron
Pearlite+austenite matrix
Hv=590,wear index=1.10

(b) 2.7%C-26%Cr iron
Austenite matrix
Hv=580,wear index=0.82

Figure 4.60

Wear surfaces of irons 5 and 6 tested in as cast conditions. ×120

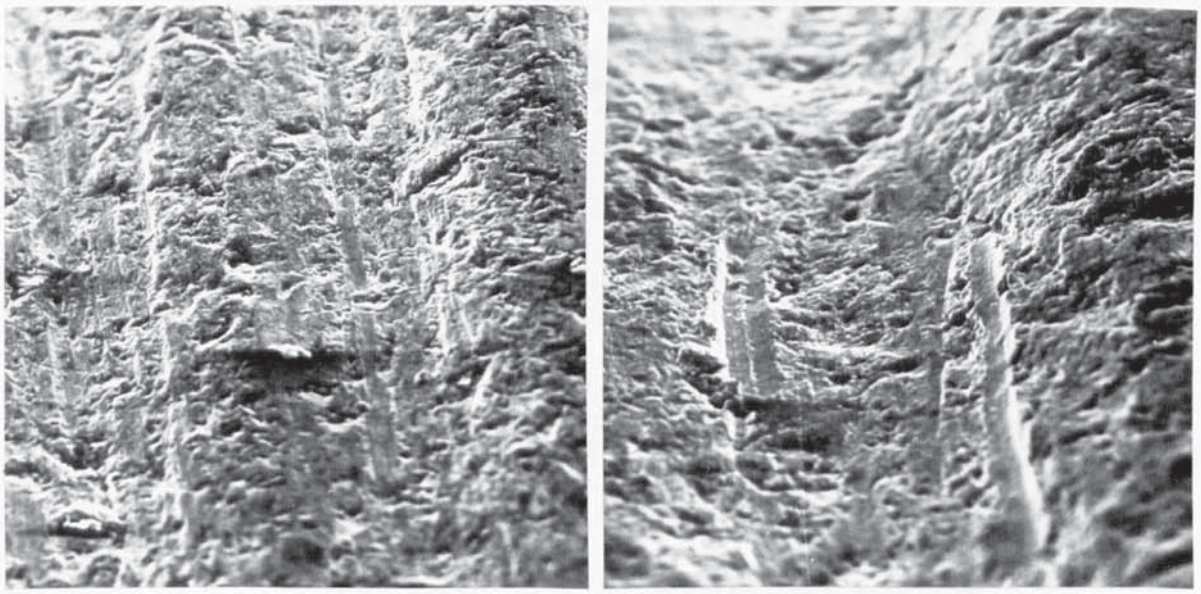

(a) View of wear grooves. x120

(b) Severe wear scars on sides of grooves.x250

Figure 4.61

Wear surface of iron 8 (2.1%C-36%Cr) tested in as cast condition. (Ferrite matrix, Hv=314, wear index=0.83.)

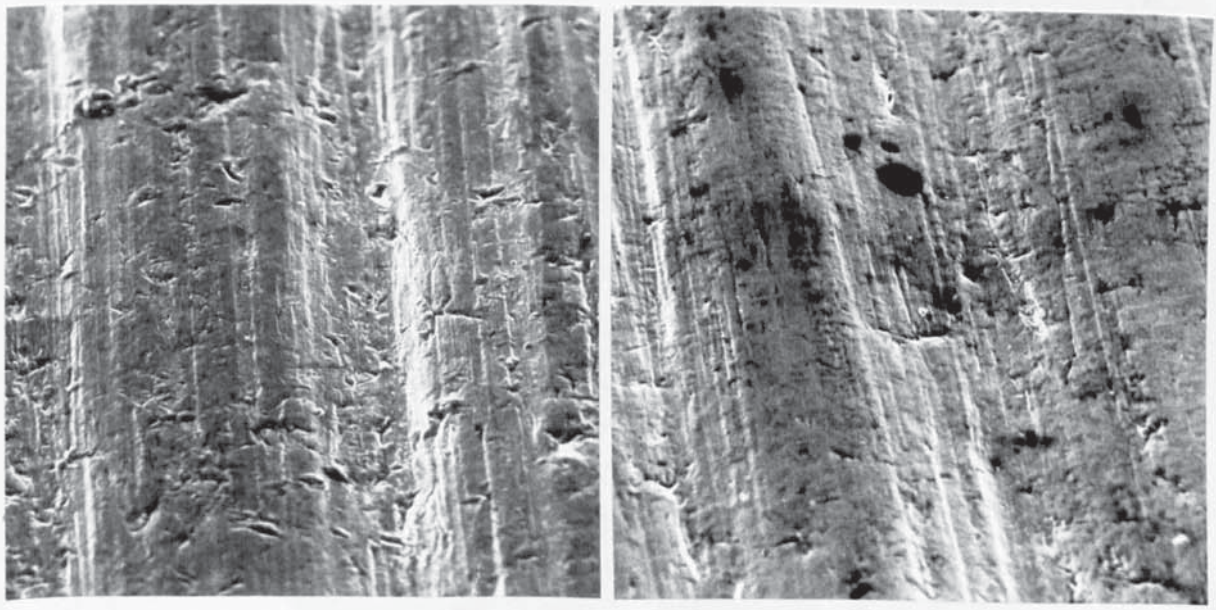

(a) 2.7%C-26%Cr iron Hv=825,wear index=1.05

(b) 3 %C-15%Cr-3%Mo iron Hv=950,wear index=2.29

Figure 4.62

Wear surfaces of irons 6 and 10 tested in the heat treated conditions.Tempered martensite matrices. x120

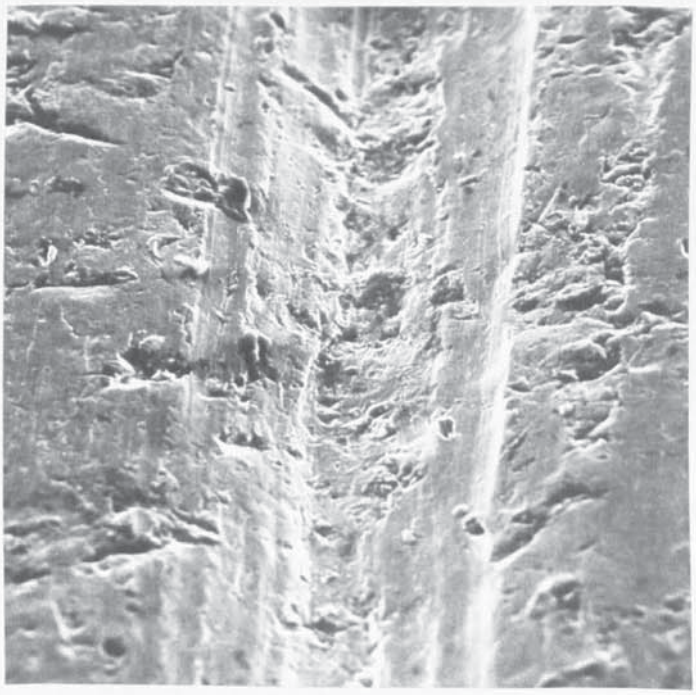

Figure 4.63
Wear surface of iron 2 (3.7%C-5%Cr) tested in as cast condition.
x300

Figure 4.64
Pitted areas on wear surface of iron 2 tested in heat treated condition. x1300

(a) 3.5%C-10%Cr iron, continuous wear scar on top of peak. Pearlite matrix (iron 3)

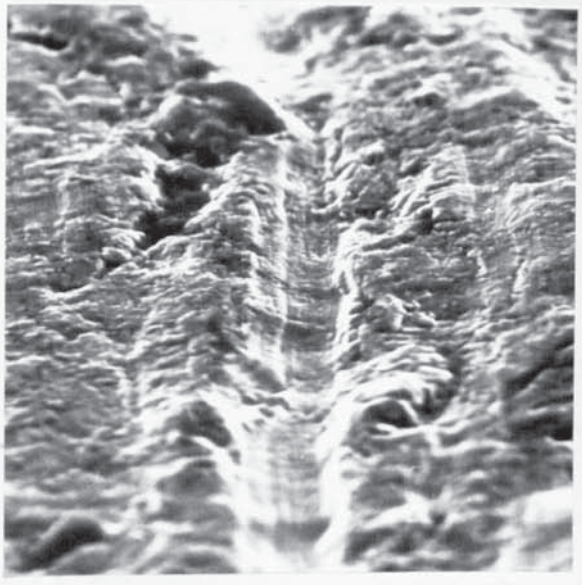

(b) 2.4%C-30%Cr iron 7 wear scar on top of peak, austenite matrix.

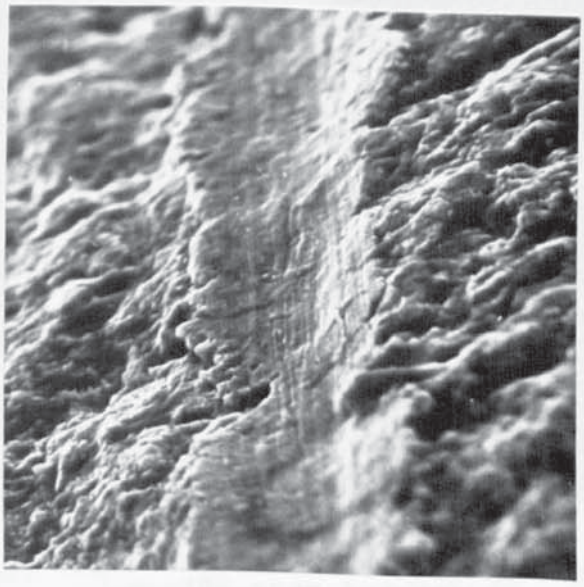

(c) 2.1%C-36%Cr iron 8, scar on side of wear groove, ferrite matrix.

Figure 4.65

Wear surfaces of irons 3,7 and 8 tested in as cast condition.

x1300

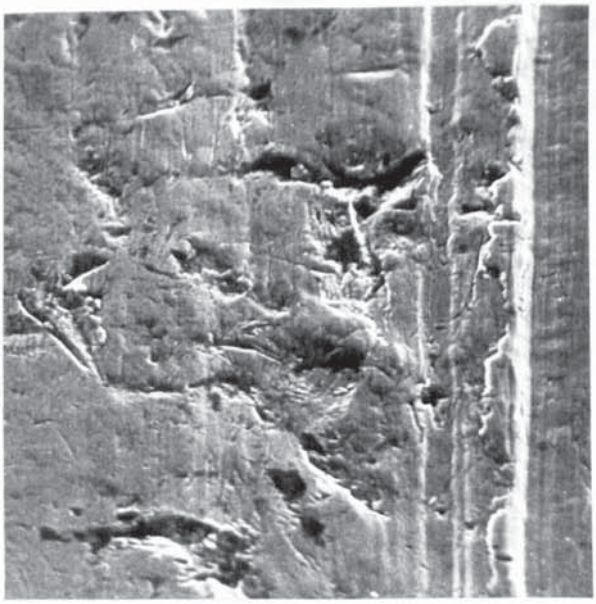

(a) Iron 3 (3.5%C-10%Cr)
Hv=917,wear index=1.34

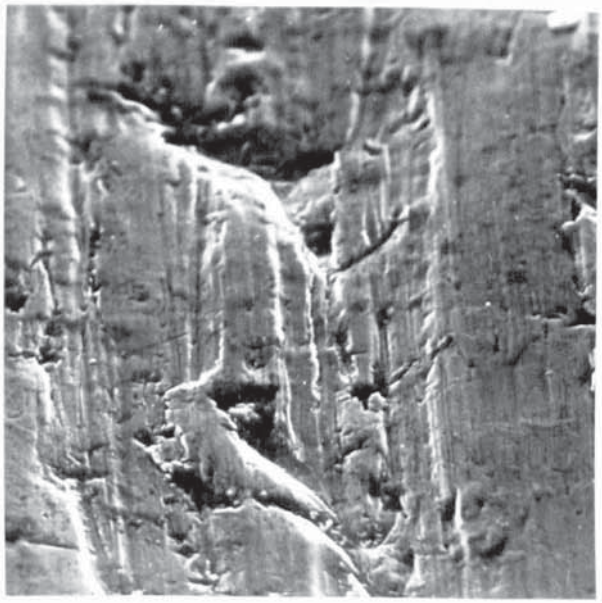

(b) Iron 4 (3%C-15%Cr)
Hv=800,wear index=1.32

(c) Iron 5 (3%C-20%Cr)
Hv=858,wear index=1.27

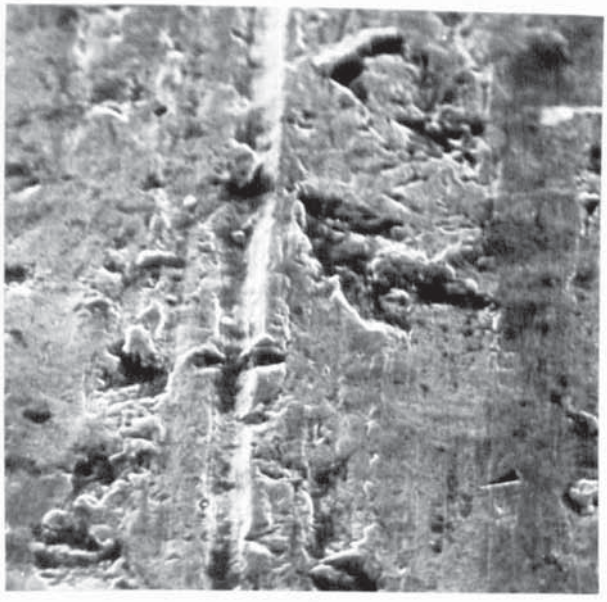

(d) Iron 7 (2.4%C-30%Cr)
Hv=794,wear index=1.06

Figure 4.66

Wear damage in irons tested in heat treated conditions.

x700

Figure 4.67
Wear surface of iron 6 (2.7%C-26%Cr) tested in heat treated condition.View across groove.Hv=825,wear index=1.05. x700

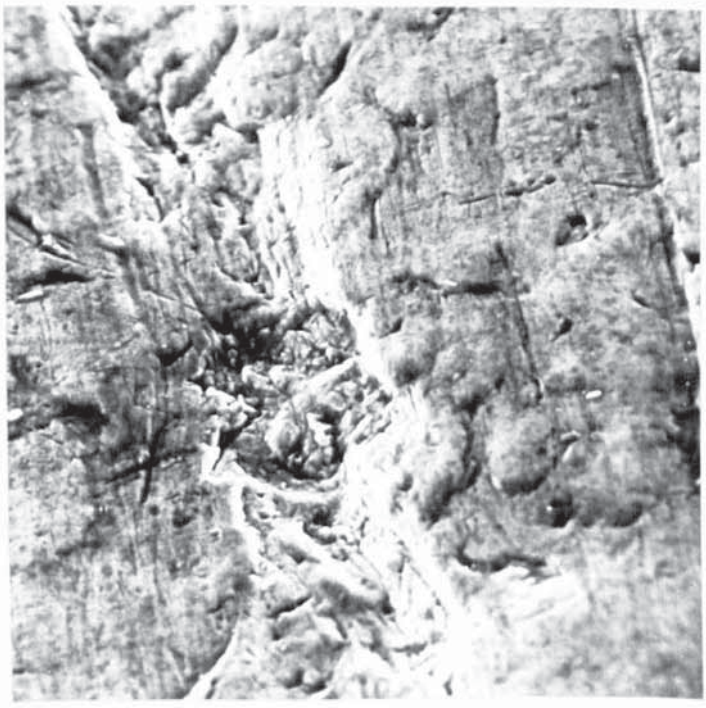

Figure 4.68
Local area of damage in iron 10(3%C-15%Cr-3%Mo) tested in hardened condition.Hv=950,wear index=2.29. x1300

figure 4.65). The damaged regions in the hardened higher chromium irons are compared in figures 4.66-4.68.

4.6.3 Examination of worn surfaces after matrix leaching.

In order to examine the severity of wear damage in the eutectic carbides by direct means several irons were subjected to deep etching which removed the matrix at the worn surface. This was achieved by leaching small specimens cut from wear test samples in 3% phosphoric acid for several hours. The specimens were washed and dried using organic solvents and were examined by scanning electron microscopy. Figure 4.69 shows severe cracking in the eutectic Fe_3C in the unalloyed white iron (iron 9) which was used as standard. In spite of the cracking the continuous eutectic carbide has remained in position. The grooving seen in the carbides corresponds to the wear direction.

Figures 4.70 and 4.71 show the 15% chromium iron where the M_7C_3 eutectic carbides are discontinuous. The flow and cracking of these carbides in the general wear direction is seen and these views confirm earlier metallographic evidence where carbides at the wear surface contained transverse parallel cracking.

In the 25% and 30% chromium irons the eutectic carbides were broken away with little apparent flow at the wear surface.

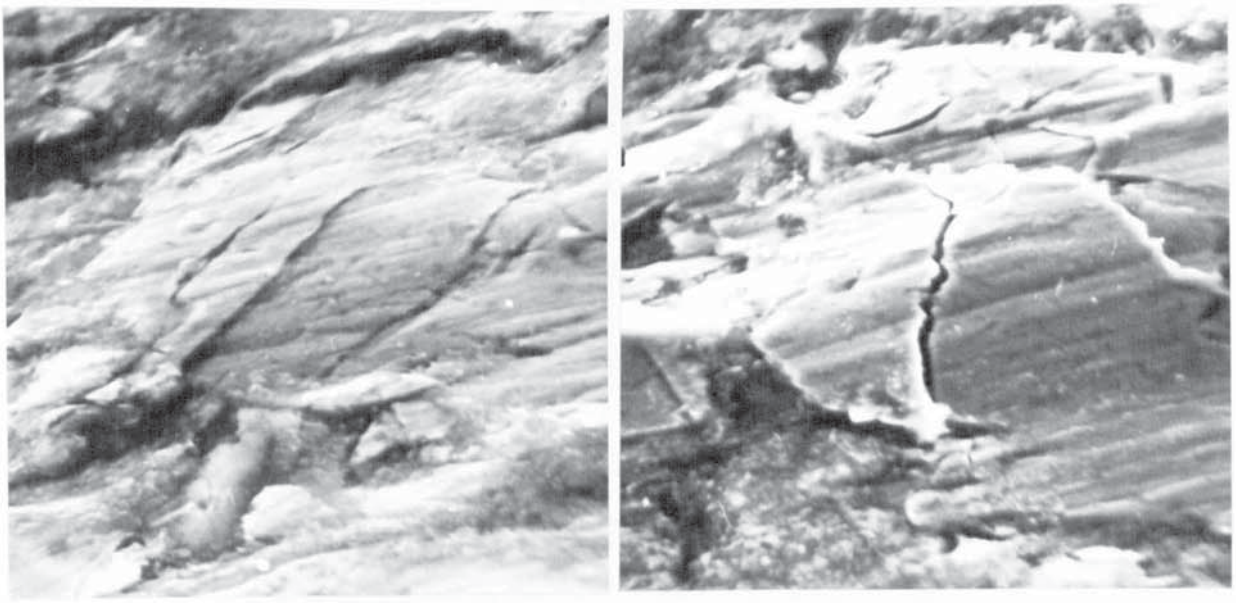

(a) (b)

Figure 4.69

SEM views after deep etching of worn surface of iron 9 tested in as-cast condition. Wear direction ←

Cracking in continuous Fe_3C eutectic carbide. (X2000).

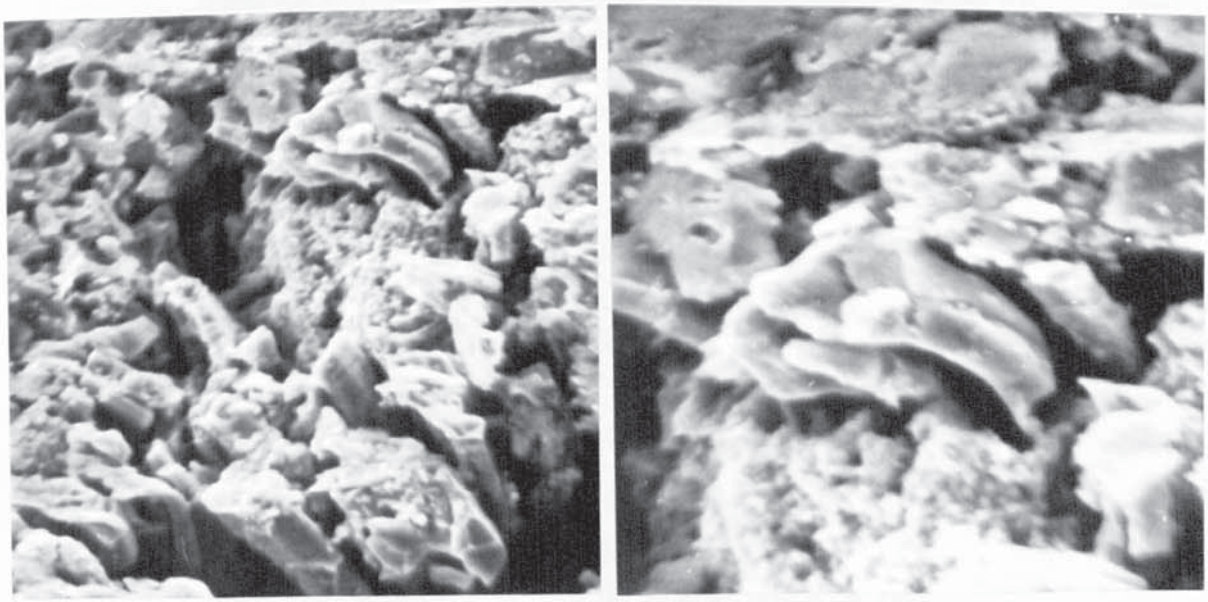

(a) X2000 (b) X3500

Figure 4.70

SEM views after deep etching of worn surface of iron 4 tested in as-cast condition. Wear direction ←

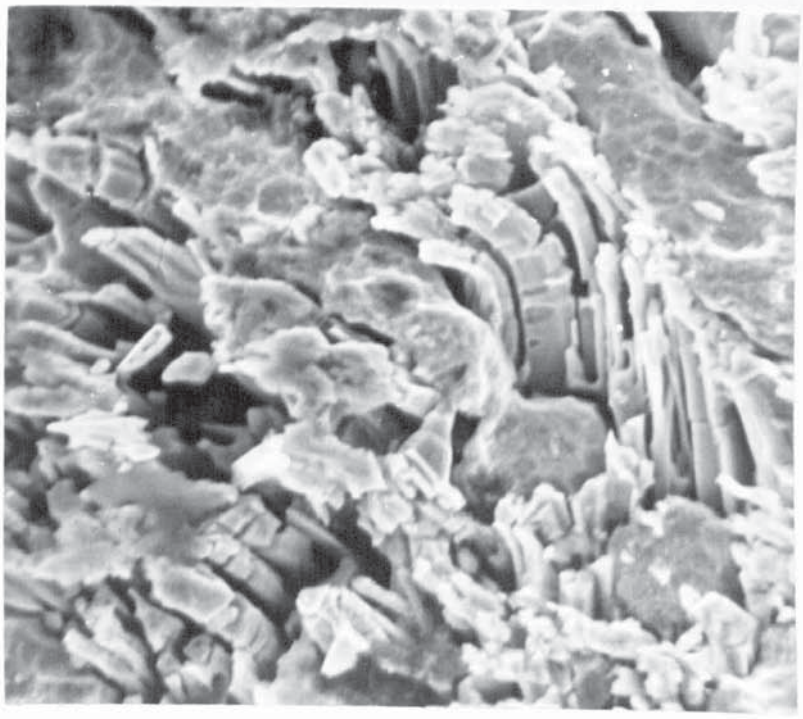

(a) General view of cracking and distortion (X1500).

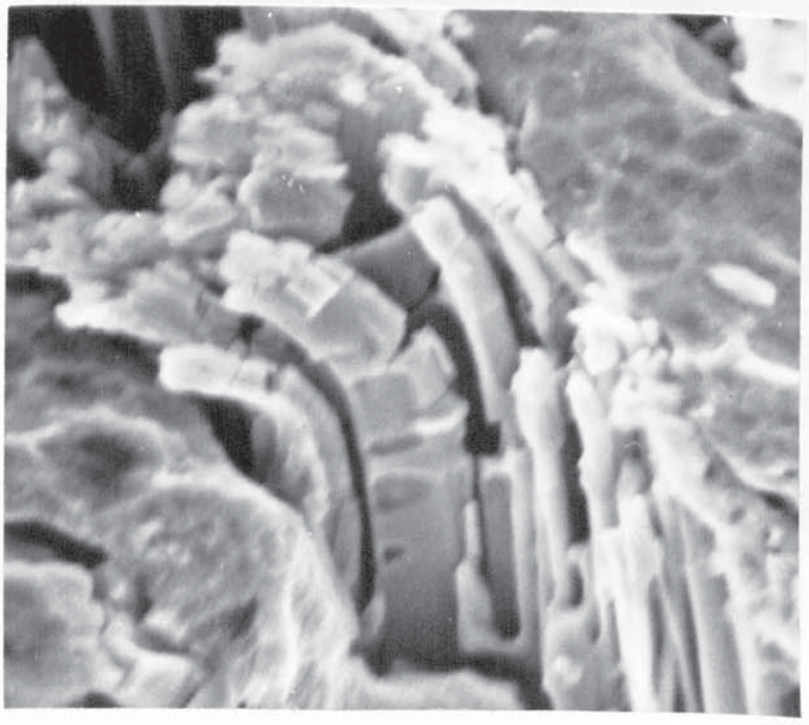

(b) Extent of fractures below original wear surface (X3000).

Figure 4.71

SEM views after deep etching of worn surface of iron 4 tested in heat treated condition. Wear direction ←

Cracking and distortion of eutectic M_7C_3 carbides.

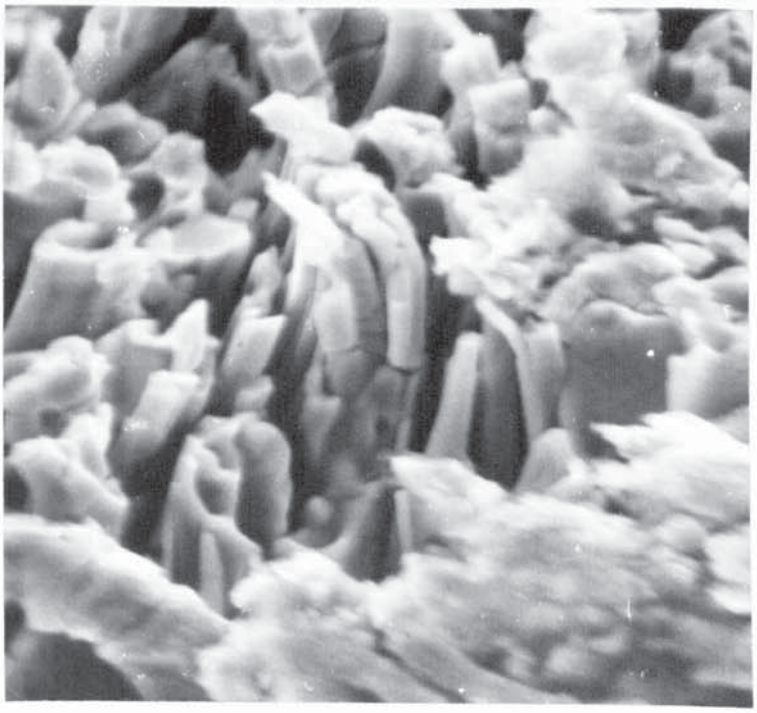

(a) X3000

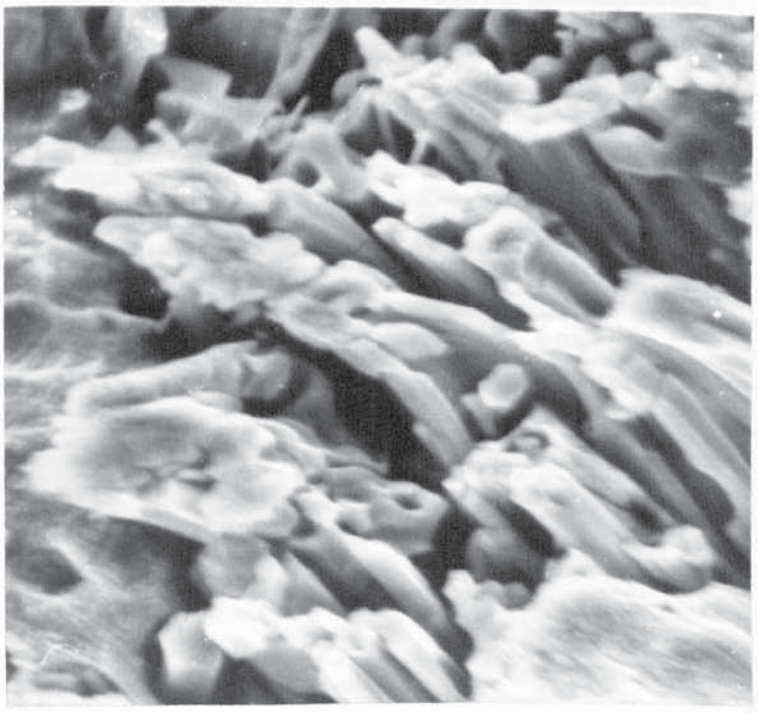

(b) X3000

Figure 4.72

SEM views after deep etching of worn surface of iron 7 tested in heat treated condition. Wear direction ←

Figure 4.72 is typical and shows the 30% chromium iron tested in the hardened and tempered condition. It was noted during these observations that some of the eutectic carbides in the higher chromium irons appear to be hollow (see 4.72(b)).

4.6.4 Examination of carbides in heat treated 30% chromium iron.

During metallographic examination of the heat treated 30% Cr iron it was seen that the "eutectic" carbides were duplex. This effect had not been observed during the development of the 28-30% Cr Superwet irons for wet abrasion resistance (196).

The duplex carbides were subjected to selective etching to aid identification. The response of carbides to etching is given below according to Woodyatt (95) and Nishizawa (204).

Etchant	M_3C	M_7C_3	$M_{23}C_6$
Murakami's reagent	NA	NA	light brown
Potassium permanganate	NA	NA	light brown

(NA - not attacked).

After etching in Murakami's reagent at 60°C for 5 seconds the outer carbide and secondary carbides were coloured brown, The inner eutectic carbide remained white. The sample was reprepared and then etched in a solution of 4g of potassium permanganate + 4g sodium hydroxide in 100 ml H_2O for 20 seconds.

The outer eutectic carbide and the secondary carbides were coloured orange-brown and the inner carbide was unaffected (see figure 4.73). The as-cast 30% Cr iron with M_7C_3 single eutectic carbides was not attacked by either etchant. Hence preliminary identification indicates that in the heat treated iron the outer and secondary carbides are $M_{23}C_6$ type.

It was not possible to analyse the two types of carbide using a Cambridge Microscan 5 Analyser due to the small sizes of the carbides. However, the "single" eutectic carbide in the as-cast material was analysed. The figures given in table 4.14 are for determinations made on three separate carbide lamellae and have been corrected for atomic number, absorption and fluorescence effects. The calculated analysis for $Cr_5 Fe_2 C_3$ is 63.7% C, 27.5% Fe and 8.8% C which corresponds approximately to those given. Examination of the heat treated iron by SEM coupled with energy dispersive analysis equipment suggested that the outer carbide (suspected $M_{23}C_6$) contained less Cr and slightly more Fe than the inner carbide but accurate Cr and Fe determinations were not possible. This effect has been studied in later work using TEM samples.

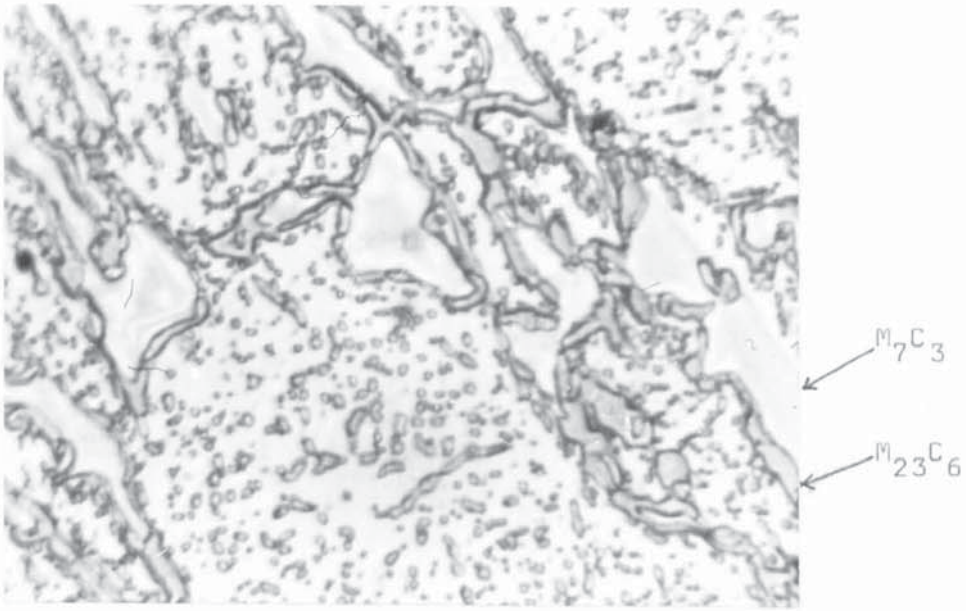

Figure 4.73.

Effect of potassium permanganate etch on carbides in heat treated 30% Cr iron.

Analysis No	%Cr	%Fe	%C	Calculated formula
1	67.64	23.89	8.47	$Cr_{5.5}Fe_{1.8}C_3$
2	68.00	23.93	8.07	$Cr_{5.8}Fe_{1.9}C_3$
3	67.00	23.73	9.27	$Cr_{4.9}Fe_{1.6}C_3$

Table 4.14

Microprobe analysis of eutectic carbide in the as cast 2.4%C 30%Cr iron (iron 7)

%C given by difference.

Calculated formula assumes M_xC_3.

5.0 DISCUSSION OF ABRASIVE WEAR BEHAVIOUR

5.1 Form of abrasion test used.

The development and initial results obtained from the specimen on track abrasion test used in the present work have already been discussed in section 4.3.1.. An assessment of reproducibility showed that the test gave greater variation than those of similar type used by other workers (4, 14). Accordingly the test conditions were modified and subsequent reproducibility tests revealed that with the modified arrangements the variations experienced were comparable with previous work (4, 14). For convenience the results are summarised as follows:

Test		Variation
Before modification	-	± 15-24%
After modification	-	± 7.2%
Boyes (14)	-	± 7-21%
Avery (4)	-	± 5.7-8%

Variation was expressed in terms of 3 standard deviations calculated as a percentage figure of the mean value for weight loss.

It is perhaps relevant at this stage to restate that the object of the current investigation was not to develop a highly reproducible abrasion test but instead to

produce high stress abrasion damage in a range of different structures under reasonably standardised conditions of testing.

The problem of producing abrasion results with a high degree of reproducibility has received particular attention from Muscara and Sinnott (13). The pin on cloth test developed by these workers was outlined in section 2.5.3 and examples of their results were given in table 2.5. It is seen from this table that the weight losses obtained were only of the order of 0.029 - 0.055 gm. At this level of metal removal variation was claimed to be less than $\pm$ 2% which is appreciably less than in the specimen on track tests and less than the $\pm$ 3 - 10% levels obtained by Richardson (18) in another pin on cloth test. Although the pin on cloth test is said to give reasonable correlation with the results from in-service trials, it has met with some criticism in that it does not truly represent grinding abrasion. The abrasive particles are not trapped and crushed between two relatively moving metal surfaces and the loads at the metal-abrasive contact point are said to be cushioned by the abrasive paper or cloth (25).

In addition the pin on cloth tests only give very small weight losses during testing. The weight losses in the present investigation were in comparison very much greater, being of the order of 4 - 10 gm and resulting in the removal of 1 - 1.5 cm^3 of material. The very small amounts of

material removed in pin on cloth tests may not be representative of the general structure of the alloy being tested in that the results could be influenced by segregation or variations in orientation of carbides within eutectic colonies or general variations in the microstructure. Tests which involve the removal of larger amounts of material may be more representative of the structure as a whole and also equate with the large amounts of material loss from components in service environments.

A further point is that the apparently lower values of surface loading in the pin on cloth type of test may not produce the same type of surface damage as experienced in service. The specimen on track test has been found during a limited study by Boyes (14) and during the present investigation to produce severe metal flow and cracking in the surface regions of the test specimens. The damage observed is very similar to that seen in worn components from service mills etc. (25).

Observations made during the course of testing revealed that the silica sand which was used as the abrasive was severely fragmented in the test. This was illustrated in figures 4.11 and 4.12 and showed that during testing high stress or grinding abrasion did occur. Since in the current work the study was centred on the wear damage produced in different types of structure little attention has been paid

to the breakdown of the abrasive and this could prove the subject of further investigation. In particular the relationships between weight loss and time at different testing loads which were non-linear (see figures 4.5 - 4.7) may be more fully understood. Figure 4.7 confirms the effects noted by Boyes (14) in that with time as the abrasive became crushed and angular the amount of wear in a given period progressively increased. However for higher test loads there was a tendancy at longer testing times when the abrasive was very finely crushed for the wear rate to decrease (figure 4.5). With fine abrasives crushing may be autogenous. There may be a range of particle shapes and sizes which is most damaging in terms of abrasive wear. A review of literature (10-13) in section 2.2 suggested that there is a value of particle size below which wear rate decreases and above which wear rate may increase or decrease depending on test conditions. Severest wear is thought most likely when the particles are not only sufficiently large so that they do not "roll" or "flow" (12) but are also angular in shape so that they can penetrate and cut wearing surfaces. However, abrasion resistant alloys are duplex and consist of hard particles within a matrix such that the abrasive effect of various grit sizes must also be related to microstructural details such as the matrix mean free path between these hard particles and their size and proportion.

5.2 Comparison of abrasion test results with previous work.

For ease of comparison between the wear rates of the different irons an abrasion index was calculated for each iron tested (see section 4.3.2.2). The larger the value of this index then the greater was the abrasion resistance of the iron under the particular condition of testing. The values of wear rate, wear index, weight loss etc. determined by the use of laboratory or in-service abrasion tests relate strictly to the abrasion conditions under which they were obtained. Hence it may be misleading to compare the wear ratios obtained under one set of conditions with those determined using some other test. It is however reasonable to look at the general behaviour of materials under different test conditions so that an approximate ranking in terms of abrasion resistance can be made.

Table 5.1 compares some of the results taken from the present work with those obtained by Boyes (14) which relate to the only alloy irons which he tested. The relative values of abrasion resistance given are for similar nominal specimen loads but the speed (1.4 m/sec) of each specimen over the wear track in the current work was over 2X greater than that used by Boyes. A faster testing speed was used in an attempt to approach the 2-2.5 m/sec rotational speeds encountered in production mills (205). In the latter case instrumented ball tests have shown that ball impact velocities may be as

Present tests Load:0.12N/mm^2 Speed:1.4m/sec		Boyes(14) Load:0.1-0.2N/mm^2 Speed:0.53m/sec	
Alloy	Wear index		Wear index
3.5C-14Cr-3Mo	2.29	3.2C-15Cr-3Mo	2.4
3.7C-5Cr	1.74	2.2C-13Cr	1.8
3.6C-10Cr	1.34	3C-5Ni-7Cr (NI-Hard 4)	1.5
3.1C-15Cr	1.32	3C-3Ni-2Cr (" " 1)	1.4
2.7C-26Cr	1.05	2.5C-27Cr	1.4
2.8C-0.1Cr *	1.00	3.2C-1Cr*	1.0

Table 5.1

Comparison of test results.Specimen on track tests in dry silica sand abrasive.

(All the irons were essentially martensitic except the white iron standards*.)

high as 7 m/sec. Testing speeds as high as this were not considered for dry wear testing because of the effects of excessive heating of the test specimens.

The present work confirmed that fully hardened 15% Cr - 3% Mo iron is of the order of 2-2.5X more abrasion resistant than ordinary white iron under dry grinding abrasion conditions in silica sand abrasive. The two sets of results also show that 10-15% Cr irons with martensitic matrix structures are more resistant than martensitic 25-27% Cr irons. It is noted that Boyes obtained a higher relative abrasion resistance for 13% Cr iron with a carbon content of 2.2% C than was obtained in the present work for 10 or 15% Cr irons with carbon contents over 3%. However, the manganese content of the 13% Cr iron was 1.56% compared to about 0.25% in the 10,, 15% Cr irons. Boyes also recorded a higher abrasion resistance relative to the white iron standard for the 27% Cr iron, whereas the present tests found that this iron was only marginally more resistant than white iron.

The behaviour of the 3.7% C 5% Cr iron in the hardened condition can be compared with that of the type 1 Ni-Hard since both irons consist of continuous M_3C carbides and martensite. The type 4 Ni-Hard with a higher chromium content was believed to contain M_3C and M_7C_3 carbides. Boyes found that the Ni-Hards were about 1.5X more abrasion resistant than white iron. The current work recorded a slightly better

performance for the hardened 5% Cr iron which has a comparable structure. The higher value of 1.7X is most probably due to the higher carbon content which gave a greater proportion of eutectic carbide in the structure.

Apart from Boyes (14) the only other published test results from a specimen on track type of test are those of Avery (4, 25) who carried out the test under wet not dry conditions. Avery found that martensitic irons with continuous M_3C carbides (Ni-Hards) were 2-3X more abrasion resistant than ordinary white iron (see figure 2.14). In the main Avery has restricted his published work to the wear behaviour of various abrasion resistant steels, particularly Mn steels and to the development of optimum compositions for abrasion resistance in heavy section 20% Cr - Mo - Ni irons (25). However, he has published some comparative results for as-cast and heat treated 25% Cr irons and these are given in table 5.2. These results show that hardening heat treatments apparently gave little improvement in abrasion resistance over the as-cast structures for heavy sections. The results were not explained in terms of the microstructure of the irons and when a small piece was heat treated an improvement of 1.4X in wet sand abrasion resistance was recorded. This is in agreement with the present work where hardening of the 25% Cr iron raised the abrasion resistance from a very low value 0.77 to 1.05; which is an increase of 1.36X.

Nominal Composition: 2.5C, 26Cr.
Hardening Treatment: 2000 F (1095 C)—2 h—Air Cooled on 12 in. by 19¾ in. (305 mm by 490 mm) section of block-type liner.

Item	Condition	HRC	HB	Grinding Abrasion Test: Weight Loss, HC250, g	Grinding Abrasion Test: Weight Loss, Std., g*	Grinding Abrasion Test: Abrasion Factor
	Thin Section (2½ in., 65 mm)					
1	As Cast	57	589	7.0	17.10	0.41
2	As Cast	59	656	7.50	17.15	0.44
3	Hardened	61	713	7.65	16.65	0.46
4	Hardened	61	668	6.45	18.00	0.36
	Thick Section (6 in., 150 mm)					
5	As Cast	50	469	9.55	16.80	0.57
6	As Cast	51	534	8.85	16.70	0.53
7	Hardened	60	652	10.00	16.00	0.63
8	Hardened	60	645	9.50	16.95	0.56
	Small Piece from Thick Section Rehardened 2000 F (1095 C)—2 h—Air Cooled					
9	Hardened	60	626	4.90	16.80	0.29
10	Hardened	60	626	4.00	16.95	0.24

* Weight loss of the annealed 1020 steel standard, in g.

Table 5.2

The effect of section size on high chromium cast iron. After Avery (25)

Other values published by Avery (4) relevant to this discussion are as follows:

Alloy	Abrasion Factor (AF)	Wear ratio ($\frac{1}{AF}$)
15% Cr - 3% Mo iron	0.21 - 0.30	3.3 - 4.7
27% Cr iron	0.22 - 0.85	1.17 - 4.5
Martensitic Ni-Cr iron	0.35 - 0.45	2.2 - 2.85
Pearlitic white iron	0.94	1.06
Normalised 1020 steel	1.00	1.00

These show the 15% Cr - 3% Mo iron to be at least 3X better than white iron under wet conditions whereas the 27% Cr iron covers a wide range of resistance. No details on structure were given but it is presumed that the lower abrasion resistance of 0.85 relates to austenitic irons which under wet conditions are only slightly better than unalloyed white iron. The present work showed that under dry conditions they are significantly worse than white iron. It must be remembered that both the wet test of Avery and the current dry test does not involve impact loading which the austenitic irons are designed to resist. It must also be stressed that even a simple comparison between wet and dry tests may not be valid because of the possible role of corrosion damage or changes in the physical nature of wear when wet conditions prevail.

The work of Muscara at Al (13) using a pin on cloth test did not include a survey of alloy irons but compared the relative performance of steels with a 3% C, 20% Cr 1.40% Mo iron and a 3.4% Cr 4% Ni Ni-Hard. The two irons were very similar in abrasion resistance, later work (119) using this test showed that austenitic 18% Cr irons (with Mo, Ni, Cu or Mn) had about 1.5X more abrasion resistance than the pearlitic 18% Cr irons without the extra alloy additions. In the present work there was no significant difference between the abrasion resistance of an essentially pearlitic 20% Cr iron and an austenitic 25% Cr iron.

The only published surveys of the wear behaviour of a series of low to high chromium irons have been made under low stress conditions (42, 83, 192, 206) and recent studies by Katavic (207), Zum Gahr (208) and Watson (209) have examined certain commercial Cr-Mo, Cr-Ni and Cr-V irons in jaw crusher, pin on disc and rubber wheel tests. The work of Garber (42) and Shabuev (83) involved tests which simulated wet low stress abrasion conditions and that of Luckin (206) involved a sliding friction test against a metal roller. The latter test did not include an abrasive and hence does not relate directly to the present work. However, it is worth noting that the maximum wear resistance was obtained with irons containing 12 - 16% Cr and that under these sliding friction conditions irons with M_7C_3 carbides were more resistant than irons with ledeburitic M_3C which were said to wear by a

spalling mechanism. The results of Shabuev (see figure 3.20) suggest that the higher Cr irons (i.e. 25 - 30 %) perform much better under wet low stress conditions than under the dry high stress conditions of the present test. Shabuev also found that the maximum wear resistance in a 26% Cr iron was obtained when 25 - 30% residual austenite was present in the heat treated condition. With more than 35% residual austenite the wear resistance was reduced as the matrix could no longer sufficiently support the eutectic carbides. Both Shabuev and Garber confirmed that increasing the proportion of eutectic carbides in the structure increased wear resistance. Garber also found that with increased rates of cooling after casting the size of the eutectic carbides decreased and the wear resistance of the iron increased. Wear resistance was said to be greatest with chromium levels of 12 - 24% and with martensitic matrix structures. Garber found that pearlite and austenitic matrix structures have equivalent abrasion resistance.

One feature of the present work and that of other authors is the relatively poor performance of austenitic high chromium irons. This confirms comments made by Dodd (188) who reported that laboratory wear tests on austenitic irons were pessimistic since these tests could not reproduce the continual pounding encountered in service and consequently did not allow the full work hardening ability of the austenite to be developed. This contradicts the claim of Avery (4) who

said that the specimen on track wet sand abrasion test was validated by ball mill service tests. This latter comment would appear only to be true for those materials which do not have to rely on work hardening for their abrasion resistance. It is also likely that during wet wear hardening is less significant due to the cushioning effects of the pulp.

5.3 Relative abrasion resistance of the irons tested.

5.3.1 Influence of hardness.

Values of the abrasion index for the 0 - 36% chromium irons in both the as-cast and heat treated conditions have been plotted with respect to carbon and chromium contents in figure 5.1. Also included in this figure are the corresponding hardness values for each iron. The numbers given above each graph in figure 5.1 relate to the % increases in abrasion index and hardness as a result of heat treatment. (The 0.1% and 36% chromium irons were not heat treated). It is seen from these % values that for all irons with the exception of the 30% chromium iron increasing the hardness by heat treatment gave a corresponding increase in abrasion resistance. For example a 57% increase in hardness of the 5% Cr iron resulted in an increase in abrasion resistance of 39%. It is to be noted that the hardness increase on heat treatment of the 15% Cr iron was smaller than for the other irons. This was due to the low

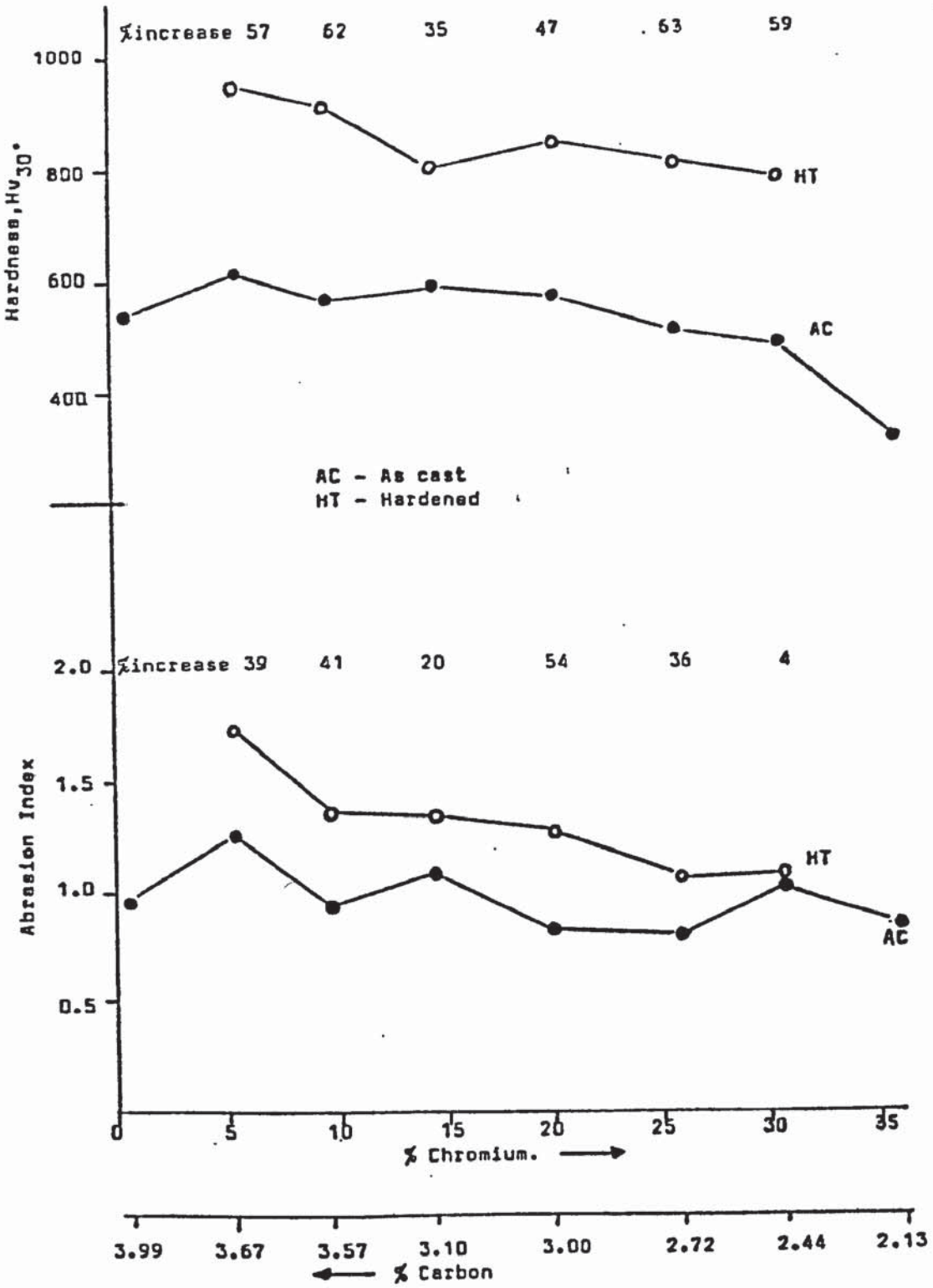

Figure 5.1

Effect of carbon & chromium content on the abrasion resistance & hardness of as-cast & heat-treated irons.

hardenability of this iron resulting in the production of non-martensitic transformation products in the structure. As a result the corresponding increase in abrasion resistance produced by heat treatment was smaller than for the other irons excluding the 30% Cr iron. For this iron there was no significant difference in abrasion resistance between the as-cast iron with an austenitic matrix and the heat treated iron with a matrix of tempered martensite and secondary carbides. This did not correlate with the measured hardness increase from about 500 to 800 as a result of heat treatment. Possible reasons for this discrepancy are discussed later.

In general it is seen that the greater the hardness of an iron then the greater tends to be its resistance to abrasion. The relationship between hardness and abrasion resistance however, was not found to be a simple one. This point is illustrated by figure 5.2 which plots Vickers Hardness Number (30 kg load) against abrasion index. It appears that there may be two relationships depending on whether the eutectic carbides are of the continuous M_3C type (ledeburite form) or are of the discontinuous M_7C_3 or $M_{23}C_6$ type (lamellar or rodlike form). Previous workers notably Richardson (18) and Boyes (14) have also found the relationship between hardness and abrasion resistance to be only approximate. Both workers presented evidence however, that there was reasonable correlation between the hardness of the work hardened wear surface and abrasion resistance. (see figure 2.16). However the present work has not supported

this suggestion as can be seen from figures 5.3 and 5.4. Figure 5.3 plots the microhardness of unworn (i.e. Unwork hardened) matrix against abrasion index and figure 5.4 plots the mean microhardness of the matrix at the wear surface against abrasion index. It is seen that both figures give similar relationships and in each case these are approximate. The results seen earlier in table 4.12 and in figure 4.37 and 4.38 show that hardness values of up to 950 Hv are produced in the austenite matrix at the wear surface of the as-cast 25% and 30% irons. However, these irons had relatively poor abrasion resistance giving index values of 0.77 and 1.02 respectively. It is therefore suggested that there may be a correlation between hardness of a worn surface and abrasion resistance only if the depth of work hardening is sufficient to strengthen the matrix to a depth which allows adequate support for the eutectic carbides present. This support is guaranteed in a martensitic matrix iron which has a uniformly high hardeness both at and below the immediate wear surface. The results of the present work are supported by evidence from Mutton (210) who found that in heat treated steels there was no straightforward relationship between hardness of worn surfaces and abrasion resistance as measured in pin on cloth tests. Mathematical models based on hardness are an oversimplification of the real situation and factors involving microstructural and fracture parameters must be considered.

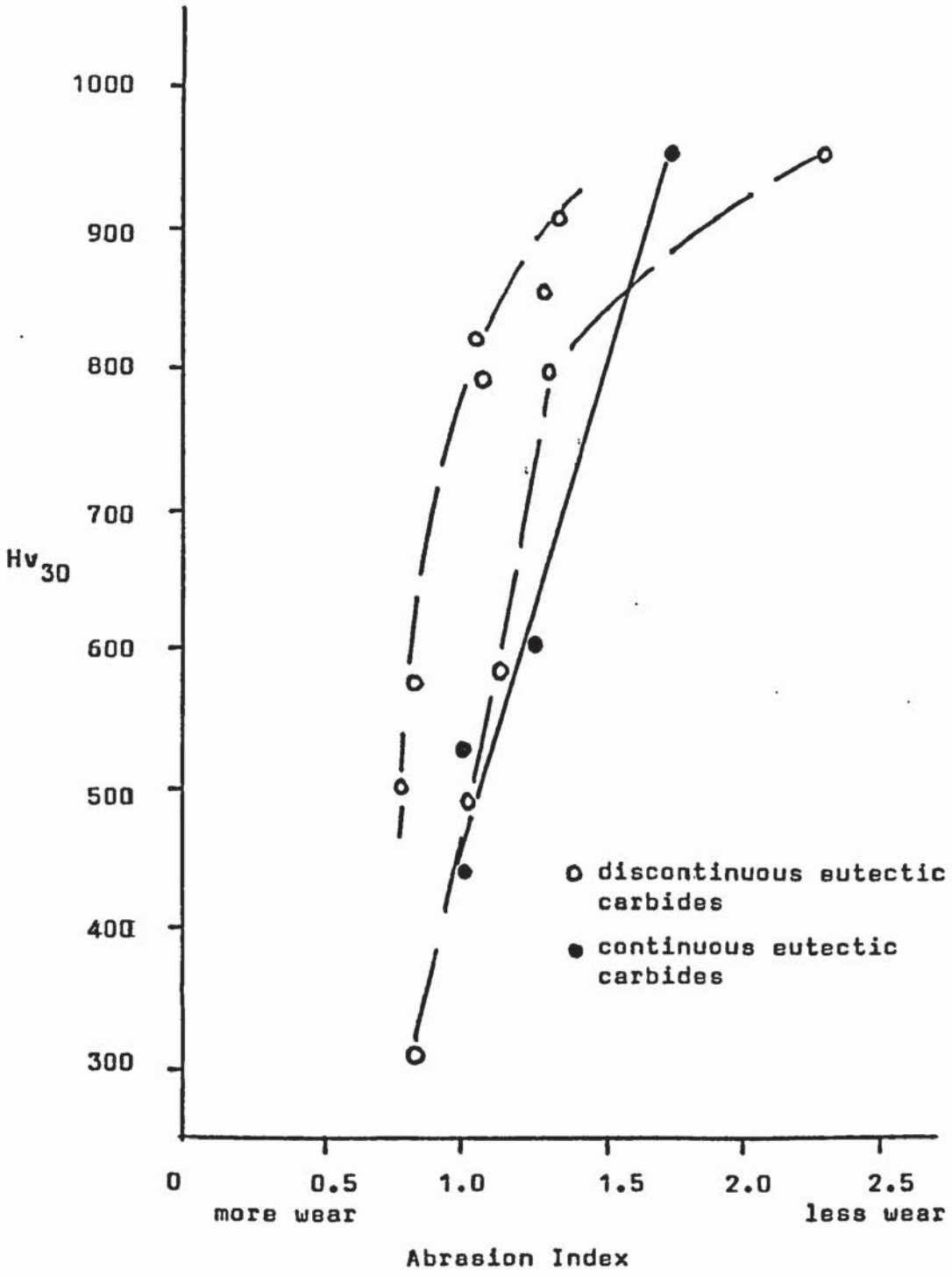

Figure 5.2

Relationship between hardness and abrasion resistance of irons tested.

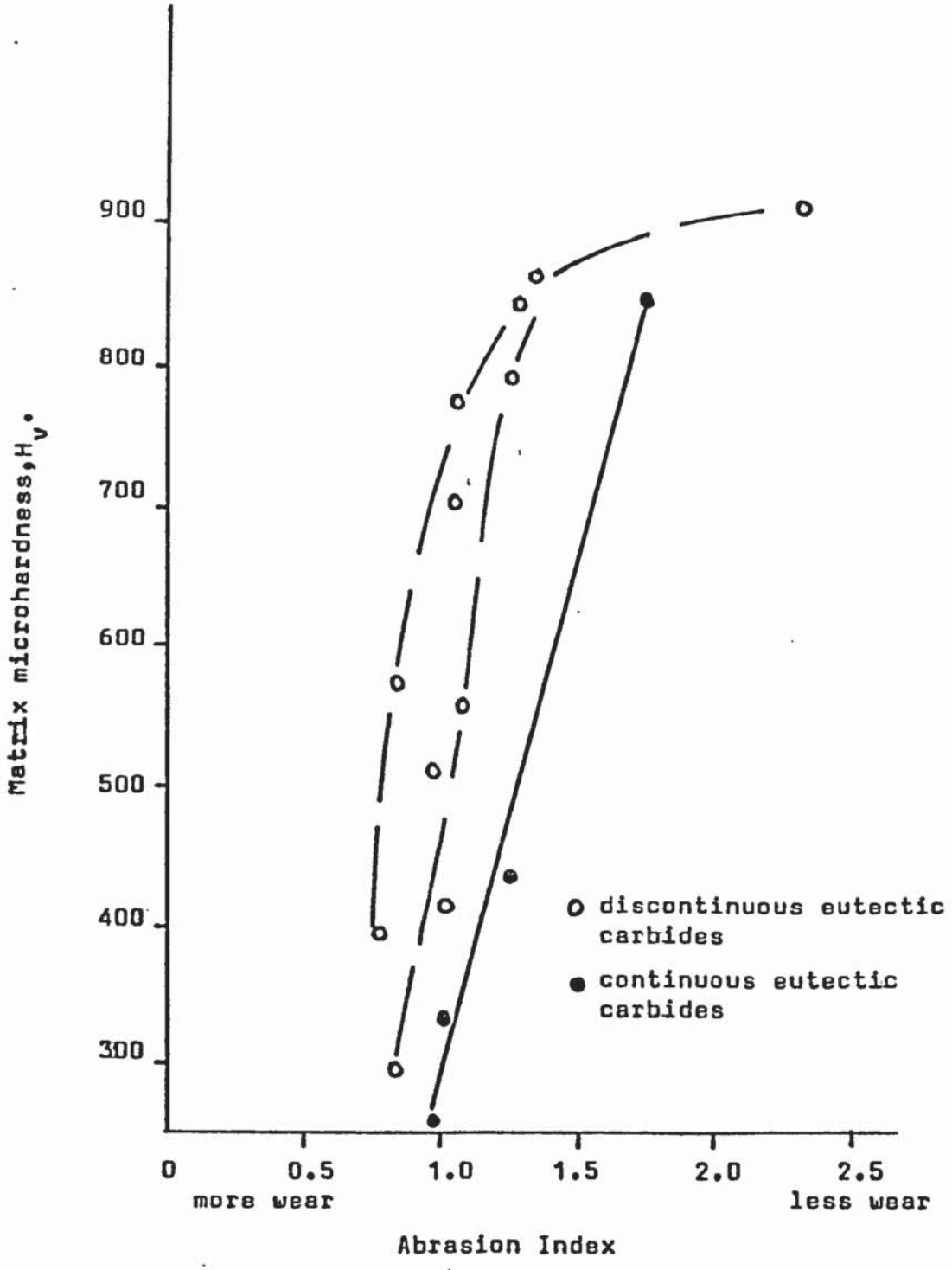

Figure 5.3

Relationship between matrix microhardness (before work hardening) and abrasion resistance.

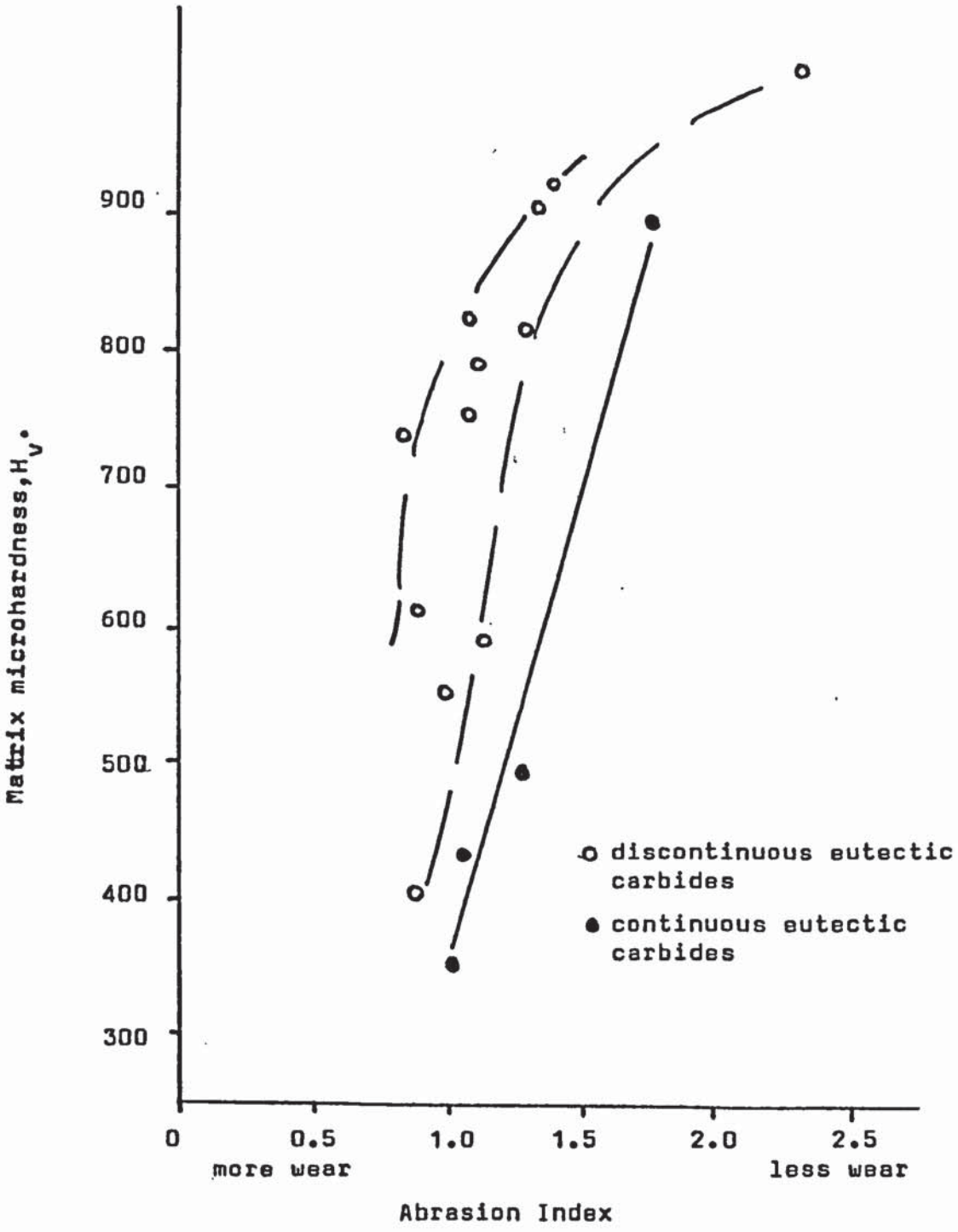

Figure 5.4

Relationship between matrix microhardness (at wear surface) and abrasion resistance.

The results in tables 4.12 and 4.13 show that all the matrix structures work hardened to some degree in their surface layers. The most significant hardening was observed in the austenitic matrix irons although there was also appreciable hardening in the ferritic 36% Cr iron and in the unalloyed pearlite matrix structures of irons 1 and 9. The increase in hardness of over 100 in the ferritic iron is believed to be due to the severe plastic flow of the surface layers. Average increases of 92 and 102 in the pearlite matrix structures of irons 1 and 9 which contained continuous M_3C carbides were significantly higher than the increases of 34-53 observed in irons 2-5 which also had pearlite matrix structures. Iron 2 contained continuous carbides and irons 3-5 discontinuous carbides. The differences in microhardness increases on wear were therefore most probably associated with the initial lower hardness values of the unalloyed pearlite in irons 1 and 9.

The irons with a martensite matrix structure also work hardened by amounts ranging from Hv 24 - 94. The greatest increase being observed in the heat treated 15 Cr/3 Mo iron (iron 10) which gave the lowest wear rate. The work by Boyes using low test loads found hardness increases of 76 to 151 for martensitic matrix structures on wear. It appears that when the rate of metal removal is low i.e. at low testing loads or when the matrix is very abrasion resistant as in iron 10 then a greater degree of work hardening is favoured

since the immediate surface layers remain intact for longer periods of time. On the other hand when the matrix is soft e.g. ferrite or soft pearlite then it flows plastically and this also results in appreciable hardening even though the rate of wear may be high.

The relationship seen earlier in figure 2.16 was determined by Boyes (14) at a very low testing load of 1.59 kg giving a nominal stress on the specimen of approximately 0.02 N/sq mm. This would give correspondingly smaller contact stress at the abraded surface and would result in less fragmentation of the abrasive and give a lower rate of metal removal from the wear surface. It is seen from figure 2.16 that the amount of metal worn away ranged from only 0.005 to 0.018 cm^3. The amount removed in the present work ranged from 1 to 1.5 cm^3. At very low loads such as those used by Boyes penetration of the surface by individual abrasive grits is expected to be less severe and hence there may be more "rubbing" and less "cutting" of the metal surface. Under these conditions it may well be that a very thin work hardened layer can sufficiently resist penetration and give adequate support to the carbides at the immediate surface. In this case the microhardness of the work hardened matrix could be expected to correlate with the measured abrasion resistance as found by Boyes. The present work infers that when the conditions of testing or indeed conditions in service are severe such that the rates of metal removal from a wear

surface are rapid then work hardening is only useful in imparting resistance to abrasive wear if it takes place to a sufficient depth below the wearing surface.

5.3.2 Influence of microstructure.

Although the influence of hardness and microstructure on wear are closely interrelated, for convenience of discussion the general effects of hardness have been dealt with in the previous section. The following sections attempt to explain the differences in wear behaviour of the various irons tested in terms of their microstructural characteristics. Since the irons consist of eutectic carbides dispersed in a matrix structure the discussion centres firstly on the influence of these carbides and secondly, on the effects of the supporting matrix. The interdependance of these two features is then considered with respect to wear damage in section 5.4.

5.3.2.1 Influence of eutectic carbides.

The alloys selected for testing were designed to provide structures containing continuous M_3C type carbides. (irons 1, 2 and 9) or discontinuous M_7C_3 type carbides. It is seen from figures 4.15, 4.16 and 4.23 that irons 1, 2 and 9 contained the ledeburite eutectic characteristic of continuous M_3C carbides. All the other irons contained the

lamellar or rodlike eutectic characteristic of the discontinuous M_7C_3 carbide. It was stated earlier that the microhardness values determined for the M_3C carbides ranged from about 1000 - 1300 Hv whereas the values for the M_7C_3 carbides ranged from 1400 - 1900 Hv. Although difficulty was experienced in performing these hardness determinations they are in general agreement with published values of 840 - 1100 for M_3C and 1200 - 1800 for M_7C_3 (2, 106, 207).

From the results of point count estimations of the proportion of eutectic carbides present given in table 4.11 it is seen that with the exception of irons 1 and 2 which each contained just over 50% eutectic carbide the irons all had approximately similar proportions of eutectic carbide present in their microstructure. The values determined ranged from 27 - 34% and gave reasonable correlation with predicted values according to Maratray (104, 105).

In the as-cast condition irons 1-4 and iron 9 which was used as standard all had pearlitic matrix structures and although the hardness of the pearlite increased with chromium content it is possible to compare the relative abrasion resistance of the irons with respect to the type and proportion of eutectic carbide in their structures. To aid this comparison results taken from previous tables have been grouped together in summary form in table 5.3.

Iron	%C	%Cr	Carbide		Hv of pearlite after wear	Wear index
			Type	%present		
9	2.8	0.1	M_3C	30.4	436	1.00
1	4.0	0.1	"	53.6	354	0.98
2	3.7	5.6	"	52.9	500	1.25
3	3.6	10.1	M_7C_3	31.8	561	0.95
4	3.1	14.7	"	33.9	596	1.10

Table 5.3

Effect of carbide in pearlite matrix irons.

For similar proportions of carbide (compare irons 9, 3 and 4) there is little, if any, difference between the abrasion resistance of irons with M_3C or M_7C_3 carbides in pearlitic matrix structures. It is suggested that the lower hardness of both the pearlite matrix and the M_3C carbide in the unalloyed iron is counteracted by the continuity of the carbide when determining abrasion resistance. The continuous carbides apparently suffer less damage than the discontinuous carbides under the conditions of testing which did not involve impact loads. Observations of the structures at worn surfaces supported this view and the level of carbide cracking was less for the M_3C continuous carbides than for the discontinuous M_7C_3 carbides. In addition when the discontinuous carbides were severely cracked they were more likely to be removed as the matrix was worn away. The most abrasion resistant of the irons given in table 5.3 was the 5% Cr iron which contained a greater proportion of eutectic carbides than irons 3, 4 or 9 and also had a pearlite hardness of 500 Hv(at wear surface). Iron 1 which also had a high proportion of eutectic carbide present was not so abrasion resistant due to the softer pearlite present and also due to the presence of eutectic graphite in mottled areas. These can be clearly seen in the surface of the test sample in figures 4.9 and 4.57. It was not possible to compare the two types of carbide in martensitic matrix structures since only iron 2 (5% Cr) was hardened and in addition the matrix hardness developed depended on chromium

content and tempering temperature. The 5% Cr iron did in fact give the second highest measured abrasion resistance of 1.74. This iron had a matrix microhardness of 850 and the value of 1.74 can be compared with values of 1.34 and 1.32 for irons 3 and 4 with respective matrix microhardness levels of 866 and 842. The higher resistance of iron 2 was therefore due to the greater proportion of eutectic carbide in its structure although the fact that its carbide was continuous must also be considered.

With a single exception the form of the eutectic carbides in the structures was not affected by the heat treatments given to the irons. There was no evidence of spheroidisation of lamellar carbides in the 15 - 30% chromium irons which were held at 1025 - 1100^{o}C for 1 hour to achieve austenite destabilisation. However, the carbide in the 30% Chromium iron became duplex after heat treatment, the as-cast M_7C_3 carbide partly transforming to $M_{23}C_6$ in its outer regions. This structural change in the carbide may be responsible for the lack of improvement in abrasion resistance on heat treatment of the 30% chromium iron. Heat treatment of this iron raised the matrix microhardness from 500 to 800 but the abrasion resistance was not improved over the as-cast value. It is interesting to compare the values of abrasion resistance determined for the higher chromium irons in that in the as-cast condition the 30% chromium iron was more abrasion resistant than the 20 and 25%

chromium irons. Since the proportions of eutectic carbide in the irons is similar it is difficult to explain this difference although the eutectic carbides in the 30% Cr iron did appear to be more finely distributed in the austenite matrix than those in the 25% Cr iron which also had a fully austenitic matrix.

The form of the carbides in the 30% Cr irons is particularly important in view of current developments in irons for wet grinding applications and further work may yield interesting results since other authors (83, 211-2) have noted that the finest distribution of eutectic carbides existed in irons containing around 30% chromium. Shabuev (83) covered a range of compositions up to 32% and Matsubara (211) studied 10-40% chromium irons. Increases in carbon level from 2.0 to 2.7% in 30% chromium irons produced greater proportions of finer carbides and increased wear resistance by 30% (212).

There is little published information on the three dimensional morphology of the M_7C_3 or M_3C eutectic carbides in cast irons and no attempts to explain carbide fineness and distribution have been recorded. However, Powell (213) has examined deep etched irons at low and high chromium levels. He noted that the M_7C_3 eutectic carbides in 17% Cr - 1.5% Mo and in 27% Cr irons exist as rods or blades, the blades being formed by the joining together of two or more rods. The rods

were hexagonal in cross section and some of them appeared to be hollow. This feature had previously been reported by Jackson (214) and in the present work some of the hexagonal eutectic carbide rods were also seen to contain "hollows" (see figure 4.72). In hardfacing deposits where growth rates on solidification are higher the eutectic M_7C_3 carbides always existed as rods with a greater proportion of these containing central hollows; the blade type of formation is known to be favoured by slower growth rates (213, 215). If finer distributions of eutectic carbide do improve wear resistance then there may be advantages in developing modification type treatments as in aluminium-silicon alloys, since the presence of finer carbides is already known to improve fracture toughness in austenitic matrix irons. (45, 134).

5.3.2.2 Influence of matrix structure.

In general the work has shown that the higher the hardness of the matrix then the greater is the resistance to abrasive wear. Consequently the heat treated irons with martensitic matrix structures gave improved abrasion resistance over their respective as-cast structures of pearlite or austenite. The performance of the austenitic matrix irons was surprisingly poor but has been explained in terms of the relatively small depth of work hardening developed in the surface layers of the test specimens during abrasion testing. This is illustrated by comparing

figures 4.37 and 4.38 with figure 4.40. In the wear test specimens the depth of hardening was confined to the immediate surface (10 - 50 μm deep) whereas in an austenitic ball which had been in service in a ball mill a hardened layer of up to 5 mm deep had been developed.

Tests of the type used in this work may therefore seriously underestimate the abrasion resistance of austenitic irons since during testing where no impact loads are used the matrix does not have chance to work harden to a sufficient depth if the rate of metal removal is high. The relative performance of the austenitic irons would probably improve if this type of test was used with smaller loads than that used in the present work. The low values of abrasion resistance observed in the austenitic and ferritic matrix irons serve to underline the role of the matrix in supporting the harder eutectic carbides. The eutectic carbides in the ferritic 36% Cr iron received little support and were therefore severely fragmented during abrasion.

Figure 5.5 shows the influence of chromium content on the microhardness of the tempered martensite matrix produced by heat treatment. As chromium content increases from 15 to 30% then the martensite becomes softer for a standard tempering temperature of 450^{o}C. This is due to the fall in carbon solubility in austenite with increasing chromium and to increased removal of carbon from the austenite during

destabilisation as secondary carbides form. Hence the higher the chromium content the lower is the carbon content of the destabilised austenite and a softer lower carbon martensite is produced on subsequent transformation. This partly explains the lower recorded abrasion resistance of the heat treated 25 and 30% chromium irons. However, these two heat treated irons had only similar abrasion resistance to the as-cast 15% Cr iron which had a pearlite matrix. Hence the nature of the carbides and how securely they are held in the matrix must also form part of the explanation for the poorer abrasion resistance of the higher chromium irons. It would be interesting to heat treat the range of irons to give a consistent level of matrix microhardness e.g. 700 - 750 Hv. Any differences in wear behaviour might then be attributed to the behaviour of the carbides and the strength of the carbide-matrix interface. The present work has used thermal treatments which were typical of those practised commercially for the various irons.

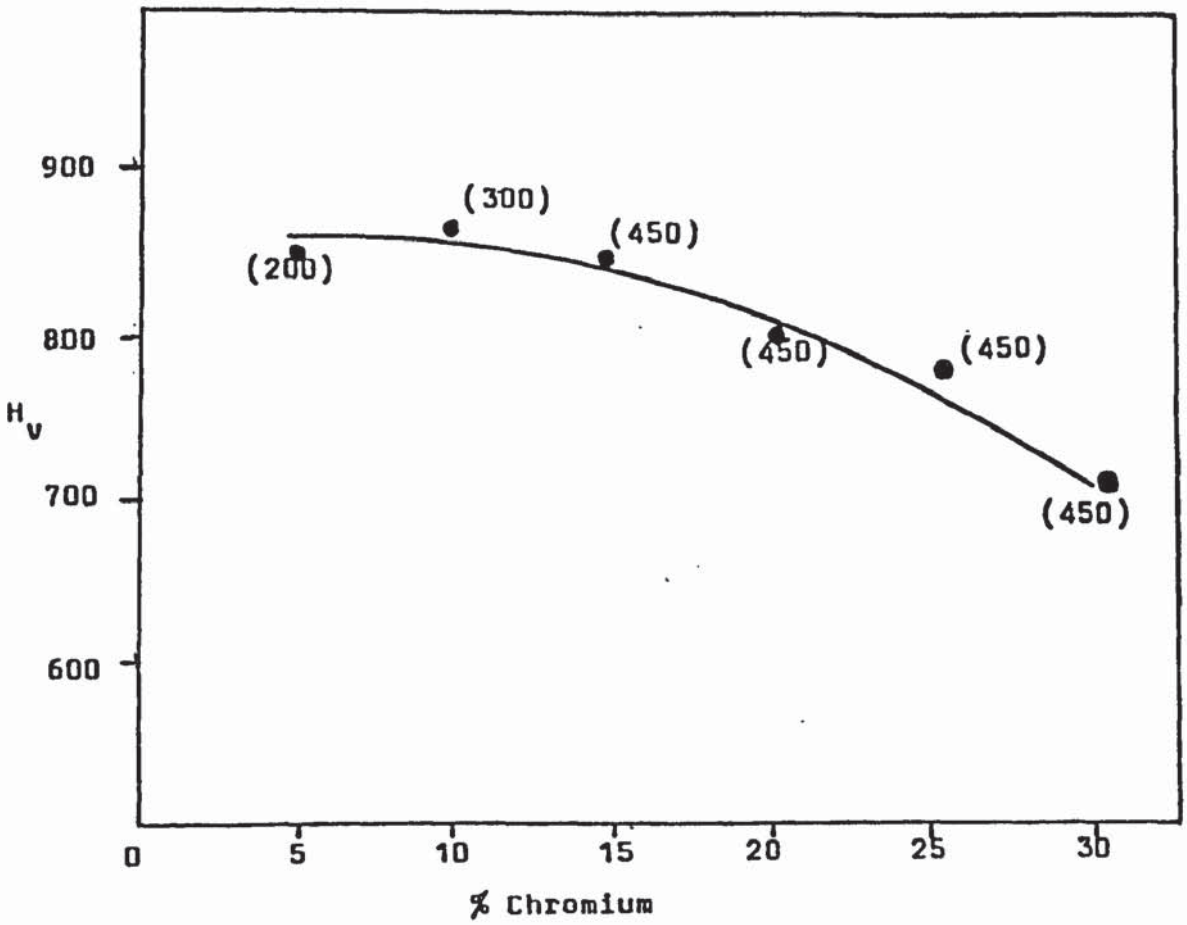

Figure 5.5

Effect of chromium content of iron on microhardness of tempered martensite.

Tempering temp. ^{o}C given in ( ).

5.4 Relationships between microstructure and the nature of wear damage.

The grooved wear patterns produced during abrasion could not be directly related to matrix structure or to the type of eutectic carbide present. For example, in figure 4.14 it is seen that there is little difference between the groove profiles developed in a pearlitic iron with continuous M_3C carbides (iron 2) and a pearlitic iron with discontinuous M_7C_3 carbides (iron 4). In addition the ferritic matrix iron (iron 8) had groove profiles which were not so severe as in irons 2 and 4 which both gave greater abrasion resistance. The deepest wear grooves were obtained in the austenitic matrix irons but the depth did not relate to the depth of the work hardened layer. Measurement of the depth of wear grooves oversimplifies the wear situation and hence cannot be used to indicate relative abrasion resistance.

The smallest values for abrasion resistance were recorded for the as-cast irons containing 20, 25 and 35% chromium. The 20% Cr iron had a pearlite + austenite matrix, the 25% Cr iron was austenitic and the 35% Cr iron was ferritic. The damage observed in the 20% Cr iron was not significantly more severe than that seen in the as-cast 15% Cr iron which was fully pearlitic, However, in the 25% Cr and 35% Cr irons more severe effects were noted. Figure 4.28 showed the severity of cracking in the eutectic carbides of

the 25% Cr iron and was typical of the damage seen in the higher chromium irons. The eutectic carbides tended to "bend" less in the general wear direction and instead produced branched fractures running both parallel and normal to the wear surface. This cracking and subsequent removal of carbide fragments from relatively undistorted carbides was a feature of both austenitic and martensitic matrix conditions and was also observed in the martensitic 20% Cr iron, (see figures 4.35 and 4.52). The removal of eutectic carbides from the matrix occured less frequently in the 15% Cr iron and lower chromium irons but was seen to occur at shallow depths in the hardened 15% Cr - 3% Mo iron (see figures 4.55-6).

The eutectic carbides in the surface regions of the ferritic 35% Cr iron were quite severely fragmented but the broken pieces were not necessarily removed from the surface and were smeared along in the soft ferrite matrix as it plastically deformed in the wear direction. The surface regions then consist of highly strained ferrite containing a dispersion of broken carbides and penetrated abrasive grits. This may produce surface armouring which would explain why this iron, which is both initially softer and work hardens less than the austenitic 25% Cr iron, does not have a lower resistance to abrasion as measured in the present test. Although the austenitic irons work harden at the immediate surface, the depth of hardening is insufficient to support the eutectic carbides and these irons, together with the

ferritic iron, contained the greatest depth of cracking of the eutectic carbides (see table 5.4).

The ease with which the austenitic and ferritic matrix irons could be worn is illustrated in figures 4.60-1 and 4.65. The surfaces show wide wear furrows superimposed on the general pattern of wear grooves. The surfaces of the wear scars are smooth suggesting a ploughing action while the surrounding region is rough and pitted.

The pearlitic matrix irons suffered less surface pitting than the austenitic or ferritic irons as is seen in figures 4.59 (a), 4.60-1. This is due to the tendency for fractured carbides in the pearlitic irons not to be removed from the matrix. (Compare figures 4.27 and 4.44 with 4.28). The eutectic carbides have also remained in position in the hardened 10-15% Cr irons when compared to the higher chromium irons. Figures 4.33 and 4.35, and, 4.49 and 4.52 illustrate this point. The apparent ease of removal of broken eutectic carbides from the matrix in the higher chromium irons coupled with the lower hardness of their low carbon martensitic matrices explains why they have lower abrasion resistance than the 10-15% Cr irons.

The tendency of eutectic carbides to fracture below the immediate wear surface and their subsequent removal from the matrix has previously been noted by Durman (59) during an

examination of the surface structures of various components damaged by abrasive wear. He observed this effect in an austenitic 25% Cr iron cyclone head which had been subjected to erosive wear. The eutectic carbides in the iron showed no evidence of deformation but appeared to have broken away just below the wear surface.

The distorted carbide fragments in the lower chromium irons tended to flow along in the matrix at the wear surface (see figure 4.31). This effect has been discussed by Harrison (44) during work on Ni-hard grinding media. Correctly heat treated balls with martensitic matrices developed a surface layer of flowed carbides giving high abrasion resistance. These surface carbides were said to be not easily removed unless they were undermined by corrosive attack of the supporting matrix under wet grinding conditions.

There have been few other reported studies of wear damage below the wear surface of alloy irons (208, 209, 216). In abrasive wear under impact conditions Strizik (216) found that in irons containing 2.5-3.6% C, 15-18% Cr, 0-3% Mo the M_7C_3 eutectic rods could develop numerous cracks without detachment. The matrix was said to remain free from cracks. Avery (25) also noted that cracking occurred parallel to the worn surface of a Paraboloy crusher segment, in this case the damaged zone was 50 μm deep.

Iron	%Cr	As cast		Heat treated	
		D	d	D	d
1	-	80-140	15	-	-
2	5	80-150	15	50-110	10
3	10	85-150	18	55-120	15
4	15	70-150	15	65-120	12
5	20	70-140	15	55-150	12
6	25	70-160	30	60-150	15
7	30	80-200	22	60-150	18
8	35	90-140	32	-	-
9	-	85-150	17	-	-
10	15/3 Mo	-	-	45-90	12

D = range of depth of wear grooves (μm)

d = depth of deepest observed cracks in carbides (μm)

Table 5.4

Depth of wear grooves and depth of cracking in eutectic carbides below worn surfaces.

In contrast recent studies of 15% Cr - 3% Mo and 27% Cr irons by Watson et Al (209) conclude that high stress abrasion as produced in a pin on cloth test takes place by a cutting mechanism in martensitic matrix irons with some ploughing also occuring in austenitic irons. They reported that there was no evidence of cracking or fragmentation of the eutectic carbides and suggested that this only occurs under impact-wear conditions as encountered in a jaw crusher test. These findings can be used to reinforce previous critical comment on the pin on cloth test covered in section 5.1 in that the rate of material removal and the resultant wear damage is much less severe than in service conditions of grinding.

In the irons with continuous M_3C type carbides it was the "matrix" of pearlite or martensite which was removed from the honeycomb of eutectic carbide. It was seen in figure 4.41 that fragmented abrasive particles had penetrated the pearlitic regions in iron 1 (4% C, 0.1% Cr) resulting in gradual removal of the pearlite. Figures 4.42 and 4.43 show similar effects in the martensitic 5% Cr iron where the martensite areas suffer cracking and removal from in between the carbides. Separation appears to have taken place along the carbide-martensite interface enabling easier removal (see figure 4.43(b)) and leading to the pit type damage seen in figure 4.64.

In iron 9 which contained 2.8% C there was only 30% eutectic carbide present compared to over 50% for irons 1 and 2. This lower carbide level has allowed more plastic flow at the wear surface. Figure 4.25 shows that the M_3C carbides have been distorted without cracking, this contrasts with the M_7C_3 carbide in the 20 + % Cr irons where cracking took place with little evidence of deformation. One interesting feature observed at the wear surface of the 2.8% C iron was the non-etching layer seen in figure 4.25 (b). This effect was at first believed to be due to uneven etching but it was visible after repeated repreparation and etching. The layer was not present all along the wear surface but only at isolated regions. It was up to 5 μm deep and microhardness tests showed that it was similar in hardness to the adjacent pearlite, although it was difficult to obtain an impression completely in the layer. The occurrence of so called white layers has been comprehensively reviewed by Eyre and Baxter (217). They discuss the formation of white layers under sliding wear conditions and do not include abrasion. The effect seen in the present work is not typical of the white layers seen on grey and nodular irons which are very distinct and completely featureless at optical microscope magnifications. Severe deformation and high surface temperature flashes which are said to be necessary for white layer formation could occur in wear of pearlite by abrasion and the feature noted in figure 4.25 may merit further study.

The effects of continuous and discontinuous type eutectic carbides during wear are summarised using figure 5.6. Under non-impact conditions (as in the present test) fracturing of the carbide phase C does not lead to its immediate removal from structure (a) where C is continuous (see figure 4.69). In structure (b) where C is discontinuous fracturing of C allows it to become more readily detached during wear. However, under service conditions where impact loads have also to be considered structure (a) may have insufficient toughness and suffer gross fracture; structure (b) with its discontinuous carbide may withstand impact and gross failure is avoided perhaps at the expense of greater wear.

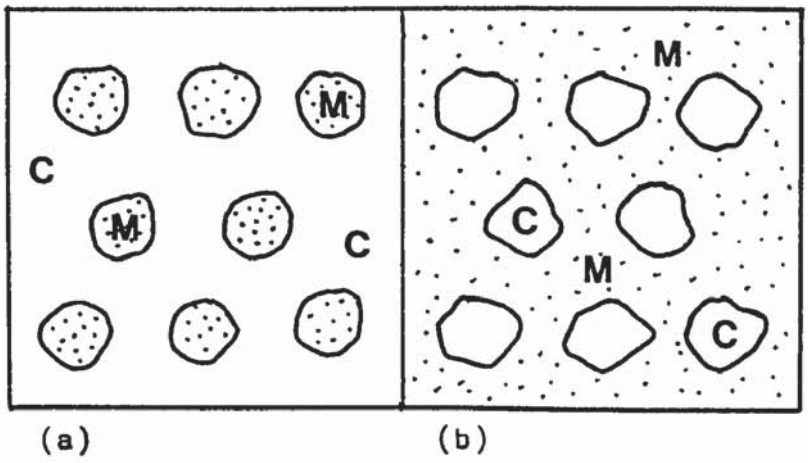

Figure 5.6 Schematic representation of microstructure in

(a) White iron with M_3C eutectic carbide

(b) White iron with M_7C_3 eutectic carbide

(C = eutectic carbide)

(M = pearlite or martensite)

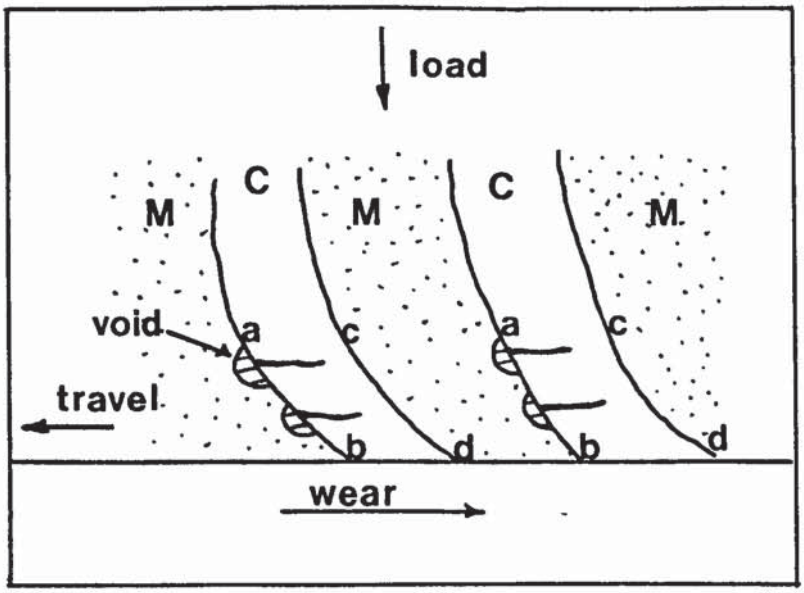

Figure 5.7

Schematic representation of eutectic carbides at wear surface. The voids once nucleated may elongate in a cumulative manner with the passage of further abrasive grits along the surface. Carbide-matrix boundary cracking may be aided by segregation of impurities to the interphase boundary.

5.5 Deformation and cracking beneath worn surfaces.

The wear damage discussed above included deformation and microcracking of both the eutectic carbide and matrix constituents and also in some cases separation at the eutectic carbide-matrix interfaces. Hence material removal during the high stress abrasive wear of white irons does not only result from the cutting and machining effect of hard sharp abrasive particles as suggested by Watson (209) but also from the effects of sub-surface deformation which leads to microspalling and eventual detachment of fragments of carbide and matrix.

The present study suggests that certain eutectic carbides can deform in the wear direction without apparent cracking and that other carbides suffer numerous fractures running parallel to the wear surface. In a small number of instances vertical cracks were also observed in the eutectic carbides. The parallel lateral cracks and the vertical cracks may correspond to the lateral and median venting discussed by Lawn (31) in single phase brittle solids.

Voids could also form at the carbide-matrix interfaces as illustrated schematically in figure 5.7. Voids of this type are seen in figure 4.43, 4.44, 4.49 and 4.51. During plastic flow of matrix regions at the surface dislocations are expected to pile up at both AB and CD type interfaces.

Because AB will be subject to tensional forces and CD subject to compression as the surface regions distort in the direction of wear the dislocation pile ups are more likely to nucleate voids or microcracks at AB interfaces (as observed in practice). The formation of these voids can correspond to severe cracks in the adjacent carbide but it was seen that carbides also crack without the formation of voids (as observed in two dimensional microsections). This was particularly noticeable in the irons containing over 20% chromium. In the present test the wear was unidirectional whereas in some service applications this is not so and the surface layers could be deformed one way and then the other leading to further decohesion at carbide-matrix interfaces and easier removal of pieces of broken eutectic carbide.

The overall effects of plastic flow at and below worn surfaces is termed deformation wear as introduced in section 2.4.1. To date the mechanisms by which plastic deformation takes place beneath worn surfaces resulting in deformation wear have only been investigated in relatively ductile metals (21, 31, 218). There is little information on deformation wear of alloy cast irons other than brief comment on the nature of spalling damage in Ni-hards (219).

Moore and Douthwaite (218) determined the strains beneath on abraded surface by direct observations on worn composite specimens consisting of copper layers interleaved

with thin films of silver solder. The extent of the plastically strained region increased with the size of the abrasive grits used and applied load and was found to be up to 70 μm deep. High strain values observed at the surface were said to be consistent with the hydrostatic stress system set up in abrasion which serves to oppose the formation of cracks and will delay fracture. Because high compressive stresses can be developed beneath an indenter the required level of shear stress to plastically deform brittle phases may be developed. A review of indentation studies on the carbides of molybenum, tantalum, niobium, vanadium and zirconium has shown that plastic deformation by slip and twinning can occur in these carbides at room temperature (27,220). These studies did not include any of the iron or iron-chromium carbides but Formichev (221) has claimed that single crystals of cementite taken from decanted hypereutectic white iron can be plastically deformed when cold by grinding on an abrasive wheel. The presence of strain was said to be proven by line broadening in X-Ray diffraction patterns.

Other work concerned with the deformation of cementite has involved studies of eutectoid cementite in pearlitic steels. In cold drawn wire steels Pickering (222) noted that thin carbide lamellae seemed capable of withstanding severe deformation without fracture whereas the coarser or the thicker the carbide then it tended to crack. Pickering

recognised three main effects:-

(a) A substructure formed on an extremely fine scale within the carbide lamellae. This was indicated by arcing of spots in electron diffraction patterns showing misorientation effects within the lamellae.

(b) Heavy deformation markings indicative of slip were produced although no dislocations were observed in the carbides; these markings appeared to develop into cracks at large deformations.

(c) Cleavage type cracks could occur with no apparent deformation.

Barnby and Johnson (223) suggested that cementite lamellae are fractured by concentrated stress from slip lines in ferrite. They did not observe any evidence of plastic deformation in the cementite although their study was made under tensile conditions and they recognised the need for further work under hydrostatic compression. Plastic deformation of cementite has been observed in cold rolled steels by Inoue (224) who proposed that cementite lamellae fractured in stages. The first stage involved the non-homogeneous movement of dislocations on certain slip planes

and resulted in the division of the crystal into several undeformed blocks. The gliding displacement between the adjacent blocks is said to increase with deformation and eventually failure occurs along the block boundaries due to stress concentration at the slip steps. This is similar to the observations of Pickering (222), however, Inoue recorded a dislocation density of 10^8 lines/cm^2 in annealed cementite and this increased from 3×10^9 lines/cm^2 to 2×10^{10} lines/cm^2 with an increase in rolling reduction from 25 to 92%. Sevillano (225) has also found that underformed cementite contains both dislocations and sub-boundaries.

Dislocation densities of 10^{10} lines/cm^2 have been observed in tungsten carbide in a cobalt bonded hard metal deformed by compression (226). The tungsten carbide is said to be able to plastically deform by a dislocation glide mechanism (226, 227) but there is evidence that deformation cracking occurs (228). A decrease in hardness and in yield and fracture strength in compression was noted after a few % plastic deformation of a hydrostatically loaded specimen.

Inoue (224) found that as a result of plastic deformation cementite lamellae in steel were divided into blocks having a width of about 0.3 μm but no dislocations were observed within the blocks. Deformation of cementite was thus considered to be concentrated at block interfaces and to be non-uniform compared to deformation in a ductile

metallic phase. The tendency for the eutectic carbide to divide into blocks along parallel fracture paths has been observed in the present work (see, for example, figures 4.26, 4.30, 4.33, 4.45, 4.49 and 4.51). These blocks were at least 2-3 μm in width but it is possible that they have developed from fractures initiated along slip steps of the type considered by Inoue (224). Cracking in eutectic carbides beneath wear surfaces could result from non-homogeneous plastic flow within carbide blades or rods as well as from the stress concentration effects of dislocation pile ups due to plastic deformation of the surrounding matrix. The latter effect is illustrated by the cracking of rod like precipitates of $M_{23}C_6$ in an austenitic stainless steel (229). The rods fractured as a result of stress concentrations generated at slip bands in the matrix with sucessively more breaks occuring with increased strain in the matrix.

Lindley et Al (230) have used a fibre loading model in addition to the pile up model to explain the carbide cracking which is observed in ferrite-carbide aggregates. It was considered that the pile-up model could not explain the influence of carbide thickness and the tendency for cracking to occur predominantly in carbide films lying parallel to the axis of tension. Gurland (231) suggested that combined dislocation and fibre loading theories can explain the influence of shape and orientation of carbides on cracking but cannot fully account for observed preferential cracking

of the largest particles of carbide in a dispersed aggregate.

In the present work a numerical analysis of the cracking in the carbides at the wear surface was not attempted since:

(a) Surface stresses can only be estimated.

(b) The stress fields around moving indenters are complex

and (c) Cracking may occur on application of a surface load and during its removal.

However, general observation has shown that both large and small carbides contained cracks but some of the thinner carbide rods had deformed in the wear direction without sign of cracking. It would be of value to perform similar studies to those mentioned above (230, 231) but in order to simplify the relationships in orientation between the eutectic carbides and the applied stress such studies would ideally be carried out on directionally solidified irons subjected to uniaxial tension or compression.

Work on directionally solidified irons would enable eutectic carbide rods or blades to be grown either parallel or perpendicular to a wear direction and to a direction of tension or compression for cracking studies. This may allow comparisons between these carbides and the behaviour of fibres in composite materials. Interface decohesion and detachment from the matrix is an observed failure mechanism in composites; when the fibre-matrix bond strength is low

failure involves fracturing of the brittle fibres e.g. carbon and then "pull out" of the broken fibres from the ductile matrix e.g. nickel (232). In contrast only a limited amount of fibre "pull out" is seen when there is a strong bond between fibre and matrix (233). Debonding has also been proposed as one of the stages of wear in the sliding wear of composites, the debonding is said to result in loose wear particles particularly when the fibres are alligned perpendicular to the sliding wear surface (234).

Since abrasion resistance depends partly on the ability of the eutectic carbide to remain in position in the matrix then the shape of the carbides and the nature of their interface with the matrix is important. It is generally recognised that a fine dispersion of small hard particles is preferred to an uneven distribution of larger hard phases for abrasion resistance and smaller particles will be less likely to crack than larger ones. The interface between carbides and matrix has received consideration in the improvement of cemented carbide tools (235). Small additions of ruthenium are said to improve the resistance to propagation of microcracks in these materials, the ruthenium is claimed to modify the bonding between carbide grains and the matrix. Other factors which may influence interface strength in alloy irons and tool materials include the relative deformation moduli of the carbides and matrix, their individual lattice types and parameters, and the orientation relationship

between them. In addition the possibility of segregation of harmful elements to interphase boundaries must be considered. In mild steels, for example, cracking along ferrite-cementite interfaces is believe to be aided by segregates of phosphorus, antimony, arsenic and sulphur building up at these interfaces and leading to easier crack nucleation (236). Segregation-sub boundary effects may also influence cracking in the matrix structure of chromium irons. In figures 4.49 - 4.51 cracks can be seen at sub-boundaries in the matrix of the hardened 15% chromium iron and a crack is also visible in the austenite matrix of the as-cast 30% chromium iron (figure 4.45). There are no reported studies of sub-boundaries in the matrix of chromium irons and it is not known whether the boundaries correspond to original boundaries between adjoining dendrite arms or are boundaries formed during holding for destabilisation or during subsequent transformation. Deleterious elements could segregate to these boundaries as well as to carbide-matrix interfaces allowing easier crack formation.

To further study the structure of the eutectic carbide and matrix phases and to determine whether plastic deformation of the carbides occurs during wear it was considered necessary to produce thin foils for examination by transmission electron microscopy. This work is described and discussed in the next chapter. There is little published information on thin foil examination of alloy white irons or

of subsurface damage in these materials although a limited study of eroded Stellite has suggested that both plastic deformation and lateral vent cracking occur at indentations in the carbide phase (237). The behaviour of carbides in the wear of Stellite has also been studied by Blomberry using deep etching to facilitate SEM examination (238). At low stress levels he reported that the carbides in the structure interupted the grooves formed by the abrasive particles but at higher stresses the carbide bridges are said to deform plastically. This lead to the suggestion that the abrasion resistance of the alloy is dependent on the ability of the matrix and the carbide to deform plastically and absorb the energy associated with the relatively moving abrasive particles rather than on the resistance of the hard carbide to micromachining as suggested by Watson (209).

Apart from wear or other mechanical tests the cracking and deformation effects discussed above could also be examined using indentation techniques. Such studies (239, 240) have been made in order to analyse the cracking patterns observed during the wear of cemented carbides but there are no reported indentation studies of alloy white irons to date. Indentation of cemented tool materials is believed to give a situation intermediate between that of a plastic metal and that of a brittle material. Median vents are said only to be formed in brittle solids and do not occur in tougher materials such as the cemented tools. Cracking is said to occur both

on loading and unloading with lateral cracks growing on unloading as in glass. One important observation is that the cracks tended to follow the interface between the carbide grains and the cobalt matrix. Indentation studies on white irons may be able to determine whether the parallel cracks in the carbide form due to the stresses on loading and/or due to the relaxation of stresses on unloading. They may also aid in understanding the occurence of carbide cracks running perpendicular to the wear surface.

6.0 TRANSMISSION ELECTRON MICROSCOPY.

When this work was initiated there was no published information on the examination of high chromium irons using thin foil transmission electron microscopy although some limited information had been obtained by Southwick (241) using foils prepared from 25% Chromium iron in the form of 3mm diameter rods. These rods, which are used as dilatometer specimens, were drawn directly from a melt into fused silica tubes and consequently this material had a very much finer microstructure than any of the irons studied in the present work on abrasion. To determine if a useful TEM study of irons with coarser sand cast structures were possible the following three irons were selected for examination.

Iron No.	%C	%Cr	Condition	Foil position *
4	3.10	14.68	Heat treated	(a), (b), (c).
7	2.44	30.60	As-cast	(a), (b), (c).
7	"	"	Heat treated	(b) only.

6.1 Preparation of thin foil specimens.

Thin slices (1 mm thick x 10 mm x 15 mm) were spark machined from sectioned wear test material using a Servomet apparatus fitted with a fed-wire electrode. Discs, 3 mm in diameter, were then spark machined from each slice using a

tube electrode. The slices were taken at positions (a), (b) and (c)* as indicated in figure 6.1.

Each disc was then carefully ground by hand on water lubricated 600 grit abrasive paper to a final thickness of 0.20 - 0.25 mm. In each case material removal was from the spark machined side of the disc. The discs were washed and degreased prior to dishing using a Struers Tenupol apparatus fitted with a Polipower controller. The polishing solution was 5% perchloric acid in 2-Butoxyethanol which was pumped from a reservoir held at -15°C. Polishing was performed at -10°C to -5°C at 70v and a current of 30 mA. Perforation was detected automatically using a light source - photocell arrangement. Average time to perforation was 30 minutes. Discs taken from positions (a) and (b) were dished from both sides but discs from position (c) were treated as follows. These discs were initially polished on both sides for 10 minutes in order to clean the wear surface. The cleaned wear surface was then protected from further thinning with stop off laquer and dishing to perforation was continued. This enabled the thinned portion of the disc to be as close to the wear surface as possible.

The perforated discs were examined at 100 Kv in a Jeol JEM 100B transmission electron microscope. It was found that only a small number of the discs (about 1 in 5) had suitable profiles around the perforation to enable TEM

examination of the structure. Even these only continued very small areas, e.g. part of a large eutectic carbide rod, thin enough for transmission of electrons. The most suitable of these discs were then subjected to further thinning using ion beam bombardment.

The ion beam thinning was carried out on an Ion-Tech machine using argon ions accelerated at 5 Kv to give a beam current of 100 Microamp, the specimen chamber pressure was maintained below 10^{-4} Torr. Each disc specimen was inclined at 15 - 20^{o} to the beam in order to thin down as evenly as possible the wedge of material around the original dished perforation. During thinning each specimen was heated to about $100^{o}C$. By trial and error it was found that satisfactory sharpening of the wedge could be achieved in about 1-2 hours giving reasonably sized areas for examination at 100 Kv. During the dishing and ion beam thinning a number of problems were encountered, these included preferential thinning of either the matrix or carbide phases, attack at the eutectic carbide-matrix interface and removal of eutectic carbides. These features are discussed where relevant in following sections.

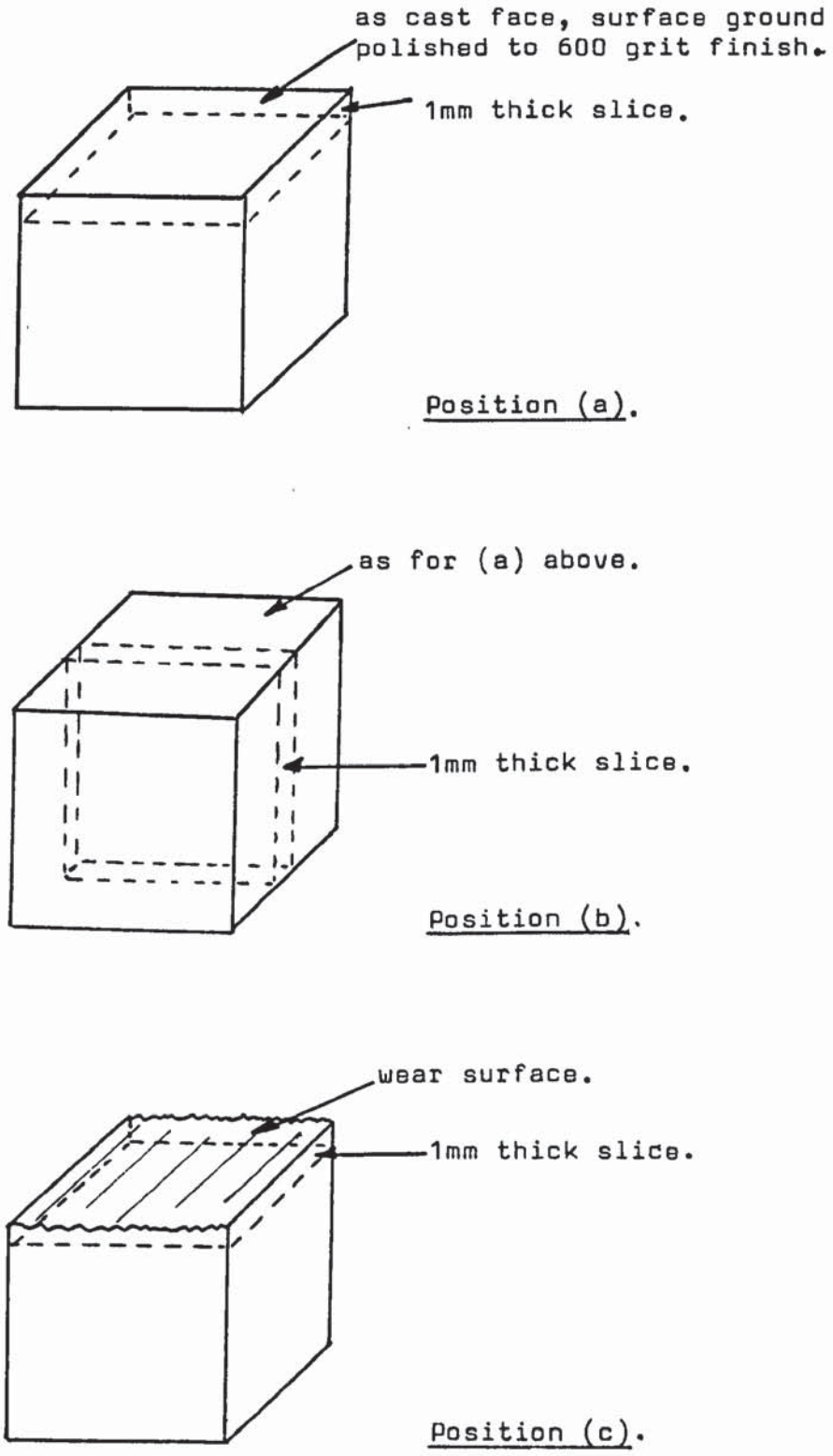

Figure 6.1

Positions of spark machined slices for TEM disc preparation

6.2 General features of the eutectic M_7C_3 carbides in the as-cast 30% chromium iron (austenitic matrix).

Figure 6.2 compares the effects of dishing on specimens taken from positions (a) and (c). In both cases the eutectic carbides have thinned preferentially to the austenitic matrix. In specimens taken from an unworn surface the eutectic carbides were not removed in the course of preparation but in specimens taken from the wear surface some of the carbides were removed due to the prior effects of wear causing their decohesion from the matrix. This removal limited the scope of the TEM study in this iron since the carbides which were most damaged by wear were lost during the preparation of thin foils.

In specimens taken from positions (a) and (c) the growth directions (C-axes) of the rods or blades of eutectic M_7C_3 carbide are at approximately 90^{o} to the plane of view. These transverse sections revealed that the carbide rods were not always single cystals but were often made up of a cluster of crystals as shown in figures 6.3(a) and 6.4. The overall diameter of the eutectic carbide rods ranged from 1 to 4 μm with the smallest diameters of crystals within a cluster being of the order of 0.4 - 0.5 μm. This observation extends the earlier SEM studies of Powell (213) and Boomgaard (242) who suggested joints between rods to form blades or lamellae of carbides but did not observe the fine sub-structures within the rods themselves.

The rods of eutectic carbide quite often contained a central core of matrix constituent which in a few cases was seen to be connected to the matrix surrounding the carbide cluster as is shown in figure 6.3(a). However, the majority of the cores observed were smaller than this and were isolated by enclosing carbide as shown in figures 6.3(b) and 6.5. Earlier metallographic examination of longitudinal sections through eutectic carbides revealed apparently isolated areas of matrix or hollows within the rods or blades in the 15% Cr, the 15% Cr - 3% Mo, and the 30% Cr irons (see figures 4.32, 4.45, 4.46, 4.51 and 4.55). Examination of a deeply etched specimen of the 30% Cr iron also showed that some eutectic rods may be hollow or may have contained matrix phases which had been removed during etching.

Although the number of observations were limited the size of the cores did not appear to relate directly to the overall diameter of the enclosing carbide rods. In figure 6.5(a) the smallest width of the core was 0.6 μm and this was equivalent to 25% of the corresponding width of the carbide. However, in the carbide shown in figure 6.5(b) the proportion was less than 15% with the smallest dimension of the core being 0.2 μm. In cross section some of the cores had an approximate hexagonal shape with straight edges which were parallel to the outside edges of the surrounding carbide. Figure 6.6 illustrates the effects of ion beam thinning after dishing. The matrix surrounding the eutectic carbides

is more clearly distinguished but the cores of matrix within the carbide have been partially removed. Figure 6.6(b) shows two adjacent cores which have developed separately as two adjacent rods grew together or may have formed by branching of an original core.

TEM examination of the 15% Cr iron also revealed the presence of cores in some of the eutectic carbide rods. Since in both irons cores were not visible in every cross section of carbide it is likely that only a proportion of the rods contain cores or that cores are present in the majority of rods but are discontinuous in nature. In longitudinal metallographic sections both long and short lengths of core or hollow have been seen. The cores may be non-uniform in cross section e.g. cigar shaped, thus explaining the observed variation in their diameter to width of enclosing carbide ratio in transverse sections. The nature of the matrix within and surrounding the carbides and the effects of wear on the matrix are discussed later.

In figures 6.4 - 6.6 sets of fine closely spaced parallel lines are seen in contrast within the eutectic carbides. This contrast is believed to result from the presence of stacking faults or twins in the structure of the M_7C_3 carbide. A maximum of three sets of faults are seen in each crystal with each set running parallel to the edges of the hexagonal rod in transverse section. In many of the carbides the

nature of the faulting was such that the crystal was sub-divided into zones with changing orientation and contrast beween the sets of faults seen in each zone. In each case the angular difference between faults in two adjacent zones was approximately 60^{o}. Figure 6.7 gives two introductory examples of this observation. The presence of these faults and those in other M_7C_3 carbides gives rise to streaking in electron diffraction patterns and a detailed account of this is given in later sections.

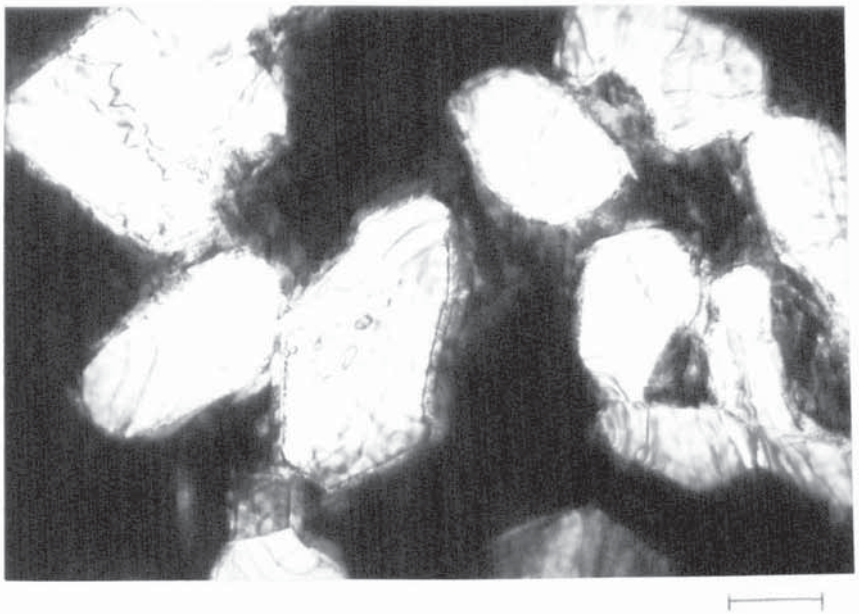

(a) Position (a), unworn. Carbide diameters range from 1-4 μm.

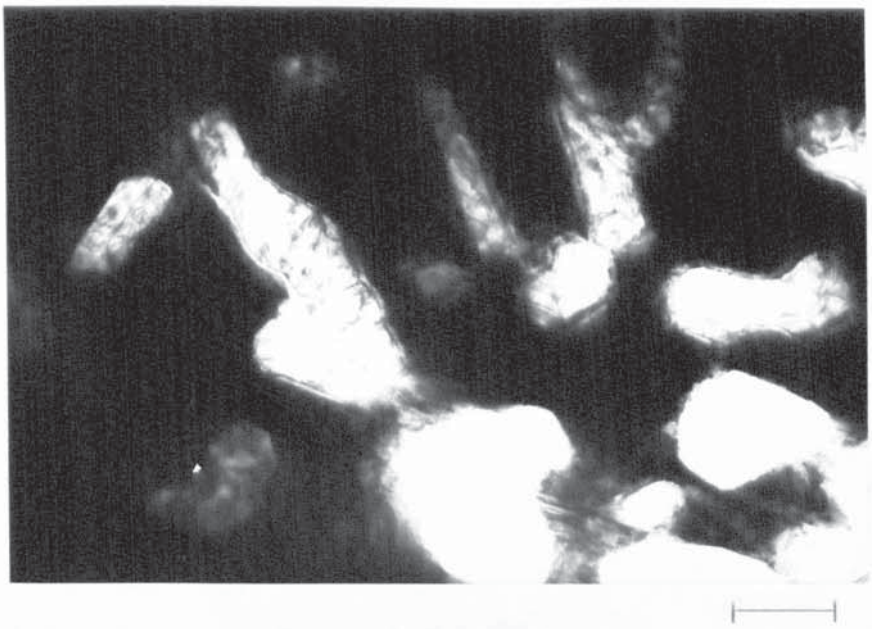

(b) Position (c), at wear surface. Note loss of eutectic carbides.

Figure 6.2

As-cast 30% Cr iron after preparation by dishing. (Marker is 1 μm).

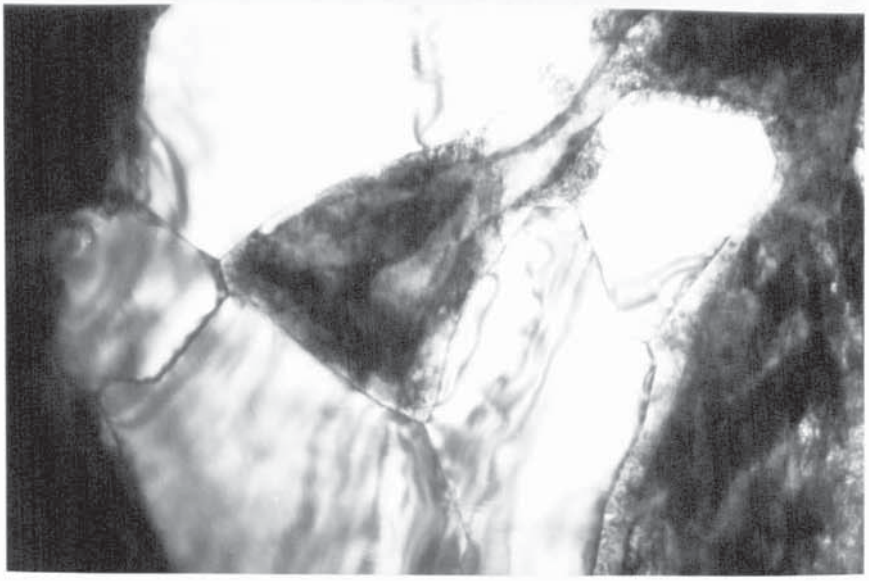

(a) Crystal boundaries in eutectic carbide.

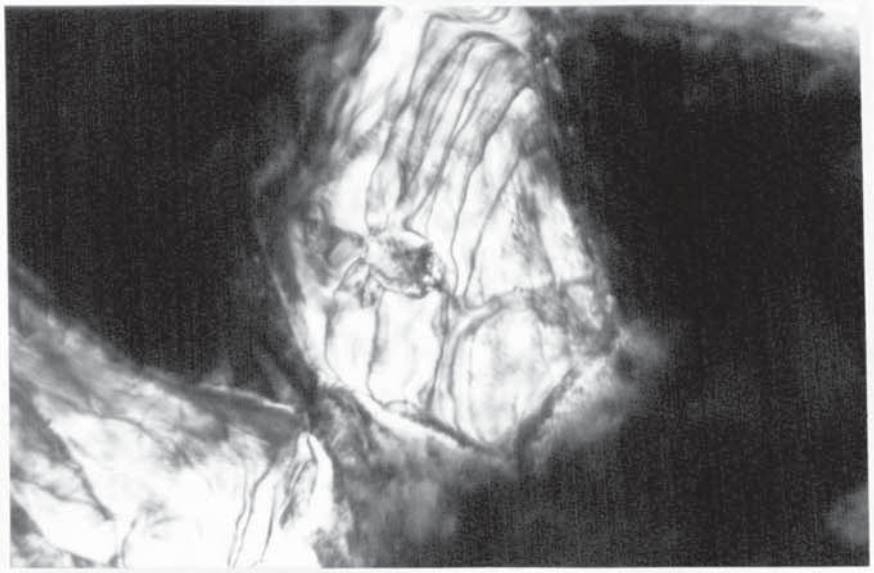

(b) Isolated core of matrix within eutectic carbide.

Figure 6.3

As-cast 30% Cr iron showing matrix cores within eutectic M_7C_3 carbide. Position (a) unworn. Preparation by dishing. (Marker is 0.5 μm).

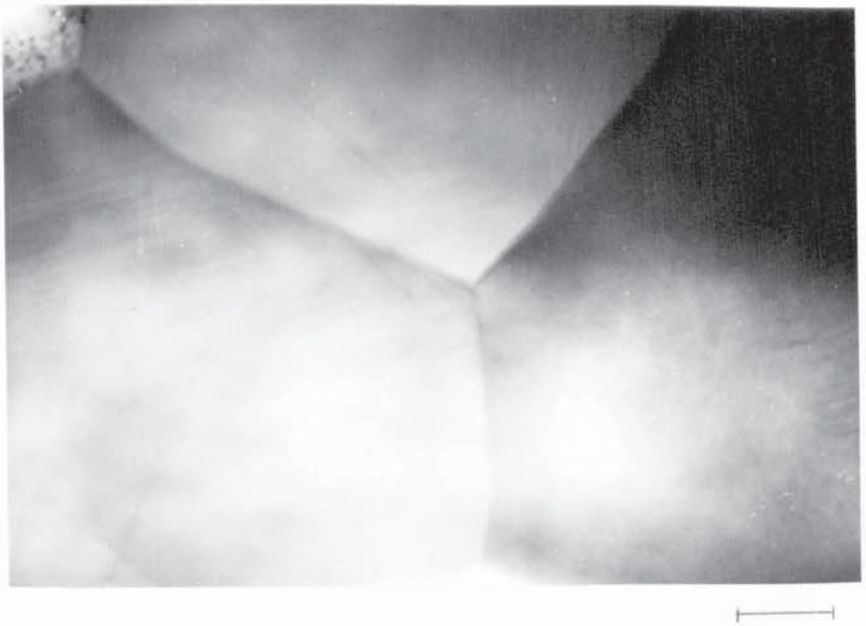

(a) Boundaries in M_7C_3 rod.

(b) Boundaries and contrast from 3 sets of faults.

Figure 6.4

As-cast 30% Cr iron showing boundaries and contrast due to faulting. Position (a) unworn. Preparation by dishing and ion beam thinning. (Marker is 0.1 μm).

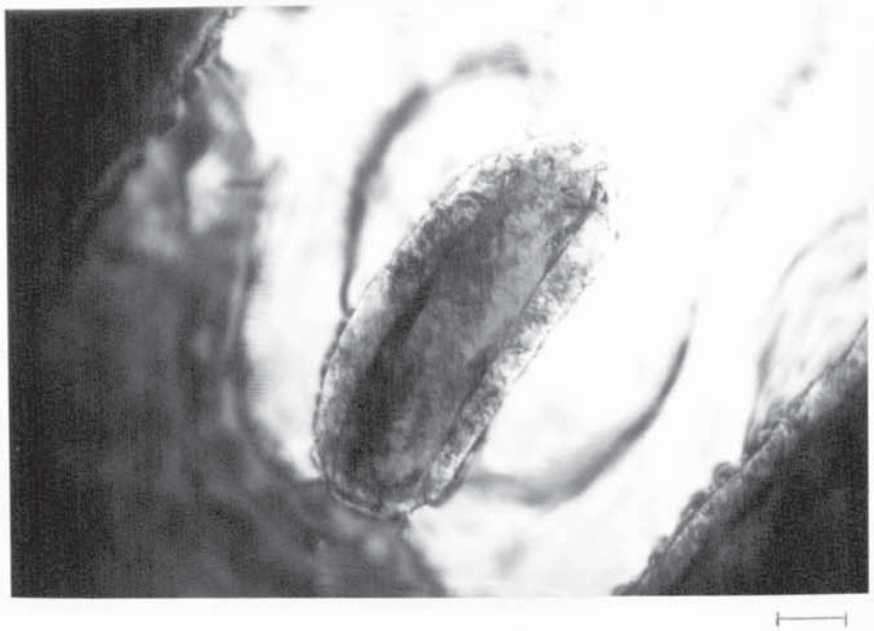

(a) Large core relative to carbide size.

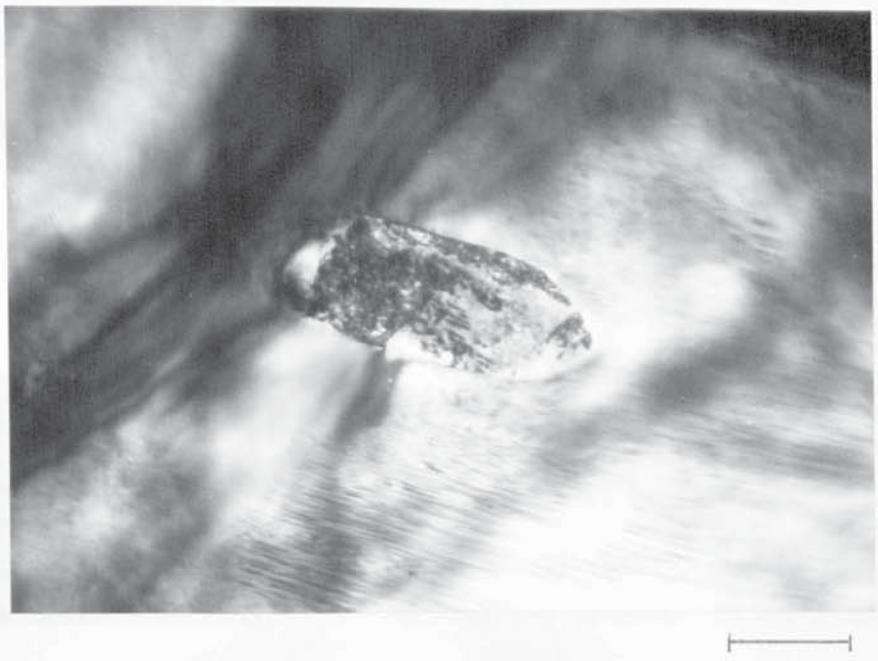

(b) Small core relative to carbide size.

Figure 6.5

Examples of matrix cores within eutectic M_7C_3 carbides in as-cast 30% Cr iron.

Position (a), unworn. Dished. (Marker is 0.2 μm).

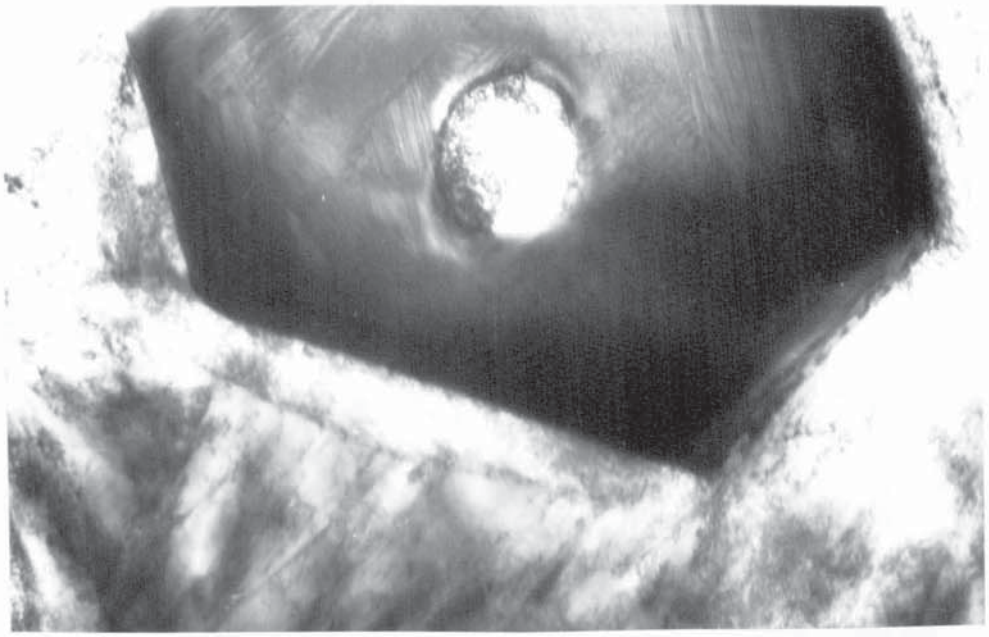

(a) Carbide with single core.

(b) Carbide with two cores.

Figure 6.6

As-cast 30% Cr iron. Partial removal and thinning of matrix. Note 60° angle between faulting and the relation to crystal edges. Position (a) Unworn. Dished + ion beam thinned. (Marker is 0.2 μm).

(a)

(b)

Figure 6.7

Further examples of contrast due to faulting within eutectic M_7C_3 carbides. As-cast 30% Cr iron.

Position (a) Unworn. Dished + ion beam thinned

(Marker is 0.2 μm).

6.3 General features of the 15% chromium iron in the heat treated condition.

The 15% chromium iron was subjected to thermal treatment in order to produce a matrix structure of tempered martensite (see section 4.2.2). During the destabilisation stage of this treatment secondary carbides were precipitated within the matrix and during subsequent cooling a small amount of very fine pearlite was also produced due to insufficient air hardenability of the destabilised austenite in the absence of molybdenum. Hence in the heat treated condition the structure of this iron contains the original eutectic carbides, secondary carbides, pearlitic carbides and tempered martensite.

The eutectic carbide rods were coarser and more variable in size than those seen in the 30% chromium iron and they appeared to contain more complex faulting within their structures. Figure 6.8 gives examples of these observations. In view (a) the nature of faulting in part of a large carbide rod (total width 6-8 μm) is seen and in view (b) two smaller rods of eutectic carbide are shown. In view (a) a mottled pattern is seen in the carbide, this effect has been observed in other specimens sometimes after dishing and sometimes after subsequent ion beam thinning. It is believed to be caused by the formation of surface films of oxide or by some form of preferential attack of the carbide. This mottled pattern is also clearly visible in figure 6.9 which

presents two of the problems encountered in thinning, i.e. attack at the carbide-matrix interface and non uniform thinning of the eutectic carbides. A mottled effect was not seen in the eutectic carbides in the as-cast 30% chromium iron but was seen in the original M_7C_3 eutectic carbides in the heat treated 30% chromium iron. It is known that alloying elements may become concentrated on the surface layers during thin foil specimen preparation and it is not yet known whether such surface layers can be removed by ion beam thinning which itself is considered to be liable to differential rates of atom removal for the various alloy constituents (243).

The size and distribution of the secondary carbide particles are seen in figure 6.10. View (a) is close to an original as-cast surface of a wear test sample and view (b) is taken from the central region of the sample. Both specimens were prepared by dishing. Many of the secondary carbides were not sufficiently thinned and any suitably thinned areas of matrix were limited in size. The advantages offered by subsequent ion beam thinning are illustrated in figure 6.11 which shows the secondary carbides and the pearlitic area seen at the right hand side of figure 6.10(b). The extra thinning revealed line contrast in the secondary carbide particles which is believed to be due to faulting as in the eutectic carbides seen earlier. It also enabled the very fine carbide lamellae in the pearlite to be clearly resolved

confirming that fine pearlite in this material is lamellar and not granular. The mean interlamellar spacing of the pearlite was 0.06 μm and the majority of the secondary carbide particles ranged from 0.25 to 0.6 μm in size. Whereas the eutectic carbides in this iron contained up to three distinctly visible sets of faults nearly all the secondary carbide particles observed contained a single visible set. A very small number of secondary carbides did contain internal boundaries, these were the largest particles which have probably formed from the coalescence of smaller particles during the period of destabilisation. There was no evidence of deposition of secondary carbide on the original eutectic carbides. The alignment of the secondary carbide particles within the matrix is seen in figure 6.10 (a) and in figure 6.11 where the line contrast believed to be due to faulting is parallel in the three larger secondary carbides.

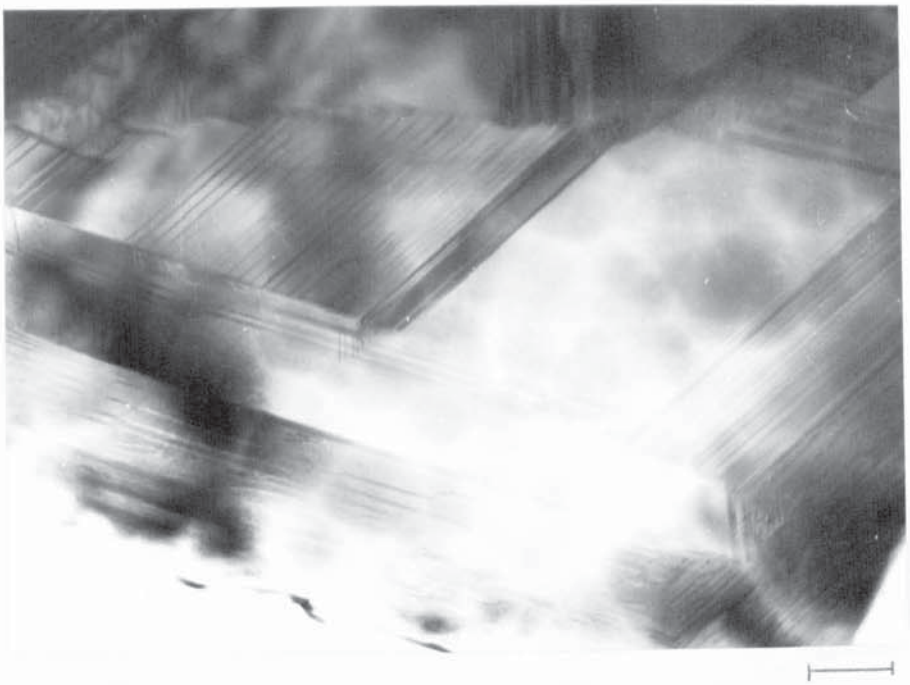

(a) View of part of a large eutectic carbide rod. (Marker is 0.4 μm).

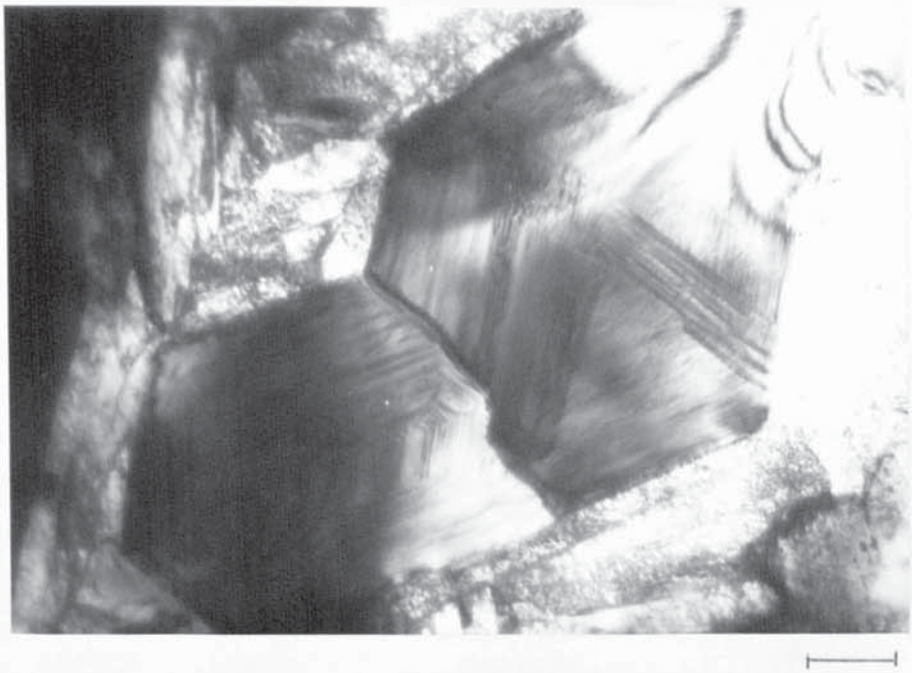

(b) Contrast due to faulting in two adjacent rods of eutectic carbide. (Marker is 0.3 μm).

Figure 6.8

Eutectic M_7C_3 carbides in 15% Cr iron (heat treated)

Position (a) Unworn, dished + ion beam thinned.

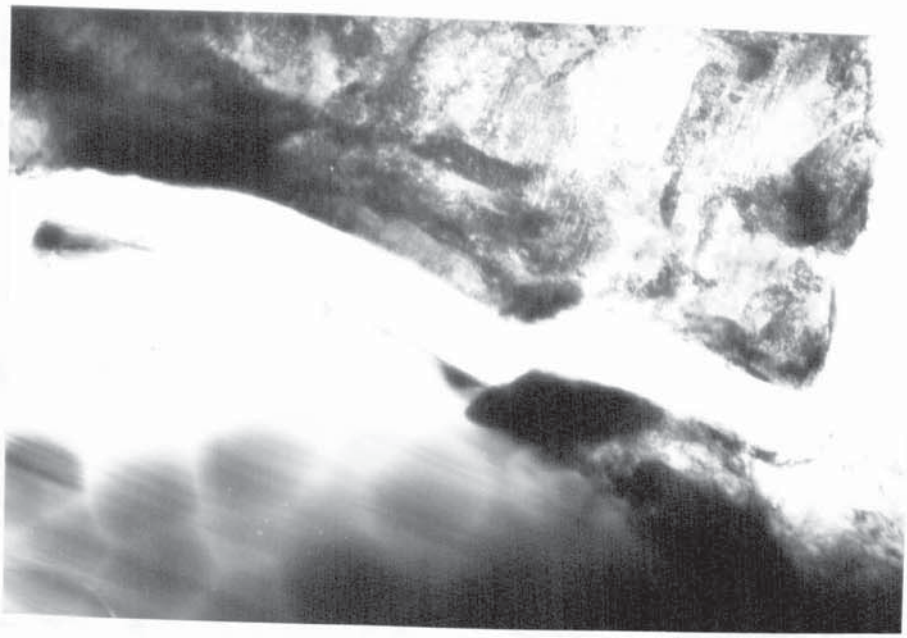

(a) Separation at eutectic carbide-matrix interface.

(b) Uneven thinning and perforation of eutectic carbide.

Figure 6.9

Examples of problems encountered during specimen preparation in 15% Cr iron (heat treated).
Position (b) unworn, dished + ion beam thinned.
(Marker is 0.25 μm).

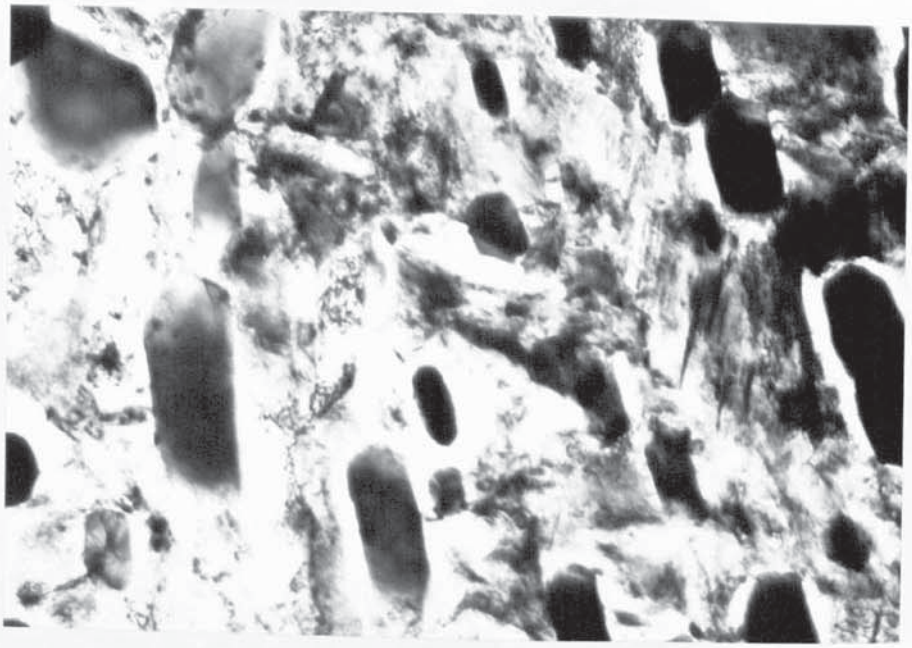

(a) Distribution of secondary carbides. Position (a) (Marker is 0.25 μm).

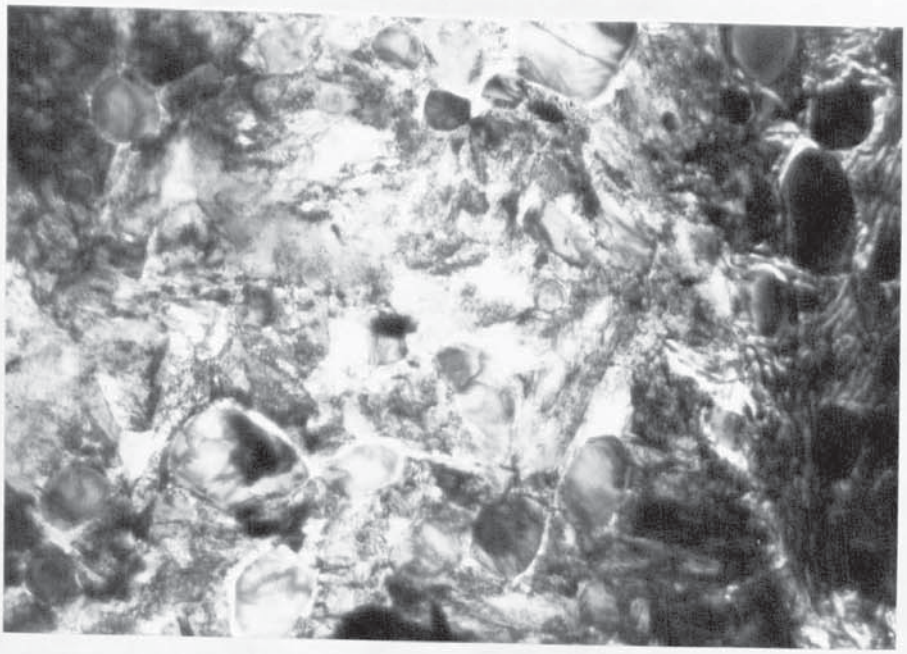

(b) Distribution of secondary carbides. Position (b). Note pearlitic area on right hand side. (Marker is 0.4 μm).

Figure 6.10

15% Cr iron (heat treated) showing secondary carbides. Dished only.

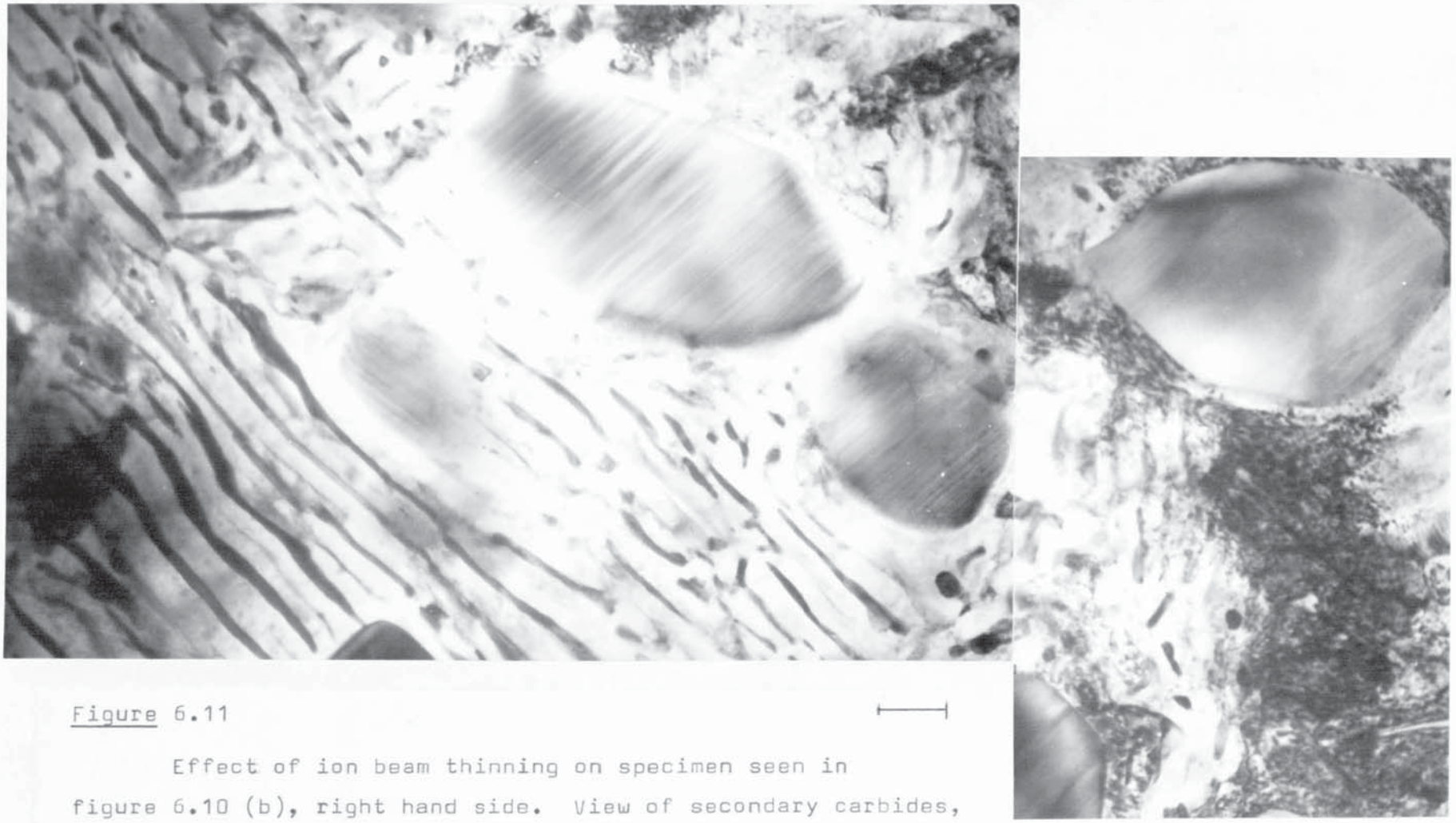

Figure 6.11

Effect of ion beam thinning on specimen seen in figure 6.10 (b), right hand side. View of secondary carbides, fine pearlite and tempered martensite. (Marker is 0.1 μm).

6.4 Microanalysis of TEM specimens.

To determine the iron and chromium contents of the core regions within the eutectic carbides a limited amount of selected area analysis was carried out using a Kevex X-ray energy spectrometer attachment on the transmission microscope. The results from this were expressed as chromium: iron ratios and are given together with the positions analysed in table 6.1. The ratios were obtained by comparison of peak heights from three minute count periods using the smallest probe diameter (beam setting 4 on the Jeol 100B microscope). Table 6.1 presents analyses from three separate carbide rods in each of the two irons examined.

Specimen (Position (a))	Analysis Position	Eutectic carbide rod		
		(i)	(ii)	(iii)
30% Cr iron (as-cast)	1	2.23	2.28	2.26
	2	0.468	0.42	0.45
	3	0.488	0.43	0.47
15% Cr iron (hardened)	1	0.94	0.925	0.938
	2	0.114	0.121	0.166
	3	0.136	0.131	0.196

Table 6.1

Chromium: iron ratios calculated from energy dispersive analysis.
(Analysis positions 1 - eutectic carbide; 2 - matrix core; 3 - surrounding matrix).

For visual comparison the traces obtained for the carbide rod seen earlier in figure 6.6(a) are given in figure 6.12. The chromium: iron ratios of 2.2 - 2.3 (uncorrected) for the eutectic carbide in the as-cast 30% chromium iron are less than the value of 2.8 (corrected) obtained by EPMA (see table 4.14). Although thin film analysis is less accurate than EPMA and is open to both instrument and specimen preparation errors it can be used to show any compositional variations between selected areas in a sample. For both irons it was found that there was little difference in the Cr:Fe ratios of the matrix cores and the corresponding matrix surrounding the carbide; in both cases there was marginally more chromium in the outside surrounding matrix. Unfortunately determination of carbon content of the two areas was not possible since energy loss spectroscopy combined with in-situ ion bombardment cleaning are required to achieve this (243).

Selected area analysis was performed on the two types of carbide, believed to be M_7C_3 and $M_{23}C_6$, in the heat treated 30% chromium iron. This information is given with electron diffraction results for this material in a later section.

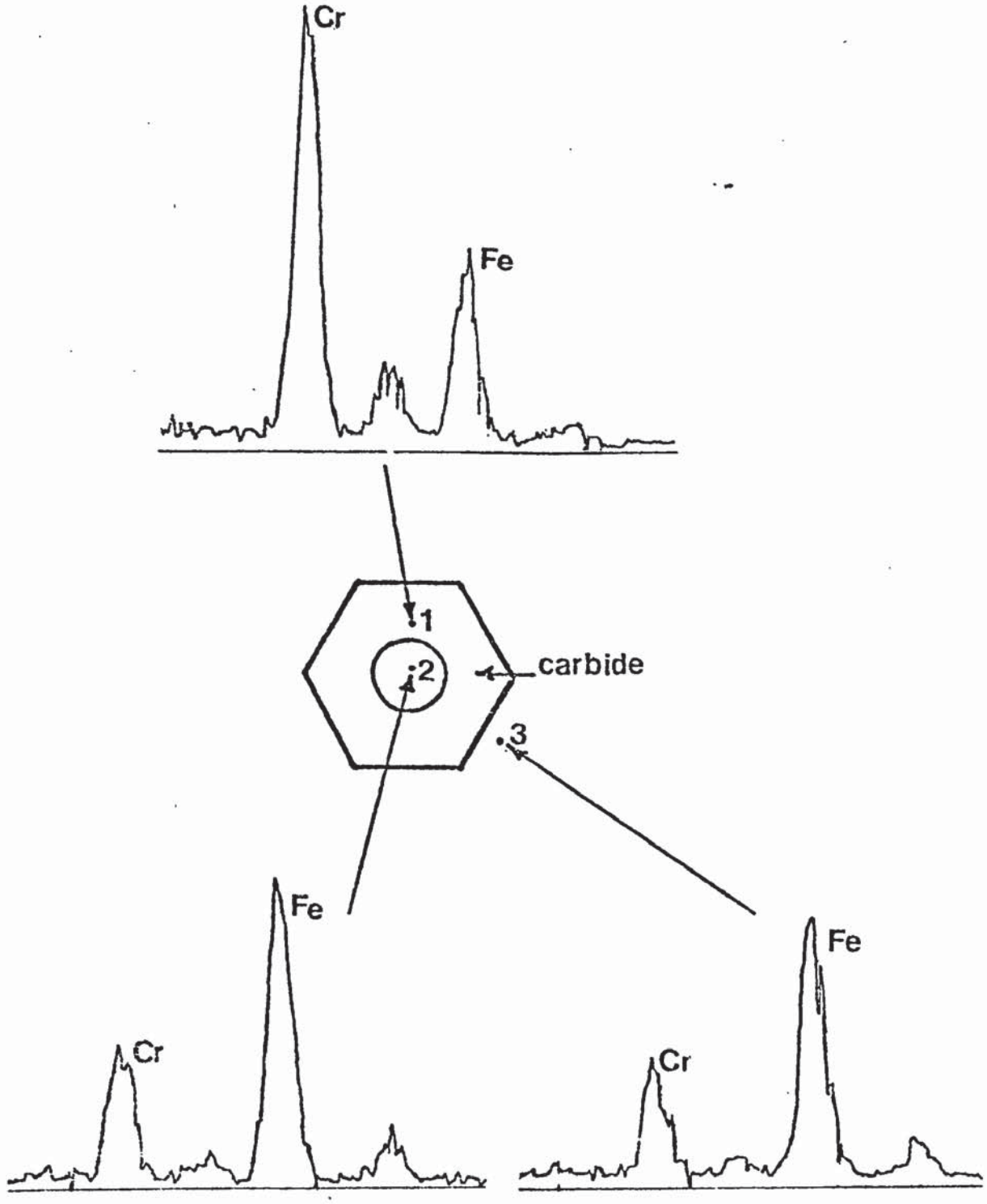

Figure 6.12

Energy dispersive X-ray microanalysis of eutectic M_7C_3 carbide and matrix in 30% chromium iron. Actual carbide analysed is shown in figure 6.6 (a).

6.5 Study of the matrix structure in the as-cast 30% chromium iron.

Earlier work has shown that the microhardness of austenite at the wear surfaces of as-cast austenitic irons reached as high as 950 Hv compared to 400 Hv for the unworn austenite (see table 4.12). Previous comments on this increase have referred, for convenience, simply to "work hardening" of the austenite. TEM examination has been used to study this effect and has produced evidence for a transformation to martensite at the wear surface by comparing specimens taken from worn and un-worn samples. It is recognised that damage can be introduced when thin foils are prepared from thicker specimens using mechanical stages such as cutting, spark erosion and grinding. However, since both sets of specimens (i.e. from positions (a) and (c) in figure 6.1) were prepared in exactly the same way any structural differences between them could be attributed to the effects of abrasive wear produced during the wear test.

Electron diffraction patterns obtained from both primary and eutectic matrix regions have been indexed using standard procedures. The theoretical background to these procedures is given in a number of comprehensive texts (244-246). Of these the work of Andrews et Al (244) was used as a working text and as a source of information on interplaner spacings and angles for phases present in ferrous alloys. To solve the initial

patterns a previously calibrated value of the camera constant λL was used but the calculated d spacings were found to be consistently 1.10-1.15 X greater than the tabulated values. Accordingly a recalibrated value for λL was used based on d spacings for unworn austenite.

Figure 6.13 is typical of the structure of the unworn dendritic austenite which is remote from the eutectic M_7C_3 carbide rods and plates. Stacking faults and dislocation lines are clearly visible but there is no evidence of martensite formation from the image or from the corresponding diffraction pattern. The defect structures are similar to those observed in austenitic stainless steels (247, 248). The density of lattice defects is slightly greater than that normally observed in an annealed austenitic steel (248), a greater number of defects probably being introduced during solidification and subsequent cooling to room temperature of the austenite. An analysis of the nature of the stacking faults observed in figure 6.13 was not attempted during the present investigation.

In comparison figure 6.14 represents the eutectic austenite adjacent to the eutectic M_7C_3 carbides in the unworn condition. Corresponding electron diffraction patterns for the eutectic austenite at positions away from and immediately adjacent to the eutectic carbide are given in figures 6.15 and 6.16. For all the patterns given correct allowance has been

made in mounting to account for image - electron diffraction pattern rotation in the microscope. Where this has not been possible (for convenience of mounting) the angular rotation between image and pattern is given. To complete the examination of the matrix structure in the unworn 30% chromium iron a diffraction pattern was obtained from the core of matrix seen earlier (Figures 6.6(a) and 6.12) within a eutectic carbide rod; this is given in figure 6.17.

Reference d spacings for austenite and ferrite and an outline of the methods used to solve the patterns given in figures 6.13 - 6.17 are given in the appendix. For the pattern in figure 6.13 the measured d spacings and angles are compared with reference and calculated values as follows:

Reflection	d_m	d_r	Angle	Measured	Calculated
111	2.06	2.070	$\bar{1}11$ $\bar{1}1\bar{3}$	28^o	29.49^o
200	1.84	1.793			
311	1.08	1.081	$00\bar{2}$ $\bar{1}1\bar{3}$	25^o	25.23^o

where d_m = d spacing measured from pattern in $\mathring{A}$

d_r = d spacing from tables in $\mathring{A}$

The electron beam direction B indicated with the patterns is conventionally taken as the vector upwards from the plane of the paper (see (245) pp 17-23).

Comparisons obtained for the patterns in figures 6.15 and 6.16 for the austenite phase were as follows:

Reflection	d_m	d_r	Angle	Measured	Calculated
111	2.08	2.070	$02\bar{2}$ ^ $\bar{1}3\bar{1}$	32°	31.48°
022	1.19	1.268	$\bar{1}3\bar{1}$ ^ $\bar{1}11$	58°	58.51°
113	1.08	1.081	$02\bar{2}$ ^ $\bar{2}40$	50°	50.76°
024	0.817	0.802			

In the pattern obtained from the matrix at position 2 which was immediately adjacent to the eutectic carbide extra reflections were obtained which corresponded to bcc iron. These are shown in figure 6.16, the d spacings calculated from the pattern for 002 and 112 reflections were 1.430 and 1.165 Å compared with corresponding tabulated values of 1.433 and 1.170 Å. The presence of bcc iron in this region is to be expected since martensite is known to form in the eutectic austenite areas due to impoverishment in carbon and chromium in the vinicity of the eutectic M_7C_3 carbide (249). The pattern for austenite in figure 6.16 corresponds to a $[2\bar{1}1]$ zone and the reflections from the bcc iron correspond to a $[\bar{1}10]$ zone. The relationship between the face centred and body centred structures found from the pattern is thus:

$(0\bar{2}2)$ fcc // (002) bcc

(211) fcc // (110) bcc

and $(\bar{1}\bar{1}3)$ fcc ~// $(\bar{1}12)$ bcc.

This fits the Nishiyama-Wasserman (N-W) relationship for austenite and martensite (see ref. (244) pp 137-147 and the stereographic projection in the appendix).

Examination of the diffraction pattern from a core of matrix phase within a eutectic carbide rod (see figures 6.6, 6.12 and 6.17) showed that this core had a bcc structure and no reflections for fcc austenite were recorded. The d spacings and angles for the bcc pattern given in figure 6.17 were as follows:

Reflection	d_m	d_r	Angle	Measured	Calculated
011	2.01	2.027	$\bar{1}\bar{2}1 \wedge \bar{2}\bar{1}1$	32^o	33.5^o
112	1.14	1.170	$\bar{2}\bar{1}1 \wedge \bar{3}01$	25^o	25.35^o
013	0.88	0.906	$\bar{3}01 \wedge \bar{1}10$	47^o	47.87^o

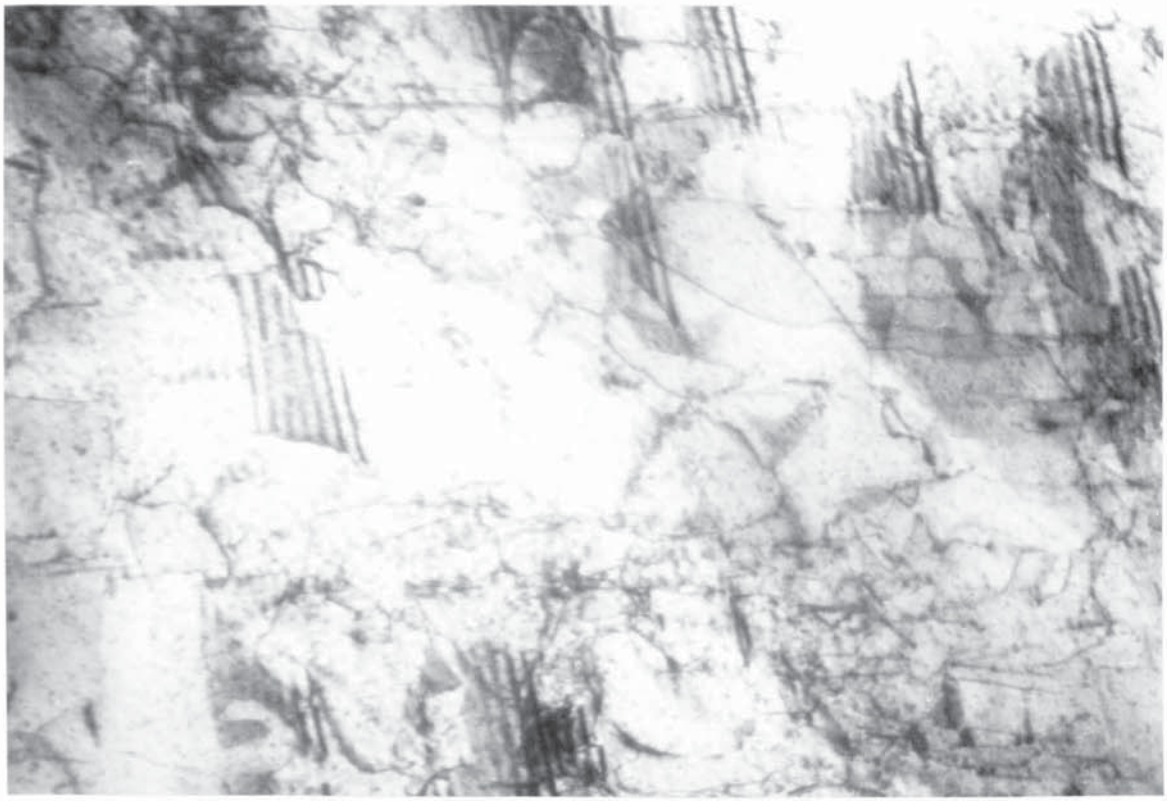

(a) Defect structures in austenite matrix remote from eutectic carbides (Marker is 0.2 μm).

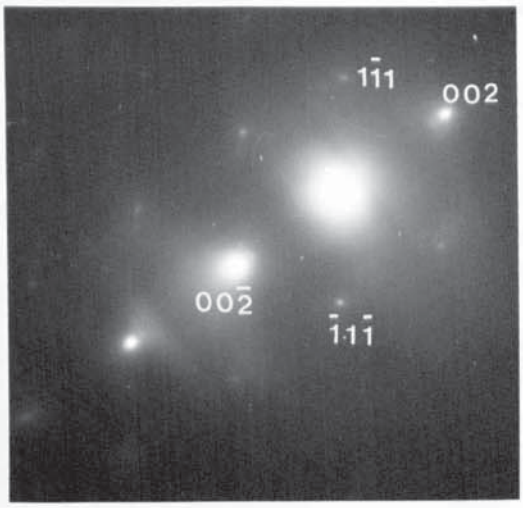

(b) Diffraction pattern for (a). The beam direction B was close to $[110]$.

Figure 6.13

As-cast 30% Cr iron. TEM view of primary austenite before abrasion. Position (a). Dished + ion beam thinned.

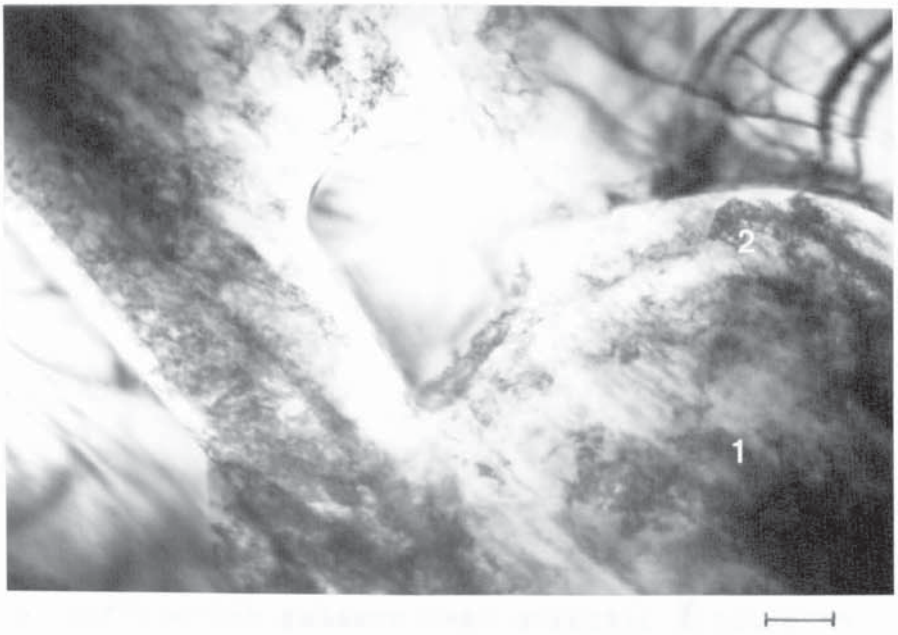

Figure 6.14

As-cast 30% Cr iron. Eutectic austenite + carbides. Position (a). Dished + ion beam thinned. (Marker is 0.2 μm).

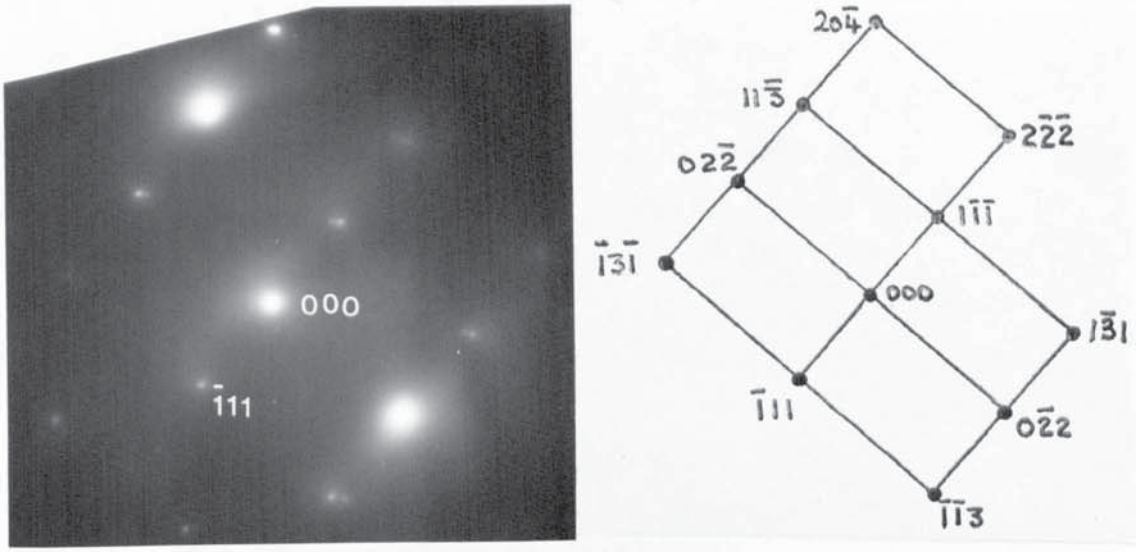

Figure 6.15

Electron diffraction pattern from position 1 in figure 6.14. B was close to $[2\bar{1}1]$.

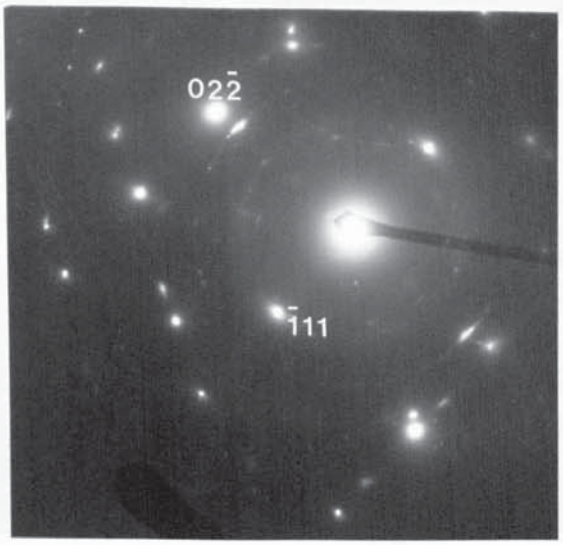

(a) Diffraction pattern from eutectic γ close to eutectic M_7C_3

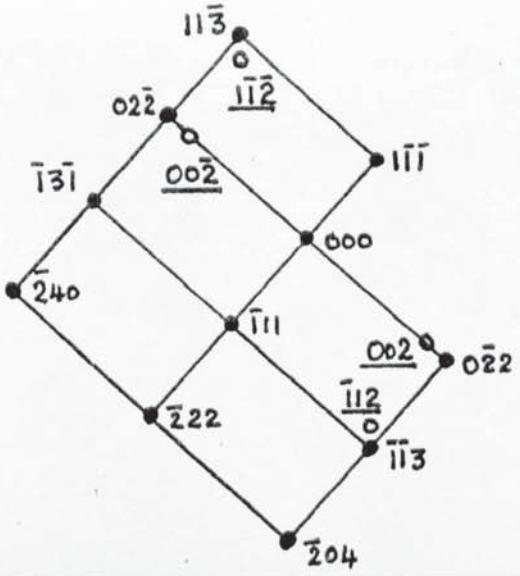

(b) Indexed pattern for fcc and bcc (underlined) reflections. For fcc B was close to $[211]$ and for bcc was close to $[110]$.

Figure 6.16

As cast 30% Cr iron. Diffraction pattern from position 2 in figure 6.14.

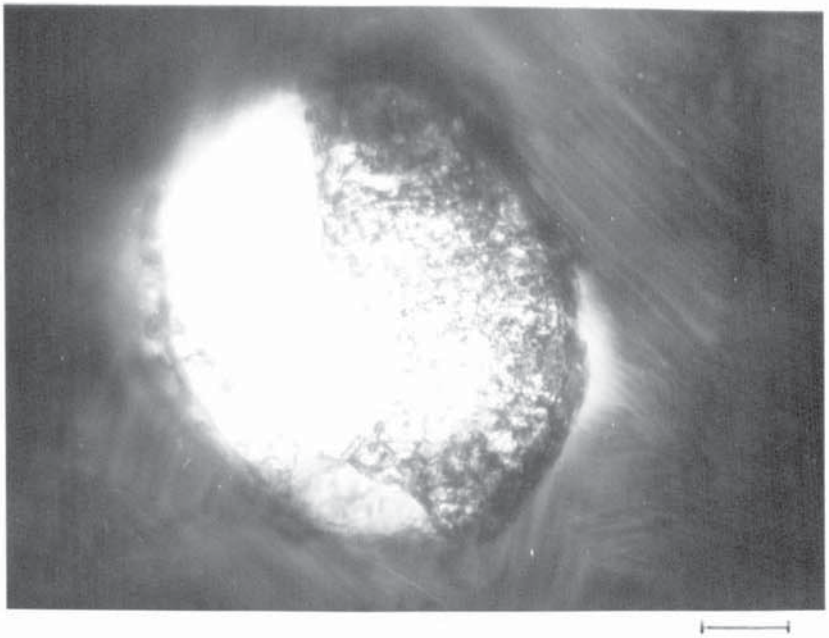

(a) Core of matrix within carbide. Marker is 0.1 μm

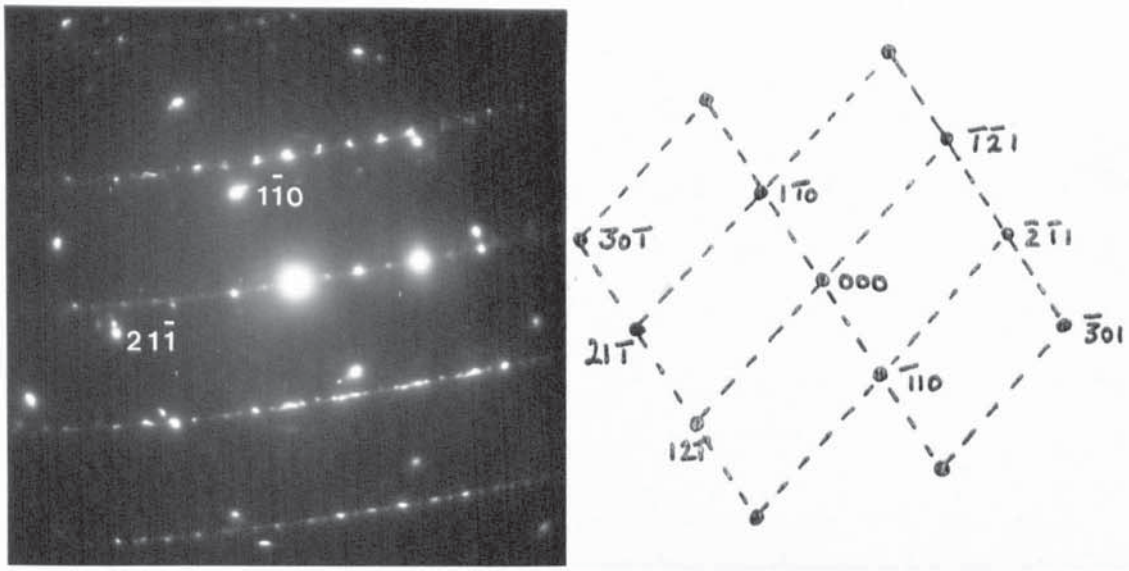

(b) Diffraction pattern from (a). B for bcc core was close to $[\bar{1}13]$. Pattern must be rotated 63° anti-clockwise relative to image. (a)

Figure 6.17

As cast 30% Cr iron. Matrix core within eutectic carbide seen in figure 6.6 (a).

From the results of figures 6.13 - 6.17 it is seen that in the as-cast condition the matrix is essentially austenitic with some transformation to body centred martensite in the eutectic austenite adjacent to M_7C_3 carbides and in the cores of matrix within the carbides. In the latter case transformation to the body centred structure is more extensive and this is probably due to extra depletion of carbon in the cores compared to the surrounding matrix. There was little difference in chromium: iron ratios but carbon analysis was not possible.

Figures 6.18 - 6.21 are used to illustrate the effects of abrasion on the above structure. In the primary austenite remote from the eutectic carbides thin crystals of ε martensite (hcp) were observed together with regions of highly dislocated matrix believed to be α martensite (body centred) as shown in figure 6.18(a). This structure is similar to that observed by Brooks (248) in austenitic stainless steel which was deformed in situ in an electron microscope. The electron diffraction pattern from the abraded structure contained diffraction rings which suggested that the area examined was polycrystalline. Before abrasion primary austenite produced spot patterns normally obtained from single crystal regions (compare figure 6.18 with figure 6.13).

Analysis of the pattern (see following table and figure 6.19(a)) confirmed the presence of a hcp structure within the austenite where the close packed planes and

directions of the hcp ε phase and the fcc. γ are parallel. The pattern has been indexed in accordance with $(011)_\gamma // (\bar{2}1.0)_\varepsilon$, this is consistent with the relationship found by Brooks (247) in γ stainless steel where

$$(111)_\gamma // (0001)_\varepsilon$$
$$\text{and } [1\bar{1}0]_\gamma // [1\bar{2}10]_\varepsilon$$

Ring No.	d_m	d_r	Reflection	
			fcc	hcp
1	2.48	*	*	*
2	2.09	2.070	111	00.2
3	1.51	1.509	-	01.2
4	1.30	1.268	022	-
5	1.14	1.170	-	01.3
6	1.03	1.035	222	00.4

The six spots seen in ring number 1* do not correspond to hcp $\{10.0\}$ reflections since these spots are not correctly positioned for a $[\bar{2}1.0]$ zone. However, these six spots are in the correct angular positions with respect to the fcc $\{111\}$ reflections to be the $\{011\}$ reflections from body centred iron i.e. α martensite. Likewise the extended reflections of ring number 3 could also correspond to $\{112\}$ body centred reflections. The measured d spacings of 2.48 and 1.51 are significantly larger than the tabulated values for bcc ferrite of 2.027 and 1.17 but the r^2 values fit the 2:6 ratio for

$\{011\}$: $\{112\}$ reflections. Hence the indexed pattern in figure 6.19(b) is tentatively suggested to account for these six reflections with the discrepancy in d spacings possibly due to the presence of a high carbon content and strain at the wear surface. This suggested solution corresponds to a $[\bar{1}11]$ zone and the two patterns are then in agreement with the relationship

$$(011)_\gamma \;//\; (111)_\alpha \;//\; (\bar{2}1.0)_\varepsilon$$

discussed by Andrews (244).

Figure 6.20(a) shows the effects of wear on an area of primary austenite closer to the eutectic region. As in figure 6.18(a) long thin parallel faults which are typical of ε martensite (A) are seen. Regions with a high defect density (B) were also visible and these may correspond to worked austenite or α martensite. Analysis of a diffraction pattern from this area confirmed the presence of both a hcp and a body centred structure and gave similar relationships to those of figure 6.18(b). Both the pattern and indexed diagram (slightly larger scale) should be rotated 108° anticlockwise with respect to the micrograph. The strong reflections at $(1\bar{1}1)_\gamma$ correspond also to $(0\bar{1}1)_\alpha$ and $(00.\bar{2})_\varepsilon$; likewise at $(\bar{1}1\bar{1})_\gamma$ are $(01\bar{1})_\alpha$ and $(002)_\varepsilon$. To be consistent with these relationships the pattern has been indexed with B as $[0\bar{1}\bar{1}]_\gamma$ and $[\bar{1}\bar{1}\bar{1}]_\alpha$. The measured values of the angles θ and ϕ of 69° and 55° relate to the theoretical values of 70.5° and 54.7°. Compared to the previous pattern the $\{011\}_\alpha$ reflections are

at their expected positions but there is also a faint inner ring visible giving a d value of 2.49 Å. Spots are seen in this ring but none is in the correct position to fit $\{01.0\}_\varepsilon$ reflections (d value = 2.20). In the previous pattern the inner six reflections assumed to be $\{011\}_\alpha$ corresponded to a d value of 2.48.

Figure 6.21 is typical of the structure of the eutectic austenite at the wear surface. Thin crystals believed to be ε martensite or stacking faults in the austenite (250) are visible (indicated by A) as are highly dislocated areas (B) believed to be α martensite. A rod of eutectic carbide is at the extreme right (C). Analysis of the diffraction pattern from this region confirmed the presence of a body centred structure as well as austenite. The pattern corresponds to a $[001]$ zone for bcc and to a $[0\bar{1}1]$ zone for fcc conforming to the relationship $(0\bar{1}1)_\gamma \;//\; (001)_\alpha$ seen earlier from figure 6.16. The pattern in figure 6.21 must be rotated 63° anticlockwise relative to the micrograph above. Measured d spacings for the two structures compared to reference values as follows:

Body Centred			Face Centred		
	d_m	d_r		d_m	d_r
110	2.04	2.027	111	2.037	2.070
020	1.45	1.433	022	1.20	1.268
130	0.903	0.906	133	0.774	0.802

Also present were reflections corresponding to hcp martensite (h and h^1 on diagram). The d spacings calculated for h and h^1 were 1.91 and 0.96 Å fitting reflections from $(10\bar{1}1)$ and $(20\bar{2}2)$ which have reference d values of 1.945 and 0.974 Å. The $(10\bar{1}1)$ type reflections were situated on streaks from the (111) and $(\bar{1}\bar{1}\bar{1})$ austenite reflections, elongation of the $(222)_\gamma$ reflection is also seen.

In the case of eutectic austenite body centred α martensite was seen to be present before wear but hcp ε martensite was not observed. The effect of wear on the eutectic region has been to introduce thin ε crystals into the austenite as for the primary dendrite austenite. Further transformation of the eutectic austenite to bcc α martensite may also take place but this cannot be proven without examining the same region of eutectic austenite both before and after wear since some α is present in the unworn condition. By comparing figure 6.21 with figure 6.15 it is seen that wear has resulted in a sub-boundary structure within the eutectic matrix with clear differences in contrast between adjacent crystals of γ and α Thin ε crystals (or stacking faults)* are clearly seen in contrast against lighter γ. At the left hand side of the micrograph in figure 6.21 the ε crystals (faults)* halt at a sub-boundary in the austenite. The areas of α martensite appear to contain large numbers of defects which may have been introduced during wear or may simply have resulted from the misfit between γ and α being accomodated by slip rather than by twinning (247, 250).

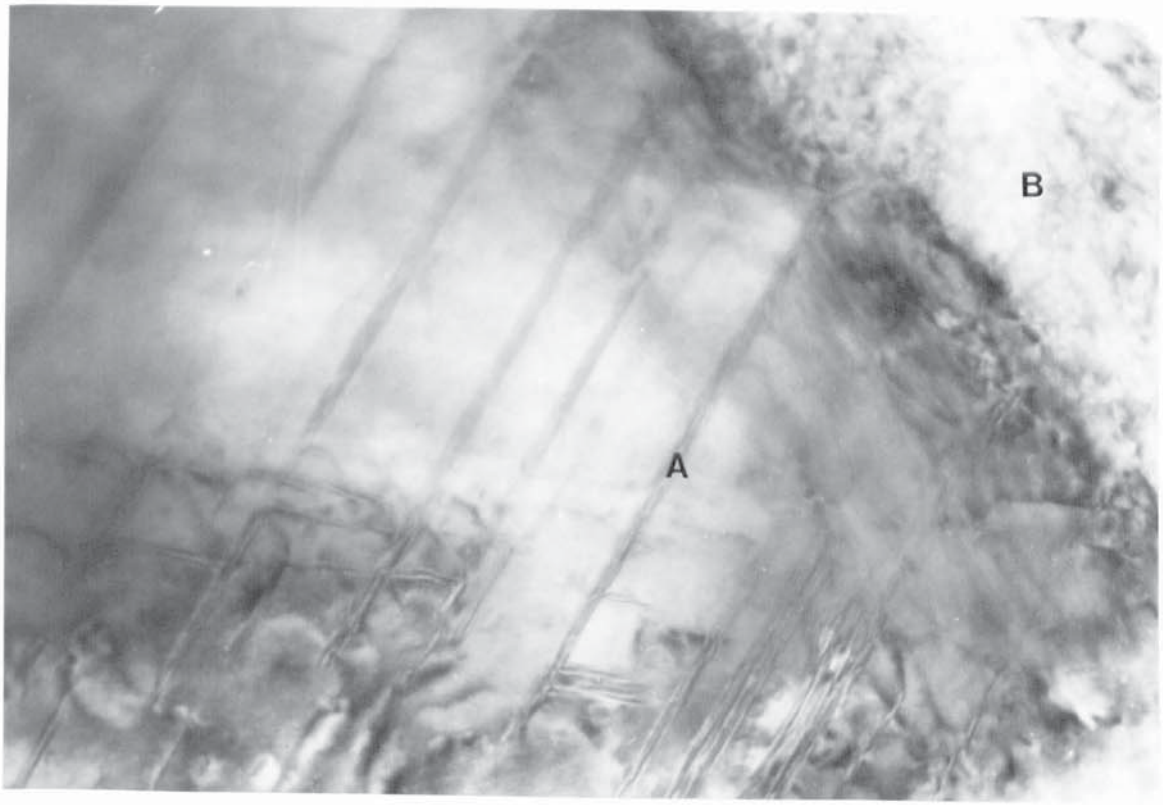

(a) Thin crystals of ε martensite (A) and highly dislocated α martensite (B). Marker is 0.1 μm.

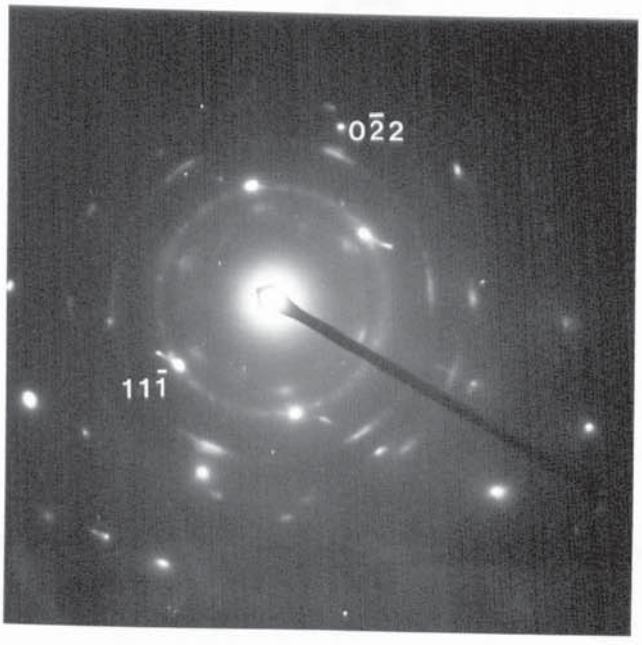

(b) Diffraction pattern from (a). B for fcc is [011].

Figure 6.18

As-cast 30% Cr iron. Effect of abrasion on primary austenite remote from eutectic carbide. Position (c), dished + ion beam thinned.

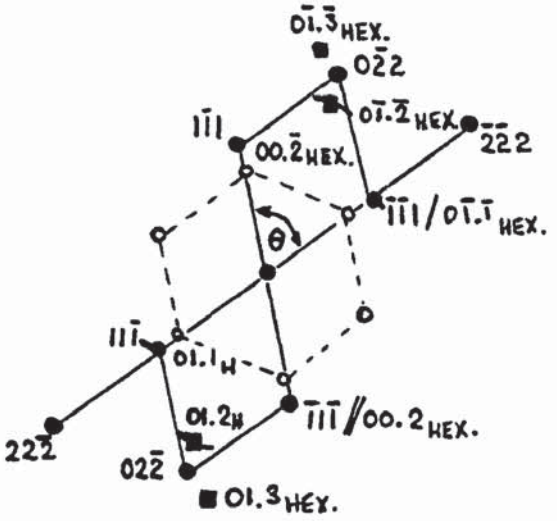

(a) Indexed as $(011)_\gamma$ // $(\bar{2}1.0)_\varepsilon$ where ε is hcp. Measured value of angle θ is 68° compared to theoretical value of 70.5°.

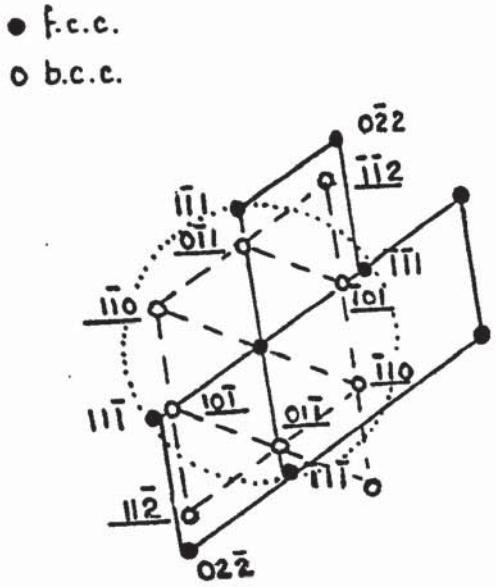

(b) Indexed such that $(011)_\gamma$ // $(111)_\alpha$. Inner six reflections assumed from $\{110\}_\alpha$

Figure 6.19

Diffraction patterns corresponding to figure 6.18. Each pattern must be rotated 41° anticlockwise relative to micrograph.

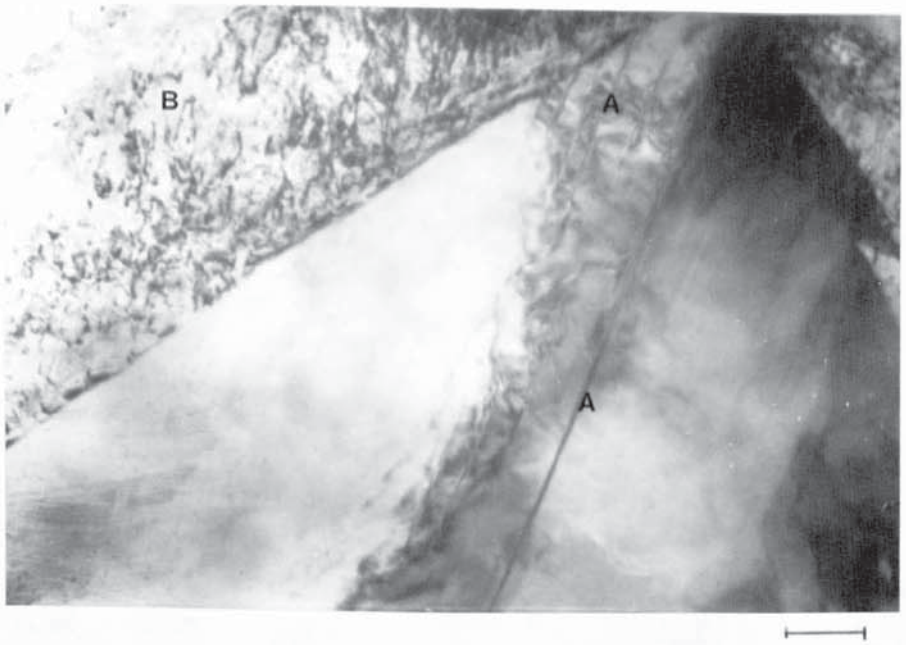

(a) Thin crystals (A) believed to be ε martensite and region (B) which may be α martensite or heavily worked γ. Marker is 0.1 μm.

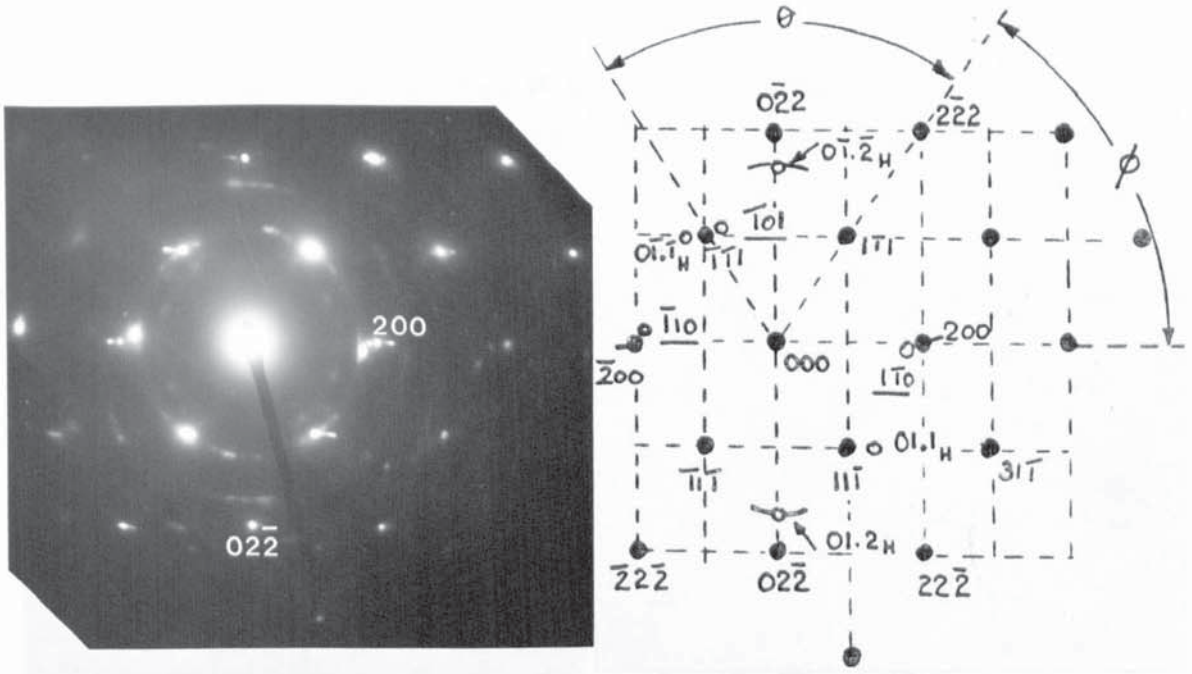

(b) Diffraction pattern from (a).

Figure 6.20

As-cast 30% Chromium iron. Effect of abrasion on primary austenite. Position (c). Dished + ion beam thinned.

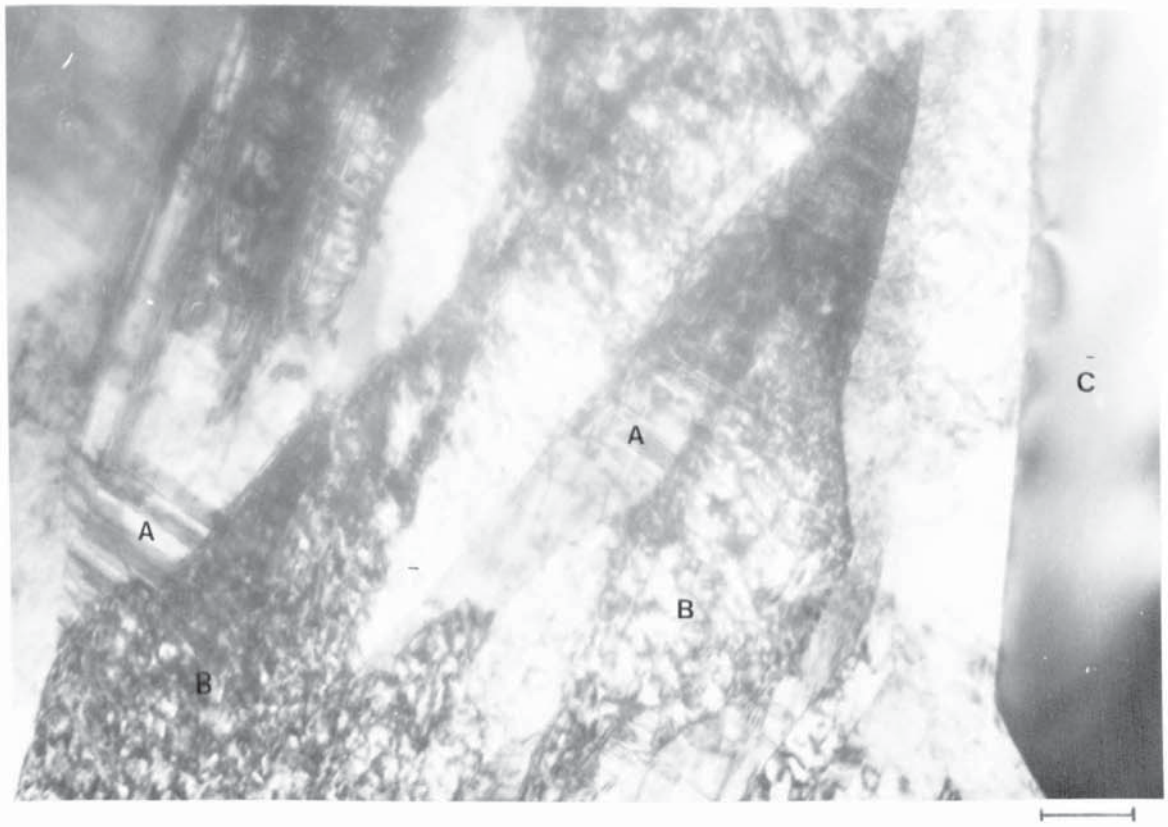

(a) Thin crystals of ε and stacking faults in γ (A). Highly dislocated α martensite (B). Eutectic carbide (C) at right of view. Marker is 0.1 μm.

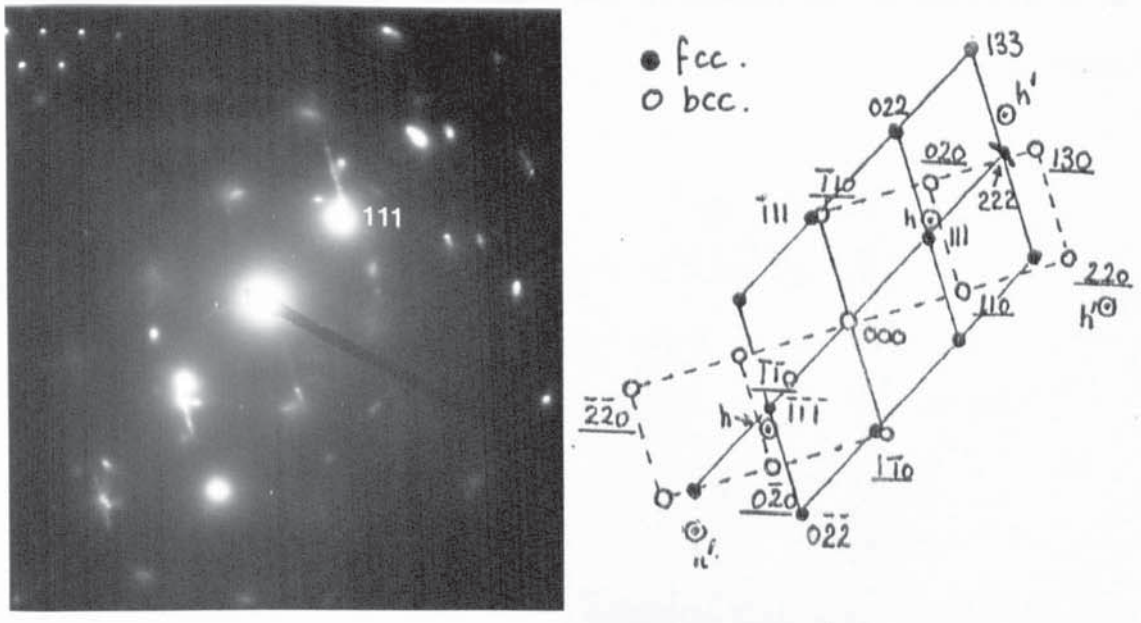

(b) Diffraction pattern from (a).

Figure 6.21

As-cast 30% Chromium iron. Effect of abrasion on eutectic austenite. Position (c). Dished + ion beam thinned.

It is to be remembered* that a single stacking fault in a fcc matrix can be considered as a small volume of material with a hcp structure and it is suggested (250) that the volume of hcp material produced by the passage of one Shockley partial is the ε nucleus. Changes in interplanar spacing are very small (1-2%) between $(111)_\gamma$ and $(0002)_\varepsilon$ and changes in interatomic spacing within $(0001)_\varepsilon$ are only $\sim$ 0.1% (251). The formation and overlapping of stacking faults is the accepted model for the production of long thin crystals of the hcp phase. Fujita (252) argues that intermediate structures (between fcc and hcp) may form causing diffuseness and shifts of diffraction spots of both the hcp structure and the matrix. In work on γ stainless steels he found that the ε phase is first indicated by the streaking of certain fcc reflections. This streaking effect is clearly seen in the present work where $\{111\}_\gamma$ type reflections are streaked as in figures 6.18 and 6.21. No such streaking was seen in the austenite patterns prior to abrasive wear.

If the same transformation sequence is followed in chromium irons as in stainless steels then α martensite is expected to form via hcp ε martensite by nucleation at junctions between ε crystals. No evidence for this was obtained in the limited study of the present work and the actual sequence of events i.e. $\gamma \rightarrow \varepsilon \rightarrow \alpha$ might only be seen in experiments involving direct observation of deforming foils. The foils produced from the irons were too brittle for such

experiments and could be broken by careless handling (30-35% eutectic carbide was present). However, such experiments may be possible in irons of lower carbon content which would have a discontinuous network of fewer eutectic carbides i.e. below 1.4% C.

Considering the work of Durman (253) the use of irons of lower carbon content would be expected to encourage strain induced martensite (SIM) formation in in-situ deformation experiments. In studying strain hardening in the plastic zone near the crack tip in fracture toughness work on 15% chromium irons Durman (253) found that SIM only occured in irons which exhibited significant plastic deformation during testing, i.e. irons with C levels of 1.1 - 1.4%. The presence of a continuous carbide network at 2.1% C restricted plastic deformation and SIM was not produced. In the 1.1 - 1.4% C irons rises in hardness in the plastic zone were said to be on a scale comparable to those observed in worn components and were attributed to work hardening of the austenite and SIM formation. The evidence from figures 6.18 - 6.21 suggests that SIM formation can also take place at higher carbon levels (C content of iron 7 is 2.44%) and that this is partly responsible for the microhardness Hv values of 850 observed at worn surfaces of the test samples.

The work described in this section has shown that the austenite matrix in high chromium irons can be studied by thin foil TEM. This means that further studies could investigate the nature of stacking faults and dislocation configurations in these materials and may allow the influence of alloying elements on the stacking fault energy, work hardenability and tendency to SIM formation of the austenite to be determined. This could lead to the design of compositions of irons which would have more effective self replacing hardened layers at wear surfaces and hence improve the lives of wear parts.

6.6 The nature of faulting in secondary and eutectic M_7C_3 carbides.

Structural studies of carbides such as M_7C_3 and $M_{23}C_6$ have largely been limited to heat treated low and high alloy steels (254-258). Tempering of these steels results in the precipitation of alloy carbides in the matrix and the nature and distribution of these carbides then has a significant influence on the properties of the steel. Particular attention has been paid to M_7C_3 (257) and to the $M_7C_3 \longrightarrow M_{23}C_6$ transition (256). Although in tempered steels these carbides are in a very much finer form than that of the destabilised or eutectic carbides being considered here there are likely to be a number of common structural features. For example, the possible presence of faults in the M_7C_3 in chromium irons has already been introduced in section 6.2; this may be similar to the faulting known to arise in M_7C_3 in steels (257).

Electron diffraction theory normally considers the case of an infinite crystal which results in diffraction patterns containing sharp spots. However, patterns are frequently observed with modified features such as elongation of the spots, division of individual spots into groups of satellite spots or the presence of continuous streaks. These effects are believed to arise either from the particular shapes of the crystalline particles of the specimen or from the presence of lattice imperfections or strains. A full consideration of

these effects is given by Hirsch et Al (246). In specimens which contain stacking faults or narrow twin platelets there is effectively a very small dimension in one direction and the effect in reciprocal space is to elongate the diffraction spot in a direction perpendicular to the fault. This extension gives rise to the streaking which is said to characterise the electron diffraction patterns from faulted M_7C_3 carbides (244, 257).

Normally faulting in a hexagonal structure would be expected due to incorrect stacking of the basal (00.1) planes giving ...ABC ABC... rather than ...AB AB... stacking, however, in the hexagonal M_7C_3 in steels faults were found in planes perpendicular to (00.1). Some arose parallel to (10.0) or (01.0), the hexagonal prism faces, while some were in planes perpendicular to these, i.e. (11.0), $(1\bar{2}.0)$. This section investigates the streaking observed in diffraction patterns from both secondary and eutectic carbides and compares the findings with those on steels and with the recent studies of Inoue (259) and Dudzinski (260) on white irons.

6.6.1 Secondary carbides.

These are considered first since they are much smaller and generally have less complicated structural features than the eutectic carbides. Figure 6.22 presents a view of the secondary carbides produced during the destabilisation of the

heat treated 15% Cr iron (iron 4). A diffraction pattern containing streaking was obtained from the central carbide particle which contains the faulting marked F on the micrograph. When allowing for image rotation of 71.5° AC for 120 K original registered magnification of picture (see calibration in appendix) then the streaking in the diffraction pattern lies at exactly 90° to the line of faults (F) seen in contrast. Previous work by Beech (256) and Dyson (257) had forwarded only electron diffraction patterns as evidence of the faulting in tempered carbides, no visual record was presented as in figure 6.22 (a) and as in figure 6.11 seen earlier.

The diffraction pattern from the carbide in figure 6.22 is given in figure 6.23. Reflections have also been recorded for the surrounding matrix region. The ferrite matrix was close to a $\langle 113 \rangle$ type zone and has been indexed with B as $[\bar{1}31]$. The M_7C_3 carbide was close to a $\langle 100 \rangle$ zone and has been indexed with B as $[0\bar{1}0]$ ie $[1\bar{2}10]$. B given as $[0\bar{1}0]$ is in Miller notation whereas $[1\bar{2}10]$ is in 4 - axis Miller-Bravais notation (see (244) pp 92 onwards and (261)). Measured and reference d values and angles for ferrite were as follows:

Reflection	d_m	d_r	Angle	Measured	Calculated
011	2.02	2.027	$101 \wedge 310$	49°	47.86°
112	1.15	1.170	$101 \wedge 21\bar{1}$	72°	73.22°
013	0.90	0.906	$\bar{1}0\bar{1} \wedge 11\bar{2}$	74°	73.22°

For the carbide measured d spacings of 3.61, 4.55 and 2.91 Å for (02.1), (00.1) and (40.0) correlate with published values of 3.615, 4.506, and 3.027 (see table A1 in appendix). Tables of d spacings for M_7C_3 conventionally denote planes by (hk.l) where the dot signifies that the third index i = -(h + k) has been omitted (244). The carbide pattern in figure 6.23 is characterised by streaking perpendicular to (10.0) i.e. along $[21.0]$. This is in agreement with the work on steels (257). The orientation relationship between the carbide and matrix found from the pattern is $(1\bar{2}10)_C \;//\; (\bar{1}31)_\alpha$ which again fits one of the relationships obtained in steels (257). However, in figure 6.23 $[00.1]_C$ is parallel to $[310]_\alpha$ and this is a 25.3° rotation from the relationship $[00.1]_C \;//\; [21\bar{1}]_\alpha$ for steels (257).

Figure 6.24 presents a view of other secondary carbides in the heat treated 15% Cr iron. As in the previous case the streaks in the diffraction pattern from the larger carbide in the centre of the view lie at exactly 90° to the line contrast seen in the image when allowing for a rotation of 14° AC for the original 90 K magnification. This pattern has also been indexed as a $[1\bar{2}10]$. Measured d spacings for (10.0), (02.2) and (00.2) were 11.91, 2.097 and 2.22 Å respectively as against tabulated reference values of 12.109, 2.1117 and 2.253 Å. As before the streaking is perpendicular to (10.0).

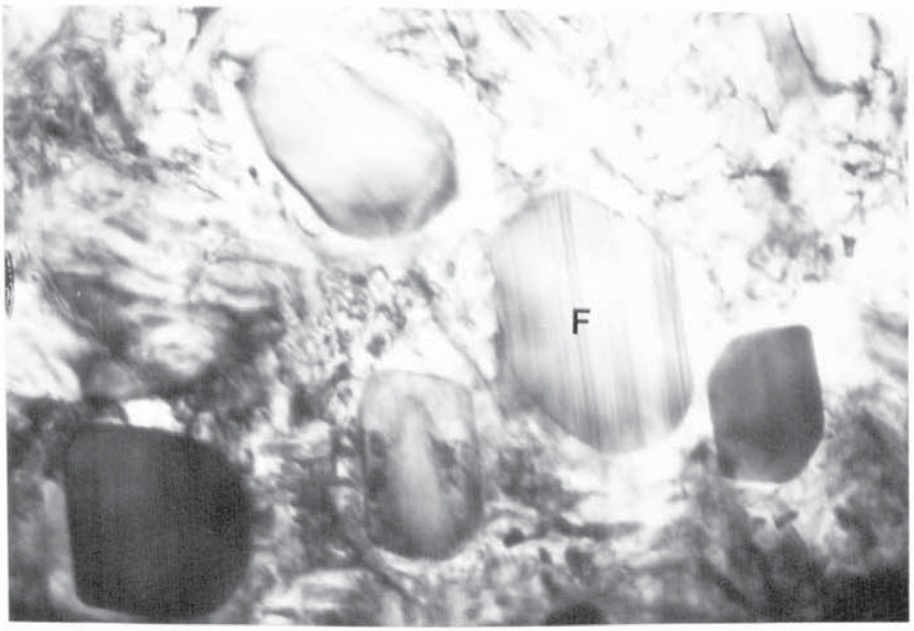

(a) Contrast due to faulting in secondary carbide. Marker is 0.1 μm.

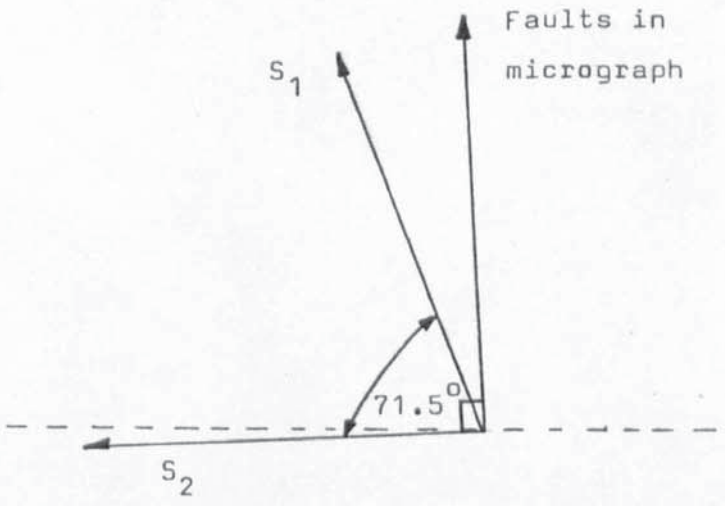

(b) Sketch to show that streaks (direction S_1) in diffraction pattern lie at 90° to faults seen in (a) when allowing for image rotation (S_2).

Figure 6.22

TEM view of secondary carbide in heat treated 15% Cr iron.

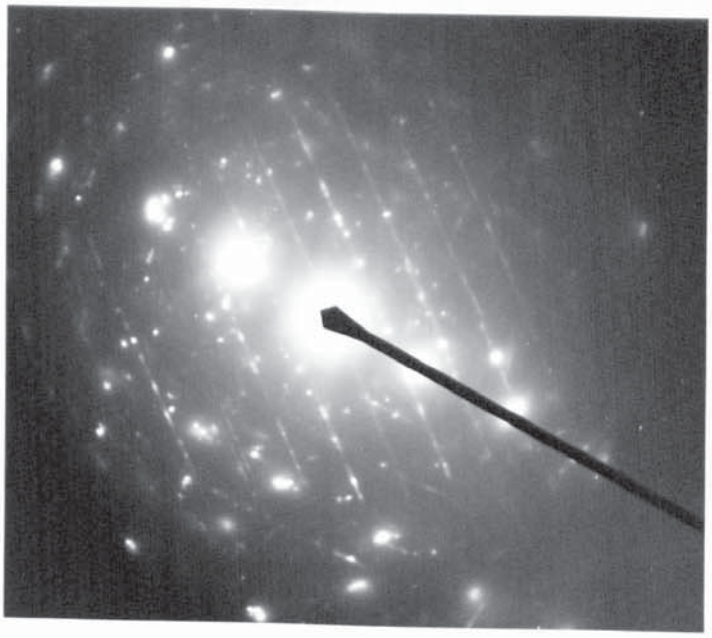

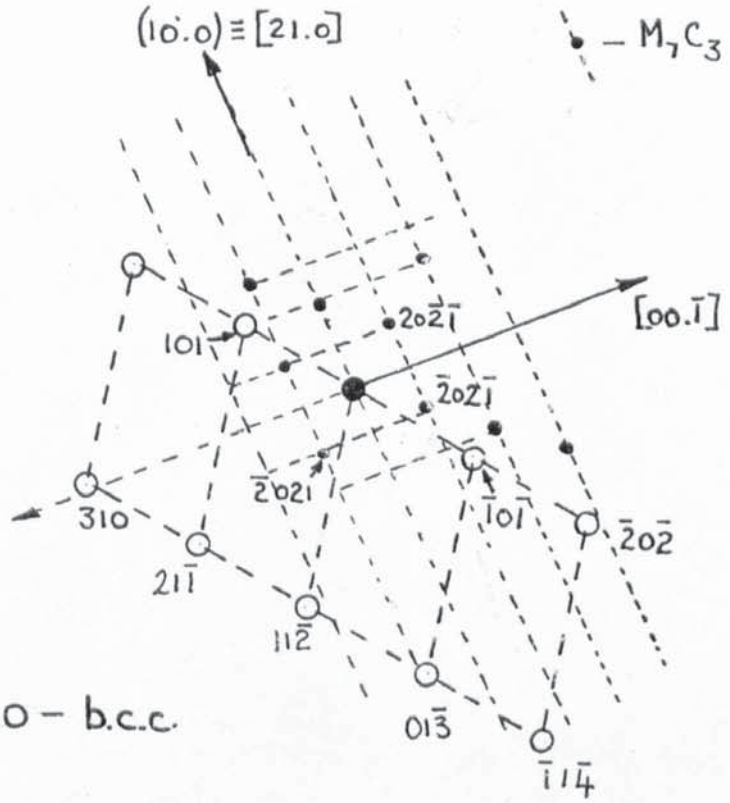

Figure 6.23

Diffraction pattern from figure 6.22.

Indexed diagram is 1.25 x scale of print. Pattern must be rotated 71.5° anticlockwise to print in figure 6.22.

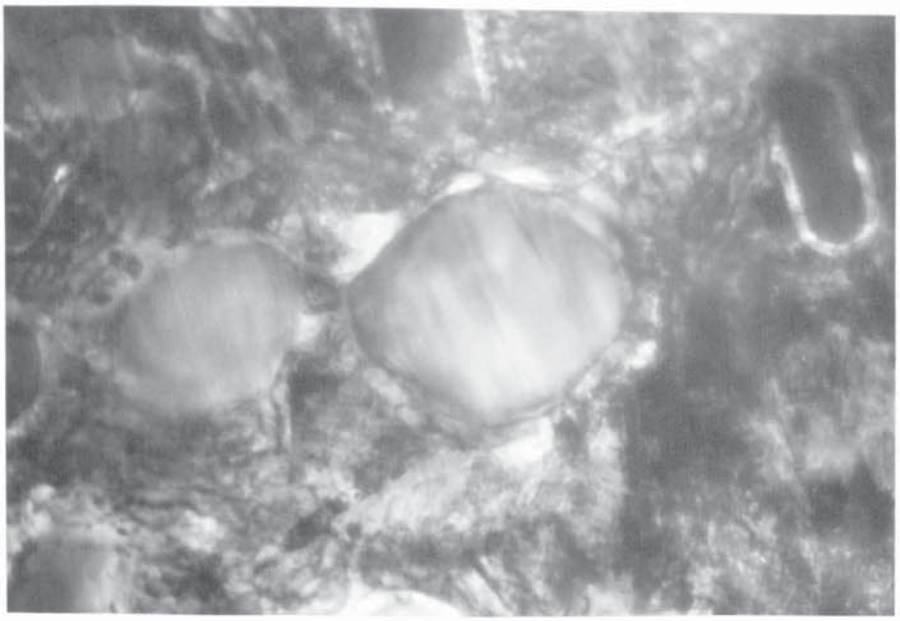

(a) Secondary carbides. Marker is 0.1 μm.

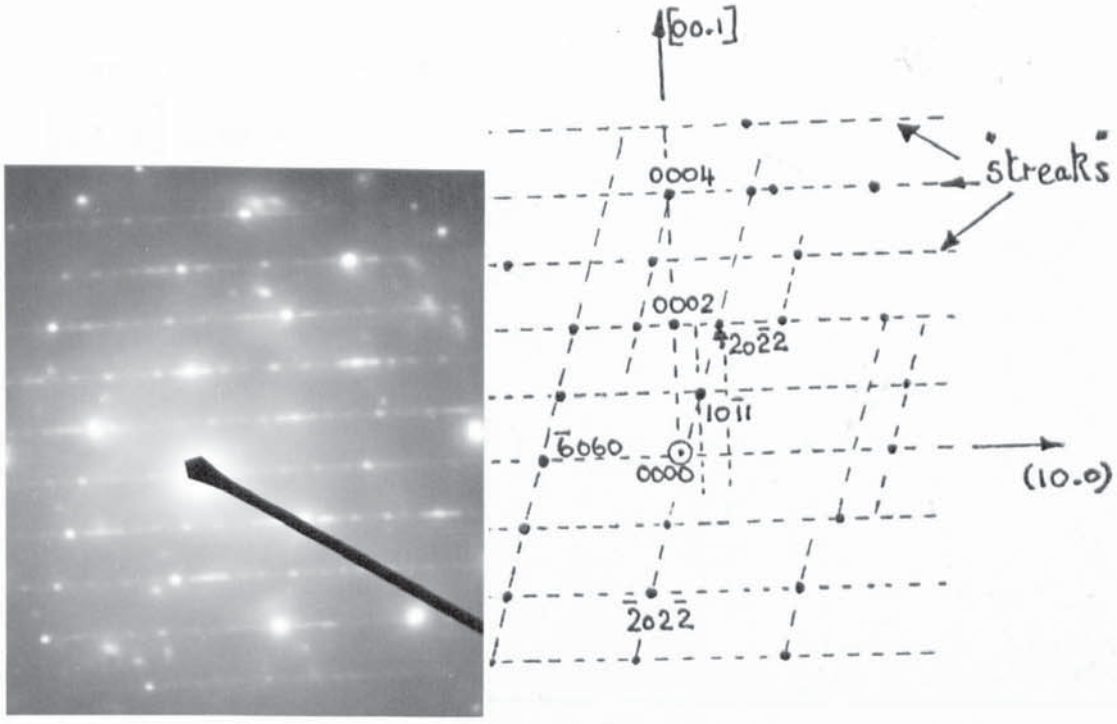

(b) Diffraction pattern from central larger carbide. Diagram is 1.28 x scale on print. Pattern must be rotated 14^{0} AC to print (a).

Figure 6.24

Further TEM view of secondary carbides in 15% Cr iron (heat treated).

6.6.2. Eutectic carbides.

The possible occurrence of faulting in the eutectic M_7C_3 carbides was introduced earlier using the evidence from figures 6.4 - 6.7 for the 30% Cr iron and 6.8 - 6.9 for the 15% Cr iron. A maximum of three sets of faults could be seen in each carbide crystal with approximately 60° angles between each set of faults. Figure 6.25 is typical of the contrast due to faulting obtained in the eutectic M_7C_3 for the as-cast 30% Cr iron samples taken from position (b), (see figure 6.1). A single set of parallel faults are visible running at an angle of 30° below the horizontal in the micrograph. When allowing for image rotation the faults lie at 90° to the streaking in the $[21.0]$ direction of the diffraction pattern as seen in figure 6.26. In this case the streaking in the pattern is faint and the positions of individual spots can be measured. This gives respective d spacings of 12.23, 4.29 and 2.18 Å for (10.0), (01.1) and $(\bar{1}2.2)$. These correspond reasonably well with the respective tabulated values of 12.1088, 4.2235 and 2.0215 Å, hence the pattern is close to a $[01.\bar{1}]$ as sketched in figure 6.26(b). This information suggests that since the faulting contrast is 90° to $[21.0]$ i.e. (10.0), it is planes of the type (10.0), (01.0) etc. which are faulted as found in steels and in the secondary carbides discussed earlier. This was confirmed in other patterns from similarly faulted carbides although in some instances a complete description of the pattern was not possible due to the effects

of streaking e.g. the pattern in figure 6.27 which is from the eutectic carbide seen earlier in the top right hand side of figure 6.15.

Streaking of the spots will result in the displacement of a spot from its correct position if the spot in question is not exactly in the Bragg position. Streaking can also result in satellite spots near to the main spots. These two effects are illustrated by the sketches of figure 6.28 and are present in the diffraction pattern in figure 6.27. For this pattern the d spacing calculated for reflections lying along the line marked ST was 12.90 Å, i.e. (10.0), (01.0) reflections.

The presence of three sets of faults was most clearly revealed in the specimens taken from position (a) i.e. the transverse slices through the carbide rods as in figures 6.4(a), 6.6, 6.7, 6.8). In some cases three sets of continuous streaks were observed in the corresponding diffraction pattern as shown in figure 6.29. This pattern consists of a number of Laue zones which suggests that the crystal is tilted by a few degrees ($1\text{-}3^{\circ}$) from a prominent zone axis, in this case the $[00.1]$.

(a) Contrast due to faulting in eutectic M_7C_3
Marker is 0.1 μm.

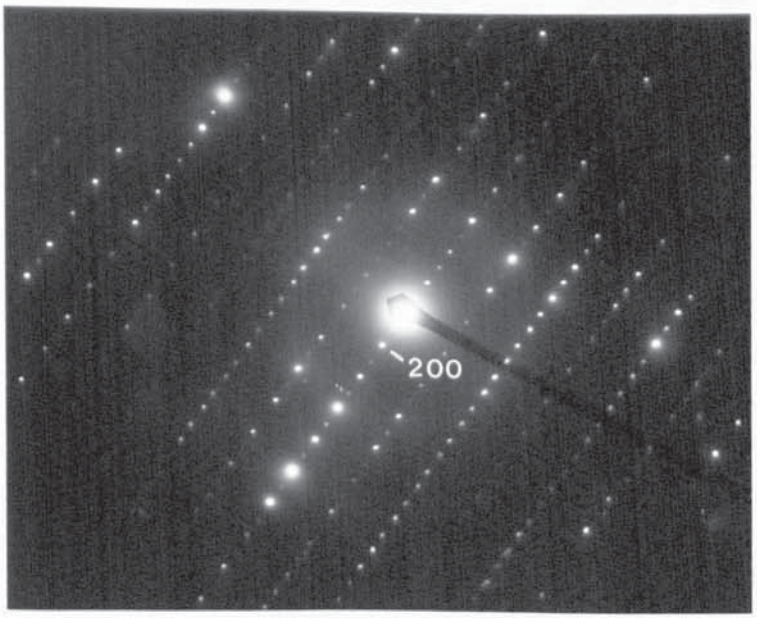

(b) Diffraction pattern from M_7C_3 above

Figure 6.25

Faulting in eutectic M_7C_3 in as-cast 30% Cr iron. Position (b). (Same region as figure 6.15).

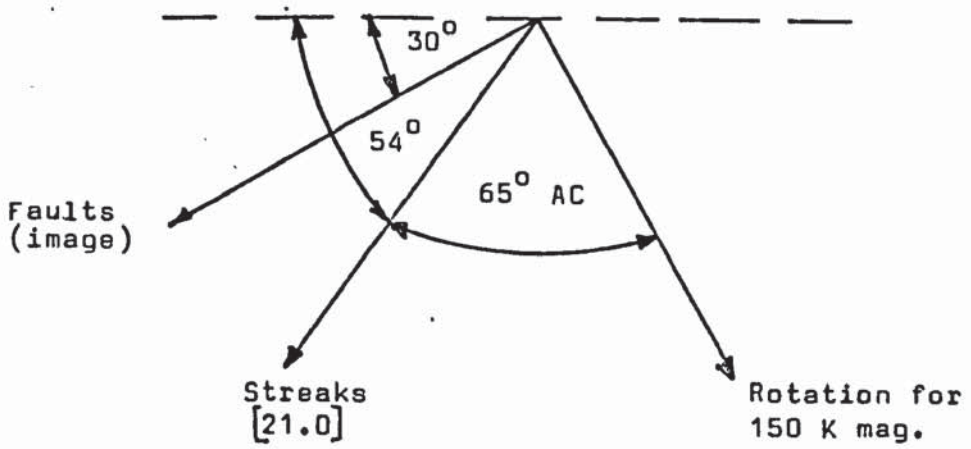

(a) Diagram to show faults in image are at 90° to [21.0], i.e. (10.0).

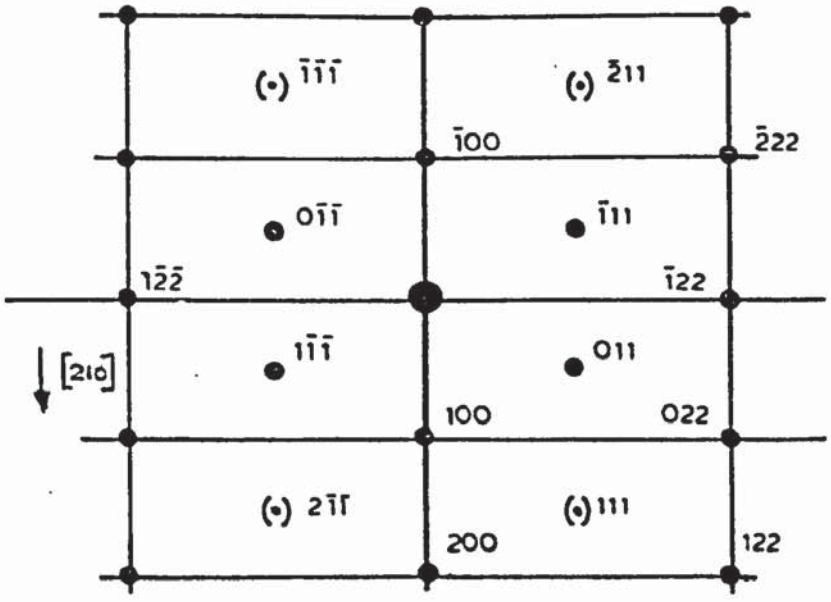

(b) Diffraction pattern, rotated 35° AC for convenient presentation.

Figure 6.26

Indexed diffraction pattern from figure 6.25.

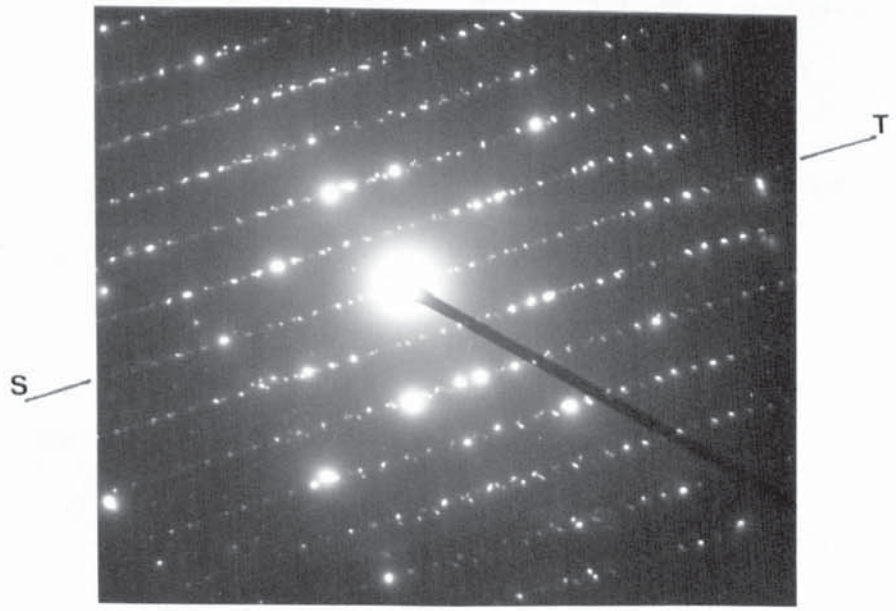

Figure 6.27

Diffraction pattern from eutectic M C seen in figure 6.15.

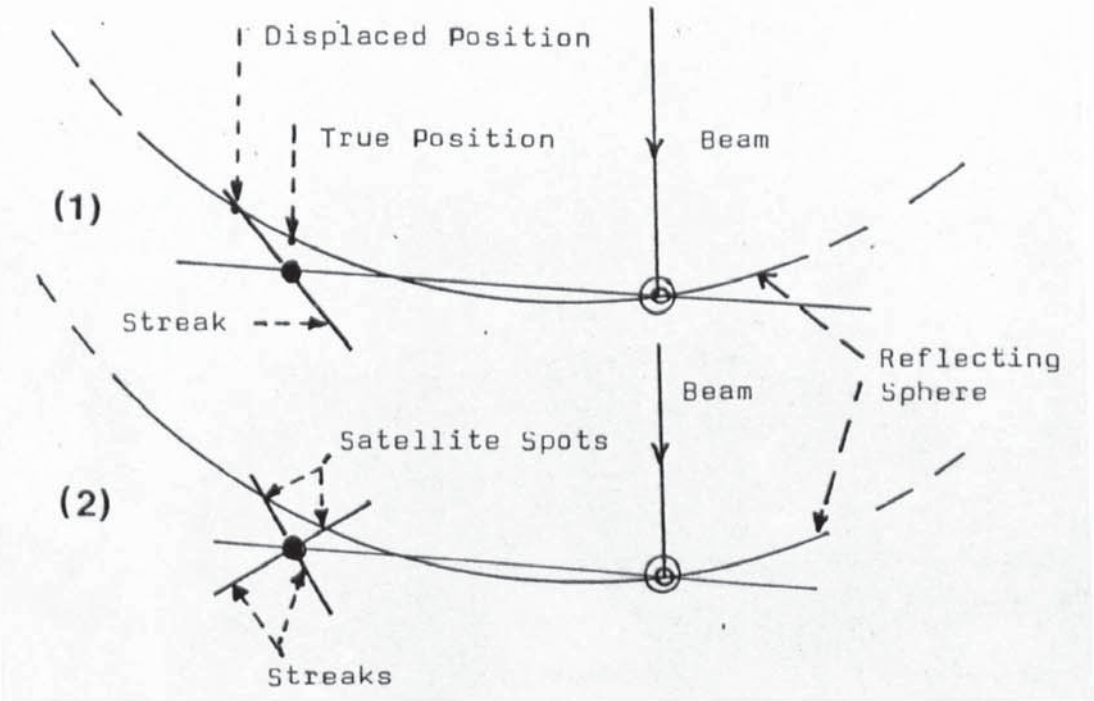

Figure 6.28

Effect of streaks: (1) spot displacement, (2) satellite spots. After Kelly (262).

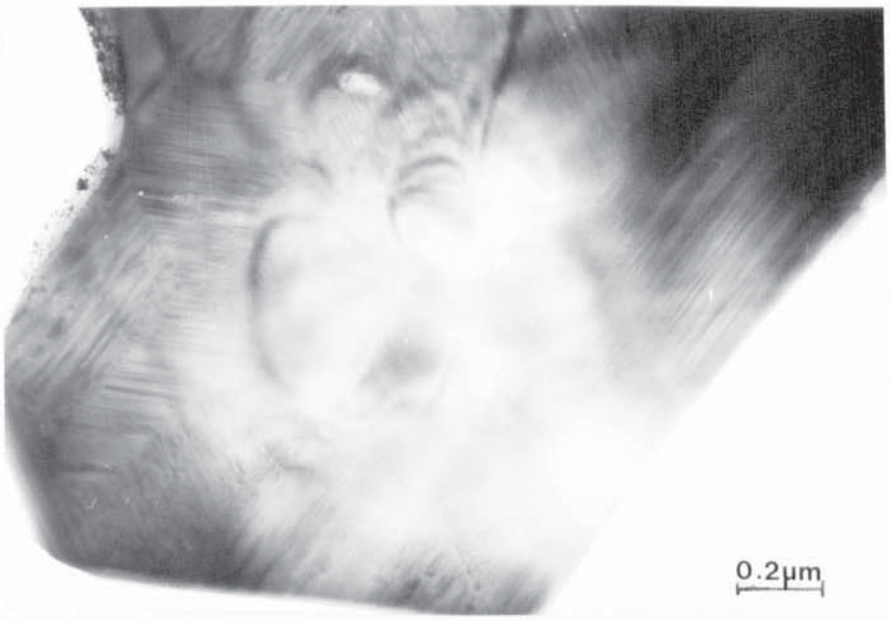

(a) Three sets of faults within eutectic carbide.

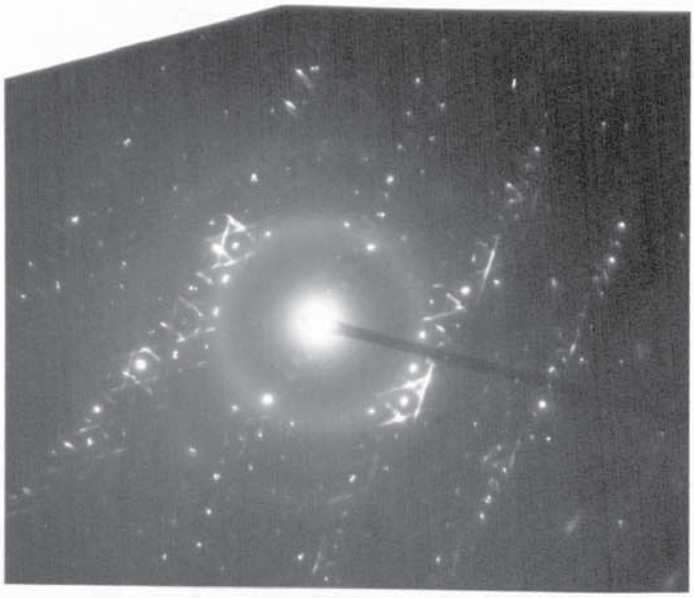

(b) Diffraction pattern from carbide in (a).

Figure 6.29

As-cast 30% Cr iron. Faulting in carbide and associated streaking in diffraction pattern. Position (a).
Dished + ion beam thinned.

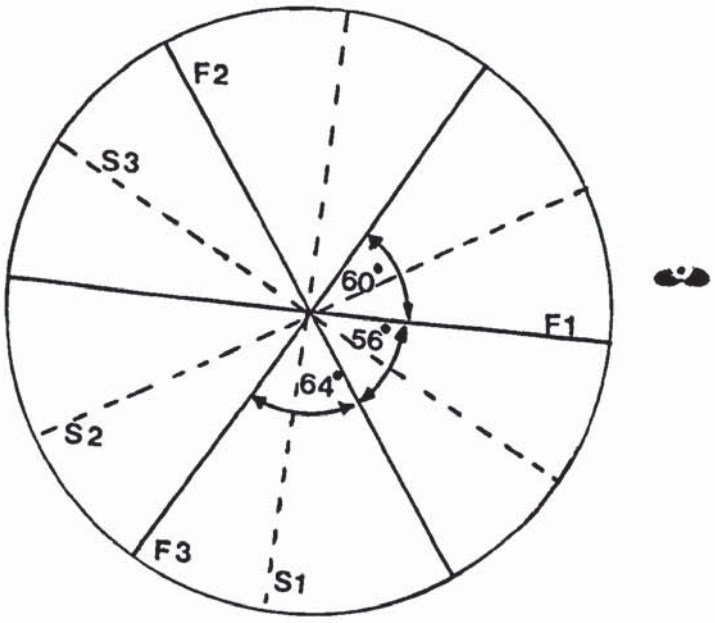

(a) Relative positions of faults (F) in micrograph and streaks (S) in diffraction pattern.

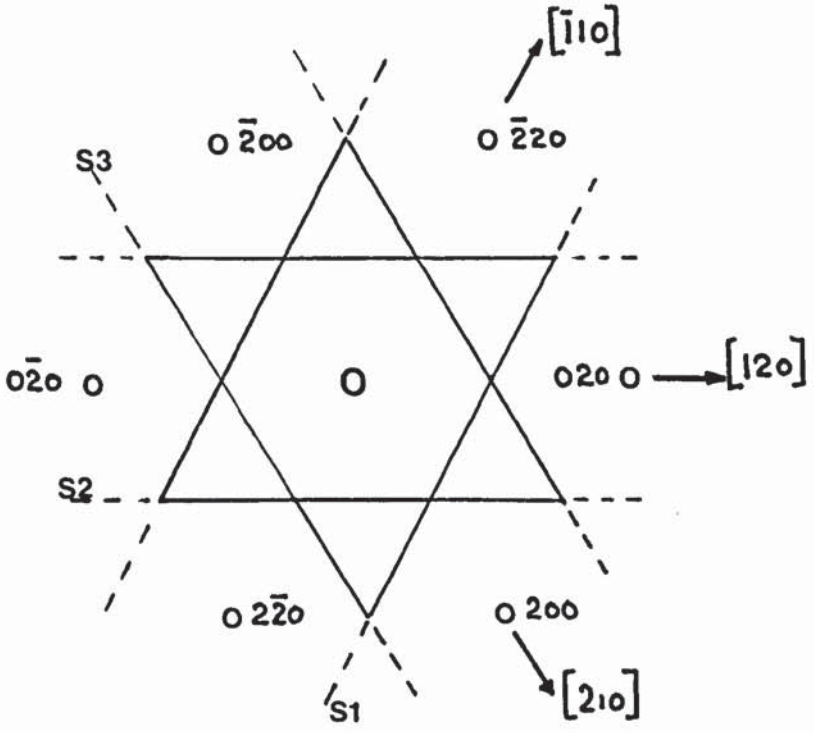

(b) Schematic indexed pattern.

Figure 6.30

Analysis of diffraction pattern in figure 6.29.

The reflections in figure 6.29 which are not streaked correspond to a $[00.1]$ zone and it is considered that these are from the central area of the carbide which does not show stacking fault contrast. Due to the effects of buckling as indicated by the presence of bend contours parts of the crystal are tilted away from this zone and for these regions stacking fault contrast is seen in the bright field image with associated streaking in the diffraction pattern (see figure 6.30). The absence of streaking in reflections of the $[00.1]$ zone is also illustrated by figure 6.31. The carbide crystal marked X is very close to a $[00.1]$ zone with the excess (bright) Kikuchi line (EL) for (09.0) passing almost through the diffraction spot increasing its intensity and the corresponding defect (dark) line (DL) passing very close to the central spot. The same holds for the $(6\bar{3}.0)$ reflection (lines EL' and DL') giving extra intensity to the (66.0) reflection. For this pattern measured d values for (06.0) and (66.0) of 2.03 and 1.12 correlate with reference values of 2.018 and 1.165 $\mathring{A}$. These findings are consistent with those from recent work on Cr-Fe-V mixed carbides ($Cr_{2.8}\ V_{0.7}\ Fe_{3.4}\ C_3$) where zero contrast was obtained for faults on the three equivalent planes (10.0), $(1\bar{1}.0)$ and (01.0) for the laue zone $[00.1]$.

For the adjacent carbide (marked Y in figure 6.31(a)) stacking fault contrast and streaking are observed. The diffraction pattern for this carbide is given in figure 6.32 and corresponds to a $[0\bar{1}.3]$ zone i.e. $[1\bar{2}19]$. Measured d

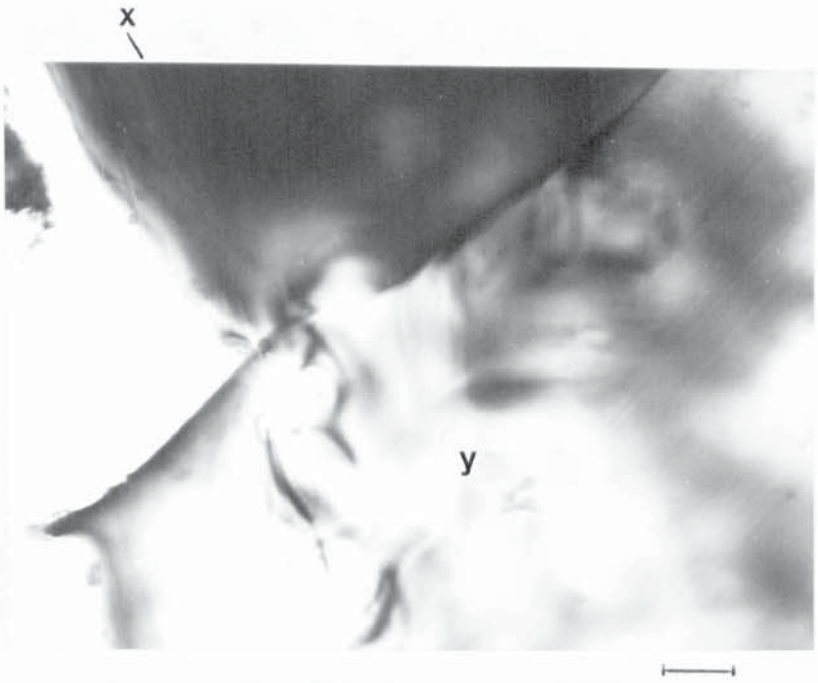

(a) Two adjacent M_7C_3 crystals. Marker is 0.1 μm.

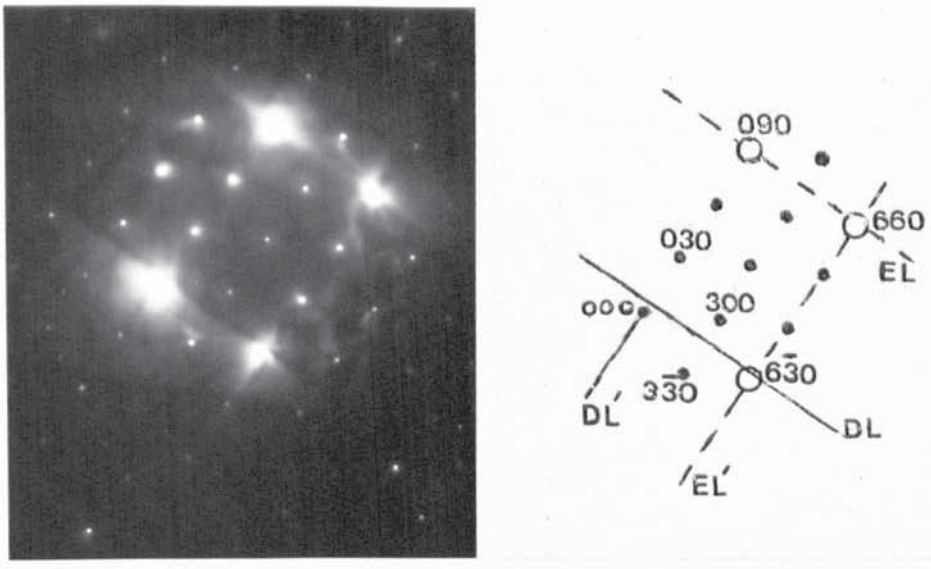

(b) Diffraction pattern from crystal marked X. The pattern must be rotated 71.5° AC relative to micrograph.

Figure 6.31

Heat treated 15% Cr iron. Absence of streaking in [00.1] pattern.

Position (a) Dished + ion beam thinned.

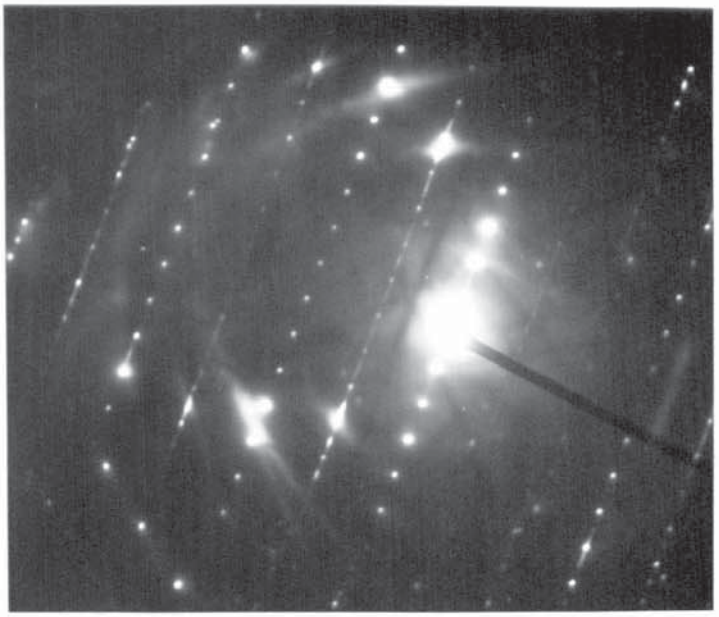

(a) Diffraction pattern must be rotated 71.5° AC relative to micrograph. F gives direction of faults in micrograph, F^1 gives direction allowing for image rotation.

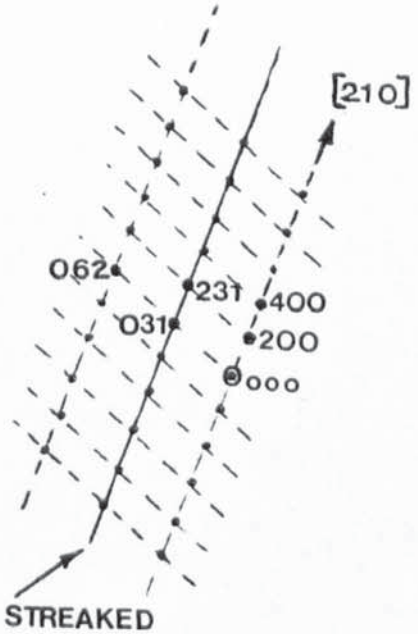

(b) Line diagram showing indexing as $[0\bar{1}3]$.

Figure 6.32

Diffraction pattern from carbide Y in figure 6.31.

spacings of 6.20, 3.03 and 2.35 for (20.0), (03.1) and (23.1) relate to reference values of 6.054, 3.006 and 2.3648 Å respectively. Measured angles between (20.0) and (23.1) and between (20.0) and (03.1) of 45° and 70° are in agreement with calculated values of 46.9° and 68.2° taking c/a as 0.32.

In addition to the contrast from stacking faults in some of the carbide crystals extra image contrast was observed which was believed to be due to the presence of antiphase domain boundaries. An example of this effect is given in figure 6.33 for the as-cast 30% iron. The darker lines marked ab and bc which run parallel to the two sets of faulting denote the boundaries between different domains in the crystal. Some of these boundaries contain a number of small steps and some of the domains appear to be quite narrow. Antiphase domain boundaries arise in ordered structures e.g. Cu Au, Cu_3 Au, and separate ordered domains. Across a boundary there is a displacement equal to a lattice vector in the disordered crystal or some fraction of a lattice vector in the ordered crystal (245). Contrast effects from antiphase domain boundaries (APB's) are reviewed by Hirsch (246) who states that for an APB inclined to the plane of the foil then a fringe type contrast is produced as for a stacking fault; for an APB the number of fringes obtained is often only two or three. This effect is seen for the boundaries ab and bc which consist of a single light inner fringe and two dark outer fringes. Dudzinski et Al (260) have given a comprehensive crystallographic arguement for the presence of domains in M_7C_3

(a) Cluster of M_7C_3 crystals. Marker is 0.1 μm.

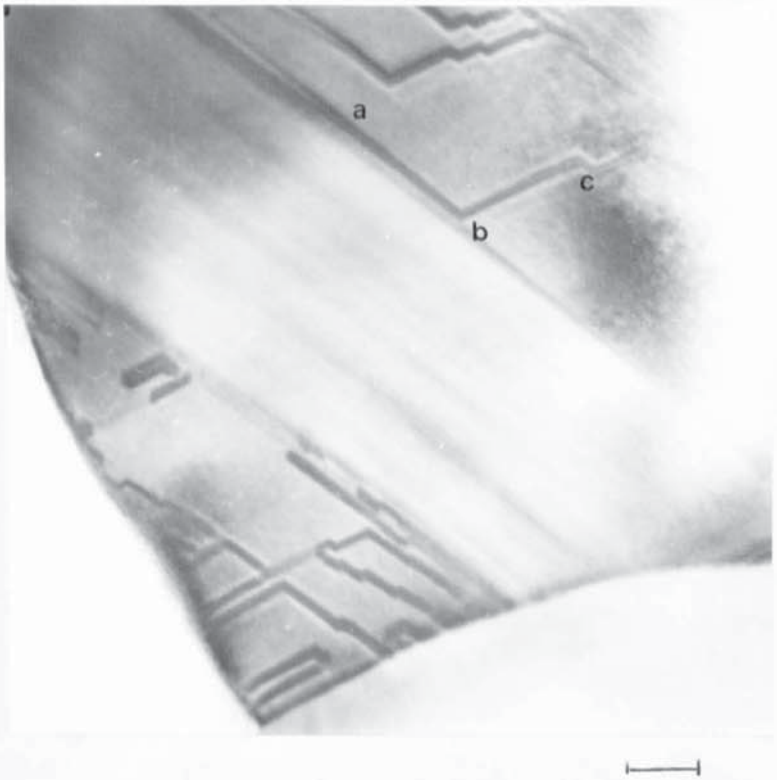

(b) View of upper crystal showing contrast from antiphase domain boundaries (ab & bc). Marker is 0.05 μm.

Figure 6.33

As-cast 30% Cr iron. Contrast from antiphase domain boundaries in M_7C_3 rod. Position (a) Dished + ion beam thinned.

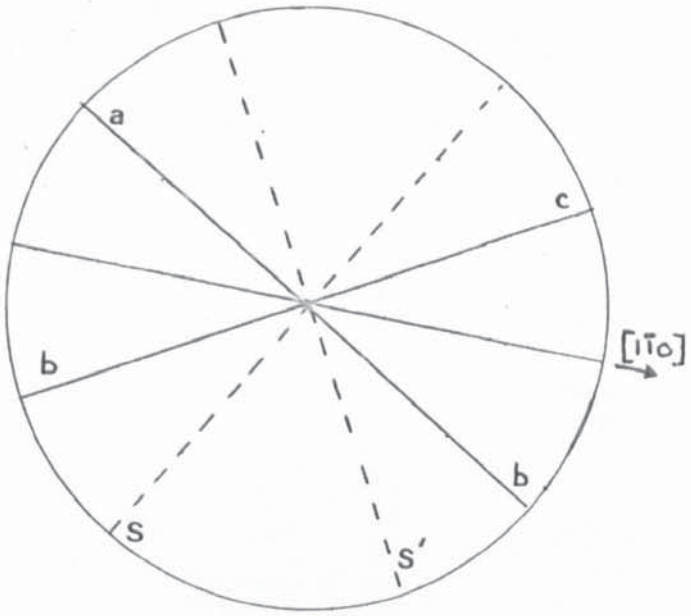

(a) Diagram to show relationships between streaking S, S^1 and antiphase boundaries ab and bc.

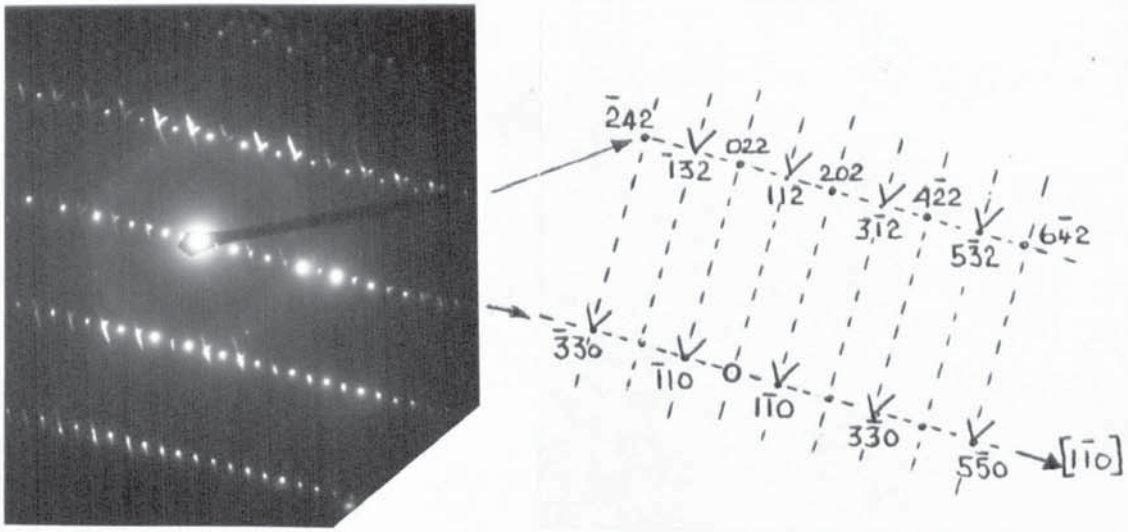

(b) Indexed diffraction pattern from M_7C_3 carbide rod seen in figure 6.33 (b).

Figure 6.34

Electron diffraction pattern corresponding to figure 6.33.

Figure 6.35

Complexity of faulting in eutectic M_7C_3 cluster in 15% Cr iron (heat treated)
Marker is 0.2 μm.

containing chromium, iron and vanadium but have not presented any electron micrographs showing contrast effects as in figure 6.33. Possible APB contrast was also seen in the M_7C_3 in the heat treated 15% Cr iron as indicated by position d in figure 6.35.

A diffraction pattern taken from the carbide crystal showing APB contrast is given in figure 6.34. This pattern has been indexed as a $[11.\bar{1}]$ zone but four expected $\{01.0\}$ reflections are absent. Measured d spacings for (112), (202) and $(3\bar{1}2)$ of 2.08, 2.03 and 1.86 match reference values of 2.144, 2.112 and 1.871 Å. Measured angles between $(1\bar{1}0)$ and (202), $(1\bar{1}0)$ and $(3\bar{1}2)$, $(1\bar{1}0)$ and $(4\bar{2}2)$ reflections of 80^{o}, 71^{o} and 62^{o} agree with calculated values of 80.02^{o}, 70.6^{o} and 62.2^{o} respectively. (Nb. The expanded indexed line diagram in figure 6.34(b) is schematic and has not been drawn to scale). The two sets of faulting and the line of the APB's ab and bc are seen to lie at 90^{o} to the two directions of streaking seen in the diffraction pattern. The two streaks are at 65^{o} to each other and at 58^{o} and 123^{o} to $[1\bar{1}.0]$, they are only present in reflections where the k index is odd i.e. (112), $(3\bar{1}2)$, $(5\bar{3}2)$ etc. This observation is in agreement with the findings of Dyson (257) in steel where M_7C_3 reflections with k odd were elongated parallel to $[12.0]$ while those with k even were sharp. This effect was also seen in figure 6.32, i.e through (031), (231) reflections.

In addition to image contrast from faulting and from antiphase domain boundaries the presence of low angle boundaries within M_7C_3 was suspected. One such boundary is shown in figure 6.36 for the 15% chromium iron. The boundary (a) is believed to consist of a number of edge dislocations which are spaced 250 to 350 Å (25-35 nm) apart. This observation is very similar to a low angle tilt boundary studied by Koreeda (263) in a cementite crystal extracted from 0.8% C steel.

Assuming a simple tilt boundary is present in figure 6.36 then the strength b of the dislocations can be related to the spacing h and orientation difference θ by:

$$\frac{b}{h} = 2 \sin \frac{\theta}{2} \qquad (264)$$

Taking h as 300 Å and b as 2.5 Å then θ is approximately 0.5^{o} In a diffraction pattern the presence of doublet diffraction spots is only possible where the misorientation is greater than about 0.5^{o} (265). Hence in this case (see figure 6.37) double spots are not produced from the region which straddles the suspected boundary. Some of the spots which are more distant from the origin are elongated but this may be due to faulting. Any misorientation present is small since it is seen from figure 6.36(b) that the lines of faulting contrast are parallel to each other on either side of the boundary. In cementite (263) dislocation spacings of 160 Å were measured giving a 1.8^{o} misorientation.

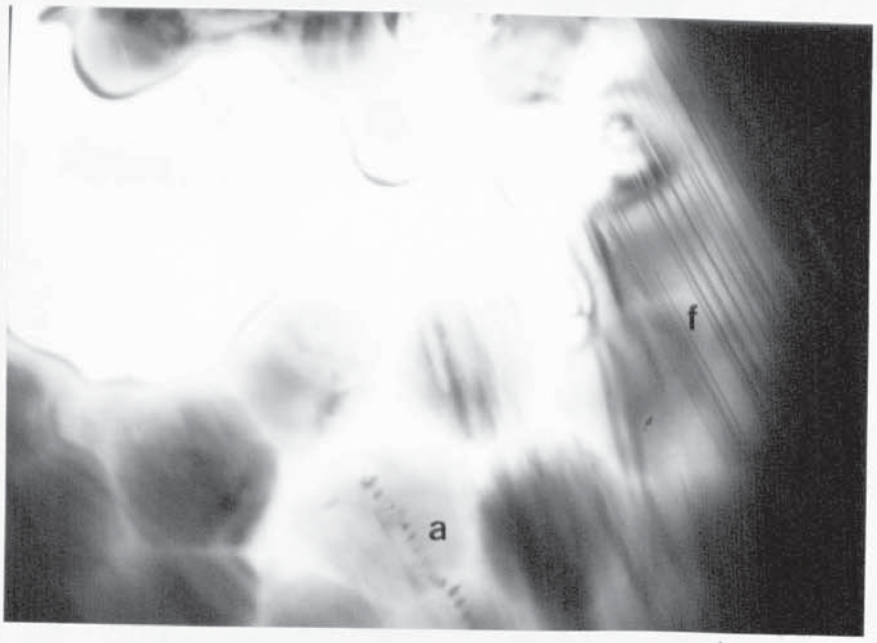

(a) Eutectic M_7C_3 showing contrast from boundary (a) and faulting (f). Marker is 0.3 μm.

(b) Section of boundary (a). Marker is 0.1 μm

Figure 6.36

Heat treated 15% Cr iron. Suspected small angle boundary revealed by contrast from uniformly spaced dislocations. Position (b), dished + ion beam thinned.

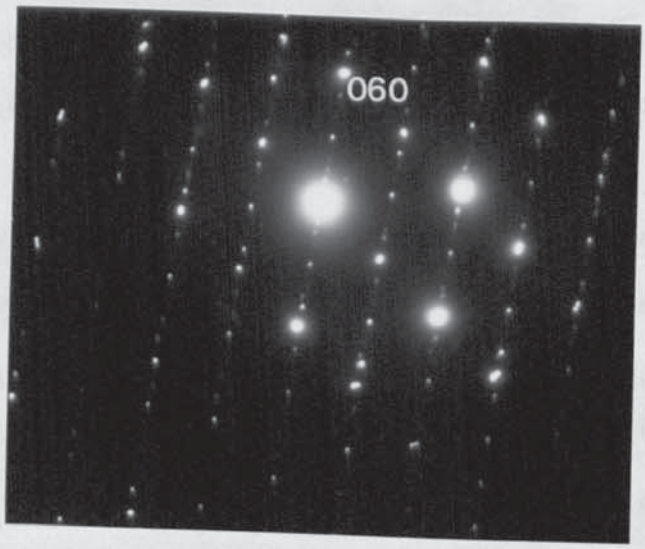

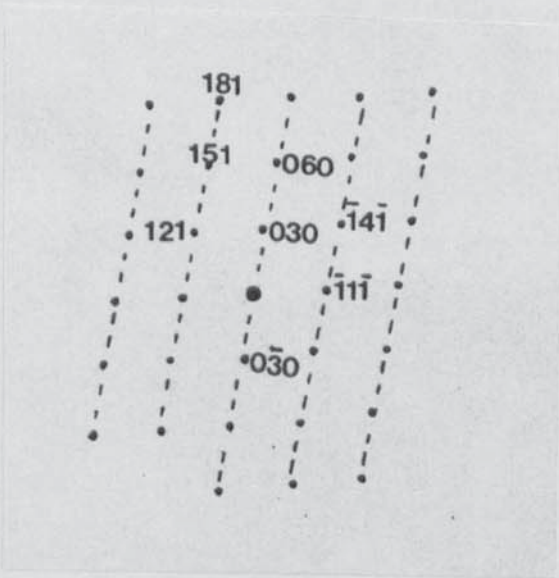

Figure 6.37

Diffraction pattern from figure 6.36. (Area covers both sides of suspected boundary).

Figure 6.37 has been indexed as a $[10.\bar{1}]$ zone. Measured d spacings of 2.10, 3.18 and 1.37 Å for (06.0), (12.1) and (18.1) correlate with tabulated values of 2.018, 3.211 and 1.3519 Å. Measured angles from (06.0) of 20° for (18.1), 40° for $(\bar{1}4.\bar{1})$ and 78° for $(\bar{1}1.\bar{1})$ correspond to the respective calculated values of 18.5°, 39.07° and 81°.

The contrast effect seen in figure 6.36 was the only evidence of the presence of dislocation type defects in the eutectic M_7C_3 carbides. Other workers (259, 260) have not observed any crystalline defects other than faulting although dislocations have been observed in eroded $M_{23}C_6$ carbide (237). Future studies could lead to the determination of the geometry of the contrast seen by using invisibility criteria. A discussion of the significance of the above TEM studies of the eutectic carbides together with comment on the effect of wear is given in section 6.8 after consideration of the features seen in the heat treated 30% chromium iron.

6.7 The $M_7C_3 \longrightarrow M_{23}C_6$ transformation in 30% Cr iron.

The partial transformation of the eutectic M_7C_3 carbide during thermal treatment was given initial consideration in section 4.6.4 using figures 4.36, 4.53-4 and 4.73 as evidence. The duplex nature of this carbide is clearly recognised under TEM examination as shown in figure 6.38. A central core of M_7C_3 is surrounded by a shell consisting of a number of crystals of $M_{23}C_6$. The diffraction pattern for this core is given with the micrograph and patterns from positions 1 and 2 (as indicated) in the $M_{23}C_6$ shell are presented in figure 6.39. (All three patterns must be rotated 42° AC relative to the micrograph). The pattern from the M_7C_3 is close to a [00.1] zone hence reflections are not streaked and faulting contrast is not observed in the image. For this pattern calculated d spacings of 3.96 and 2.29 Å correlate with reference values of 4.036 and 2.3303 Å for (03.0) and (33.0) respectively. From the image it is seen that the dappled contrast effect previously mentioned is present in the M_7C_3 core but disappears in the outer $M_{23}C_6$.

For the pattern from position 1 the measured d spacings and angles can be compared with reference and calculated values as shown overleaf, where

d_m = d spacing measured from pattern in Å

and d_r = d spacing in Å from table A2

Reflection	d_m	d_r	Angle	Measured	Calculated
422	2.195	2.168	$4\bar{2}\bar{2}$ ^ 511	53.5	51.1
133	2.296	2.437	511 ^ 133	56.5	60.9
511	1.942	2.044	133 ^ $\bar{3}55$	36.0	36.2
335	1.389	1.383	$4\bar{2}\bar{2}$ ^ 644	79.0	78.6

For the pattern from position 2 in the $M_{23}C_6$ the following comparisons can be made.

Reflections	d_m	d_r	Angle	Measured	Calculated
204	2.366	2.375	$\bar{2}04$ ^ $\bar{1}35$	30.5	33.7
131	3.293	3.203	$\bar{1}35$ ^ 131	48.0	48.5
135	1.720	1.795	$\bar{2}04$ ^ $\bar{1}55$	49.0	46.5
155	1.473	1.487	$\bar{1}55$ ^ 151	39.0	38.6

Hence the pattern from position 1 corresponds to a $[0\bar{1}1]$ zone and for position 2 there are two zones which can be indexed i.e. $[2\bar{1}1]$ and $[10,\bar{3}5]$. This suggests that there are misorientations within the $M_{23}C_6$ shell associated with the presence of individual crystals. Calculated angles between $[0\bar{1}1]$ and $[2\bar{1}1]$ and $[2\bar{1}1]$ and $[10,\bar{3}5]$ are 54.7^o and 9.07^o respectively. The presence of distinct grains of $M_{23}C_6$ is clearly seen in figure 6.40. In this view the M_7C_3 which shows faulting contrast has not become completely surrounded by $M_{23}C_6$ and part remains in contact with the matrix (bottom right of micrograph). Diffraction patterns from the two $M_{23}C_6$ crystals, A and B are given in figure 6.41

(a) Core of M_7C_3 surrounded by a shell of $M_{23}C_6$ containing boundaries. Region at top is matrix. Marker is 0.4 μm.

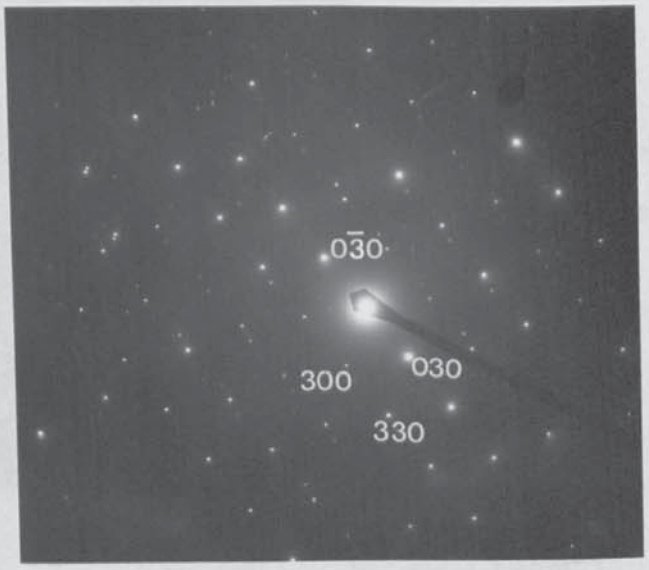

(b) Diffraction pattern from M_7C_3 core.

Figure 6.38

TEM view of 30% Cr iron (heat treated) showing duplex nature of "eutectic" carbide. Position (b).

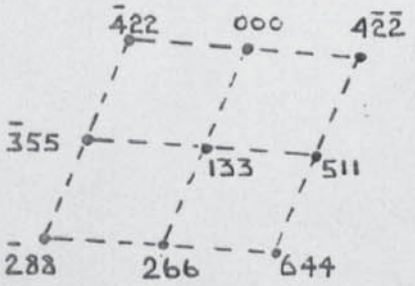

(a) Position 1. Indexed as $[0\bar{1}1]$ zone.

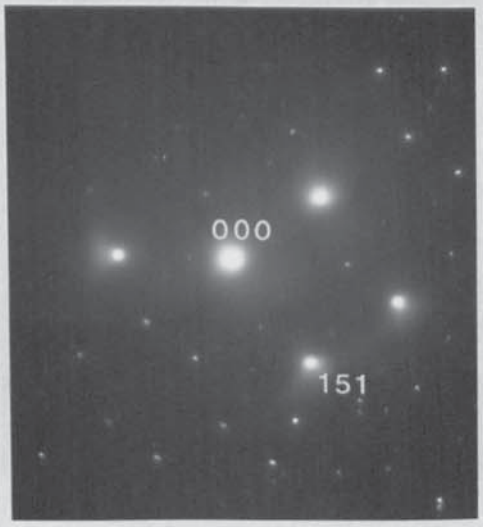

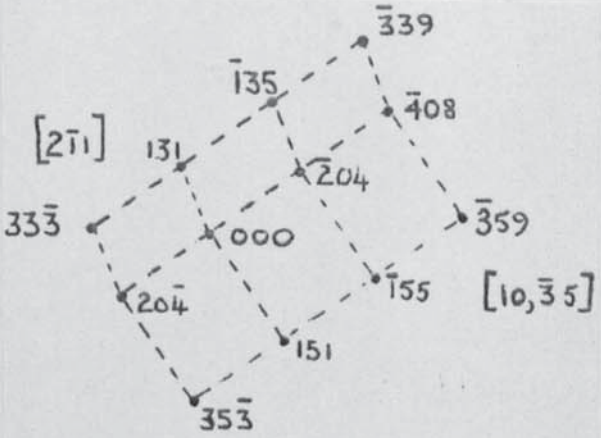

(b) Position 2. Indexed as $[2\bar{1}1]$ and $[10, \bar{3}5]$.

Figure 6.39

Diffraction patterns from positons 1 and 2 in $M_{23}C_6$ shell seen in figure 6.38.

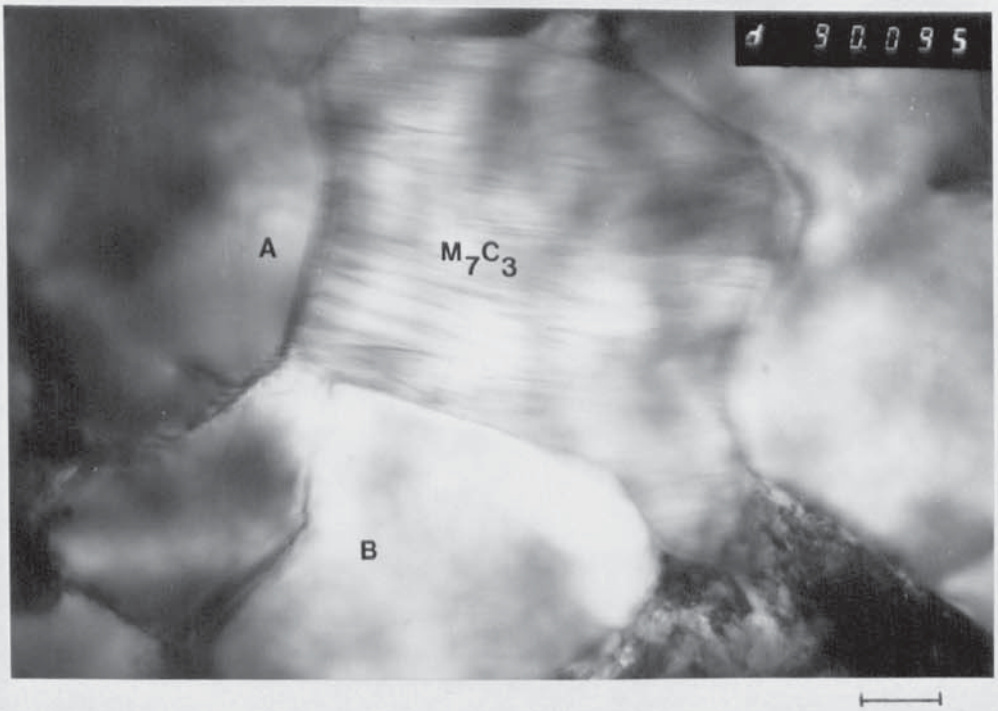

(a) Central crystal of faulted M_7C_3 almost completely surrounded by grains of $M_{23}C_6$. Marker is 0.2 μm.

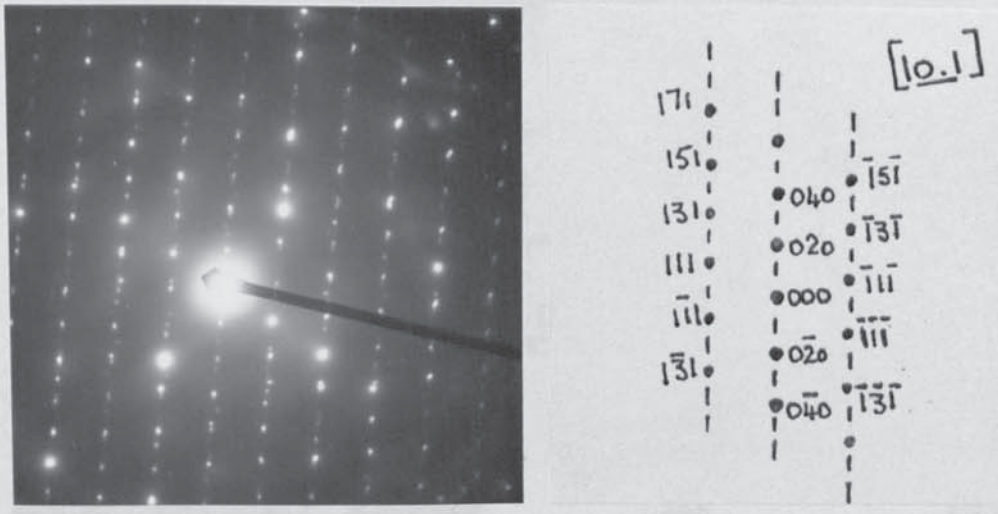

(b) Diffraction pattern from central M_7C_3 carbide.

Figure 6.40

Further example of duplex carbide. Position (b).

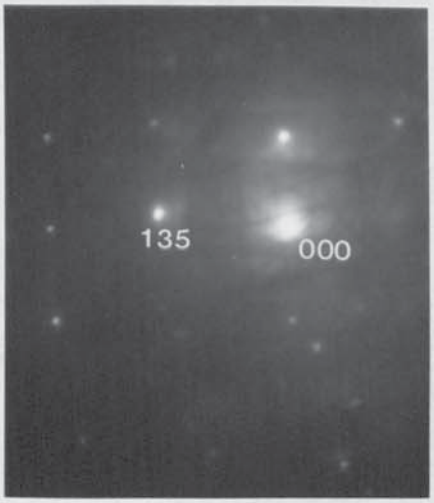

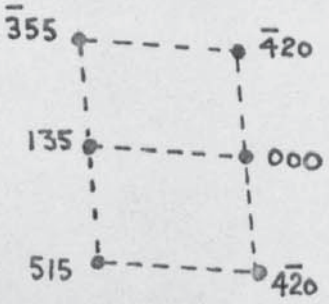

(a) Pattern from crystal A.

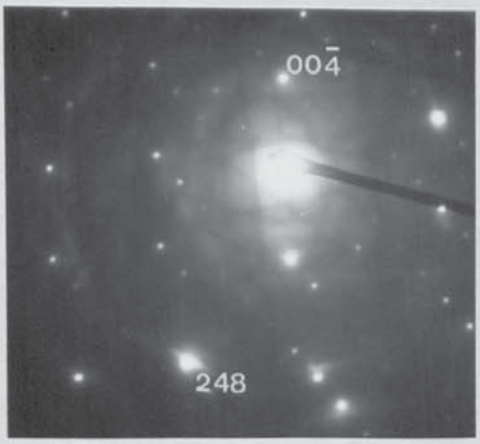

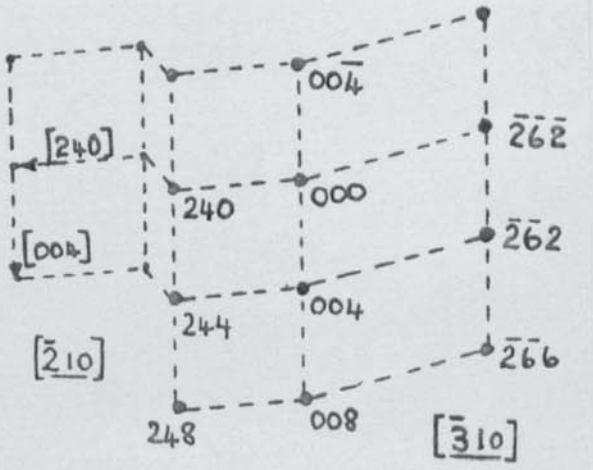

(b) Pattern from crystal B.

Figure 6.41

Electron diffraction patterns from $M_{23}C_6$ in figure 6.40.

Crystal A was identified as $M_{23}C_6$ using the following comparisons:

Reflection	d_m	d_r	Angle	Measured	Calculated
420	2.30	2.375	$\bar{4}20 \wedge \bar{3}55$	49.5^o	50.2^o
135	1.84	1.795	$135 \wedge \bar{3}55$	32^o	35.4^o
355	1.40	1.383	$135 \wedge 515$	40^o	38.6^o

The pattern in figure 6.41 (a) has therefore been indexed as a $[\bar{5}, 10, 7]$ zone.

The diffraction pattern from crystal B which is seen to contain a boundary consisted of a number of zones. The two zones closest to the origin have been indexed as $[\bar{2}10]$ and $[\bar{3}10]$ as in figure 6.41 (b) and this crystal is also confirmed as $M_{23}C_6$. Measured and reference d spacings, etc were as follows:

Reflection	d_m	d_r	Angle	Measured	Calculated
004	2.65	2.655	$004 \wedge \bar{2}\bar{6}2$	73.5^o	72.5^o
262	1.57	1.601	$004 \wedge \bar{2}\bar{6}6$	47^o	46.5^o
266	1.19	1.218	$004 \wedge 244$	48^o	48.2^o
240	2.33	2.375	$004 \wedge 248$	29^o	29.2^o
244	1.74	1.770	$004 \wedge 240$	87^o	90^o
248	1.14	1.159	$004 \wedge \bar{2}\bar{6}\bar{2}$	75^o	72.5^o

Further examples of the duplex carbides are seen in figures 6.42 - 6.44.

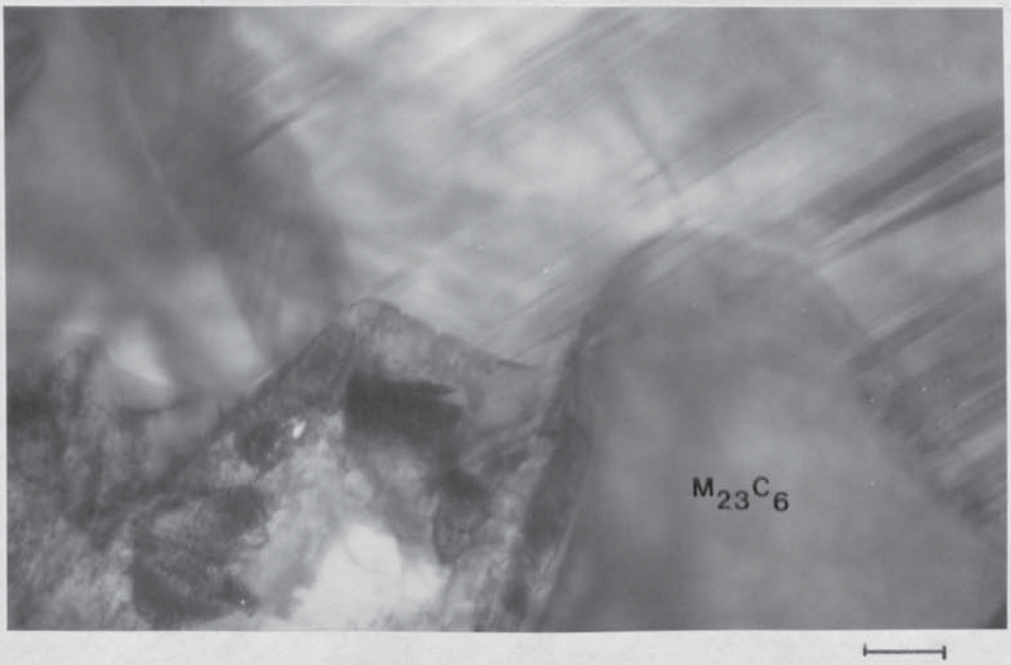

(a) Faulted M_7C_3 and adjacent $M_{23}C_6$. Matrix at bottom left. Marker is 0.2 μm.

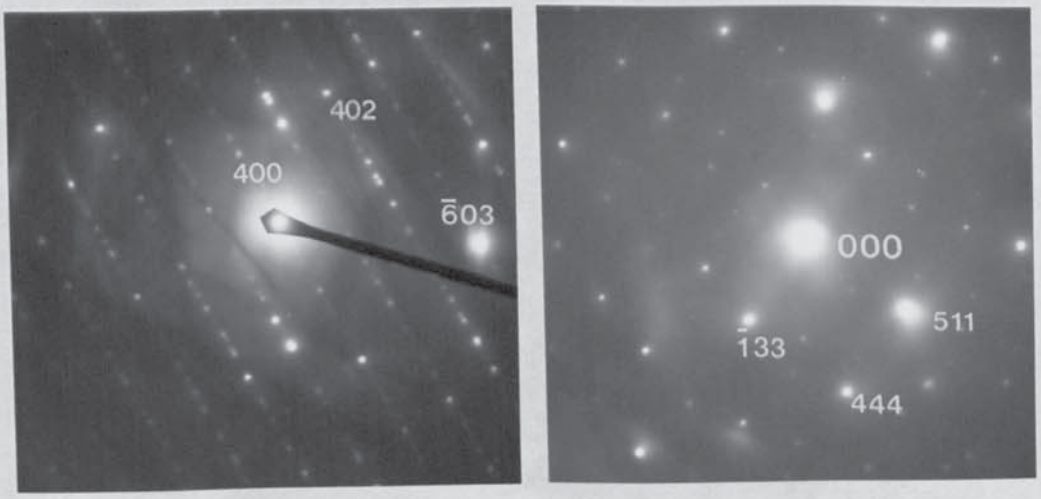

M_7C_3 $M_{23}C_6$

(b) Diffraction patterns.

Figure 6.42

Further example of $M_7C_3 \longrightarrow M_{23}C_6$.

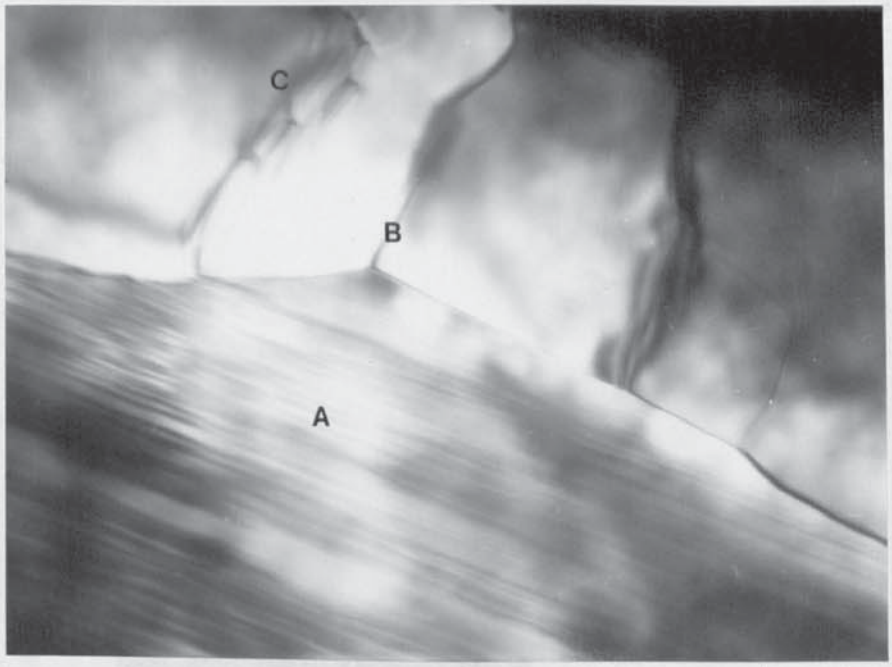

(a) Faulting in M_7C_3 (A). Boundaries (B) and dislocations (C) in adjacent $M_{23}C_6$. Marker is 0.2 μm.

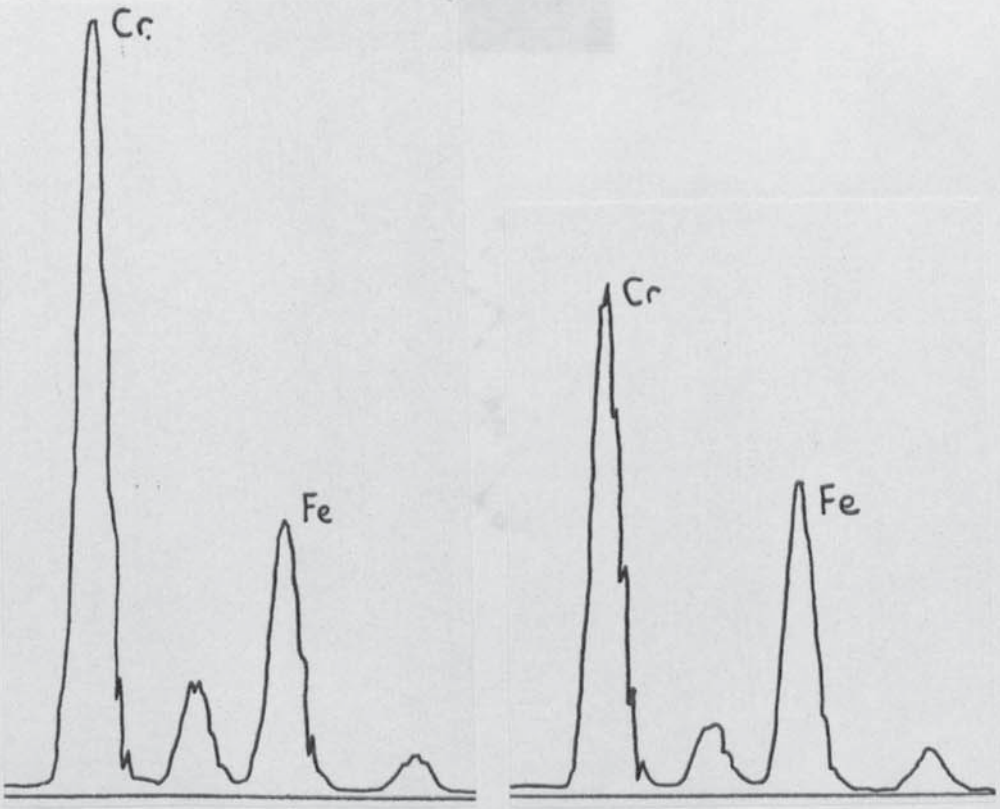

(b) M_7C_3 (c) $M_{23}C_6$

Figure 6.43

Chromium and iron peaks for M_7C_3 and $M_{23}C_6$. (Kevex).

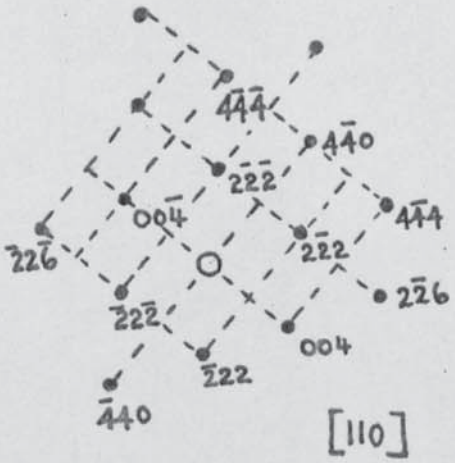

Figure 6.44

Electron diffraction pattern from $M_{23}C_6$ carbide seen in figure 6.43

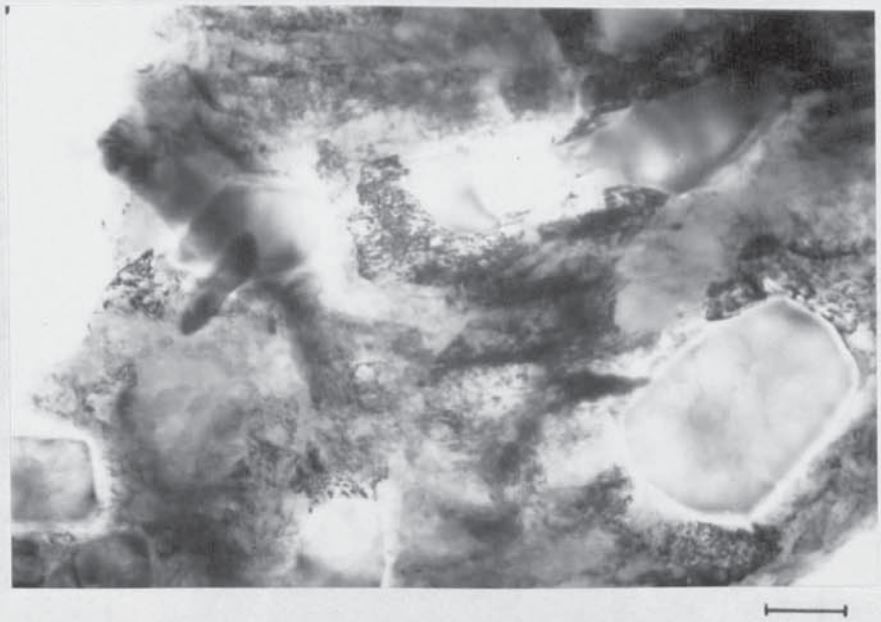

(a) Matrix containing secondary carbides.
Marker is 0.25 μm.

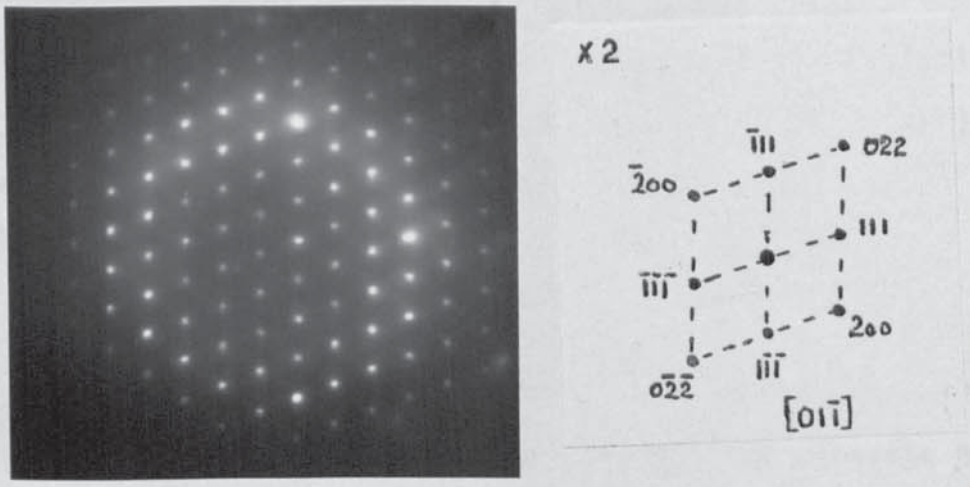

(b) Diffraction pattern from a large secondary carbide particle.

Figure 6.45

Secondary carbides in heat treated 30% Cr iron.

Figure 6.42 presents a second example where the original M_7C_3 carbide has not been fully surrounded by $M_{23}C_6$. The presence of the latter was confirmed from the following information

Reflection	d_m	d_r	Angle	Measured	Calculated
133	2.49	2.437	$\bar{1}33$ ^ 444	50°	48.52°
115	1.97	2.044	444 ^ 511	39.5°	38.94°
444	1.54	1.533	511 ^ $6\bar{2}\bar{2}$	39.0°	41.0°
226	1.58	1.601	$0\bar{2}\bar{2}$ ^ $1\bar{3}\bar{3}$	73.5°	71.07°
022	3.77	3.755	$\bar{1}\bar{3}\bar{3}$ ^ $\bar{1}\bar{3}\bar{5}$	27.5°	26.88°

Hence the diffraction pattern in figure 6.42 (b) has been indexed with the main zone as $[01\bar{1}]$ and with a second adjacent zone containing $(\bar{3}31)$, $(\bar{2}0\bar{2})$ and $(\bar{1}3\bar{5})$ reflections as $[34\bar{3}]$. The pattern for the M_7C_3 is shown alongside and is near to a $[0\bar{1}.0]$ zone with measured d spacings of 3.02, 4.50, 2.51, 1.78, 1.38 and 1.23 Å relating to table values of 3.027 (40.0), 4.5065 (00.1), 2.513 (40.1), 1.807 (40.2), 1.346 (40.3) and 1.205 ($\bar{6}$0.3).

Chromium and iron traces were obtained by X-ray energy dispersive analysis (see section 6.4) of five separate M_7C_3 - $M_{23}C_6$ composite carbides. The chromium: iron ratio found for the M_7C_3 varied from 2.29 to 2.77 with the ratio for the outer $M_{23}C_6$ ranging from 1.61 to 1.68. Figure 6.43 shows one of the areas used for analysis and gives the K_α and K_β peaks for chromium and iron in the two carbides.

The identity of the $M_{23}C_6$ seen in figure 6.43 was confirmed by the diffraction pattern given in figure 6.44. This was close to a $[1\bar{1}0]$ zone with calculated d spacings of 3.05, 1.63, 2.73 and 1.80 Å relating to reference values of 3.066 (222), 1.601 (226), 2.655 (004) and 1.878 (440). Measured angles between (004) and $(2\bar{2}6)$, $(4\bar{4}4)$, $(\bar{4}40)$ of 26.5°, 57°, 91° agree with calculated angles of 25.24°, 54.7° and 90°.

The secondary carbide particles present in the iron were also confirmed as $M_{23}C_6$. In earlier selective etching work (see section 4.6.4) the isolated secondary particles had responded in the same way as the outer carbide layers discussed above. Contrast effects due to the presence of structural faulting were not obtained in any of the secondary carbide particles observed as illustrated in figure 6.45. A diffraction pattern from a larger secondary carbide particle is also given and has been index as a $[01\bar{1}]$ zone using the following information:

Reflection	d_m	d_r	Angle	Measured	Calculated
111	6.18	6.132	$\bar{1}11 \wedge 022$	35°	35.26°
002	5.36	5.311	$022 \wedge 111$	35°	35.26°
022	3.76	3.755	$111 \wedge 200$	54.5°	54.73°

Analysis of secondary particles suggested that their chromium : iron ratio was approximately 0.85 with the ratio being 0.32 - 0.36 for the surrounding matrix. The ratio for the carbides is questionable since the reported maximum level of iron in $M_{23}C_6$ is 42.8%. The small particle size may have lead to higher iron counts due to Xrays originating from adjacent matrix areas.

Previous work (196, 266, 267) has not reported any evidence of transformation in the eutectic carbides during the heat treatment of 30% chromium irons. However, the present study of TEM foils has confirmed that an in-situ $M_7C_3 \longrightarrow M_{23}C_6$ transition does take place. This transition is known to occur in steels although there has been some discussion over whether the change involves separate nucleation or in-situ type mechanisms (256). In a attempt to obtain direct evidence of the in-situ transformation Inoue (259) has studied TEM foils of rapidly solidified high carbon Cr-W-Fe and Cr-Mo-Fe alloys which he has termed steels but which contain carbides which form direct from the melt. These alloys contained 18% chromium and either 3-8% tungsten or molybdenum and were produced by directing a stream of molten alloy onto the outer surface of a rapidly revolving steel roll giving ribbons 3mm wide by 0.05 mm thick. Their as-cast structures then consisted of an extremely fine mixture of austenite and metastable M_3C carbides, the formation of M_7C_3 and $M_{23}C_6$ both being suppressed by the very rapid cooling rate. Tempering of this material above 600^{o} gave rise to a series of changes i.e. $M_3C \longrightarrow M_7C_3 \longrightarrow M_{23}C_6 \longrightarrow M_6C$ where each stage occurred by an in-situ mechanism. Inoue (259) did not investigate alloys with higher chromium contents and did not comment on the possibility of such transitions in normal commercial irons which solidify at low rates of cooling and have very much coarser structures.

Irons solidified at lower rates of cooling are less likely to contain non-equilibrium eutectic carbides although it has been suggested (268) that crystals of $Cr_{23}C_6$ are not readily formed so that moderate cooling of liquid compositions corresponding to this carbide gives a metastable system of Cr_7C_3 and chromium. The joint presence of M_7C_3 and $M_{23}C_6$ has been noted by Nishizawa (204) and by Edington (237). In the latter case TEM examination of Stellite (supplied as 6 mm wrought plate of composition 2.5 Fe, 2.8 Ni, 30.7 Cr, 1.4 Mn, 4 W, 1.4 Mo, 1.06 C, balance Co) revealed that some of the carbide particles consisted of a small core of M_7C_3 with a surrounding shell of $M_{23}C_6$ although in many of the thin foil sections examined only single phase $M_{23}C_6$ particles were observed (237). Nishizawa (204) obtained duplex carbide structures by gradual carburisation of a 39.7% Cr alloy. The first carbide to form was $M_{23}C_6$ and this decomposed to M_7C_3 and austenite with further carburisation, the M_7C_3 being formed with small fibres or inclusions of austenite.

The findings in the present work that duplex carbides can exist with a core of M_7C_3 being partially or fully encased in a shell of $M_{23}C_6$ are in general agreement with the non-equilibrium studies of Inoue (259) and the observations on Stellite (237). The evidence from figures 6.38 - 6.44 suggests that the $M_{23}C_6$ is nucleated at the original interface between eutectic M_7C_3 and eutectic austenite. This is to be expected since the ratio M: C increases on forming $M_{23}C_6$ and

this requires a reaction between M_7C_3 and the matrix according to:

$$2M_7C_3 + 9M \longrightarrow M_{23}C_6$$

Inoue (259) proposed that $M_{23}C_6$ is nucleated over the entire interface between a M_7C_3 crystal and the matrix and then grows inwards consuming the M_7C_3. Inoue did not report the presence of boundaries in the resultant $M_{23}C_6$ shell (as seen in the present work) but his carbides were produced by quenching of liquid iron and were extremely fine. His alloys also contained tungsten or molybdenum which are believed to encourage nucleation and growth of $M_{23}C_6$ (255, 256). The small size of the carbides and the presence of these elements may have contributed towards uniform growth around each M_7C_3 crystal. For the much coarser carbides studied here and in the absence of tungsten and molybdenum (although at higher chromium levels) the formation of $M_{23}C_6$ was less uniform resulting in some cases in incomplete $M_{23}C_6$ shells and in all observed cases in $M_{23}C_6$ containing boundaries. At lower chromium levels of 15% Biner (269) has reported no evidence of any carbide transformations during high temperature spheroidisation treatments in spite of the presence of up to 5% tungsten or molybdenum. However, either of these two elements was necessary for spheroidisation of the M_7C_3 eutectic carbides and replacing them with vanadium or manganese produced little alteration of eutectic carbide morphology during heat treatment.

No strict crystallographic relationships were found between M_7C_3 and $M_{23}C_6$. For example in figure 6.38 (0001) M_7C_3 is parallel to $(0\bar{1}1)$ and $(2\bar{1}1)$ in adjacent $M_{23}C_6$ crystals and the boundaries between the two carbides are curved. This feature was also noted by Inoue (259) and he suggested that any orientation relationships between M_7C_3 and $M_{23}C_6$ were weak although he did observe (0001) M_7C_3 // $(\bar{1}2\bar{1})$ $M_{23}C_6$ which is similar to the observation above.

The presence of $M_{23}C_6$ around the M_7C_3 and as secondary carbides (instead of M_7C_3 as in the 15% Cr iron) is believed to be responsible for the lack of improvement in abrasion resistance on heat treatment of the 30% Cr iron (see figure 5.1). Although no microhardness measurements were possible $M_{23}C_6$ is known to be softer and less wear resistant than M_7C_3. In addition the $M_{23}C_6$ shell tended to crack away during abrasion (see figures 4.53-4, 4.72) and this may have contributed to easier removal of the carbides. In view of the TEM observations of grain boundaries in the $M_{23}C_6$ shells it is likely that cracks produced during wear follow these boundaries although this effect could only be proven by further studies. These observations are significant to the continuing development of 28-30% Cr irons for corrosive wear applications. For example, Dodd (270) has reported that 28% Cr irons heat treated to a martensitic condition gave substantially better resistance to corrosion than unheat-treated irons with austenitic matrix structures.

The austenitic irons were said to suffer marked attack at the boundaries of the eutectic carbide and the austenite with chromium depletion of the matrix at the carbide-matrix interface being forwarded as a possible explanation of this effect. No comments were made about the carbides in the heat treated material and it is not known whether $M_{23}C_6$ was present. In the 30% Cr iron considered above the formation of $M_{23}C_6$ at the interface would be expected to influence corrosion behaviour but a lowering of resistance might be expected since $M_{23}C_6$ is reported to be less corrosion resistant than M_7C_3 (114). In view of the effects of $M_{23}C_6$ on abrasion resistance and its possible effects on corrosion behaviour further development of Superwet type irons (197) must involve studies of the respective fields of stability of M_7C_3 and $M_{23}C_6$ at the 28-32% Cr level. This should enable compositions and thermal treatments to be selected to avoid the formation of $M_{23}C_6$. Considering the possible suppression of $Cr_{23}C_6$ formation by rapid cooling (268) a thermal analysis study at different cooling rates for the solidification of the 30% Cr irons may form the useful basis of such an investigation. Jackson (94) has shown that the Cr_7C_3 liquidus is significantly depressed by increased cooling rates (about 4X greater than for ferrite or austenite). If the $Cr_{23}C_6$ liquidus is similarly depressed but by a greater amount then this could give rise to a "stable-metastable double system" for $Cr_{23}C_6$ and Cr_7C_3 analogous to the graphite-Fe_3C system. In each case the Cr_7C_3 and Fe_3C is favoured by non-equilibrium

fast cooling. Indeed Inoue (259) has already shown that M_7C_3 itself can be suppressed in favour of M_3C at very rapid cooling rates. Such constitution studies may also help to resolve the continued arguements over the positioning of the M_7C_3 - $M_{23}C_6$ boundary in the liquidus surface of the Fe-Cr-C system and determine whether a reation of the form

$$L + M_{23}C_6 \longrightarrow \gamma + M_7C_3$$

takes place at a temperature of around 1250°C. These studies should be linked to structural examination of the morphology of the carbides and may explain why the eutectic structure of the 30% Cr iron was significantly finer than those observed in the lower chromium irons, which is a feature also noted by other workers (83, 211-2).

6.8 Discussion of TEM studies.

Other than the studies by Southwick (241), Inoue (259) and Dudzinski (260) there has been no further report of TEM examination of chromium irons other than the recent brief comment that foils had been successfully prepared from martensitic irons (271). A more recent review of alloy white iron developments does not even mention the possible use of transmission techniques using foils to research these materials (272). The present work, however, has clearly demonstrated that foils for examination at 100 Kv can be prepared from high chromium irons which have relatively coarse multiphase microstructures by use of conventional dishing and ion beam thinning. In both the 15% and 30% chromium irons both the matrix and the carbide constituents could be satisfactorily thinned and hence be studied by visual contrast and electron diffraction. The use of higher voltage electron microscopy (1 Mv) is expected to be of even more value since this should enable information to be obtained from the thicker parts of the foils. At 100 Kv the number and size of examinable areas of the foils was limited and this restricted the scope of the study. In this respect when discussing the TEM studies it must be remembered that small isolated areas are being examined in a relatively coarse heterogeneous structure and one must always question whether these small fields of examination can be regarded as a true representation of the structure as a whole.

In response to this problem a number of examples, rather than single cases, have been used in the preceeding text to illustrate the various TEM observations. The question of possible structural damage and change, e.g. the introduction of lattice defects, during foil preparation also arises. However, the foils from the alloy irons were produced by recognised techniques i.e. spark machining, dishing and ion beam thinning, and these foils were less likely to suffer structural damage than foils prepared from softer alloys such as those based on aluminium or copper. Where comparisons have been made between unworn and worn structures foil preparation has been exactly the same in each case. The obvious problems which did arise during specimen preparation have already been mentioned; these included mottled contrast in carbides, non-uniform thinning, attack at carbide-matrix interfaces and the loss of eutectic carbides from foils taken close to the wear surface.

The use of TEM examination to study the matrix structure of austenitic irons has been fully considered in section 6.5 and the value of the technique discussed in relation to future work (see pages 315-7). This could be extended to cover the martensitic matrix irons so that the nucleation and growth characteristics of both secondary (destabilised) carbides and tempered carbides could be investigated. This may lead to improved thermal treatments which give more effective distributions of these fine carbides resulting in higher levels of matrix hardness and increased resistance to abrasion.

Examination of the secondary carbides in the heat treated 15% and 30% chromium irons revealed that in the 15% Cr alloy these carbides were of the type M_7C_3 whereas at the 30% Cr level they were identified as $M_{23}C_6$. To illustrate this figure 6.22 may be compared with figure 6.45. The pearlitic carbides (see figure 6.11) and the very fine tempered carbides were not identified. As considered in section 6.7 the presence of $M_{23}C_6$ rather than M_7C_3 will reduce abrasion resistance and may also lower resistance to corrosion. In view of this for the continued development of 28-30% chromium irons additions of elements such as vanadium which is known to stabilise M_7C_3 and delay $M_{23}C_6$ formation in steels may prove advantageous. In contrast additions of molybdenum, used to improve hardenability, or tungsten may encourage transition to the unwanted $M_{23}C_6$ form.

The secondary M_7C_3 carbide particles were seen to contain structural faulting giving line contrast in bright field images and associated streaking in electron diffraction patterns. The streaking was perpendicular to {10.0} suggesting faults in planes parallel to (10.0) or (01.0) as observed in M_7C_3 carbides produced during tempering of steels (257). Such streaking was not present in patterns obtained from $M_{23}C_6$ secondary carbides, which is also in agreement with previous work on steels (256). The faulted M_7C_3 carbides in steels were produced by tempering at temperatures up to 700°C and the size of the tempered carbide particles examined ranged from 0.01 to 0.1 μm (256).

The present work has extended the knowledge gained from the studies on steels in that it has obtained image contrast from the faulting in the secondary M_7C_3 carbide particles and does not rely solely on evidence from electron diffraction patterns. It has also been shown that the faulting is present when M_7C_3 particles form at the higher temperature of 1025°C having nucleated and grown from a matrix of austenite. This is in comparison with 550-700°C in a matrix of bcc tetragonal martensite for steels. The M_7C_3 secondary carbides in the alloy iron were also much coarser having sizes between 0.25 and 0.6 μm. These different conditions suggest that the faulting is a characteristic of the growth behaviour of the M_7C_3 type carbide when it forms by precipitation in the solid state and that the faulting may occur in particles of varying sizes growing from both fcc and bcc matrices over a wide temperature range. In the $M_{23}C_6$ type carbide observed in the structure of the heat treated 30% chromium iron no evidence was seen of the structural faulting which according to Inoue (259) may exist in this phase.

The studies of the eutectic M_7C_3 carbides showed that structural faulting is also characteristic of the growth behaviour of this type of carbide during solidification of the γ + M_7C_3 eutectic in the 30% chromium iron. The faulting was present in the remaining M_7C_3 "eutectic" carbides in this alloy after oestabilisation + hardening and did not appear to have been modified by the heat treatment. Although the M_7C_3

eutectic carbides in the 15% chromium iron were not examined in the as-cast condition it is assumed that the faulting observed in these carbides in the heat treated condition was originally produced during solidification. However, without examination of faulted carbide structures both before and after thermal treatments it is not known whether the nature of the faulting has been affected during the annealing-destabilisation-hardening-tempering sequence.

Studies of M_7C_3 carbides in tempered steels (257) have confirmed the original work of Westgren (273) on the structure of Cr_7C_3. This structure is illustrated in figure 6.46 which represents symmetry elements and the unit cell and shows the positions of the chromium and carbon atoms as projected on to the (00.1) plane. Iron atoms replace chromium atoms in this lattice to give $(Cr\ Fe)_7C_3$ carbides. It is seen that the projection of the atoms onto the basal plane can be divided into four equal parts and that a displacement of $^a/2$ in certain of the planes parallel to the diagonal glide planes moves atoms into coincident positions at the same heights and does not alter any of the nearest neighbour distances. This was noted by Beech (256) who suggested that the glide planes would be favourable for mechanical slip. Dyson and Andrews (257), having obtained from extracted M_7C_3 particles diffraction patterns which had streaks only in one set of parallel directions, concluded that once the $^a/2$ translation occurred parallel to one cell face then a corresponding fault

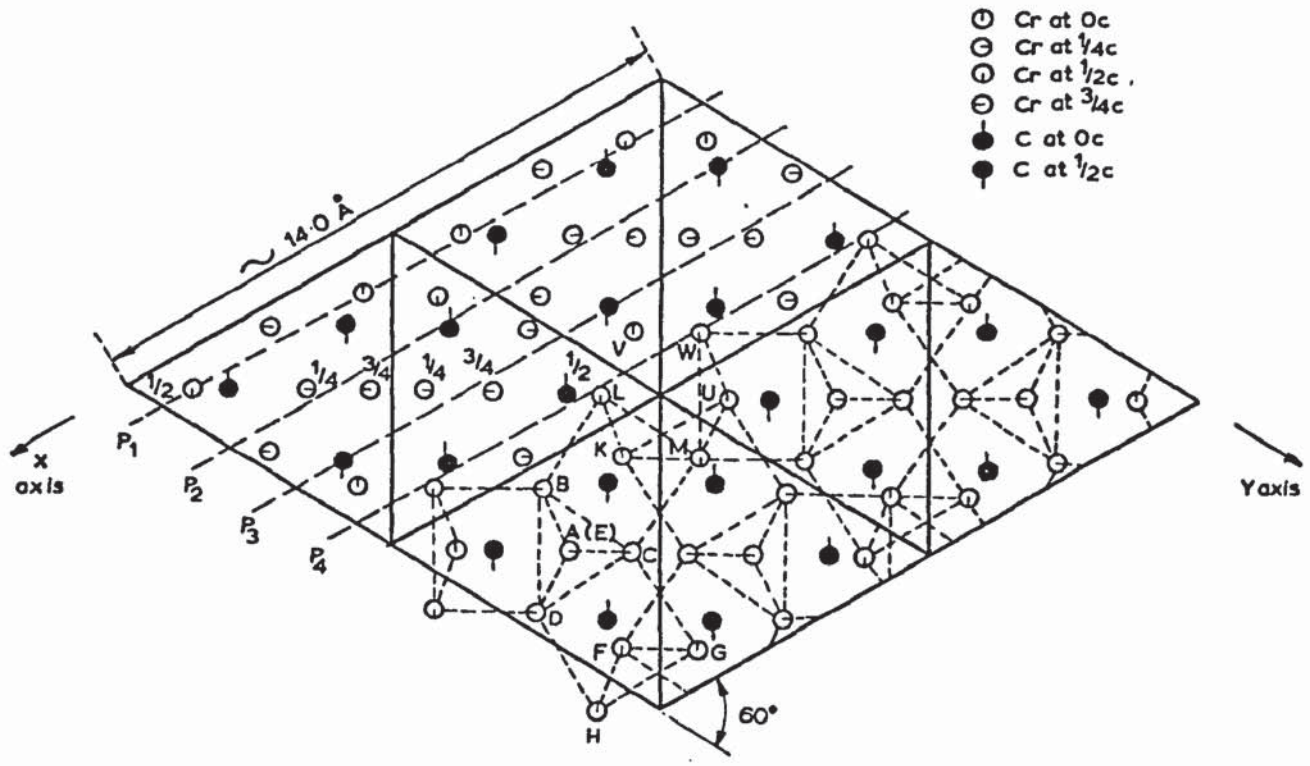

(a) Atomic positions in Cr_7C_3

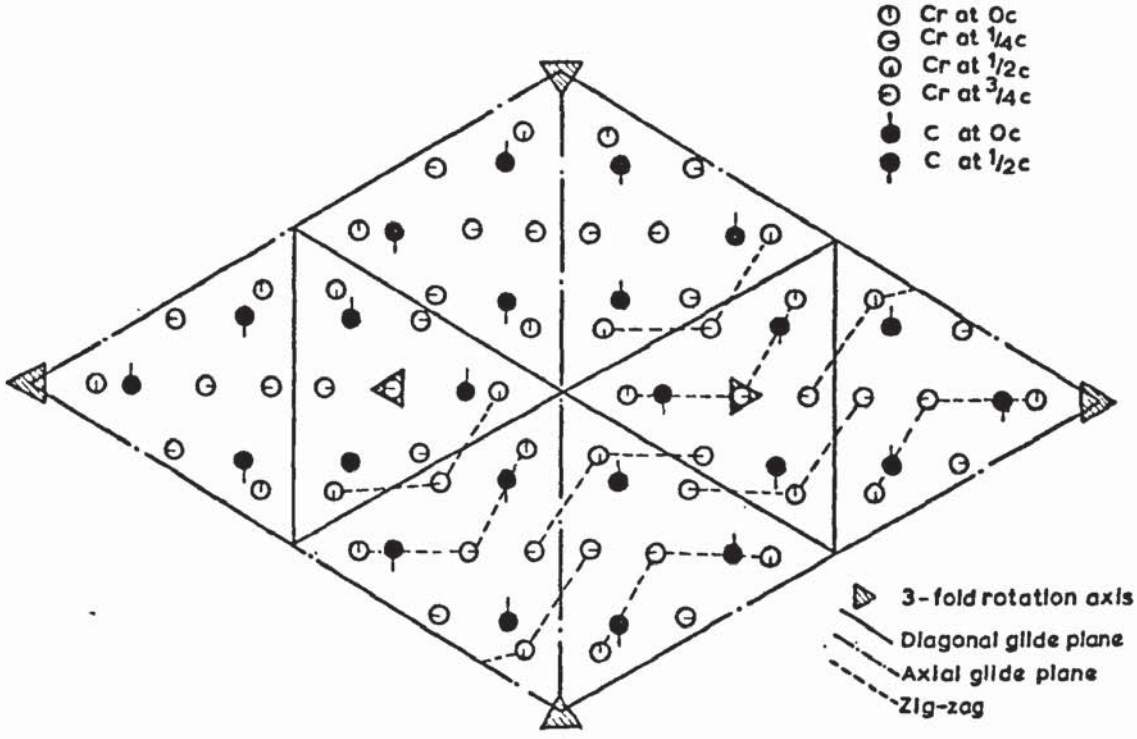

(b) Unit cell of Cr_7C_3 showing symmetry elements and zigzag rows.

Figure 6.46 Structure of Cr_7C_3
After Westgren (273) and Dyson and Andrews (257).

could not form parallel to another face. However, up to three sets of faults, and corresponding streaking, have been observed in the eutectic M_7C_3 carbides in the chromium irons. This observation is in agreement with the work (260) on eutectic $(Cr, Fe, V)_7C_3$ as is the condition of zero contrast for the [00.1] zone (see page 332).

In explaining the M_7C_3 structure previous workers have shown that the metal atoms are positioned at the corners of octahedrons, tetrahedrons, acute angled prisms and prisms which are approximately right angled. Examples are given in figure 6.47. There is a trigonal bi-pyramid of height AE=c at the centre of each triangular division of the (00.1) projection seen in figure 6.46. The bi-pyramids are each surrounded by three double prisms; some are surrounded by two of the left hand combination and one of the right hand (in figure 6.47), i.e. two down and one up, or vice versa. The bi-pyramids marked with a triangle in figure 6.46 are surrounded by three double prisms of the same type. The metal atoms surrounding a carbon atom are at the corners of a right triangular prism and it is suggested (260) that in this prism all metal-carbon interatomic distances are identical; this then corresponds to a perfectly symmetrical environment as for carbon atoms in cementite. Based on this it was further proposed that M_7C_3 can be considered as a stacking sequence of the right angled prisms containing carbon atoms (260). This model is illustrated in figure 6.48, where the right angled prisms can be considered as zig-zag rows and as isolated groups.

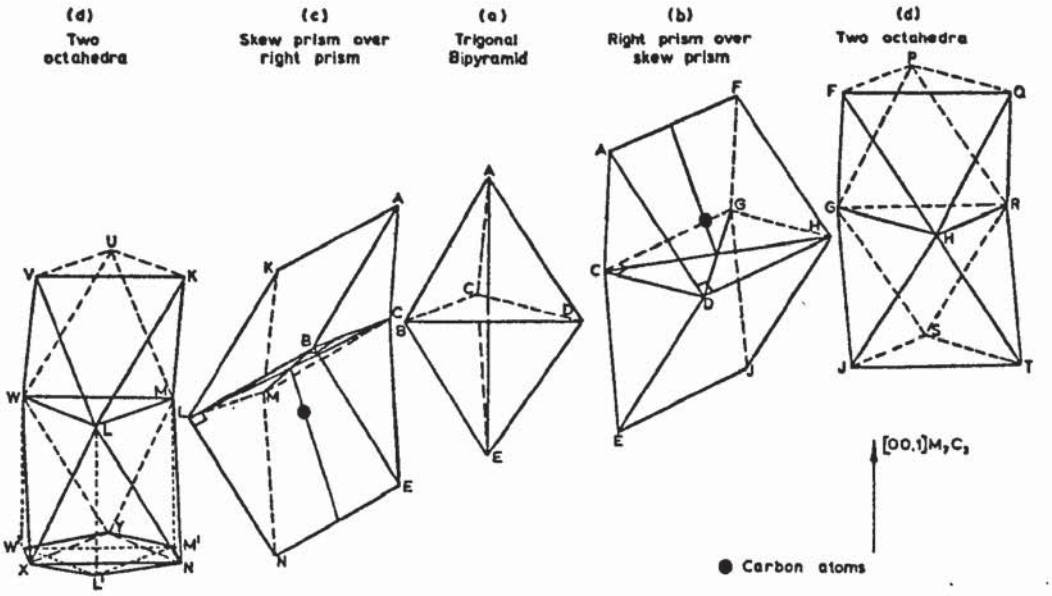

Figure 6.47

Build up of atomic structure of M_7C_3.

(Dyson and Andrews model (257)).

(a) Zig-zag rows (AA', BB', DD',) and isolated prisms (E,E')

(b) Prisms grouped parallel to axis b.

Figure 6.48

Description of Cr_7C_3 structure.
(Dudzinski model (260)).

The six zig-zag rows are termed A, A'; B, B'; and D, D' and are respectively parallel to three axes a, b and d. (a and b correspond to X and Y in figure 6.46). In the model shown only the prisms from one of each double row parallel to the three axes are shaded. The isolated prisms do not form continuous rows and are called E and E'. Dudzinski et Al (260) suggest that these can be arranged parallel to the (10.0) into the two types I and II shown in figure 6.48 (b). An unfaulted crystal can thus be described as a stacking sequence ... $.\alpha\beta\alpha\delta\alpha\beta\alpha\delta...$ of types I and II. The type I arrangement contains the rows B and B' parallel to b where all the atoms have a repeat distance for a $^{b}/2$ movement. Hence a $^{b}/2$ displacement produces a stacking fault with a fault plane (10.0) and a fault vector $^{b}/2$. Similarly faulting arises due to a $^{a}/2$ displacement in (01.0) and to a (a+b)/2 displacement for $(1\bar{1}.0)$. The fault planes identified in the present work for 15 and 30% chromium irons are all consistent with this model, although fault vectors have not been determined.

Using the above crystallographic model Dudzinski et Al (260) discussed the possible presence of ordered faulted structures i.e. ordered domains separated by antiphase domain boundaries. One of their schematic descriptions is given in figure 6.49. In this a fault arises every n type I arrangement for domains where n = 1 and for when n = 2; i.e. $\alpha\beta\alpha\beta$ or $\alpha\delta\alpha\delta$ for n = 1 and $\alpha\beta\alpha\delta\alpha\delta$ for n = 2. Type I and II arrangements are shown schematically as XXX and XOX.

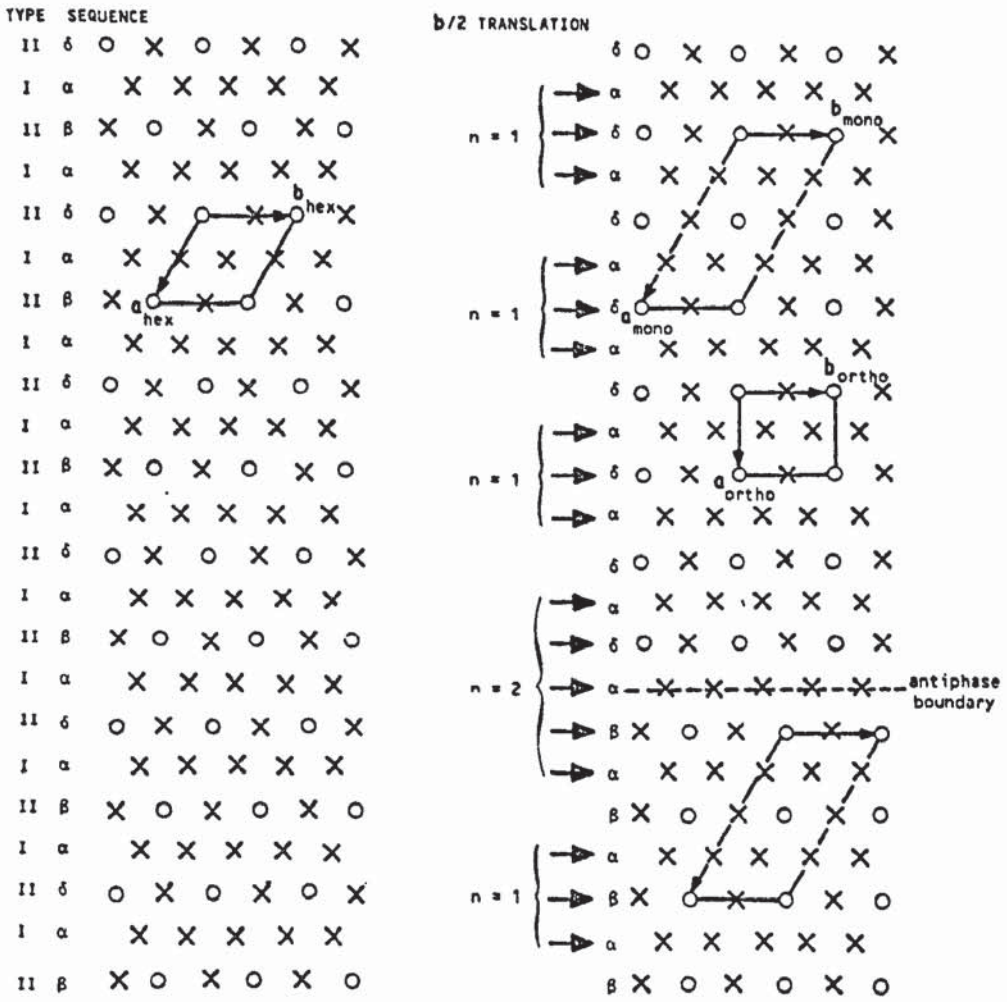

(i) Non-faulted; stacking sequence is

$\alpha\beta\alpha\delta\alpha\beta\alpha\delta$

(ii) Faulted; domains with n = 1 are separated by a domain with n = 2

Figure 6.49

Non-faulted and faulted Cr_7C_3 showing stacking of types I and II, and creation of antiphase boundary. (After Dudzinski et Al (260)).

Dudzinski did not present any visual TEM contrast from antiphase domain boundaries, however in the M_7C_3 crystal seen earlier in figure 6.33 a contrast effect believed to result from the presence of antiphase boundaries was obtained. For this crystal the lines of the antiphase boundaries were parallel to the lines of faulting contrast (i.e. at 90^o to diffraction pattern streaking). This observation fits the model given in figure 6.49. Steps observed in the antiphase boundaries are at 120^o and are expected to correspond to $^a/_2$ translations in the A,A' rows. (A,A' rows are parallel to axis a; B,B' rows are parallel to axis b and a makes 120^o with b). When ordered faulted domains are extensive additional sharp reflections are expected in diffractions patterns as superlattice reflections and stacking faults are said to be invisible (260). This suggests that the domains in figure 6.33 are narrow since their boundaries are contrasted and no superlattice reflections are seen.

The presence of (10.0),(01.0) and $(1\bar{1}.0)$ faulting has been confirmed in both eutectic and secondary M_7C_3 carbides. The faulting must originate directly as the M_7C_3 crystals grow either from the melt or in the solid state or the faulting must arise, as suggested (260), from mechanical or thermal stresses acting on already formed M_7C_3 crystals. In the latter case the faulting would be expected to be associated with the presence of partial dislocations. To date there is no published evidence of dislocations in M_7C_3 other than that seen earlier in figure 6.36, where an array of dislocations is suspected to compensate for mis-match at a low angle sub-boundary.

When M_7C_3 occurs as a primary phase or in a eutectic mixture in chromium irons it exists as crystals with sharply defined hexagonal prism shapes resulting from a faceted growth behaviour. The growth forms of faceted phases have been reviewed by Chadwick (274) who suggests that the solid-liquid interfaces of such phases may be described as perfect crystallographic surfaces on which a small number of atoms reside or from which a small number of atoms are missing. When undercooling requirements for growth are satisfied then growth takes place by the lateral movement of growth steps along the interface and atoms must become attached to the growing crystal at specific ledges on the crystal surface. Hence there must be a continuous source of ledges or growth would be arrested. Chadwick listed three means by which growth steps could be continually available. These are represented in schematic forms in figure 6.50. The first requires the repeated nucleation of groups of atoms on the crystal surface which develop in two dimensions as indicated. The second, and more likely, mechanism involves a perpetual growth site produced by an emergent screw dislocation. This gives rise to a growth step which winds around the dislocation to form a spiral. Atoms can then be added to the ledges around the spiral. This type of growth has been observed in crystals grown from the vapour and from the melt. The final possibility arises when a twin or sub-boundary-surface intersection produces a groove at the surface. Growth proceeds by attachment of atoms to both sides of the twin at the groove root.

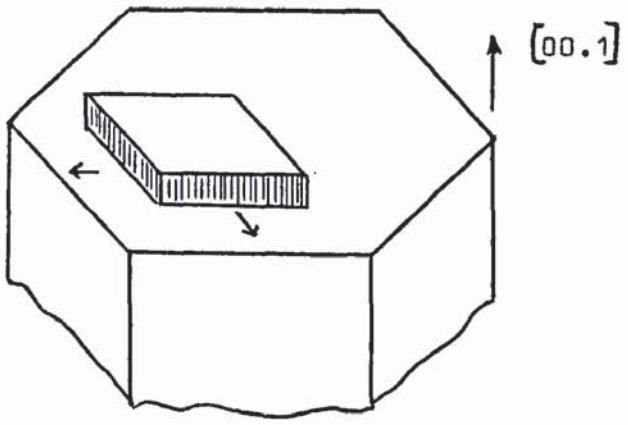

(a) Repeated nucleation of layers on interface.

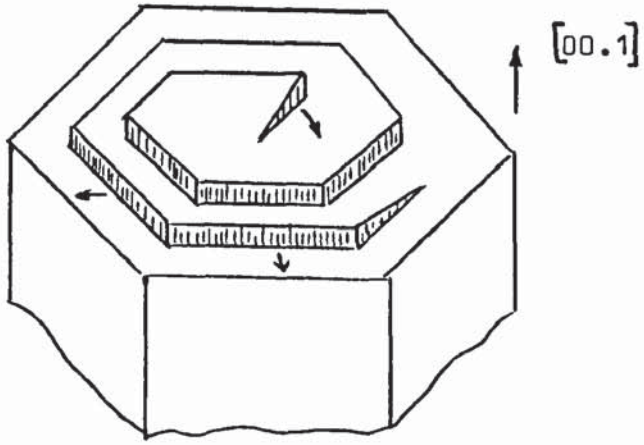

(b) Spiral growth - screw dislocation mechanism.

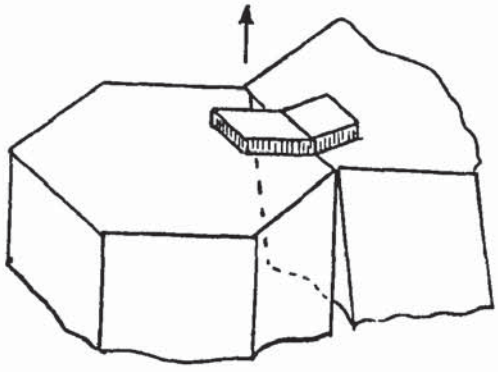

(c) Groove produced at sub-boundary intersection.

Figure 6.50

Production of growth steps (schematic).

In each situation seen in figure 6.50 the growth steps (shaded) could correspond to $\{10.0\}$ so that variation in the attachment of atoms at these steps could give rise to the $\{10.0\}$ faulting. Direct SEM observation of growth fronts in carbide crystals exposed by decanting the remaining liquid from partially solidified irons may be of use in determining whether such growth steps exist and whether they are significant to the origins of the faulting. This observation could aid in understanding how the central cores of matrix are produced within the eutectic carbides.

Hole formation during the growth of graphite crystals has been explained by Minkoff (275) in terms of the adsorption of impurity atoms at the spiral ledges produced during the screw dislocation growth mechanism (see figure 6.50(b)). He suggested that adsorbed impurities could stop the sidewise movement of a step across the crystal surface leading to void formation. This produces a number of holes situated around the spiral ledge. However the M_7C_3 carbides generally contain only a single core so that this impurity adsorption effect cannot be used as a possible explanation of core formation.

Two alternative suggestions can be considered, these involve nucleation at austenite dendrites or the formation of an intermediate carbide. These are illustrated in schematic form in figure 6.51. In the first mechanism eutectic austenite is nucleated at the surface of a primary austenite dendrite and

grows from the eutectic liquid between an initial eutectic M_7C_3 crystal and the dendrite. The M_7C_3 then grows around the extended dendrite arm and since it is likely to be the leading phase of the eutectic it overgrows and surrounds the austenite. The isolated austenite then develops as a core within the M_7C_3 as further growth takes place. The situation may arise where a cluster of M_7C_3 crystals grow around a dendrite arm and develop to produce the effect seen in figure 6.3. This nucleation mechanism relies on the presence of primary austenite dendrites and could not explain the formation of hollow primary M_7C_3 carbides observed by other workers in hypereutectic irons.

The alternative suggestion involves the initial nucleation of a carbide, possibly $M_{23}C_6$ which requires fewer carbon atoms for nucleation than M_7C_3 . This first formed carbide then "transforms" to austenite and M_7C_3 due to its instability or due to its inability to grow at a sufficient rate for solidification to proceed. In the first case transformation may involve a peritectic reaction i.e. $M_{23}C_6 + L \longrightarrow M_7C_3 + \gamma$ (see page 362). The second case may cause nucleation of M_7C_3 which then grows rapidly and consumes the original $M_{23}C_6$. In both situations austenite remains to grow within the M_7C_3 as a core. The formation of $M_{23}C_6$ is more likely in the higher chromium irons and the present observations suggested that the incidence of matrix cores was higher in the carbides in the 30% Cr iron than in the 15% Cr iron. However, no evidence was seen of any $M_{23}C_6$ particles in the matrix cores to support this theory.

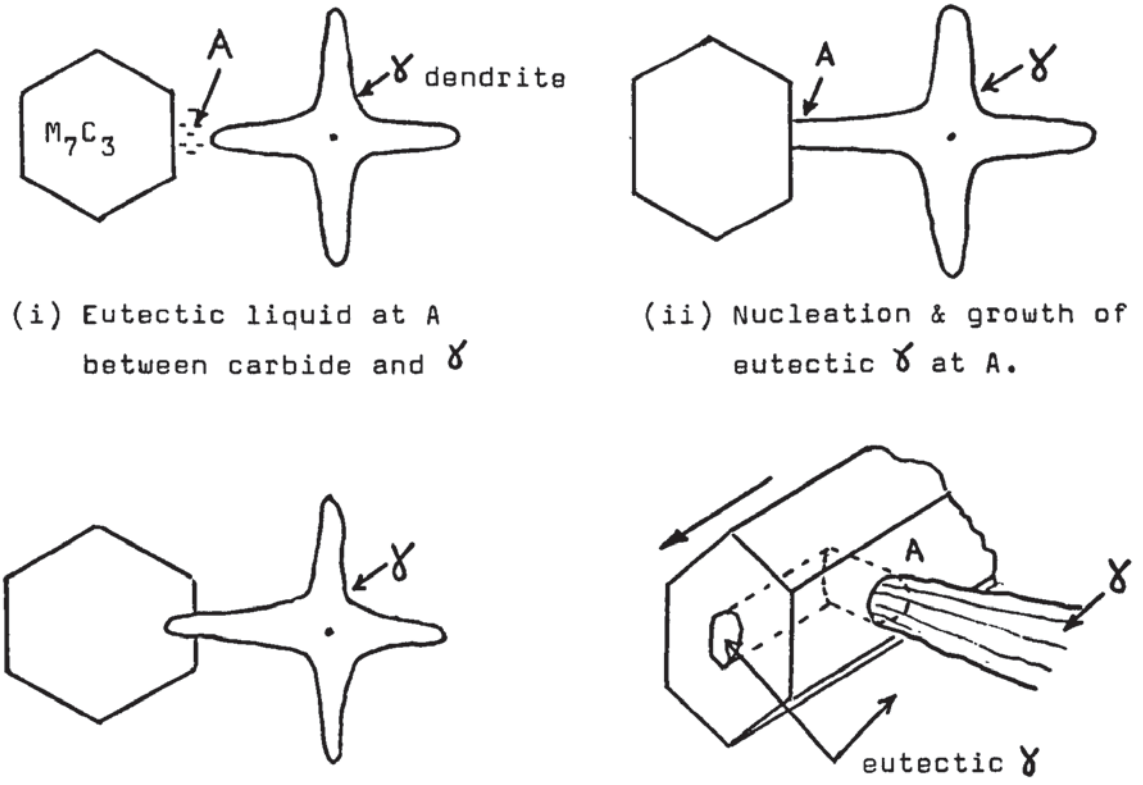

(i) Eutectic liquid at A between carbide and γ

(ii) Nucleation & growth of eutectic γ at A.

(iii) Carbide surrounds γ

(iv) Development of core

(a) Nucleation at austenite dendrite arm.
(Growth direction for (i)-(iii) is normal to paper).

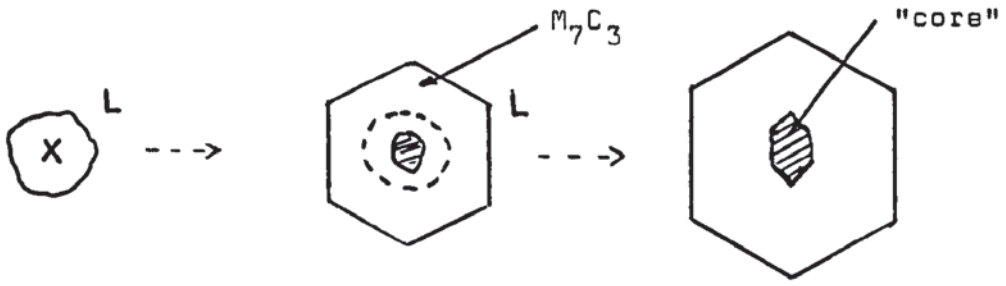

(b) "Decomposition" of initial carbide, X.

Figure 6.51

Origin of cores in M_7C_3. (Schematic).

The development of a core will involve modification of the growth of a carbide rod and may facilitate a spiral type growth mechanism. From figure 6.50 (b) and figure 6.52 it is seen that for the case of a complete rod if atoms are added uniformly along the step then the angular velocity of the step is greater at the centre and the step distorts and produces a spiral. If a central core of matrix develops then the length of the step is reduced by r, the radius of the core, and this should result in a lowering of the lattice elastic strain associated with the original screw dislocation. The reduction in step length will also reduce the differences in angular velocity along the step as growth occurs. Variations in the attachment of atoms at the step would give rise to faulting. The presence of a core may assist carbide growth since iron atoms can be rejected into eutectic austenite at the inner and outer edges of the step.

It is recognised that M_7C_3 carbide may be anisotropic but the presence of internal softer matrix cores could also contribute to the wide variation in published hardness figures, low values being recorded when the indenter penetrates near or into the softer core. The core may also influence microcracking behaviour of the carbide and two possible effects may be considered. In the first of these the cores could delay microcrack propagation during wear. A crack nucleated in a carbide rod without a core may propagate across the rod section without obstruction or deflection and may then be able to nucleate microcracking in the adjacent matrix.

This is an observed failure mechanism in austenitic matrix irons (134, 269). The core may effectively decrease the size of the microcrack in the carbide and will thus increase the stress level required to initiate propagation into the matrix. It may also cause deflection of the crack along the core-carbide interface. This effect is illustrated in figure 6.53 and if the crack is deflected for a sufficient distance to create additional surface area of fracture faces then extra energy will be consumed in cracking the carbide. Such a deflection could be responsible for the steps in the fracture path seen in the eutectic M_7C_3 in figure 6.46. It has been suggested that hollow rods are produced at fast growth rates (213), hence chilling of wear surfaces in castings production would be expected to give smaller diameter rods containing cores and resulting in improved resistance to fracture and wear for austenitic matrix irons. Any beneficial effect would be much less significant in heat treated irons where failure is initiated around destabilised carbide particles (134, 269) but the possible deflection of a crack in a carbide rod would still hold.

In contrast if a microcrack is not deflected at the internal interface and if no energy is consumed in plastically straining the core then a second and opposite effect could arise. The microcrack could be accelerated through the carbide on either side of the core and in this case transverse cracking of the carbide would be easier, although the undamaged core may help retain the broken carbide in position.

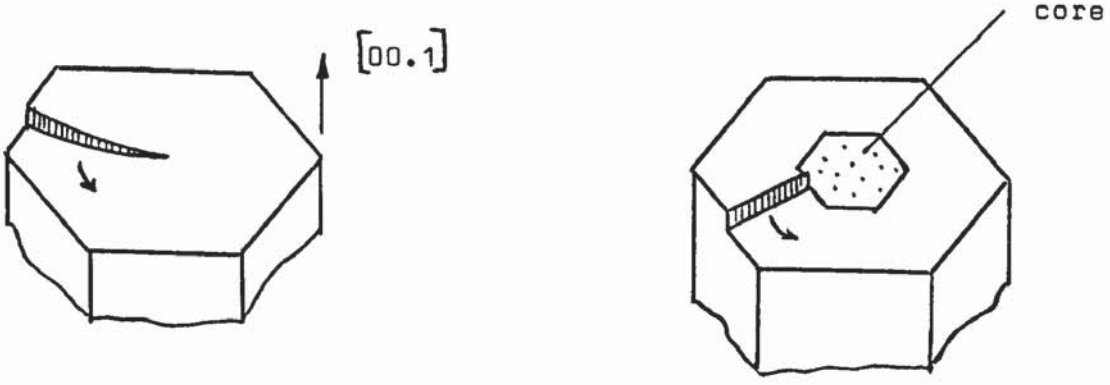

(a) No core, step distorted

(b) Core, shorter straight step.

Figure 6.52

Possible effect of core on growth step in M_7C_3.

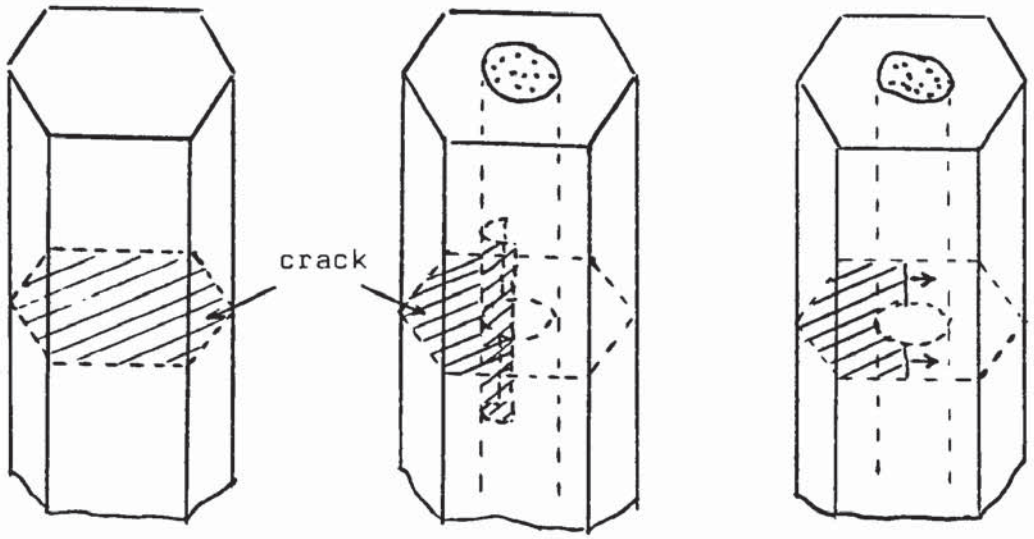

(a) No obstruction to crack

(b) Deflection along internal interface

(c) Acceleration of crack at

Figure 6.53

Possible effects of core on microcracking in M_7C_3.

The TEM examination of eutectic carbides at the wear surfaces was limited by the loss of these carbides from thin foils during specimen preparation. The problem may be overcome in future work by plating the wear surface with a relatively thick layer of iron or nickel. Foils may then be taken normal to the wear surface with the aim of achieving perforation at the plating-wear surface interface with suitably thinned regions in the carbide adjacent to this interface.

Some observations were made of eutectic carbides which had remained in position during preparation. In the majority of these carbides the structural effects seen, i.e. faulting and sub-boundaries, were no different to those seen in the carbides examined in specimens prepared from unworn surfaces. However, in two separate rods of carbide in the 15% Cr iron additional contrast effects were obtained which had not been noted in samples from unworn surfaces. These effects are illustrated in figure 6.54. In view (a) a number of wavy faults are seen at position 1, These make angles of 65^{o} with the main family of faults seen and they intersect the latter producing steps in the fringe contrast (see position 2). Also visible are two more intense lines of contrast (position 3) which are not straight and which are approximately alligned with the wavy faults. The lower of these lines in the micrograph is seen to cross a number of faults. A similar effect is seen in view (b) where a line of contrast is seen

at position 1. In this case there is a displacement in the intense fringe along the line of faulting. Also seen in view (b) are contrast effects at position 2 which may be due to the presence of dislocations associated with the growth of bands of faulted structure. An additional feature is seen at position 3, here the contrast is similar to that from a domain boundary but is believed to have been caused by the presence of a dislocation loop or dipole. It is seen in figure 6.55 that the suspected dislocation line has produced a displacement in the fringe contrast from fault F. Additional intersections of adjacent faults have occurred at X, Y and Z. The measured angle between F_1 and F_2 is 58^o and between F_2 and F_3 is 67^o, it is assumed that F_1, F_2 and F_3 correspond to $\{10.0\}$ faulting, since an electron diffraction pattern was not obtained for this area. The section AB of the suspected dislocation is not parallel to the line of faulting F_1 and makes an angle of 45^o with F_2. The fault intersections at X, Y and Z are all parallel to AB and meet F_2 at 45^o producing changes in diffracting conditions and hence in the contrast from F_2 faults. It is therefore unlikely that AB corresponds to a domain boundary since this would be expected to run parallel to the faults F_1. Such a boundary does exist in the top part of the field of view as indicated by D.

(a) Wavy faults (1) producing steps in straight fault (2) Two lines of intense contrast (3) crossing into faulted region.

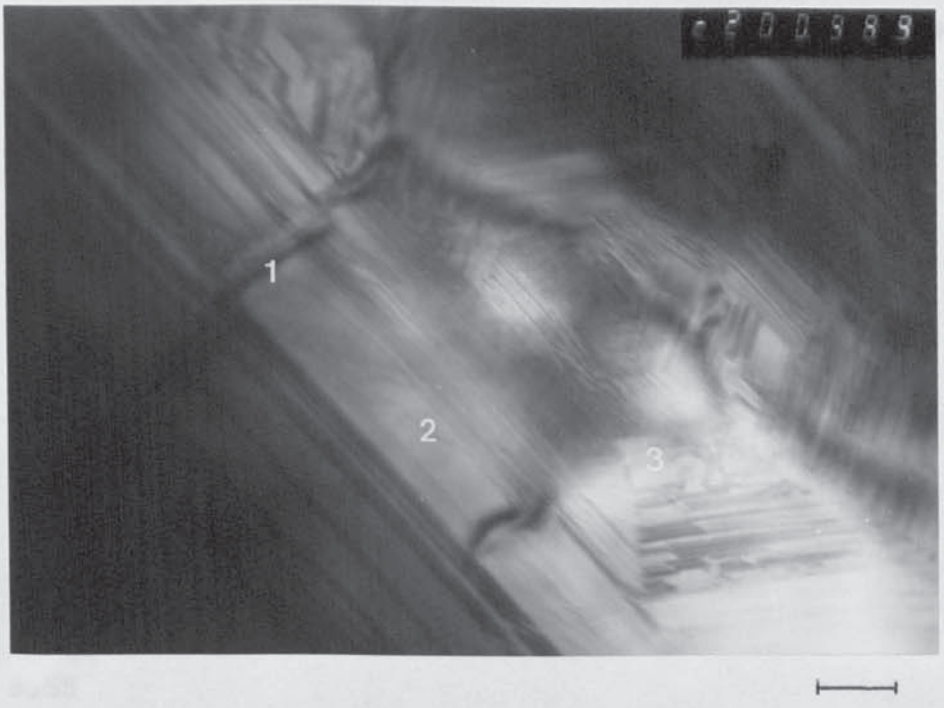

(b) Intense line contrast (1). Dislocations associated with faults (2). Possible loop dislocation at (3).

Figure 6.54

TEM views of M_7C_3 eutectic carbide at wear surface of 15% Cr iron (heat treated). Marker is 0.1 μm.

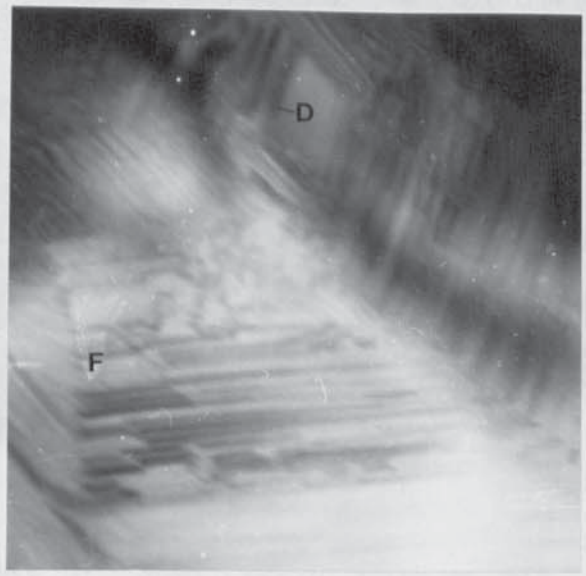

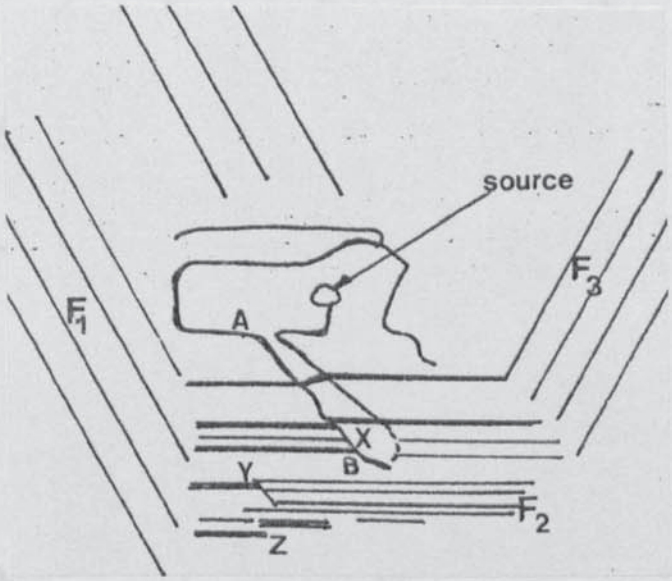

Figure 6.55

Magnified view of position 3 in figure 6.54(b). Marker is 0.05 μm.

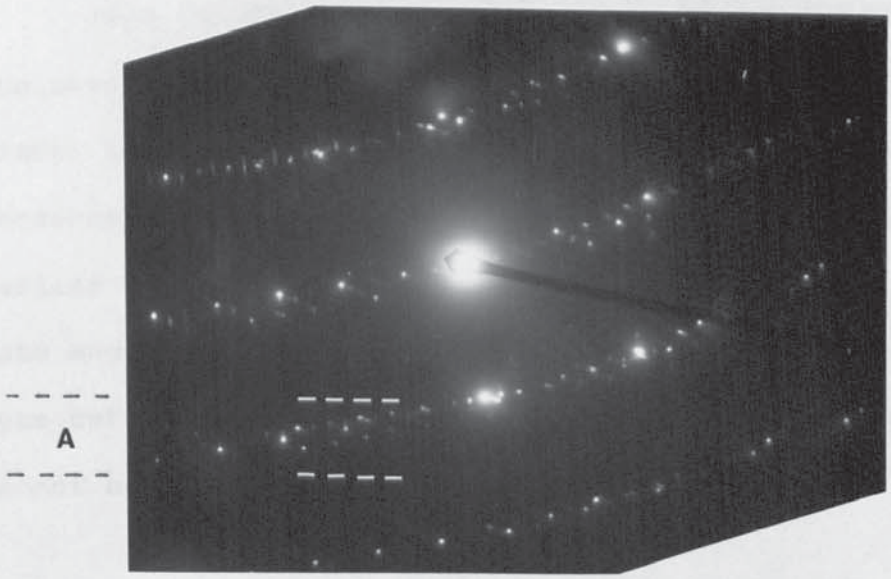

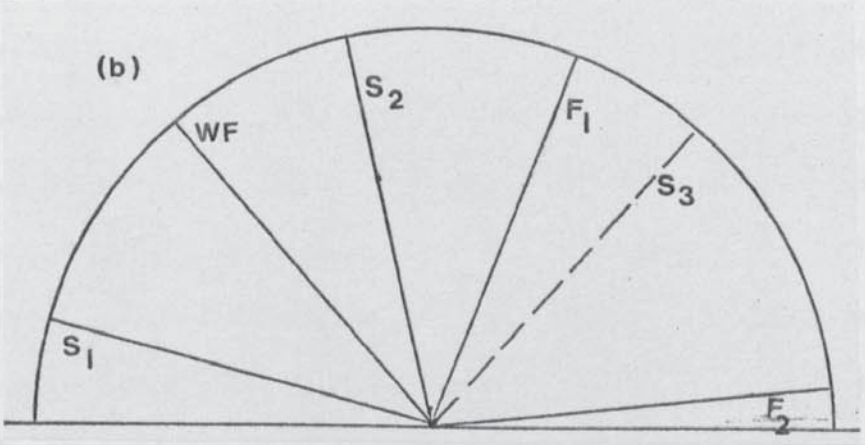

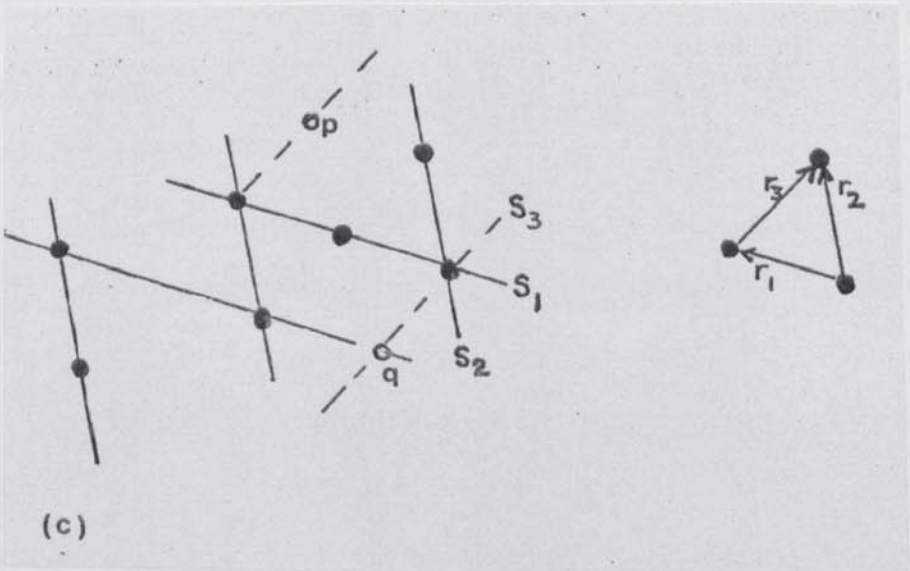

Figure 6.56

Diffraction pattern from view (a) in figure 6.54.

View (b) in figure 6.54 was the only evidence seen for the possible existence of slip dislocations in the carbides either in the unworn condition or at the wear surface. The presence of suspected sub-boundary dislocations was considered earlier (see page 340). In the absence of electron diffraction data and contrast experiments the presence of a dislocation type defect and hence plastic deformation in the carbide cannot be confirmed.

One other possible deformation mechanism in the carbide may involve mechanical twinning and it was thought that the wavy faults and heavier traces (position 3) seen in figure 6.54 (a) might correspond to fine twins. However, this was not confirmed from the electron diffraction pattern for this area (see figure 6.56). The part of the carbide examined was tilted away from a prominent zone axis and this has resulted in an "imperfect" pattern with the reflections lying along curved paths. The reflections have been analysed with regard to the micrograph view (a) using the region A as indicated in the diffraction pattern.

The faint streaking, S_1 and S_2, seen in the pattern correlates with the faulting F_1 and F_2 observed in view (a) as illustrated in figure 6.56 (b). Sharp reflections are seen lying along S_1 and S_2 and their spacings r_1, r_2 and r_3 give a calculated d spacing of 12.0 Å, i.e. the reflections correspond to $\{10.0\}$ planes.

A magnified schematic view of region A of the diffraction pattern is given in figure 6.56 (c). Included in this view are reflections p and q which are missing from the actual pattern. Their inclusion in the schematic diagram is in order to show that this area of the pattern is a few degrees from a Laue zone, [00.1] and, also, to enable the line of "missing" streaks S_3 to be shown. It can then be seen from diagram (b) that S_3, if present, would be at approximately 90^{o} to the wavy faults WF. This suggests that these faults correspond to normal {10.0} type faulting and could have been present before wear of the carbide. No twin reflections were present in the pattern.

Although the above TEM study has not been able to show that plastic deformation of eutectic carbides occurs during abrasive wear it has nevertheless given rise to a number of interesting points. Among the effects that merit further consideration are the following.

(i) How are the stacking faults affected by thermal treatments, is the fault density reduced or are further faults created ?

(ii) Is the frequency of the faulting related to compositional effects and do elements such as chromium and molybdenum alter stacking fault energy ?

(iii) Can partial dislocations exist in association with the faults and will their presence allow plastic deformation of the carbide ?

The answers to these questions might only be obtained after an intensive study of individual carbide crystals. In this respect it may be necessary to use a technique similar to that recently reported by Hibbs (276) in a study of deformation mechanisms and defect structures in tungsten carbide. This would require the production of large "single" crystals (3 mm x 1 mm) of M_7C_3 carbide using controlled solidification or by sintering of compacted carbides obtained by matrix dissolution. Deformation may be induced by indentation with a microhardness tester as in the work on tungsten carbide. Lattice defects introduced by this could then be examined using bright and dark field contrast experiments (245).

7.0 SUGGESTIONS FOR FUTURE WORK.

7.1 The conclusions in the present work are based on a limited number of abrasion tests since the main studies have centred on the nature of wear damage rather than on producing highly reproducible wear ratio data. Clearly there is always scope for larger numbers of repeat tests to be performed on various irons and other materials so that abrasion resistance can be compared with more confidence. In addition the effects of variables such as the load, speed and time of testing and the type, particle size and breakdown characteristics of the abrasive can be investigated. For example, further work could be carried out using selected mineral ores as the abrasive since these tend to be less hard than silica. They may therefore produce different wear damage and hence give a different ranking of the relative abrasion resistance for the alloys under investigation.

7.2 Although the present work has been confined to alloy white irons a number of other abrasion resistant materials are available and are being developed. One of the newer materials is polyurethane and during the wear testing of the cast irons a small number of polyurethane samples were also tested. The white iron standard suffered a volume loss of 1.10 cc. whereas the polyurethane tested under identical conditions lost only 0.30 cc. It must be remembered that a low wear rate may not be an end in itself because in grinding applications

the pulp must be successfully crushed and ground and this may not be so efficiently performed with plastic liners. However, there is little information on the abrasion resistance of polymer materials and a study of these and how they compare with conventional hard materials and rubbers under a variety of abrasive conditions could be the subject of a wide range of research projects.

7.3 The effects of section size on the abrasion resistance of alloy irons is worthy of study since the coarser structures of heavier cast sections may be less abrasion resistant as well as having inferior toughness to lighter sections. It is generally accepted that a fine distribution of small hard particles is preferred to an uneven distribution of larger hard phases. It is also known that abrasion resistance can vary considerably between alloys of the same nominal composition if their manufacturing conditions differ.

7.4 Wear test specimens could be etched before wear to study the effects of matrix corrosion. Alternatively the specimens could be wear tested under a variety of corrosive conditions to determine the extent to which the abrasion resistance ranking of the various alloys alters and to study if the wear damage is different to that observed in dry wear.

7.5 Further useful information regarding the development of wear damage may be obtained from experiments which involve the movement of a single loaded stylus across a suitably prepared surface e.g. polished metallographic surfaces in the unetched condition and with varying degrees of etchant attack.

7.6 Indentation studies similar to those reported for cemented carbide tools (239, 240) may also aid in the understanding of the cracking behaviour of the eutectic carbides.

7.7 The present work used typical commercial heat treatments and these gave variations in matrix microhardness from 850 to 720 H_V with composition (see figure 5.5). Wear tests on irons heat treated to the same level of matrix microhardness e.g. 700 H_V may allow the effects of the type and form of the eutectic carbides in the irons to be more readily correlated with wear behaviour.

7.8 In view of the relatively high measured abrasion resistance of the hardened 5% chromium iron the development of spheroidising treatments may be possible to improve the toughness of this cheaper material by breaking down the continuity of the embrittling carbide.

7.9 High temperature treatments have been used by Biner (269) to improve the fracture toughness of austenitic 15% Cr irons by spheroidisation of the eutectic carbides. Although toughness is increased the effect of such treatments on wear resistance has still to be determined. One consequence of the treatment is that the mean inter-carbide spacing increases from about 10 μm in the as-cast structure to 25-30 μm after spheroidisation. This increase may allow easier penetration by abrasive grits into the matrix areas between the carbides resulting in greater wear damage. The rounded carbides themselves may be more readily removed from the matrix than the "as-cast" rodlike carbides which are usually orientated normal to wear faces in cast balls and liners. Durman (134) has noted that high temperature treatments can weaken the carbide-matrix interface as revealed by the presence of entire carbide particles on fracture surfaces rather than cleavage facets of fractured carbides. However, later work (269) has suggested that interface cracking was less significant than carbide cracking in propagation of fracture toughness cracks.

7.10 In the higher Cr irons the use of sub-zero treatments needs consideration. Conventional hardening requires prior destabilisation which depletes austenite in carbon and consequently gives a low hardness, low carbon martensite. Refridgeration treatments of 12-22% Cr, 1-3% Mo irons are claimed to give martensitic matrix structures with improved

abrasion resistance (277). Such treatments e.g. the Cryotough process, are already being used to improve the lives of alloy steel tools (278) and could be readily applied to small grinding media.

7.11 In view of the observed carbide-matrix interface decohesion during wear, interface cracking in toughness studies (134, 269, 279) and interface attack in corrosive wear (270, 280) useful knowledge may be gained by the use of Auger electron spectroscopy and STEM to study the possible segregation of alloy elements and impurities in the interphase boundary regions.

7.12 An examination of the mechanical behaviour of directionally solidified irons may allow comparisons to be made between eutectic carbides in white irons and the fibres in a composite material. Carbide-matrix bond strength may be assessed at different chromium contents if the eutectic carbides can all be aligned parallel to a tension axis.

7.13 The present TEM work used a polishing solution of 5% perchloric acid in butoxyethanol which had been developed for the dishing of stainless steels. Difficulties such as preferential thinning of phases and eutectic carbide- matrix interface attack were encountered. These may be reduced if an alternative polishing solution can be found and may be avoided by ion beam thinning to perforation without the use

of a dishing stage, although this would involve much longer thinning times. Chemical thinning may also be possible to decrease the amount of mechanical polishing required for initial reduction of the spark machined discs and hence to lessen the danger of structural damage in specimen preparation.

7.14 The transmission studies were limited to three of the irons examined in the abrasion programme. Thin foils may also be prepared from the other alloys used for wear tests to enable their finer structural features to be investigated.

7.15 Additional TEM work on austenitic matrix irons may be used to determine the effects of composition and condition of the austenite upon its stacking fault and dislocation configurations and upon its work hardening behaviour and its tendency to form strain induced martensite during wear. Further observations of eutectic and secondary carbides may allow a greater understanding of their structures and physical behaviour. The occurrence of matrix cores, structural faulting, domain and grain boundaries and other defects may be considered with respect to composition, solidification and thermal treatments variables.

8.0 CONCLUSIONS.

8.1 The specimen on track type of abrasion test produces conditions of high stress abrasion in that the abrasive particles are crushed at the wearing surfaces.

8.2 In all the irons examined the matrix and the eutectic carbides in the surface regions were distorted in the general wear direction. This caused cracking in the eutectic carbides and lead to material removal by the detachment of the broken carbides from the matrix as well as by the penetration and cutting effects of the abrasive grits.

8.3 Martensitic matrix structures gave higher resistance to abrasion than austenitic or pearlitic structures under the particular testing conditions used. Martensitic 15% Cr - 3% Mo iron had the highest measured resistance to abrasion. Martensitic 10 - 15% Cr irons were more abrasion resistant than martensitic 25 - 30% Cr irons due to the lower carbon martensite produced after destabilisation of the higher chromium irons. Observations of wear damage suggested that removal from the matrix of broken carbides was more likely to occur in the 25% Cr iron than in the 10 - 15% Cr irons.

8.4 Martensitic 5% Cr iron with continuous M_3C carbides gave higher abrasion resistance than 10 - 15% Cr iron without molybdenum. 5% Cr iron may be useful as a cheap abrasion resistant alloy for non-impact service conditions.

8.5 In the irons containing 5% Cr or less which had continuous M_3C type carbides the matrix was removed from the honeycomb of eutectic carbide during abrasion but fractured carbides could retain their positions and were less likely to be removed than the cracked carbides of the discontinuous M_7C_3 type. In the unalloyed white iron the presence of flake graphite resulted in severe local damage in the mottled areas.

8.6 Increases in hardness produced by suitable thermal treatments gave rise to corresponding increases in abrasion resistance for all the heat treated irons with the single exception of the 30% Cr iron. The poor performance of this alloy was explained by the presence of the softer $M_{23}C_6$ carbide in the heat treated structure.

8.7 There is no simple relationship between general hardness or matrix microhardness at the wear surface and abrasion resistance. There may be a correlation between the hardness of a wearing surface and abrasion resistance if the depth of hardening below the worn surface is sufficient to allow adequate support for the eutectic carbides.

8.8 Where matrix support is limited as in the soft ferritic matrix 35% Cr iron severe distortion and cracking of the carbides occurs in the sub-surface layers and abrasion resistance is relatively low.

8.9 All the matrix structures work hardened to some extent at the wear surface. The most significant hardening occurs in austenitic irons but the depth of hardening observed after wear testing was much less than that observed in austenitic balls from production mills.

8.10 The specimen on track test does not give impact conditions and consequently it yields pessimistic results for austenitic matrix irons which rely on impact conditions to achieve sufficient depth of work hardening in their surface layers for abrasion resistance. Such a test is only useful in assessing the wear behaviour of matrices which do not rely on work hardening for abrasion resistance. It may be of some use for wear testing under wet conditions since it is believed that less work hardening of grinding media and liners occurs during wet milling.

8.11 TEM foils for examination at 100 Kv can be prepared from high chromium cast irons with relatively coarse microstructures using a combination of dishing and ion beam thinning. Both the matrix and eutectic and secondary carbide constituents can be successfully thinned in this way.

The following conclusions are based on TEM thin foil observations of the as-cast 30% Cr iron and the heat treated 15% Cr iron.

8.12 Several of the rodlike eutectic M_7C_3 carbides consisted of clusters of smaller diameter rods of hexagonal cross section. Individual crystals of M_7C_3 quite often contained a central core of matrix constituent which in many cases was seen, in transverse sections, to be isolated from the surrounding matrix.

8.13 In the as-cast 30% Cr iron the matrix was essentially austenitic with some transformation to body centred martensite in the eutectic austenite adjacent to eutectic M_7C_3 carbides and in the cores of matrix within the carbides. There was little difference in the Cr : Fe ratios of the matrix cores and the corresponding matrix surrounding the carbides.

8.14 Strain induced martensite formation occurred at the wear surface of the as-cast austenitic 30% Cr alloy and this contributed to the observed increase in microhardness i.e. from 400 to 850 Hv.

8.15 The secondary carbides produced during the destabilisation treatment of the 15% Cr alloy were identified as M_7C_3. The fine pearlite produced during incomplete hardening of this iron was found to be lamellar and not granular.

Additional conclusions based on all TEM observations are given below.

8.16 The secondary carbides produced during the destabilisation of the 30% chromium iron were identified by electron diffraction as $M_{23}C_6$. During the heat treatment of this alloy the original M_7C_3 eutectic carbide partly transformed to $M_{23}C_6$ by an in-situ mechanism. This resulted in duplex "eutectic" carbides consisting of a central core of M_7C_3 fully or partially surrounded by a shell of $M_{23}C_6$. This outer shell contained grain boundaries along which separation may occur during the sub-surface deformation produced by high stress abrasive wear.

8.17 The secondary and eutectic M_7C_3 carbides in the 15% chromium iron and the eutectic M_7C_3 in the 30% chromium iron were all found to contain structural faulting. This gave rise to visible contrast in bright field images and caused streaking in the electron diffraction patterns from these carbides. No evidence of faulting was seen in the $M_{23}C_6$ carbides in the hardened 30% chromium alloy.

8.18 The secondary M_7C_3 carbide particles generally contained only one set of faults but up to a maximum of three sets of faults could be seen in the crystals of eutectic M_7C_3. The fault planes were identified as the three equivalent planes (10.0), ($1\bar{1}$.0) and (01.0) with the Laue zone [00.1] giving zero contrast conditions.

9.0 APPENDIX.

Solution of cubic patterns.

A single crystal electron diffraction pattern is an image of a plane in reciprocal space normal to the electron beam. The points in the two dimensional lattice represent reflections from planes in direct space and these planes all lie in a zone which is defined by the electron beam as zone axis. The solution of a single crystal pattern therefore involves the determination of the indices of the reflections and calculation of the zone axis. Single crystal patterns for austenite (fcc) and ferrite (bcc) were solved as follows.

On the pattern two directions such as OX and OY are drawn from O, the centre of the pattern which represents the undeviated electrons. Along lines OX and OY relection spots lie at equal intervals x and y respectively and other spots will occupy the corners of parallelograms formed as shown in Figure A.1. The pattern is then analysed by measuring

(i) the distances of 3 spots from O i.e. r_1, r_2 and r_3 from which corresponding d spacings can be calculated using

$$d = \frac{\lambda L}{r}$$

and where λL = camera constant.

(ii) the angles θ_1, θ_2 and θ_3 between the reciprocal vectors and hence between the planes producing the diffraction spots which subtend these angles at the origin O.

To perform the above measurements each diffraction pattern was magnified to 2-3x the scale shown in the text. The distances r_1, r_2 and r_3 were determined using the maximum number of reflection spots along each particular direction, e.g. along OX, to give a mean value for r in each case. The corresponding d spacings d_1, d_2, d_3 were calculated and compared with tabulated reference values for austenite and ferrite and the reflections were then assigned possible Miller indices.* These possible indices* were checked using r^2 ratios:

$$\left(\frac{r_1}{r_2}\right)^2, \left(\frac{r_1}{r_3}\right)^2 \text{ and } \left(\frac{r_2}{r_3}\right)^2.$$

These ratios are related to the ratios:

$$\frac{N_1}{N_2}, \frac{N_1}{N_3} \text{ and } \frac{N_2}{N_3}.$$

N is the line number and is given by:

$$N = \left(n^2 h^2 + n^2 k^2 + n^2 l^2\right)$$

where n = order of reflection, and

$\{hkl\}$ = indices of reflecting plane.

For fcc crystals N has values 3, 4, 8, 11, 12, 16, etc. and for bcc crystals N has values 2, 4, 6, 8, 10, 12, etc.

Each spot was then given definite indices such that by addition $h_1 + h_2 = h_3$, $k_1 + k_2 = k_3$ and $l_1 + l_2 = l_3$. This satisfies the vector addition $r_1 + r_2 = r_3$

(* "Possible" refers to a family of indices e.g. $\{112\}$ without deciding whether the values of hkl are positive or negative).

The definite* indices were confirmed by comparing the measured angles θ_1, θ_2 and θ_3 with values calculated from the corresponding pairs of indices, i.e. $(h_1k_1l_1)$ and $(h_2k_2l_2)$ using the relationship:

$$\cos\theta = \frac{h_1h_2 + k_1k_2 + l_1l_2}{\sqrt{\left[(h_1^2 + k_1^2 + l_1^2)\,(h_2^2 + k_2^2 + l_2^2)\right]}}$$

This enabled the measured and calculated or reference values for angles θ and d spacings to be presented in simple tabular form in the text for each pattern considered. The zone axis [uvw] for each pattern was then conventionally determined as the vector upwards from the plane of the paper using the equations:

$$u = k_1l_2 - k_2l_1$$

$$v = l_1h_2 - l_2h_1$$

$$w = h_1k_2 - h_2k_1$$

for any pair of indices $(h_1k_1l_1)$, $(h_2k_2l_2)$ where the reflection spot for $(h_1k_1l_1)$ is in the clockwise sense to that of $(h_2k_2l_2)$. All the indices in the pattern then should satisfy the condition:

$$hu + kv + lw = 0$$

For the polycrystalline type ring patterns obtained from the matrix at the wear surfaces interplanar (d) values were determined from measurements of ring diameter.

(* "Definite" refers to specific index values e.g. $(\bar{2}11)$, (121), $(1\bar{1}2)$ or $(\bar{1}12)$ etc.).

Solution of carbide patterns.

The patterns for the hexagonal M_7C_3 and the cubic $M_{23}C_6$ carbides were analysed as outlined above. For the hexagonal patterns r^2 and N ratios could not be used and spots were indexed using table A.1. by comparison of calculated and reference d values. Because the d spacing of $\{01.0\}$ planes is large (12.11 Å) the corresponding r value was small and for these reflections identification was based on higher orders i.e. for (03.0), (04.0), etc. Although the presence of streaking caused some problems, in most of the patterns obtained definite reflections could be indentified along the streaked lines. Measured angles between indentified reflections were compared with calculated angles using the equation:

$$\cos \phi = \frac{h_1h_2 + k_1k_2 + \frac{1}{2}(h_1k_2 + k_1h_2) + \frac{3}{4}\frac{a^2}{c^2} l_1l_2}{\sqrt{\left[(h_1^2 + k_1^2 + h_1k_1 + \frac{3}{4}\frac{a^2}{c^2} l_1^2)(h_2^2 + k_2^2 + h_2k_2 + \frac{3}{4}\frac{a^2}{c^2} l_2^2)\right]}}$$

where ϕ = angle between $(h_1k_1l_1)$ and $(h_2k_2l_2)$.

The ratio $\frac{c}{a}$ for M_7C_3 was taken as 0.32.

A zone axis was assigned to each pattern in order to satisfy the relationship:

$HU + KV + LW = 0$ for Miller indices

$hu + kv + it + lw = o$ for Miller-Bravais indices

The equation $UVW = (K_1L_2 - K_2L_1): (L_1H_2 - L_2H_1): (H_1K_2 - H_2K_1)$ was applied to (HK.L) indices with the redundant figure - (H + K) omitted to give a zone axis in Miller form.

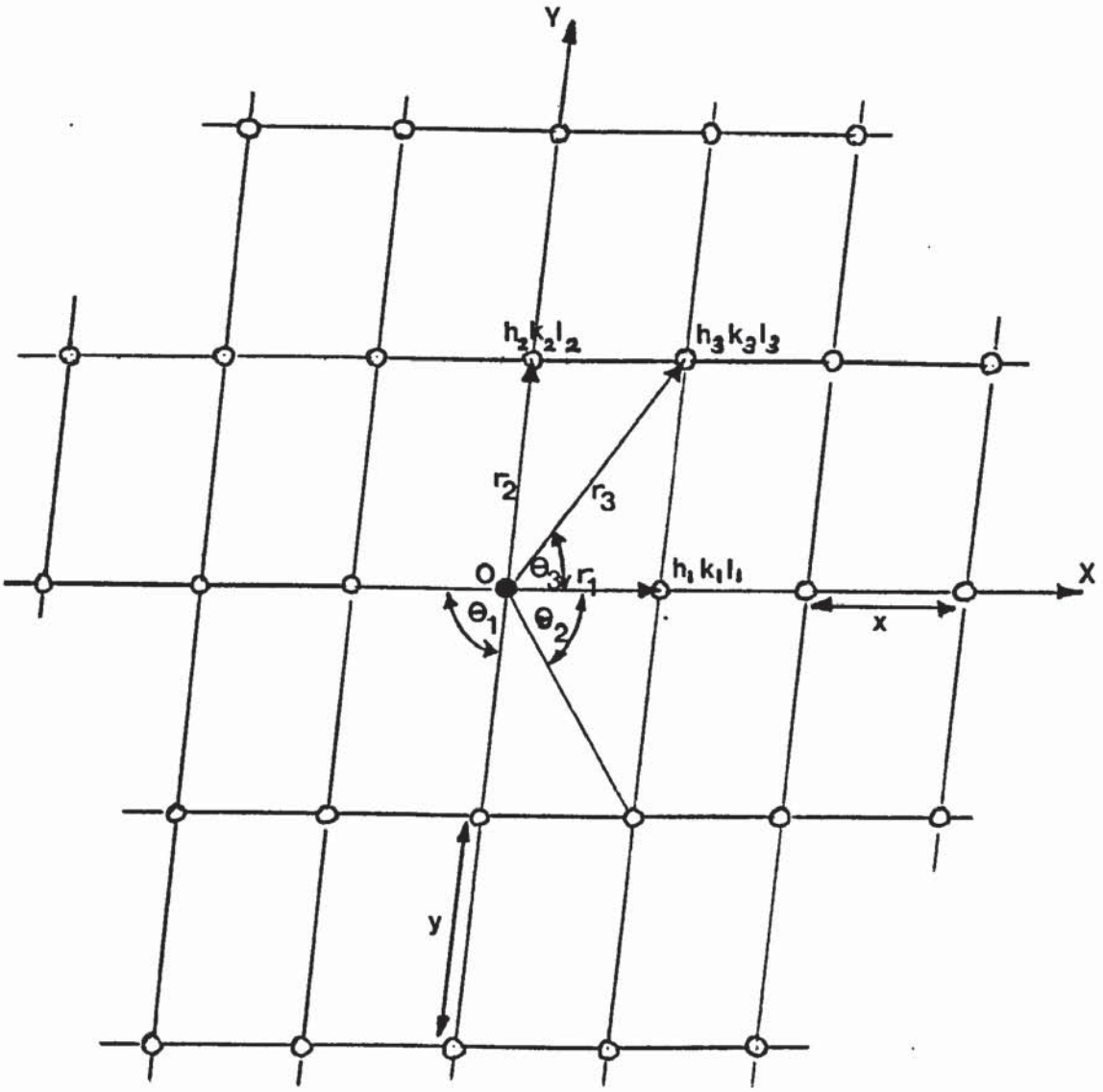

Figure A.1 Representation of a spot pattern.

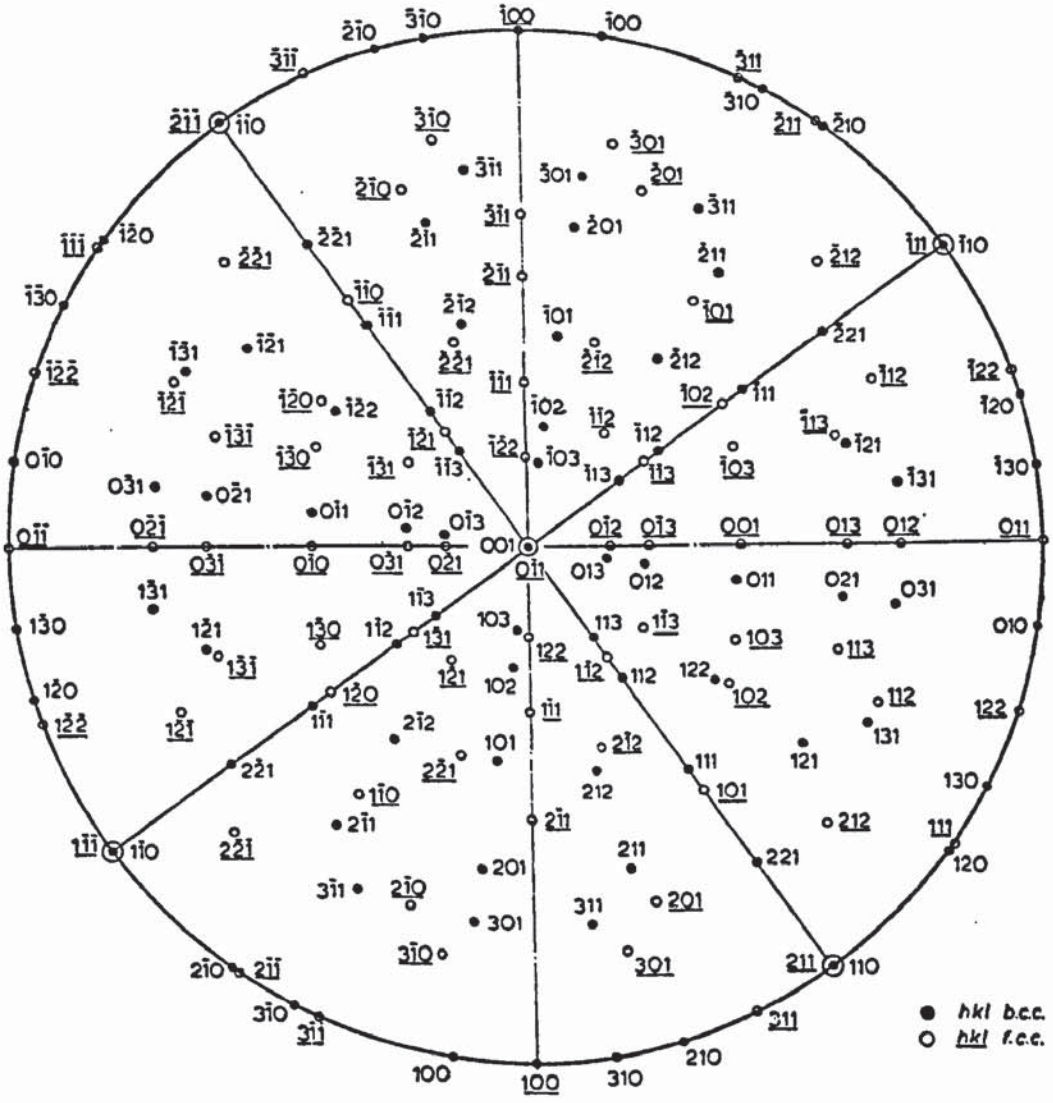

Stereographic projection representing the N–W orientation relationship between body- and face-centred cubic materials.
(001) b.c.c. //(0$\bar{1}$1) f.c.c.
($\bar{1}$10) b.c.c. //($\bar{1}$11) f.c.c.
(110) b.c.c. //(211) f.c.c.

After Andrews et Al (244).

Figure A.2

Table A1

Interplanar spacings of $M_7C_3=(Cr,Fe)_7C_3$

Crystal structure: Pseudo-hexagonal

Unit cell: $a_0 = 13{\cdot}982_0$ Å, $c_0 = 4{\cdot}506_3$ Å

hk.l	*d*-spacing (Å)	*hk.l*	*d*-spacing (Å)	*hk.l*	*d*-spacing (Å)	*hk.l*	*d*-spacing (Å)	*hk.l*	*d*-spacing (Å)
00.1	4·5065	0,10.0	1·2109	19.0	1·2693	2,10.0	1·0874	46.0	1·3890
00.2	2·2532	0,10.1	1·1694	19.1	1·2218	2,10.1	1·0571	46.1	1·3274
00.3	1·5022	0,10.2	1·0666	19.2	1·1059	2,10.2	0·9793	46.2	1·1824
00.4	1·1266			19.3	0·9695			46.3	1·0198
		0,11.0	1·1008			2,11.0	0·9987		
01.0	12·1088	0,11.1	1·0694	1,10.0	1·1493	2,11.1	0·9751	47.0	1·2556
01.1	4·2235	0,11.2	0·9891	1,10.1	1·1137			47.1	1·2095
01.2	2·2152			1,10.2	1·0238	33·0	2·3303	47.2	1·0968
01.3	1·4907	0,12.0	1·0091			33.1	2·0700	47.3	0·9634
01.4	1·1218	0,12.1	0·9847	1,11.0	1·0500	33.2	1·6199		
				1,11.1	1·0226	33.3	1·2626	48.0	1·1442
02.0	6·0544	11.0	6·9910	1,11.2	0·9517	33.4	1·0143	48.1	1·1090
02.1	3·6150	11.1	3·7877					48.2	1·0202
02.2	2·1117	11.2	2·1446	1,12.0	0·9664	34.0	1·9907		
02.3	1·4580	11.3	1·4686			34.1	1·8209	49.0	1·0500
02.4	1·1076	11.4	1·1123	22.0	3·4955	34.2	1·4919	49.1	1·0226
				22.1	2·7620	34.3	1·1991	49.2	0·9517
03.0	4·0363	12.0	4·5767	22.2	1·8939	34.4	0·9805		
03.1	3·0066	12.1	3·2111	22.3	1·3801			4,10.0	0·9695
03·2	1·9674	12.2	2·0215	22.4	1·0723	35.0	1·7298		
03.3	1·4078	12.3	1·4273			35.1	1·6149	55.0	1·3982
03.4	1·0851	12.4	1·0940	23.0	2·7779	35.2	1·3721	55.1	1·3354
				23.1	2·3648	35.3	1·1342	55.2	1·1881
04.0	3·0272	13.0	3·3584	23.2	1·7500			55.3	1·0235
04.1	2·5129	13.1	2·6929	23.3	1·3214	36.0	1·5256		
04.2	1·8075	13.2	1·8711	23.4	1·0440	36.1	1·4450	56.0	1·2693
04.3	1·3456	13.3	1·3712			36.2	1·2633	56.1	1·2218
04.4	1·0559	13.4	1·0681	24.0	2·2883	36.3	1·0704	56.2	1·1059
				24.1	2·0404			56.3	0·9695
05.0	2·4218	14.0	2·6423	24.2	1·6056	37.0	1·3623		
05.1	2·1332	14.1	2·2794	24.3	1·2558	37.1	1·3041	57·0	1·1598
05.2	1·6496	14.2	1·7145	24.4	1·0108	37.2	1·1658	57.1	1·1232
05.3	1·2765	14.3	1·3059			37.3	1·0091	57.2	1·0312
05.4	1·0215	14.4	1·0364	25.0	1·9390				
				25.1	1·7811	38.0	1·2295	58.0	1·0661
06.0	2·0181	15.0	2·1748	25.2	1·4697	38.1	1·1861	58.1	1·0375
06.1	1·8419	15.1	1·9586	25.3	1·1875	38.2	1·0793	58.2	0·9637
06.2	1·5033	15.2	1·5648	25.4	0·9741	38.3	0·9514		
06.3	1·2050	15.3	1·2360					59.0	0·9854
06.4	0·9837	15.4	1·0004	26.0	1·6792	39.0	1·1195	59.1	0·9627
				26.1	1·5735	39.1	1·0864		
07.0	1·7298	16.0	1·8466	26.2	1·3464	39.2	1·0025	66.0	1·1652
07.1	1·6149	16.1	1·7087	26.3	1·1196			66.1	1·1281
07.2	1·3721	16.2	1·4282			3,10.0	1·0271	66.2	1·0350
07.3	1·1342	16.3	1·1653	27.0	1·4793	3,10.1	1·0014		
		16.4	0·9618	27.1	1·4055			67.0	1·0745
08.0	1·5136			27.2	1·2366	44.0	1·7478	67.1	1·0452
08.1	1·4348	17.0	1·6038	27.3	1·0540	44.1	1·6295	67.2	0·9699
08.2	1·2564	17.1	1·5110			44.2	1·3810		
08.3	1·0662	17.2	1·3066	28.0	1·3212	44.3	1·1392	68.0	0·9953
		17.3	1·0964	28.1	1·2678			68.1	0·9719
09.0	1·3454			28.2	1·1397	45 0	1·5504		
09.1	1·2892	18.0	1·4172	28.3	0·9921	45.1	1·4660	77.0	0·9987
09.2	1·1552	18.1	1·3519			45.2	1·2772	77.1	0·9751
09.3	1·0022	18.2	1·1997	29.0	1·1931	45.3	1·0788		
		18.3	1·0309	29.1	1·1534				
				29.2	1·0544				

After Andrews et Al (244)

Table A2

Interplanar spacings of an $M_{23}C_6$ carbide

Crystal structure: Face-centred cubic
Unit cell: $a_0 = 10{\cdot}621_4$ Å

hkl	*d*-spacing (Å)	*hkl*	*d*-spacing (Å)	*hkl*	*d*-spacing (Å)	*hkl*	*d*-spacing (Å)
111	6·132	006, 244	1·770	337	1·298	139	1·113
002	5·311	026	1·679	028, 446	1·288	448	1·084
022	3·755	335	1·620	228, 066	1·252	557, 177, 339	1·068
113	3·203	226	1·601	157, 555	1·227	00,10, 068	1·062
222	3·066	444	1·533	266	1·218	02,10, 268	1·042
004	2·655	117, 155	1·487	048	1·188	159, 377	1·023
133	2·437	046	1·473	119, 357	1·166	22,10, 666	1·022
024	2·375	246	1·419	248	1·159		
224	2·168	137, 355	1·383	466	1·132		
333, 115	2·044	008	1·328				
044	1·878						
135	1·795						

Table A3

Interplanar spacings of an M_6C carbide

Crystal structure: Face-centred cubic (diamond type)
Unit cell: $a_0 = 11{\cdot}082_3$ Å

hkl	*d*-spacing (Å)	*hkl*	*d*-spacing (Å)	*hkl*	*d*-spacing (Å)	*hkl*	*d*-spacing (Å)
111	6·398	006, 244	1·847	028, 446	1·344	557, 177, 339	1·114
002	5·541	026	1·752	228, 066	1·306	00,10, 068	1·108
022	3·918	335	1·690	157, 555	1·280	02,10, 268	1·087
113	3·341	226	1·671	266	1·271	159, 377	1·071
222	3·199	444	1·600	048	1·239	22,10, 666	1·066
004	2·771	117, 155	1·552	119, 357	1·217	359	1·034
133	2·542	046	1·537	248	1·209	04,10, 468	1·029
024	2·478	246	1·481	466	1·181	24,10	1·012
224	2·262	137, 355	1·443	139	1·161		
333, 115	2·133	008	1·385	448	1·131		
044	1·959	337	1·354				
135	1·873						

Table A4

Interplanar spacings of α-iron

Crystal structure: Body-centred cubic
Unit cell: $a_0 = 2{\cdot}866_4$ Å

hkl	*d*-spacing (Å)	*hkl*	*d*-spacing (Å)	*hkl*	*d*-spacing (Å)	*hkl*	*d*-spacing (Å)
011	2·027	013	0·906	114, 033	0·676	233	0·611
002	1·433	222	0·828	024	0·641	224	0·585
112	1·170	123	0·766			015, 134	0·562
022	1·013	004	0·717				

Table A5

Interplanar spacings of γ-iron

Crystal structure: Face-centred cubic
Unit cell: $a_0 = 3{\cdot}585_2$ Å

hkl	*d*-spacing (Å)	*hkl*	*d*-spacing (Å)	*hkl*	*d*-spacing (Å)	*hkl*	*d*-spacing (Å)
111	2·070	133	0·823	044	0·634	335	0·547
002	1·793	024	0·802	135	0·606	226	0·541
022	1·268	224	0·732	006, 244	0·598	444	0·518
113	1·081	333, 115	0·690	026	0·567	117, 155	0·502
222	1·035						
004	0·896						

After Andrews et Al (244)

Table A6. Interplanar Spacings of Hexagonal ε-Iron.

$a = 2.54$ Å, $c = 4.14$ Å, $c/a = 1.63$

hkl		d Å
0001	F	4.14
$10\bar{1}0$		2.20
0002		2.07
$10\bar{1}1$		1.945
$10\bar{1}2$		1.509
0003	F	1.38
$11\bar{2}0$		1.27
$11\bar{2}1$	F	1.215
$10\bar{1}3$		1.17
$20\bar{2}0$		1.10
$11\bar{2}2$		1.083
$20\bar{2}1$		1.063
0004		1.035
$20\bar{2}2$		0.974
$10\bar{1}4$		0.938
$11\bar{2}3$	F	0.935
$20\bar{2}3$		0.860
$21\bar{3}0$		0.833
0005	F	0.830

Reflections marked F are forbidden by the structure factor but may occur by double diffraction. (After Kelly (262)).

Table A7

CALIBRATION OF THE JEOL JEM 100B TRANSMISSION ELECTRON MICROSCOPE AT 100 KV ACCELERATING VOLTAGE

Registered Magnification (K)	True Magnification (K)	Rotate Diffraction Pattern Relative to Micrograph
6	1.84	-
8	2.68	-
10	3.45	83° anticlockwise
15	4.98	88° " "
17	5.75	92° " "
20	6.25	62° " "
25	8.43	58.5° " "
30	9.96	56.0° " "
35	11.5	52° " "
40	13.0	48° " "
50	16.1	42° " "
60	19.2	35° " "
70	22.2	28° " "
80	25.0	22° " "
90	29.5	14° " "
100	32.6	7° " "
120	37.6	71.5° " "
150	45.0	65° " "
200	59.0	-
50 Diffraction Setting	16.1	17° clockwise

Dept. of Metallurgy and Materials
University of Aston
April 1979

10.0 REFERENCES

1. Abrasion resistant cast irons.
   Durman R.W.
   British Foundryman, 1979, Anniversary Supplement, 159-163.

2. Abrasion resistant high chromium white cast irons
   Fairhurst W.A. Rohrig K.
   Foundry Trade Journal 1974, 136, 685-698.

3. The use of cast iron under conditions of abrasive, dry and lubricated wear.
   Angus.H.T.
   BCIRA Journal 1962, 10, 80-103.

4. The measurement of wear resistance.
   Avery H.S.
   Wear 1961, 4, 427-449.

5. A review of two body abrasive wear.
   Moore M.A.
   Wear 1974, 27, 1-17.

6. A study of abrasive wear under three body conditions.
   Rabinowicz E.
   Wear 1961, 4, 345-355.

7. Abrasive wear of metals.

Norman T.E.

Ch 13, Handbook of mechanical Wear, 277-314.

Editors: Lipson C & Colwell L.V.

University of Michigan, 1961.

8. Selection and performance of hard facing alloys.

Farmer H.N.

Proceedings of Materials for the Mining Industry, Vail, Colorado. July 1974, 85-91.

9. The abrasion resistance of metals.

Haworth R.D.

Transactions American Society for metals 1949, 41, 819-869.

10. Wear resistance.

Avery H.S.

Ch 14, Handbook of Mechanical Wear, 315-352.

Editors: Lipson C & Colwell L.V.

University of Michigan, 1961.

11. Resistance of metals to wear by abrasion

Khruschev M.M.

Proc. Conf. on Lubrication and Wear, Institution of Mechanical Engineers, London, October 1957.

12. Ferrous castings for abrasion resistance.
Dunlop G.E. and Fellows J.A.
American Brake Shoe Company, New York, 1952.

13. Construction and evaluation of a versatile abrasive wear testing apparatus.
Muscara J and Sinnott M.J.
Metals Engineering Quarterly, 1972, 12, 21-32

14. Development and use of abrasion testing at BCIRA
Boyes J.W.
BCIRA Journal, 1967, 15, 572-585.

15. Erosive wear of metals by sand erosion.
Stauffer W.A.
Metal Progress, 1956, 69, 102-107.

16. Abrasive wear.
Report of iron and steel Technical Committee, J965
Society of Automotive Engineers, New York, August 1966.

17. The friction and lubrication of solids (pts 1 and 2).
Bowden F.P. and Tabor D.
Claverdon Press, Oxford, Part 1 (1954), Part 2 (1964).

18. The wear of metals by hard abrasives.
Richardson R.C.D.
Wear, 1967, 10, 291-309.

19. A theory of friction and wear during the abrasion of metals.
Goddard J and Wilman H.
Wear, 1962, 5, 114-135.

20. The abrasion of metals.
Mulhearn T.O. and Samuels L.E.
Wear, 1962, 5, 478-490.

21. A study of erosion phenomena.
Bitter J.G.A.
Part 1, Wear, 1963, 6, 5-21
Part 2, Wear, 1963, 6, 169-190.

22. Erosion of surfaces by solid particles.
Finnie I.
Wear, 1960, 3, 87-103.

23. Principles of abrasive wear.
Khruschov M.M.
Wear, 1974, 28, 69-88.

24. How microstructure affects abrasive wear resistance.
Zum Gahr K.H.
Metal Progress, 1979, 116, 46-52.

25. Work hardening in relation to abrasion resistance.
Avery H.S.
Proceedings of Materials for the Mining Industry.
Colorado, July, 1974, 43-78.

26. The hardness of metals.
Tabor D.
Oxford University Press, New York, 1951.

27. The science of hardness testing and its research applications.
Westbrook J.H. and Conrad H.
American Society for Metals, Ohio, 1973.

28. The mathematical theory of plasticity.
Hill R.
Clarendon Press, Oxford, 1950.

29. A new approach to plasticity and its application to blunt two dimensional indenters.
Shaw M.C. and De Salvo G.J.
Trans. ASME, Journal of Engineering for Industry, 1970, 92, 469-479.

30. Plastic flow beneath a blunt axisymmetric indenter.
As (29), pp 480-494.

31. Abrasive wear by soil.

Moore M.A.

Tribology International, 1975, 8, 105-110.

32. Indentation fracture: principles and applications.

Lawn B.R. and Wilshaw R.

Journal of Materials Science, 1975, 10, 1049-1081.

33. Microfracture beneath point indentations in brittle solids.

Lawn B.R. and Swain M.V.

As (32), pp 113-136.

34. On the mode of chipping fracture in brittle solids.

Lawn B.R., Swain M.V. and Phillips K.

As (32), pp1236-1239.

35. Equilibrium penny-like cracks in indentation fracture.

Lawn B.R. and Fuller E.R.

As (32), pp 2016-2024.

36. The influence of sample preparation on toughness testing of cemented carbides.

Exner H.E.

Trans. Met. Soc. AIME, 245, 677-683.

37. Abrasive wear resistance of ferritic materials.

Moore M.A.

Wear, 1974, 28, 59-68.

38. The abrasion resistance of some hardened and tempered carbon steels.
Larsen-Badse J.
Trans. AIME, 1966, 236, 1461-1466.

39. Influence of structure on abrasion resistance of 1040 steel.
Larsen-Badse J. and Matthew K.G.
Wear, 1969, 14, 199-206.

40. Fracture of carbides in the abrasive wear of alloy steels.
Popov V.S.
Russian Engineering Journal 1969, 49, 78-81.

41. Wear of metals by relatively soft abrasives.
Richardson R.C.D.
Wear, 1968, 11, 245-275.

42. Effect of structure on the wear resistance of white cast irons.
Garber M.E., Levi L.I. et Al.
Metal Science & Heat Treatment 1968, 11, 895-898.

43. Abrasive wear of tungsten carbide - cobalt composites. II. Wear mechanisms.
Blombery R.I., Perrot C.M. & Robinson P.M.
Materials Science & Engineering 1974, 13, 93-100.

44. Martensitic alloy cast iron development.
Harrison G.L. and Dixon R.H.T.
British Foundryman 1962, 55, 164-176.

45. Optimising abrasion resistance and toughness in steels and irons for the mining industry.
Diesburg P.E. and Borik F.
Proceedings of Materials for the Mining Industry.
Vail, Colorado, July 1974, 15-41.

46. The wear of metal shares in agricultural soils.
Richardson R.C.D.
Ph.D Thesis London, 1969.

47 Research on wear of metals.
Khruschov M.M. and Babichev M.A.
ASME Translation 12, 1958, 25-38.

48. Corrosion inhibitors reduce ball wear in grinding sulphide ore.
Hoey G.R., Dingley W. & Freeman C.
CIM Bulletin 1975, 68, 120-123.

49. Corrosion control in Canadian sulphide ore mines and mills.
Hoey G.R. and Dingley W.
CIM Bulletin 1971, 64, 62-69

50. Corrosive and erosive wear of metals in mineral slurries.
Lui A.W. and Hoey G.R.
Canadian Metallurgical Quarterly 1973, 12, 185-190

51. Mechanisms of corrosive wear of steel balls in grinding hematite ore.
Lui A.W. and Hoey G.R.
Canadian Metallurgical Quaterly 1975, 14, 281-285

52. Metal wear in crushing and grinding.
Bond F.C.
Chemical Engineering Progress 1964, 60, 90-93

53. Nickel alloys in the mining and mineral processing industries.
Renof S.M.
Australasian Corrosion Engineering 1970, 14, 7-28

54. Dry grinding at the Wabush mines pellet plant
Sobering A. and Carlson G.N.
CIM Bulletin 1971, 64, 38-42

55. Corrosion principles for the mining engineer.
Steigerwald R.F.
Proceedings of Materials for the Mining Industry,
Vail, Colorado, July 30,31 1974, 93-104.

56. Examination of a damaged chilled cast iron cam follower by SEM.
Lamb A.D.
BCIRA Journal 1970, 18, 545-550

57. Effect of a reactive environment on the Hertzian strength of brittle solids.
Langitan F.B. and Lawn B.R.
J Applied Physics 1970, 41, 3357.

58. Comparative study of the fracture of various silica modifications.
Swain M.V., Williams J.S., Lawn B.R., Beek J.J.H.
Journal of Material Science 1973, 8, 1153.

59. The role of work hardening in wearing processes.
Durman R.W.
Bradley and Foster Research Report RD67/26 September 1967.

60. High Cr cast iron for use at elevated temperatures.
Boyes J.W.
Iron and Steel 1966, 39, 102-109.

61. High Cr-Mo alloy iron rolls
Dodd J.
Climax Molybdenum, Denver, Colorado 1975.

62. Hot hardness characteristics of high Cr cast irons
Boyes J.W.
BCIRA Journal 1964, 12, 54-63

63. Hot hardness of hard facing alloys.
Avery H.S.
Welding Journal 1950, 29, 552-576.

64. The wear testing of hot work die steels.
Aston J.L., Hopkins A.D., Kirkham K.E.
Metallurgia and Metal Forming 1972, 39, 46-50

65. Gouging abrasion test for materials used in ore and rock crushing. Part I.
Borik F. and Sponsellor D.L.
Journal of Materials 1971, 6, 576-589.

66. Frictional heating during abrasive wear.
Moore M.A.
Wear 1971, 17, 15-58.

67. Requirements of iron castings subject to wear and abrasion.
Lamb A.D.
Conference papers. Engineering Properties and Performance of Iron Castings, University of Loughborough April 1970, 181-205.

68. Wear of cast iron.
Lamb A.D.
British Foundryman 1976, 69, 279-289.

69. Using tests to define the influence of metallurgical variables on abrasion.
Borik F.
Metals Engineering Quarterly 1972, 12, 33-39

70. Surface protection against wear and corrosion.
Avery H.S.
Ch 3, ASM Publication 1954, 22-24.

71. Gouging abrasion test for materials used in ore and rock crushing. Part II
Borik F. and Scholz W.G.
Journal of Materials 1971, 6, 590-605

72. Gouging wear test and scratching abrasion results.
Abrasion Resistant News June 1972, Climax Molybdenum.

73. Properties of cast iron grinding balls.
Farge J.C. and Barclay G.A.
Metals Engineering Quarterly 1975, 15, 41-46.

74. How to select Cr-Mo steels for ball and rod mill liners.
Norman T.E.
Eng. and Mining Journal 1957, 158, 102-106.

75. Study of ball wear using radioactive tracer techniques.
Wesner A.L.
Trans. AIME 1960, 217, 429-434.

76. Relative wear rates of grinding balls in production mills.
Norquist D.E. and Moeller J.E.
Mining Engineering 1950, 187, 712-714.

77 Abrasive wear of ferrous materials in Climax operations.
Norman T.E. and Hall E.R.
Evaluation of Wear Testing ASTM, STP 446 (1969), 91-114.

78. The wear of metallic materials by soil-practical phenomena.
Richardson R.C.D.
J. Agricultural Eng. Res. 1967, 12, 22-39

79. Wear resistant manganese cast iron.
Lambert B., Poyet P., Dancoisne P.L.
British Foundry 1975, 68, 179-183.

80. Evaluating wearing performance under abrasive and adhesive sliding.
Stahli G. and Beuler H.
Sulzer Technical Review 1976, 58, 33-40.

81. Rubber wheel abrasion test.
Borik F.
Society of Automotive Eng. Conference, Milwaukee.
September 1970, Reprint 700687, 10pp.

82. Field and laboratory abrasion tests on plowshares.
Stolk D.A.
AS (81) Reprint 700690, 8pp.

83. Abrasive wear resistance of chromium alloys in relation to composition and structure.
Shabuev et Al
Russian Castings Production 1972, 3, 110-111.

84. Low stress (scratching) abrasion, gouging and grinding abrasion.
Abrasion Resistant News, June 1974, Climax Molybdenum 16 pp.

85. Abrasive wear behaviour of alloy cast irons.

Pearce J.T.H.

Transfer Thesis, University of Aston, November 1978.

86. Special cast irons.

Barton R.

BCIRA Journal 1960, 8, 857-882.

87. Chill and mottle formation in cast iron.

Boyes J.W. and Fuller A.G.

BCIRA Journal 1964, 12, 424-472

88. Influence of chromium on chill and mottle formation.

Boyes J.W.

BCIRA Journal 1961, 9, 499

89. Progress and problems in understanding of cast irons.

Morrogh H.

British Foundryman 1964, 57, 297-307.

90. The application of alloyed white irons in crushing and grinding processes.

Durman R.W.

British Foundryman 1976, 69, 141-149.

91. Das system Fe-Cr_7C_3-Fe_3C

Tofaute W., Kuttner C., Buttinghaus A.

Archiv Fur Eisenhuttenwesen 1935-6, 9, 607-617.

92. Iron-Carbon-Chromium system.
Bungardt K., Kunze E., Horne E.
Archiv Fur Eisenhuttenwesen 1958, 29, 193-203

93. C-Cr-Fe liquidus surface.
Griffing N.R., Forgeng W.D., Helay G.
Trans AIME 1962, 224, 148-159.

94. The austenite liquidus surface and constitutional diagram for the Fe-Cr-C metastable system.
Jackson R.S.
J1S1, 1970, 204, 163-167.

95. Fe-Cr-C system at 870°C
Woodyatt L.R. and Krauss G.
Met. Transactions 1976, 7A, 983-989.

96. Forgeng W.D. and Forgeng W.D. Jr.
Metals Handbook V8, 402-404, ASM Metals Park, Ohio.

97. Thermodynamics of the carbides in the system Fe-Cr-C.
Benz R., Elliott J.F., Chipman J.
Met. Transactions 1974, 5, 2235-2240.

98. A study of the solidification process in grey and white irons.
Fuller A.G. and Hughes I.C.H.
BCIRA Journal, 1958, 7, 288-298.

99. Eutectic cells in cast iron.
Merchant H.D.
Trans AFS 1962, 70, 973-992.

100. The structure of White iron eutectic.
Hillert M and Steinhauser H.
Jernkontorets Annaler 1960, 144, 520.

101. A relationship of microstructure to mechanical properties of white irons.
Williams W.J.
BCIRA Journal 1953, 5, 132-134

102. Eutectic structure in white cast iron.
Rickard J and Hughes I.C.H.
BCIRA Journal 1961, 9, 11-25.

103. The iron, iron carbide eutectic.
Pearce K and Gill D.
Iron and Steel 1969, 42, 158-160

104. Choice of appropriate compositions for Cr-Mo white irons.
Maratray F.
Climax Molybdenum Co. ,1971, 4 pp.

105. Factors affecting the structure of Cr-Mo white irons.
Maratray F. and Nanot R.V.
Climax Molybdenum Co. ,1971, 32 pp.

106. Basic metallurgical concepts and the mechanical testing of some abrasion resistant alloys.
Durman R.W.
Foundry Trade Journal 1973, 134, 645-651.

107. Metallurgical and production aspects of high Cr irons for abrasion resisting applications.
Jackson R.S.
British Foundryman 1974, 67, 34-41.

108. The distribution of Cr between carbide and matrix in Fe-C-Cr alloys.
Ballinger J. ,Hughes I.C.H. & Mulvey T.
BCIRA Journal 1960, 8, 232-237.

109. Experiments concerning as-cast grain size in 30% Cr irons.
Rickard J.
BCIRA Journal 1960, 8, 200-216.

110. Influence of grain size and stripping time on the incidence of hot tearing in white iron castings.
Twitty M.D.
BCIRA Journal 1960, 8, 844-856.

111. Nature and causes of hot tears in white iron sand castings.
Bryant M.D.
BCIRA Journal 1966, 14, 264-289.

112. Mould coatings to prevent hot checking in malleable iron castings.
Bryant M.D. and Moore A.
British Foundryman 1971, 64, 215-229.

113. Modification of grain structures of chromium irons by use of mould coatings and ladle additions.
Moore A.
BCIRA Journal 1971, 19, 469-472.

114. High chromium irons for crushing and grinding machinery.
Dodd J. and Jackson R.S.
Metallurgia 1967, 76, 107-110

115. Cr-Mo white cast irons for abrasive applications.
Fairhurst W and Stolk D.A.
Foundry Trade Journal, 1972, 132, 401-408

116. Cr-Mo white cast irons for abrasive applications.
Fairhurst W.
BCIRA Journal 1970, 18, 503-511.

117. Powder welding.
Westwood C.G. and Lamb A.D.
BCIRA Journal 1966, 14, 453-474.

118. Abrasion resistant cast iron.
British Standards Institution, London, Parts 1,3 - 1974,
Part 2 - 1972.

119. Microstructure, hardness and abrasion resistance of as-cast 17.5% Cr irons.
Gundlach R.B.
Trans AFS 1974, 82, 309-316.

120. Alloyed abrasion and wear resisting white irons.
Maratray F.
B.C.I.R.A. Conference Proceedings.
University of Warwick, April 1979.

121. The production of Ni-Hard martensitic white cast iron.
International Nickel Ltd. 1963, London, 57 pp.

122. Electric furnace melting and production of abrasion resistant steels and irons.
Fisher G.A. and Woodling J.H.
21st Annual Electric Furnace Conf, Chicago, Dec. 4th, 1963.

123. Isothermal transformatiom characteristics on direct cooling of alloyed white iron.
Rote F.B., Conger G.A., De Longe K.A.
Trans AFS 1951, 59, 509-521.

124. Copper alloyed white iron.
Dilewlijins J. and Bromage K.
Foundry Trade Journal 1969, 126, 3-11

125. New wear resistant iron.
Farge J.C.T., Chollet P., Yernaux J.
Foundry Trade Journal 1971, 130, 319-326

126. Effects of heat treatment upon the impact fatigue life of Ni-Hard grinding balls.
Dixon R.H.T.
JISI 1961, 195, 40-48

127. Ni-Cr white irons for abrasion service.
Provias P.J.
Canadian Mining and Met. Bulletin 1965, 58, 923-930.

128. Ni-Hard v Abrasion.
Whitelaw R.B.
IBF (Australian Branch) Convention Proceedings
1959, 10, 57-75.

129. Martensitic white irons for abrasion resistant castings.
Norman T.E., Solomon A., Doane D.V.
Trans AFS 1959, 67, 242-256.

130. Heat treated martensitic white irons.
Fraser W.W.
Report C6-17-2, National Metal Congress, Chicago,
Oct.-Nov. 1966.

131. 15% Cr/Ni/Mo Martensitic white cast irons for abrasion resistant applications.
Cox G.J.
Foundry Trade Journal 1974, 136, 31-38

132. Structure of 15% Cr cast iron alloyed with up to 5% Mn or V.
Stefanescu et al.
AFS International Cast Metals J. 1976, 1, 19-30

133. Austenite transformation kinetics and hardenability of heat treated 17.5% Cr white irons.
Cias W.W.
Trans AFS 1974, 82, 317-328.

134. Fracture toughness of a series of high Cr alloys.
Durman R.W.
Ph.D. Thesis, Univ. of Aston. Aug 1970.

135. Effect of heat treatment on hardness and microstructure of 30% Cr irons.
Boyes J.W.
BCIRA Journal 1960, 8, 726-741.

136. Effect of cobalt in high Cr irons.
Allen J.K.
Unpublished work at Bradley and Foster Ltd.

137. Kamaras L. and Korsnak P.
Proceeding IX, Congress on heat treatment, Bratislava 1972, 81-90.

138. Room and elevated temperature mechanical properties of 30% Cr irons.
Boyes J.W.
BCIRA Journal 1963, 11, 715-731.

139. Fracture toughness of hard high speed steels, Tool steels and white irons.
Erikson K.
Scandinavian J of Metallurgy 1973, 2, 197-203.

140. Fracture toughness tests for abrasion resistant white irons using compact specimens.
ASTM STP 559, 1974, 3-14.

141. Fracture toughness of Cr cast irons.
Diesburg D.E. and Rohrig K.
Giesserei 1976, 63, 25-31.

142. Effect of forging on the properties of white iron castings.
Ensor T.
BCIRA Journal 1968, 16, 580-592.

143. Development of ultrafine superplastic structures in white cast irons.
Wadsworth J. et Al
Materials In Eng. Applications, 1979, 1, 143-153.

144. Wear characteristics of metals.
Eyre T.S.
Tribology International 1976, 9, 203-212.

145. Wear of steel during rubbing against loose powder abrasive.
Serpik N.H. and Kantor M.M.
Friction and Wear in machinery 1965, 19, 28.

146. Designing with high strength steel castings.
Climax Molybdenum Co., 171 pp.

147. Steel grinding media used in the United States and Canada.
Nass D.E.
Proceedings of Materials for Mining Industry, Vail, Colorado. July 1974, 173-183.

148. The properties and applications of Mo alloy steel castings.
Jackson W.J.
Climax Molybdenum Co, p12-15.

149. Development of IN 646, a cast wear resistant air hardening Steel.
Cox G.J.
Foundry Trade Journal 1975, 139, 633-658

150. Melting practice, heat treatment and properties of Hadfield Mn steel.
Farrar C.W.
21st Annual Electric Furnace Conference, Chicago, Dec. 4th 1963.

151. Manganese steels in crushing and grinding service,
Fabert H.A.
Proceedings of Materials for the Mining Industry,
Vail, Colorado. July 1974, 163-168.

152. Austenitic manganese steels.
Norman T.E., Doane D.V., Solomon A.
Trans AFS 1960, 68, 287-300

153. Technical note.
Dancoisne P.L.
British Foundryman 1975, 68, p(xvi) Oct.

154. Hardness and abrasive wear resistance of Ni-Cr-Mo-C
hardfacing alloys.
Whelan E.P.
Journal of Metals,1979, 31, 15-19.

155. Hardfacing against abrasive and impact types of
wear with iron base alloys.
Moeshie H.
Phillips Welding Reporter 1973, 9, 1-6

156. Abrasion and corrosion resistant cobalt alloys for
hardfacing.
Drapier J.M.
Wear 1975, 33, 271-282

157. Tribology and hard surfacing.

Moore A.J.W.

Tribology 1976, 9, 265-271

158. Surface coatings.

Donavan M.

Tribology 1972, 5, 205-224.

159. Selection of hardfacing alloys.

Evans C.J.

Welding and Metal Frabrication 1977, 45, 62-64.

160. Some characteristics of tungsten carbide weld deposits.

Avery H.S.

Welding Journal 1951, 30, 144-160.

161. Welding in the foundry.

Cookson C.

British Foundryman 1976, 69, pXV Feb.

162. The wear of metals by relatively soft abrasives.

Richardson R.C.D.

Wear 1967, 10, 291-309

163. A review of materials for grinding mill liners.

Norman T.E.

Proceedings of Materials for the Mining Industry,

Vail, Colorado. July 1974, 209-218.

164. Materials and technology VII.
Longman - de Bussy 1971, 60-62.

165. Slagceram, a new construction material.
Klemantaski S. and Kerrison E.
Chemistry and Industry 1966, Oct. 15th, 1745-1753.

166. Wear resisting metal slag pipes.
Parasyuk P.F.
Russian Castings Production 1975, 270.

167. Durafrax wear resistant ceramic materials.
The Carborundum Company, New York, 11 pp.

168. ZAC 1681 - anti abrasion material.
Electro-Refractaire Publication, Paris July 1974, 48 pp.

169. Durafrax wear alumina.
Resistant Materials Bulletin No.4.
The Carborundum Co. Ltd., St. Helens, July 1976.

170. Alfrax and Mullfrax.
Refractories and Electronics Bulletin No. 11.
The Carborundum Co. Ltd., St. Helens, May 1974.

171. Silicon Carbide super refractories (Carbofrax).
Refractories and Electronics Bulletin No.5.
The Carborundum Co. Ltd., St. Helens, May 1974.

172. Using silicon nitride for gas turbine engines.
Stoddart D.E.
Gas turbine International July 1972, 4 pp.

173. Wear resistant rubber.
Trelleborgs Gummifabriks Publication, Sweden 1976, 56 pp.

174. Polyurethanes
Phillips L.N. and Parker D.B.
Illiffe, London 1964, 53-56.

175. Assessment of polyurethane as a wear resistant material.
Bradley and Foster Internal Report RD/75/8.

176. Skega-lining for grinding mills.
Skega publication, Ersmark 1975, 32 pp.

177. Trellex mill linings,
Trelleborgs Gummifabriks Publication, Sweden, 1976, 44 pp.

178. Use of abrasion resisting alloys and design factors in producing underground mine scrapers.
Wilson J.A.
Farm, Construction and Machinery Conf. Milwaukee, Sept. 1966.
Society of Automotive Eng. Report 660611.

179. Materials and metallurgy related to Taconite mining abrasion problems.
Judkins K.R.
As (178) Report 660610.

180. Selection and performance of abrasion resistant materials.
Lampman J.
Pit and Quarry 1963, March, 114-118.

181. Extraction Metallurgy.
Gilchrist J.D.
Pergammon Press London 1967.

182. Utilization and application of a superior abrasion resistant material for severe crushing applications.
Hegmegee P.E. Jr.
Proceedings of Materials for the Mining Industry, Vail, Colorado, July 30,31 1974, 201-205.

183. Laminated martensitic white irons.
Kempe P.C.
Canadian Mining and Metallurgical Bulletin 1967, Sept., 225-230.

184. Skega rubber screen decks.
Skega Publication, Eramark 1975, 32 pp.

185. Wear resistant lining materials for steelworks chutes.
Hocke H.
Tribology in Iron and Steel Works, London 1969
ISI Publication No 125 pp 17-22.

186. Wear resistant materials for steelworks plant handling coke and sinter.
Hocke H.
Symposuim on Storage and Flow of Solids.
Chicago, 17-20 September 1972, 11 pp.

187. An approach to mill liner materials for critical grinding service.
Dougall J.R.
Proceedings of Materials for the Mining Industry,
Vail, Colorado July 30,31, 1974, 169-172.

188. The role of cast alloys in resisting abrasion by cement clinker.
Dodd J.
Wear 1969, 14, 255-262.

189. High Cr-Mo alloy irons for the mining industry.
Dodd J. and Dunn D.J.
Molybdenum Mosaic,1978, 3, 2-9.

190. Forum on ball and rod mill liners.

Zieman W.H.

Canadian Mining & Met. Bulletin 1959, 52, 511-28,776-7.

191. Polyurethane as a lining plate material.

Buster R.G.

Bradley & Foster Internal Report RD 76/16.

192. Abrasion resistance and fracture toughness of white irons.

Sare I.R.

Metals Technology 1979, 6, 412-419.

193. Testing abrasion resistance of slurry pipeline materials.

Hocke H. and Wilkinson H.N.

Tribology International 1978, 11, 289-294.

194. Skega heavy duty wear components.

Skega Publication, Eremark, Sweden, 1975.

195. Hi-Chrome Alloy castings.

Auto Alloys Ltd. Publication, Blackwell, 1977, 23 pp.

196. Private communication.

Taylor D.
Director, Auto Alloys Ltd.

197. Production of stainless high Cr irons for wet milling.

Buster R.G.

Bradley & Foster Internal Report RD 76/1.

198. Effect of rare earth additions on electrochemical properties of Cr and Cr-Mo cast irons.
Kinevskiĭ et al.
Fiziko-Khimicheskaya Mekhanika Materialov 1972, 8, 16-18.

199. The erosion-corrosion resistance of modified chromium cast irons.
Lisogar A. et al.
Korroziya i Zaschita Metallov 1972, 64-67.

200. Grinding media for wet mills.
Data Sheet 2 p.
Bradley and Foster Ltd., Darlaston 1977.

201. Unpublished work.
Higginson G.M.
Bradley and Foster Ltd., Darlaston.

202. BIS Foundry Sand Data Book.
British Industrial Sand Ltd., Surrey.

203. Moroney M.J.
Facts from figures.
Penguin Books. 1963.

204. An experimental study of the Fe-Mn-C & Fe-Cr-C systems at 1000°C.
Nishizawa T.
Scand.J. of Metallurgy, 1977, 6, 74-78.

205. Measurement of impact forces in ball mills.
Dunn D.J. & Martin R.G.
Society of Mining Eng. 1978, April, 384-388.

206. Factors influencing the wear resistance of chromium white irons.
Luckin V.S. et Al.
Russian Castings Production, 1976, (11), 446-447.

207. The influence of structure on the abrasive wear resistance of cast iron.
Katavic I.
Wear, 1978, 48, 35-53.

208. Abrasive wear of white cast irons.
Zum Grahr K.H. & Eldis G.T.
Wear, 1980, 64, 175-194.

209. Abrasive wear of white cast irons.
Watson J.D., Mutton P.J. & Sare I.R.
Metals Forum, 1980, 3, 74-88.

210. Some effects of microstructure on the abrasion resistance of metals.
Mutton P.J. & Watson J.D.
Wear, 1978, 48, 385-398.

211. Quantitative analysis of eutectic structures in high Cr irons.
Matsubara Y. & Ogi K.
Imono, 1976, 48, 784-789.

212. Increasing the wear resistance of high Cr cast irons.
Stepina A.I. & Vagin V.V.
Metal Science & Heat Treatment, 1976, 18, 828-830

213. Morphology of eutectic M_3C & M_7C_3 in white iron castings.
Powell G.L.
Metals Forum, 1980, 3, 37-46.

214. Private Communication.
Jackson R.S.
Univ. of Aston in Birmingham.

215. On the rod to blade transition in the Al-Al_3Ni eutectic.
Smart H.B. & Courtney T.H.
Metallurgical Transactions, 1972, 3, 2000-2002.

216. Wear properties of eutectic chromium carbides in Cr-Mo cast materials subjected to impact.
Strizik P.
Giesserei-Rundschau 1976, 23, 129-133.

217. Formation of white layers at rubbing surfaces.
Eyre T.S. & Baxter A.
Metals and Materials 1972, October, 435-439.

218. Plastic deformation below worn surfaces.
Moore M.A. & Douthwaite R.M.
Metallurgical Transactions, 1976, 7A, 1833-9.

219. Metallographic observation of abrasive wear mechanisms.
Watson J.D. & Mutton P.J.
Journal of Australian Inst. of Metals, 1976, 21, 182-186.

220. Microctructure and mechanical behaviour of carbides.
Hollox G.E.
Materials Sc. & Eng., 1968, 3, 121-137.

221. Plastic deformation of cementite.
Formichev O. & Nikitchencko V.
Physics of Metals and Metallography, 1971, 31, 223-225.

222. Some aspects of the relationship between microstructure and mechanical properties.
Pickering F.B.
Iron and Steel, 1965, 38, 110-114.

223. Fracture in pearlite steels.
Barnby J.T. and Johnson M.R.
Metal Science Journal, 1969, 3, 155-159.

224. TEM study of deformation and fracture of cementite in cold rolled steels.
Inoue A., Ogura T. etAl
Trans. Japan Inst. of Metals, 1976, 17, 149-157.

225. Room temperature plastic deformation of pearlitic cementite.
Sevillano J.G.
Material Sc. & Eng. 1975, 21, 221-225.

226. Ion beam thinning applied to electron microscopy of hard metals.
Almond E.A. & Roebuck B.
Metallurgist & Materials Tech. 1973, April, 184-185.

227. The deformation of WC - Co cemented carbides.
Sarin V.K. & Johannesson T.
Metal Science, 1975, 9, 472-476.

228. Effect of plastic deformation on the strength of WC - Co alloy.
Exner N. & Gurland J.
Journal of Materials, 1970, 5, 75-85.

229. Initiation of ductile failure by fractured carbides in an austenitic stainless steel.
Barnby J.T.
Acta Met. 1967, 15, 903-909.

230. Critical appraisal of carbide cracking mechanisms in ferrite/carbide aggregates.
Lindley T.C. at Al
Acta Met. 1970, 18, 1127-1136.

231. Observations on fracture of cementite particles in a 1% C steel deformed at room temperature.
Gurland J.
Acta Met. 1972, 20, 735-740.

232. Some mechanical property and fracture studies of carbon fibre-nickel composites.
Braddick D.M. et Al
Journal of Mat. Science, 1971, 6, 419-426.

233. Some aspect of the fracture of boron-aluminium components.
Jackson P.W. et Al
Journal of Mat. Science, 1971, 6, 427-438.

234. Wear mechanisms in composites.
Eliezer Z. & Khanna V.D.
Wear 1978, 51, 169-179.

235. Technical Note.
Metalworking Production, 1978, June, p13.

236. Some practical aspects of graim boundaries in metals.
Honeycombe R.W.
Inst. of Metallurgists Conf. Proceedings.
Series 3 No 5, April 1976.

237. Study of particle erosion damage in Stellite.
Edington J.W. & Wright I.G.
Wear 1978, 48, 131-155.

238. Wear mechanisms in hard facing alloys.
Blomberry K.I.
Tribology International 1975, 8, 33.

239. Indentation fracture of cemented carbide.
Ogilvy I.M., Perrot C. & Suiter J.W.
Wear 1977, 43, 239-252.

240. Elastic plastic indentation, hardness and fracture.
Perrot C.M.
Wear 1977, 45, 293-309.

241. Private communication (January 1979).
Southwick P.D.
University of Cambridge.

242. Growth and properties of the monovariant (Fe, Cr) - $(Fe, Cr)_7C_3$ eutectic system.
Van den Boomgaard J, Wolfe L.R.
Journal of Crystal Growth 1972, 15, 11-19.

243. Techniques used in the study of phase transformations.
Edington J.W.
Phase Transformations Volume 1, Inst. of Metallurgists, 1980, pp 1-16.

244. Interpretation of electron diffraction patterns.
Andrews K.W., Dyson D.J., Keown S.R.
Hilger and Watts, London, 1967, 188 pp.

245. Defect analysis in electron microscopy.
Loretto M.H., Smallman R.E.
Chapman and Hall, London, 1975, 131 pp.

246. Electron microscopy of thin crystals.
Hirsch P.B., Howie A., Nicholson R.B.,
Pashley D.W. and Whelan M.J.
Butterworths, London , 1970, 549 pp.

247. In-situ observations of the formation of martensite in stainless steel.
Brooks J.W., Loretto M.H., Smallman R.E.
Acta Met., 1979, 27, 1829-1838.

248 Private communication (November 1980).
Brooks J.W.
Inco-Europe Research, Birmingham.

249 Research into new abrasion resistant materials.
Maratray F.
Metals Forum, 1980, 3, 28-36.

250 Direct observations of martensite nuclei in stainless steel.
Brooks J.W., Loretto M.H. and Smallman R.E.
Acta Met., 1979, 27, 1839-1847.

251 Martensitic transformation in single crystals of iron-chromium-nickel alloys.
Breedis J.F. and Robertson W.D.
Acta Met., 1962, 10, 1077-1088.

252 Stacking faults and fcc → hcp transformation in stainless steel.
Fujita H. and Ueda S.
Acta Met., 1972, 20, 759-767.

253 Fractography of high chromium irons.
Durman R.W.
British Foundryman, 1981, 74, 45-55.

254 The structure of carbides in alloy steels.
Goldschmidt H.J.
J.I.S.I., 1948, 160, 345-362.

255 Role of carbides in low-alloy creep resisting steels.
Woodhead J.H. and Quarrell A.G.
J.I.S.I., 1965, 203, 605-620.

256 M_7C_3 to $M_{23}C_6$ transformation in chromium containing alloys.
Beech J. and Warrington D.H.
J.I.S.I., 1966, 204, 460-468.

257 Carbide M_7C_3 and its formation in alloy steels.
Dyson D.J. and Andrews K.W.
J.I.S.I., 1969, 207, 208-219.

258 Constitution diagrams for Cr-Mo-V steels
Andrews K.W., Hughes H. and Dyson D.J.
J.I.S.I., 1972, 210, 337-350.

259 Carbide reactions ($M_3C \rightarrow M_7C_3 \rightarrow M_{23}C_6 \rightarrow M_6C$) during tempering of rapidly solifified high carbon Cr-W and Cr-Mo steels.
Inoue A. and Masumoto T.
Met. Transactions, 1980, 11A, 739-747.

260. Stacking faults in chromium, iron and vanadium mixed carbides of the type M_7C_3
Dudzinski W, Morniroli J.P., Gantois M.
Journal of Mat. Science 1980, 15, 1387-1401.

261. The crystallography and deformation modes of hexagonal close packed metals.
Partridge P.G.
Met. Reviews No 118,, 1967, 169-194.

262. Electron diffraction in the electron microscope..
Kelly P.M.
University of Leeds, 1967, 46 pp.

263. Dislocations in cementite.
Koreeda A. and Shimizu K.
Phil. Mag., 1968, 17, 1083-1086.

264. Introduction to dislocations.
Hull D.
Pergammon, London, 1969, see Ch. 9.

265. Modern Metallography.
Smallman R.E. and Ashbee K.H.
Pergammon, London, 1969, pp 156-157.

266. Room and elevated temperature mechanical properties of 30% Chromium cast irons.
Boyes J.W.
BCIRA Journal, 1963, 11, 715-731.

267. Effect of heat treatment on the hardness and microstructure of 30% chromium cast irons.
Boyes J.W.
BCIRA Journal 1960, 8, 726-741.

268. Refractory hard metals
Schwarzkopf P. and Kieffer R.
Macmillan, New York, 1953, (see p 125).

269. The effects of metallurgical variables on the mechanical properties of high Cr cast irons.
Biner S.B.
PhD Thesis, Univ. of Aston, November,1981.

270. Trends in the production, utilisation and development of abrasion resistant alloys in America.
Dodd J.
Climax Molybdenum Pulication, 1975, 18 pp

271. Factors affecting the production and performance of thick section high Cr-Mo alloy iron castings
Dodd J. and Parks J.L.
Metals Forum 1980, 3, 3-27.

272. Wear and impact resistant white cast irons
Bereza J.M.
British Foundryman 1981, 74, 205-211.

273. On the structure of the Fe-Cr-C system.
Westgren A., Phragmen G., Negresco T.R.
J.I.S.I. 1928, 117, 383-400.

274. Metallography of phase transformations.
Chadwick D.A.
Butterworths, London, 1972, (See Ch 3).

275. Crystal growth of graphite from the melt.
Minkoff I.
The Solidification of Metals, 151 Spec. Report 110,
1968, 251-255.

276. Room temperature deformation mechanisms and the
defect structure of tungsten carbide.
Hibbs M.K. and Sinclair R.
Acta Met., 1981, 29, 1645-54.

277. Abrasion resistant refridgeration hardenable white iron.
Norman T.E. and Stolk D.A.
U S Patent No. 3941589, Feb. 13, 1975.

278. Cold plunge gives tools an extra lease of life.
Taylor J.
Metalworking Production, 1978, May, 73-77.

279. Fracture toughness of white cast irons.
Zum Gahr K.H. and Scholz W.G.
Journal of Metals, 1980, 32, 38-44.

280. Sand erosion behaviour of heat treated white iron.
Usami T., Ikawa K., Serita Y.
Journal of Japan Foundrymens Soc., 1978, 50, 531-536.